

***PROCEEDINGS OF THE***

***GEOLOGICA***

***CARPATHICA 70***

***CONFERENCE***

***Earth Science Institute of the Slovak Academy of Sciences  
Bratislava 2019***



***PROCEEDINGS OF  
THE GEOLOGICA CARPATHICA 70 CONFERENCE***

Smolenice Castle, Slovakia  
October 9–11, 2019

*Edited by:*

Igor Broska, Milan Kohút and Adam Tomašových

Earth Science Institute of the Slovak Academy of Sciences  
Bratislava, 2019

***Organizing committee:***

Ján Madarás, Igor Broska, Milan Kohút, Ľubica Puškelová, Silvia Antolíková, Nataša Halašiová, Kamil Fekete, Monika Szabóová, Pavel Uher

***Scientific committee:***

Members of the Editorial board of *Geologica Carpathica* including Associate Editors

***Reviewers:***

Peter Bačík, Vladimír Bezák, Miroslav Bielik, Igor Broska, František Hrouda, Stanislav Jeleň, Peter Koděra, Milan Kohút, Júlia Kotulová, Lukáš Krmíček, Segiy Kurylo, Ján Madarás, Jozef Madzin, Štefan Méres, Jozef Michalík, Martin Ondrejka, Igor Petřík, Marián Putiš, Adam Tomašových, Pavel Uher, Ján Vozár

***Edited by:***

Igor Broska, Milan Kohút and Adam Tomašových

***Technical editor:***

Ľubica Puškelová

The authors are fully responsible for the language and copyright of submitted figures and data in their articles.

***Organized by:***



***Partnership:***



***Sponsors and Supporting Organizations:***



## Foreword

The history of a scientific journal is recorded by the quality and rigour of articles reflecting the current methods and knowledge, by their impact on the next research, and by broad acceptance by readers and by the scientific community. The importance of *Geologica Carpathica* can also be perceived in this light. Firstly, the editors of this journal were successful in soliciting diverse contributions from authors from diverse institutions. Secondly, they were able to assess the quality of submissions, filter out and reject inadequate research, and find and engage with appropriate reviewers: these components of the editorial and review process represent the most significant components of any successful scientific journals, and *Geologica Carpathica*. The progress in the quality of concepts, models and analytical methods was enormous in all geological fields and branches during the existence of *Geologica Carpathica*. This progress was mirrored in all journals, for example, by the plate tectonic theory which explains the orogenesis by an “active subduction engine”, replacing the former theory of “passive geosynclinal subsidence”; or the influence of mantle plumes; and/or extraterrestrial events from research on meteorites. The development of

analytical methods in mineralogy and petrology shifted towards determination of thermo–barometric conditions using electron microprobe and special spectroscopic methods as is visible in many recent papers published in *Geologica Carpathica*. This shift happened along with a boom in geochronology, which is now in many cases in fact petrochronology, because we want determine the geodynamic conditions of rock genesis and reconstruct tectonic events on large spatial and temporal scales. Paleontological, sedimentologic, and stratigraphic research was similarly affected by increasing availability of instrumental methods in elemental and isotopic geochemistry, shifting the fields towards multiproxy and high-resolution studies. The *Geologica Carpathica* constantly reflects these latest trends in geoscience research. The contributions in this issue devoted to its 70<sup>th</sup> anniversary are represented by review papers that can represent a building block or foundation for further development of geoscience research. This special issue of *Geologica Carpathica* was prepared in order to highlight the importance of a long-living scientific journal with a strong tradition in impartial peer-review assessment.

*Editors*



## Table of contents

<b>I. Broska, A. Tomašových, M. Kohút &amp; E. Puškelová:</b> Geologica Carpathica: History and future of the open access international geoscience journal.....	9
<b>I. Broska &amp; P. Uher:</b> Bohuslav Cambel: An outstanding geochemist and his role in history of Geologica Carpathica (100 years since his birth).....	12
<b>Theme 1: Tectonic history of the Alpine–Carpathian–Balkan orogenic belt</b>	
<b>Keynote talk F. Neubauer, Y. Liu, S. Cao &amp; S. Yuan:</b> What is the Austroalpine mega-unit and what are the potential relations to Paleotethys Ocean remnants of southeastern Europe? .....	16
<b>Keynote talk D. Plašienka:</b> The Western Carpathians — record of 180 Myr lasting orogenic progradation and its drivers.....	21
<b>T. Csibri, M. Kováč &amp; S. Rybár:</b> Neogene exhumation and denudation of the Central Western Carpathian nappe units in the Danube Basin.....	25
<b>P. Ivan, Š. Méres &amp; D. Plašienka:</b> Lithology and tectonic structure of the HP/LT metamorphosed composite Bôrka Nappe: An important clue to the Meliata Ocean geological history.....	29
<b>E. Márton, D. Plašienka, J. Madzin, J. Grabowski, J. Bučová, R. Aubrecht &amp; M. Putiš:</b> A new era of the paleomagnetic research in the pre-Cenozoic of the Central Western Carpathians: Concepts, first results and ongoing studies.....	33
<b>F. Neubauer, Y. Liu, S. Yuan, S. Yu, J. Genser, B. Liu &amp; Q. Guan:</b> The Wechsel Gneiss Complex of Eastern Alps: A Cambrian continental arc and its Early Proterozoic hinterland.....	37
<b>T. Potočný, Š. Méres &amp; D. Plašienka:</b> Succession of tectonometamorphic processes in the Veporic–Gemic contact zone revealed by monazite age data (Western Carpathians, Slovakia).....	39
<b>J. Soták, M. Kováč, D. Plašienka &amp; R. Vojtko:</b> Orogenic wedging and basin formation in the Central Western Carpathians: New insights from Súľov–Domaniža and Žilina–Rajec basins.....	43
<b>R. Vojtko, P. Žitňan, J. Prcúch, J. Lexa, P. Koděra, M. Chovan &amp; A. Kubač:</b> Structural control of the Banská Hodruša ore deposit (Štiavnica Stratovolcano).....	45
<b>Theme 2: Petrology and geochemistry: Towards geodynamics and metallogeny</b>	
<b>Keynote talk V. Janoušek:</b> Variscan odyssey of the Bohemian Massif and the related plutonic activity.....	50
<b>Keynote talk A. von Quadt, S.J.E. Large, Y. Buret, I. Peytcheva &amp; C.A. Heinrich:</b> How long does it take to make a giant porphyry copper deposit? Advances in high-precision geochronology and modelling of magmatic–hydrothermal processes.....	54
<b>P. Bačík:</b> The influence of cationic partitioning among crystallographic sites based on bond-valence constraints and the genetic environment geochemistry on the composition of tourmaline-supergrain minerals.....	56
<b>E. Balkanska, I. Gerdjikov, S. Georgiev, A. Lazarova &amp; A. Kounov:</b> Mylonitic Late Variscan granites from the central Balkan fold-thrust belt, Bulgaria.....	60
<b>F. Finger, H. Fritz, C. Hauzenberger, E. Hejl, W. Kurz &amp; M. Lindner:</b> Variscan I-type granitoids in the Eastern Alps and their geodynamic setting: An updated discussion based on new geochronological results.....	64
<b>H. Georgieva, R. Nedialkov &amp; I. Krumov:</b> Hydrothermal amphiboles from Na–Ca and Na–Ca–K-silicate alterations: An example from Elatsite porphyry copper–gold deposit, Bulgaria.....	65
<b>M. Janák:</b> Eclogites of the Western Carpathians revisited.....	69
<b>P. Jirman, E. Geršlová &amp; L. Medvecká:</b> The geochemical characteristics of the Menilite Formation in the Czech Carpathians: A short review.....	71

<b>M. Kohút, R. Anczkiewicz, A. Biroň, M. Danišík, V. Erban, A. Gerdes, A. Halton, K. Jesenák, C. Kirkland, Y. Kochergina, T. Magna, T. Mikuš, S. Milovská, R. Milovský, N. Pearce, C. Recio, S. Sherlock, J. Šurka, J. Westgate &amp; P. Bačo:</b> Genesis of the Carpathian obsidians.....	75
<b>L. Krmíček &amp; L. Ackerman:</b> Regionally dependent metasomatism of orogenic mantle revealed by highly siderophile elements and Re–Os isotope geochemistry of Variscan lamproites: A pilot study from the Bohemian Massif.....	79
<b>J. Lexa, B. Rottier, K. Yi, A. Audétat, I. Broska, P. Koděra &amp; M. Kohút:</b> Magmatic evolution of the Štiavnica volcano.....	83
<b>N. Lyzhachenko, S. Kurylo, S. Bondarenko &amp; V. Syomka:</b> Mineralogy of Nb–Ta bearing apatite–cordierite metasomatised metabasite from Mostovyi ore occurrence (Ukrainian Shield).....	87
<b>M. Maraszewska, I. Broska &amp; S. Kurylo:</b> Hybrid I/S nature of Prašivá granite type, Low Tatra pluton: Evidence from mineralogical data.....	91
<b>D. Ozdín, M. Gargulák, P. Povinec, S. Strekopytov, V. Porubčan &amp; Š. Farsang:</b> Meteorite Smolenice — a new iron of IVA group from Slovakia.....	95
<b>I. Petrík:</b> Two types of titanite in I-type tonalites from Tatric and Veporic units: Magmatic vs. post-magmatic oxidation.....	99
<b>S. Shnyukov, I. Lazareva, O. Andrieiev, O. Mytrokhin, A. Aleksieienko &amp; L. Gavryliv:</b> Geochemical modeling of magmatic–hydrothermal systems: Petrological evaluations and metallogenic application.....	102
<b>P. Uher, P. Bačík &amp; J. Fridrichová:</b> Beryllium silicate minerals in granite–pegmatite suites: Tracers of magmatic to hydrothermal and tectonic evolution (examples from Western Carpathians).....	106
 <i>Theme 3: Permian evolution: Joining the Variscan and Alpine orogenic events</i>	
<b>Keynote talk G. Zulauf:</b> From Variscan to Cimmerian Europe as revealed from case studies in the Bohemian Massif and the eastern Mediterranean.....	110
<b>I. Broska &amp; M. Kubiš:</b> Whole rock chemistry of the Permian Gemeric specialised S-type granites (Western Carpathians) and remark to their correlation.....	112
<b>R. Demko:</b> The Permian basalts in Hronic Unit (the Western Carpathians): Their physical and regional variations.....	115
<b>M. Putiš, F. Koller, X-H. Li, Q-L. Li, A. Larionov, P. Siman, M. Ondrejka, P. Uher, Z. Németh, P. Ružička &amp; O. Nemeč:</b> Geochronology of Permian–Triassic tectono–magmatic events from the Inner Western Carpathian and Austroalpine units.....	119
<b>J. Spišiak, L. Vetráková, D. Chew, Š. Ferenc, T. Mikuš &amp; P. Siman:</b> Calc–alkaline lamprophyres from the Nízke Tatry and Malá Fatra Mts.: Petrology and geochronology.....	123
 <i>Theme 4: Stratigraphy, sedimentology, and paleobiology of the Tethyan and Paratethyan realms</i>	
<b>Keynote talk K. Holcová, F. Scheiner, N. Doláková, S. Nehyba, J. Kopecká, R. Brzobohatý, A. Demeny, Š. Hladilová, J. Hrabovský, H. Kuhnert, R. Milovský, J. Rigová, M. Seko &amp; T. Utescher:</b> An imprint of the middle Miocene paleoceanologic and paleoclimatic events in a satellite sea during the Langhian: A case study from the Central Paratethys.....	126
<b>Keynote talk M. Kováč &amp; The Neogene Tigers (E. Halásová, J. Hók, K. Holcová, N. Hudáčková, M. Hyžný, M. Jamrich, P. Joniak, M. Kováčová, A. Ruman, S. Rybár, M. Sabol, K. Šarinová, M. Šujan, R. Vojtko, T. Csibri, P. Kiss, P. Nováková, I. Pavičič, L. Šamajová, T. Vlček):</b> Implication of the global and regional tectonics and eustasy on the Central Paratethys paleogeography: Reflection in the regional and standard time scale correlation.....	130
<b>Keynote talk J. Michalík:</b> Mesozoic sedimentary basins, current systems and life domains in northern part of the Mediterranean Tethys Ocean.....	134

<b>Keynote talk D. Reháková:</b> Plankton evolution and biostratigraphy during Late Jurassic and Early Cretaceous..	137
<b>A. Ali, R. Mohamed, K. Zaki &amp; M. Wagreich:</b> Influence of deformation bands on Nubian sandstone reservoir quality, Eastern Desert, Egypt.....	141
<b>S. Antolíková:</b> Biostratigraphic and paleoecological evaluation of Lower Jurassic sediments from Myjava Highlands.....	142
<b>J. Hrabovský, D. Basso, G. Coletti &amp; A. Pisera:</b> The paleogeographic distribution of the coralline algae of the genus <i>Mesophyllum</i> in Central Paratethys during the Middle Miocene.....	143
<b>N. Hudáčková, A. Ruman, I. Plašienková, M. Jamrich, E. Halásová, P. Kiss, M. Kováčová, J. Babejová-Kmecová &amp; M. Kováč:</b> Badenian/Sarmatian foraminifera shift in the Central Paratethys: Two methods comparison — a morphogroup and species approach.....	144
<b>M. Krobicki, A. Feldman-Olszewska, O. Hnylko and J. Iwańczuk:</b> Peperites and other volcano-sedimentary deposits (lowermost Cretaceous, Berriasian) of the Ukrainian Carpathians.....	146
<b>V. Šimo:</b> <i>Bathysiphon</i> microfacies and trace fossils association of the Lower Jurassic Fleckenmergel marly limestone from the Central Western Carpathians, the Pieniny Klippen Belt and the Betic Cordillera.....	151
<b>P. Siwek &amp; M. Wendorff:</b> Research into mixed turbidite systems: Macro- and microscopic-scale observations — case study from the Szczawa Tectonic Window, the Fore-Magura zone of the Polish Outer Carpathians.....	153
<b>P. Siwek &amp; M. Wendorff:</b> The Cergowa Sandstone at Stasiana and Iwla: An example of turbidity hyperpycnal flow deposits in the Outer Carpathians (Dukla region).....	157
<b>J. Soták, S. Antolíková &amp; T. Elbra:</b> End-Cretaceous extinction and Paleogene recovery of planktonic microfauna in the Western Carpathians: Stratigraphic constraints and paleoenvironmental proxies.....	160
<b>L. Švábenická &amp; R. Šefců:</b> Provenance of natural chalk used in ground layers of the Bohemian Gothic paintings determined by nannofossils.....	162
<b>A. Tomašových, N. Hudáčková &amp; T. Fuksi:</b> Actualistic paleoecology and taphonomy of the Holocene benthic assemblages in the northern Adriatic Sea: Links with the Middle Miocene ecosystems of the Vienna Basin.....	163
 <b>Theme 5: Applied geophysics: Deep structures in orogenic belts</b>	
<b>Keynote talk M. Bielik, H. Zeyen, Z. Alasonati Tašarová, V. Starostenko, I. Makarenko, O. Legostaeva, H-J. Goetze, †F. Horváth, R. Pašteka, J. Dérerová, J. Pánisová, M. Grinč &amp; B. Šimonová:</b> Integrated geophysical modelling of the lithosphere in the Carpathian–Pannonian region: A review.....	166
<b>Keynote talk R. Pašteka, P. Zahorec, M. Bielik, V. Szalaiová, J. Mikuška, I. Marušiak, J. Papčo, D. Kušnirák &amp; M. Krajňák:</b> Revision of Bouguer gravity anomalies map of Slovak Republic and interpretation of their enhanced higher derivatives.....	171
<b>V. Bezák, J. Vozár, D. Majcin, M. Bielik, D. Bilčík, J. Pek, R. Klanica &amp; J. Telecký:</b> Research of deep crustal structures by electromagnetic sounding and other geophysical methods in the northern part of Slovakia.....	172
<b>F. Hrouda:</b> Contrasting magnetic fabrics in sedimentary rocks of the accretionary prisms of the Flysch Belt of the Western Carpathians and the Rhenohercynian Zone of E Bohemian Massif.....	176
<b>L. Šamajová, J. Hók, M. Bielik &amp; T. Csibri:</b> The contact of the Bohemian Massif, Western Carpathians and Eastern Alps: Density modelling.....	180
<b>P. Vajda, P. Zahorec, J. Papčo, D. Bilčík, F. Greco &amp; M. Cantarero:</b> Advances in volcano gravimetry: Handling topographic effects.....	184
Register.....	188



# Geologica Carpathica: History and future of the open access international geoscience journal

## Geologica Carpathica celebrates 70 years anniversary

The mission of Geologica Carpathica (GC) — as an International open access geological journal — is to cover a broad spectrum of geological topics by high-quality publications. Of course, such focus only gradually evolved and broadened over the past 70 years. It was initially concentrated on geological problems of the Western Carpathians, but its scope currently expanded towards the geological evolution of the Alpine–Carpathian–Dinaride–Balkan regions. The journal began its existence in 1950 as the Geological Proceedings (“Geologický Sborník”) of the Slovak Academy of Sciences (Fig. 1), founded as a scientific journal devoted to the dissemination of scientific results from geological research in the Czechoslovak part of the Western Carpathians. It was founded by professors Dimitri Andrusov and Rudolf Lukáč from the Comenius University (Bratislava). The early articles were published in the Slovak language, with abstracts in two other languages, typically German and Russian. The creation of the journal resulted from an effort to encourage the development of the geological knowledge of Slovakia and the expansion of the Slovak raw material basis. Thanks to international contacts of geologists from the Slovak Academy of Sciences, the Comenius University, and Dionýz Štúr Geological Institute, and through collaborations with members of the Carpathian–Balkan Geological Association, number of articles from abroad published in the journal were increase since late sixties and seventies.

## Globalisation of journal

The first foreign contribution (in Slovak translation), which appeared in Geologica Carpathica was written on request of Professor Andrusov by Krzysztof Birkenmajer (1957, Vol. 8, No.1) and clarified stratigraphy of the Pieniny Klippen Belt. Since 1963, with some exceptions, the contributions in Geologica Carpathica were mainly published in German, Russian and English, less commonly also in French. The papers published later on 1982 were almost only in English. The first really international article has been published by the leading Austrian geologist Alexander Tollmann who correlated the Tatricum with the Unterostalpin in 1965. The first international issue of Geologica Carpathica appeared in 1967, with articles published by authors from Austria, Poland, Romania, Bulgaria, Yugoslavia and the Soviet



Fig. 1. Timeline of the history of Geologica Carpathica.

Union. This issue was prepared on the occasion of the 70<sup>th</sup> birthday anniversary of Dimitri Andrusov with bibliography written by Bohuslav Cambel who later innovated and transformed the journal “Geologický Sborník”, into a truly international journal named “Geologický Zborník — Geologica Carpathica”. The dissemination of geoscience research in world languages became the new publishing concept of the Geologica Carpathica, and a base for further scientific growth of the journal. Bohuslav Cambel expanded the editorial office establishing a position of English interpreter at the Geological Institute of the Slovak Academy of Sciences (now Earth Science Institute). Under the leadership of Editor-in-chief Eduard Köhler since 1991, the journal published articles in English only, it changed the size format from B4 to A4, the title was simplified to “Geological Carpathica”, established international editorial board and the number of foreign authors increased, mainly from the Carpathian–Balkan region.

### Period after registration in Current Content database

In 1996, the journal was already indexed in the Current Contents Database, with the initial impact factor of 0.27. Then, under the direction of the Editor-in-chief Jozef Michalík, the contributors from abroad increased and came also from the eastern continuation of the Alpine zone, and the proportion of Slovak authors declined to ~20 %. The impact factor (IF) > 1 was reached for the first time in 2008, and is persistently above 1 since 2015 (Table 1). The journal importance was growing mutually up to 2016, when Web of Science (WOS) IF (2-year window) reached 1.52; together with Scimago index SJR=0.58, and the Scopus CiteScore computed over 3-year window is 1.49. In the WOS category “Geosciences-Multidisciplinary”, Geologica Carpathica belongs to the 3<sup>rd</sup> quartile, while the Scopus in category “Geology” ranks the journal to the 2<sup>nd</sup> quartile. Noteworthy, the paper published in Geologica Carpathica over the past 20 years have 90~98 % chance to be cited in the future according to Scimago evaluation of their titles and abstract. However, the reality is that only

67~78 % from the published papers recorded some citations. The peer-review process within last year’s brought expecting results and Sci evaluation of Geologica Carpathica for 2018 year recorded highest impact with WOS (Clarivate) IF=1.70; Scimago index SJR=0.63; Scopus CiteScore=1.76 and SNIP=1.20. Noteworthy that Geologica Carpathica is in the 2<sup>nd</sup> quartile on the 66<sup>th</sup> place from 218 similar journal of the Earth and Planetary Sciences/Geology category.

Since 1997, the co-publisher of journal is also the Geological Institute of the Czech Academy of Sciences in Prague and the Polish Geological Institute in Warsaw. The journal is published electronically since 2009, since 2014 the correspondence is in own electronic editorial system. The cooperation with the Versita/De Gruyter publishing House which helped journal with dissemination of electronic version of journal and organising of doi (Digital Object Identifier) for articles terminated in 2019. The history of the journal summarizes the timeline (Fig. 1) with the names of editors-in-chiefs. Figure 2 provides geographic coordinates of the sites described in the journal since 1996.

### Research output

Geologica Carpathica influenced the thinking of several generations of geologists, with 2403 articles published until now.

Several principal articles covered the crystalline basement of the Western Carpathians were published in Geologica Carpathica, including those that expanded basic knowledge on their genesis, revealed their Carboniferous age during 80-ties up to our knowledge of their development in several age and geodynamic evolutionary stages. The metamorphic crystalline basement was described from main areas in the Western Carpathians showing their pT history and on many places metamorphic zonality. Advances in stratigraphic, sedimentological, and paleontological studies of the Western Carpathians published by Geologica Carpathica included (1) paleogeographic and paleoenvironmental analyses of Mesozoic and Paleogene successions in the Pieniny Klippen Belt and Central Western Carpathians and bio-, magneto- and chemostratigraphic correlations

**Table 1:** Geologica Carpathica impact factor history.

<b>1997</b>	<b>1998</b>	<b>1999</b>	<b>2000</b>	<b>2001</b>	<b>2002</b>	<b>2003</b>	<b>2004</b>	<b>2005</b>	<b>2006</b>	<b>2007</b>
0.271	0.273	0.486	0.156	0.167	0.147	0.397	0.494	0.449	0.364	0.517
<b>2008</b>	<b>2009</b>	<b>2010</b>	<b>2011</b>	<b>2012</b>	<b>2013</b>	<b>2014</b>	<b>2015</b>	<b>2016</b>	<b>2017</b>	<b>2018</b>
1.081	0.963	0.909	0.787	1.143	0.835	0.761	1.523	1.358	1.169	1.699



Fig. 2. Sites assessed in the journal since 1996.

between the Tethyan and Boreal realms and (2) establishment of the chronostratigraphic and paleogeographic framework for the Miocene Paratethys and its correlation with the Mediterranean Miocene. In addition to the focus on paleogeographic and stratigraphic analyses, Ján Seneš was one of the first pioneers who introduced actualistic paleoecological analyses focusing on Holocene assemblages to improve paleoenvironmental analyses of Miocene deposits in the Paratethys. This work was primarily published in *Geologica Carpathica*, starting in 1953 (southern France) and 1966 (Cuba), and in 1989–1991 (Adriatic Sea), effectively pre-dating similar works in the western countries in 1960s and 1970s that became influential in the foundation of conservation paleobiology.

*Geologica Carpathica*, with its 70-year-old tradition, presents high-quality research papers devoted to all aspects of the Alpine–Carpathian–Balkan region and

adjacent regions derived from the Mediterranean Tethys and its continental foreland. *Geologica Carpathica* is an official journal of the Carpathian–Balkan Geological Association. We hope the heritage of journal will successfully keep on the future and *Geologica Carpathica* becomes even larger platform in higher number of fundamental and review contributions for dissemination of geoscience information.

Thousands of papers have been published in the seventy years of the history of our journal, and we think that this open-access scientific journal has a great future ahead. *Geologica Carpathica* is an open-access platform for all members of the geoscience community, including students. Therefore, the standard twelve printed papers with black and white pictures are cost-free, in accordance with the recommendations of the European Commission to eliminate the recent plethora of predator journals.

*Igor Broska, Adam Tomašových, Milan Kohút and Lubica Puškelová*

## Bohuslav Cambel: An outstanding geochemist and his role in history of *Geologica Carpathica* (100 years since his birth)

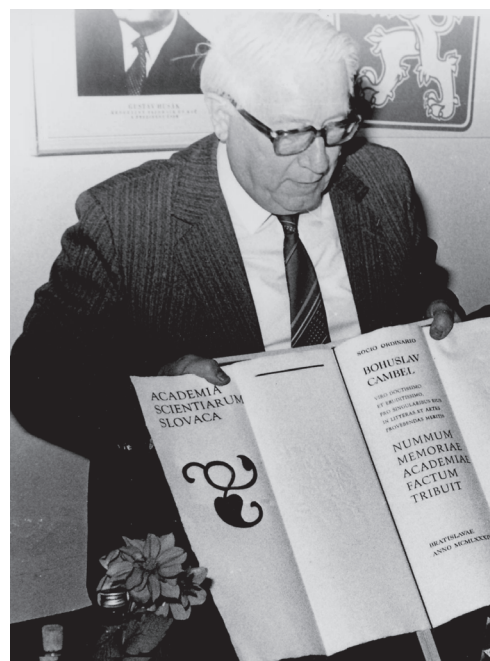


Bohuslav Cambel  
1919–2006

The Academician Bohuslav Cambel, Doctor of Science, was born on October 29, 1919 in Slovenská Ľupča. He studied at the secondary school (Gymnasium) in Banská Bystrica where he graduated in 1939. He continued his studies at the Faculty of Natural Sciences at the Comenius (at that time Slovak) University in Bratislava, where he began as a research assistant at the Mineralogy and Petrography Institute, Faculty of Natural Sciences. He received a Doctor of Natural Sciences title (RNDr.) in 1949, he became an Associate Professor in 1953 and finally a full Professor of the Comenius University in 1957. He founded and led the Department of Mineral Resources and Geochemistry (1952–1963) and later the Department of Geochemistry (1969–1980). During that time, he held positions of the Vice-Dean (1952–1953) and the Dean (1959–1961) of the Faculty of Natural Sciences, and lastly the Rector (Chancellor) of the Comenius University (1966–1969). While holding the last position, Prof. Cambel had to face a difficult period during the invasion of the Warsaw Pact military troops into Czechoslovakia (1968), and he helped many capable young scientists to migrate abroad at that time. He was also a member of the Presidium of the Slovak Academy

of Sciences (1964–1969). Prof. Cambel obtained the highest scientific degrees: Doctor of Sciences (DrSc.) in 1963, Corresponding Member of the Slovak Academy of Sciences (1964) and the Czechoslovak Academy of Sciences (1968), as well as Academician, an ordinary member of the Slovak Academy of Sciences (1972). He was also appointed as Doctor honoris causa (Dr. h. c.) of the Taras Shevchenko National University in Kyiv, Ukraine (1968).

Between 1963 and 1989, Bohuslav Cambel was the director of the Geological Institute (the Geological Laboratory before 1966), within the frame of the Slovak Academy of Sciences (SAS) in Bratislava. He re-established laboratory into a modern scientific institute mainly by creating the Geochemical Department with an appropriate and well-accessible instrument base, including electron probe X-ray microanalyser (JEOL JXA-5A), scanning electron microscope, X-ray fluorescence spectrometer and other analytical instruments. In 1981, Prof. Cambel founded the Mineral Resources Department within the Geological Institute of the Slovak Academy of Sciences, in Banská Bystrica, where currently the Institute has its main high-level instrumental base. He was the Editor-in-chief of the *Geologica Carpathica* (formerly *Geologický Zborník — Geologica Carpathica*) journal during 1965 to 1990, which was gradually transformed to a prestigious international geological magazine. Bohuslav Cambel enthusiastically organised the work of the the editorial board for more





than 30 years, as well as editorial office in effort to maintain an excellent level and reputation of the journal.

Bohuslav Cambel focused his scientific activities on the research of magmatic and metamorphic rocks (granites, metapelites, amphibolites, metacarbonates and skarns), their minerals and the associated mineral deposits, especially in the Paleozoic basement of the Malé Karpaty (Small Carpathians) Mountains near Bratislava. On the basis of geological, petrographic and geochemical data and results, he elaborated the geological, especially magmatic and metamorphic evolution of the Malé Karpaty crystalline basement (published in numerous papers in 1950–1990; see ref. in Babčan 1979), which he depicted also on a geological map in the scale of 1:50,000 (Mahel' & Cambel 1972). Prof. Cambel was a leading author of monographs concerning chemical composition of pyrite and pyrrhotite from various genetic types (Cambel & Jarkovský 1967, 1969; Cambel et al. 1977) and geochemistry of the West-Carpathian metamorphic basic rocks (Cambel & Kamenický 1982). At the time when the crystalline basement of the Western Carpathians was considered almost all Precambrian in age, he advocated their Paleozoic age, based on detailed geological, petrological, geochemical and geochronological investigations. In collaboration with geochemists from the Russia, Ukraine and Armenia (at that time the Soviet Union), he gathered the modern isotopic dating of granitic rocks from various regions of the Western Carpathians (published in *Geologica Carpathica*) and these results showed their correct Carboniferous age. The geochronological investigations of Paleozoic granitic and metamorphic rocks from the West-Carpathian area were summarized in monograph

(Cambel et al. 1990), which gave the basis for today's knowledge of the age and origin of Variscan granitic magmatism and related metamorphic processes. He has always focused his scientific work on practical outputs and therefore worked closely with the companies Ore Mines, Uranium Survey and Geological Survey. Prof. Bohuslav Cambel left behind a geochemical science school representing a continuation of his practical and scientific way of thinking.

The name of Bohuslav Cambel joined the list of the 2000 most important scientists of 20<sup>th</sup> century according to the University of Cambridge in 1998. Moreover since 2013, due to his enormous scientific contribution, the Earth Science Institute of the Slovak Academy of Sciences started awarding outstanding personalities of geoscience research by the Medal of Academician Bohuslav Cambel.

## References

- Babčan J. 1979: Academician Bohuslav Cambel, DrSc. – 60 years old. *Geol. Zborník – Geol. Carpath.* 30, 395–411.
- Cambel B. & Jarkovský J. 1967: Geochemie der pyrite einiger Lagerstätten der Tschechoslowakei. *SAV*, Bratislava, 1–493.
- Cambel B. & Jarkovský J. 1969: Geochemistry of pyrrhotite of various genetic types. *Comenius University*, Bratislava, 1–333.
- Cambel B. & Kamenický L. 1982: Geochemistry of metamorphosed basic magmatites of West Carpathian Tatroverporides. *Veda*, Bratislava, 1–514 (in Slovak with English resume).
- Cambel B. & Viliňovič V. 1987: Geochemistry and petrology of the granitoid rocks of the Malé Karpaty Mts. *Veda*, Bratislava, 1–247 (in Slovak with English resume).
- Cambel B., Král J. & Burchart J. 1990: Isotopic geochronology of the Western Carpathians crystalline complex with catalogue data. *Veda*, Bratislava, 1–183 (in Slovak with English resume).
- Mahel' M. & Cambel B. 1972: Geologická mapa Malých Karpát 1:50000. *Geologický ústav Dionýza Štúra*, Bratislava.

Igor Broska and Pavel Uher



**Theme 1:**

Tectonic history of the Alpine–Carpathian–Balkan orogenic belt

# What is the Austroalpine mega-unit and what are the potential relations to Paleotethys Ocean remnants of southeastern Europe?

FRANZ NEUBAUER<sup>1</sup>, YONGJIANG LIU<sup>2,3</sup>, SHUYUN CAO<sup>1,4</sup> and SIHUA YUAN<sup>1,5</sup>

<sup>1</sup>Paris-Lodron-University of Salzburg, Department of Geography and Geology, Geology Division, Hellbrunnerstraße 34, 5020 Salzburg, Austria. franz.neubauer@sbg.ac.at; sihua.yuan@sbg.ac.at

<sup>2</sup>Key Lab of Submarine Geoscience and Prospecting Techniques, MOE, Institute for Advanced Ocean Study, College of Marine Geosciences, Ocean University of China, Qingdao 266100, China. liuyongjiang@ouc.edu.cn

<sup>3</sup>Laboratory for Marine Mineral Resources, Qingdao National Laboratory for Marine Science and Technology, Qingdao 266237, China

<sup>4</sup>State Key Laboratory of Geological Processes and Mineral Resources, School of Earth Sciences, China University of Geosciences, Wuhan 430074, China; shuyun.cao@cug.edu.cn; shuyun.cao@sbg.ac.at

<sup>5</sup>College of Earth Science, Institute of Disaster Prevention, Sanhe, 065201, Hebei Province, China

**Abstract:** In Eastern Alps, basement units of the Cretaceous-aged Austroalpine nappe stack is considered to represent a relatively uniform continental mega-unit formed during the Variscan orogeny. Large new U–Pb zircon data sets from all, virtually Variscan and pre-Variscan, basement units east of the Tauern window reveal that the Plankogel Complex of the Saualpe is of oceanic affinity and contains Middle–Upper Triassic magmatic protoliths and detrital zircons excluding a depositional age older than Middle–Late Triassic. Based on these observations, we review Middle–Late Triassic palaeogeography and magmatic belts from both strands extending from Alps to western Turkey. We propose a new model with Triassic supra-subduction magmatic belts along margins of the Paleotethys Ocean as well as a model how the Triassic oceanic unit was emplaced within the Austroalpine nappe stack.

## What is the Austroalpine mega-unit?

The Austroalpine mega-unit of Eastern Alps and Western Carpathians is a thick-skinned continental nappe stack of Cretaceous age. Its cover is considered to represent a uniform Triassic passive continental margin succession opening towards to Meliata Ocean in the S to SE during late Middle Triassic times (Fig. 1; Froitzheim et al. 2008; Schmid et al. 2008; Plašienka 2018). The basement, particularly east of the Tauern window, is considered to have formed during Variscan orogeny, mainly during early Pennsylvanian. The basement units are highly diverse and include pre-Variscan sedimentary and magmatic units (e.g., Neubauer & Frisch 1993), which are now intensely investigated by U–Pb zircon dating of magmatic protoliths. Based on literature data and new results, the Austroalpine mega-unit comprise several major units, which include: (1) fossil-bearing Early Ordovician to Early Pennsylvanian passive margin units formed along the northern Gondwana margin; (2) a magmatic belt with abundant Ordovician to Silurian granitoids; (3) a Late Devonian–Mississippian tonalite–granite belt due to Variscan subduction processes, (4) a zone of Middle Permian granite–gabbros (Grob-Gneiss Complex), which is interpreted to have formed by rifting and crustal thinning of mid crustal levels; and (6) (Neopro-

terozoic to) Cambrian magmatic arc successions (Neubauer et al., this volume).

Previous work on this basement demonstrated Permian tectonothermal processes (e.g., Schuster & Stüwe 2008; Thöni & Miller 2009) but no post-Variscan lithostratigraphic was known, and even not expected (Froitzheim et al. 2008).

The pre-Alpine Austroalpine amphibolite-grade metamorphic basement of Eastern Alps contains a number of ophiolitic sutures (Neubauer & Frisch 1993), which are poorly constrained in age. All of them have been considered to have formed not later than during Variscan plate collision during the Carboniferous. Major portions of this basement is then overprinted by Permian rift processes, which also include low-pressure rift metamorphism (Schuster & Stüwe 2008; Thöni & Miller 2009). As a result, the location of a Paleotethyan suture has not been considered to extend into the Alps.

## Plankogel Complex of the Saualpe

Here we report preliminary results of an extensive U–Pb zircon dating campaign on the Plankogel Complex in Eastern Alps (Saualpe and Koralpe). The Plankogel Complex, a tectonic mélange, is composed of coarse-grained

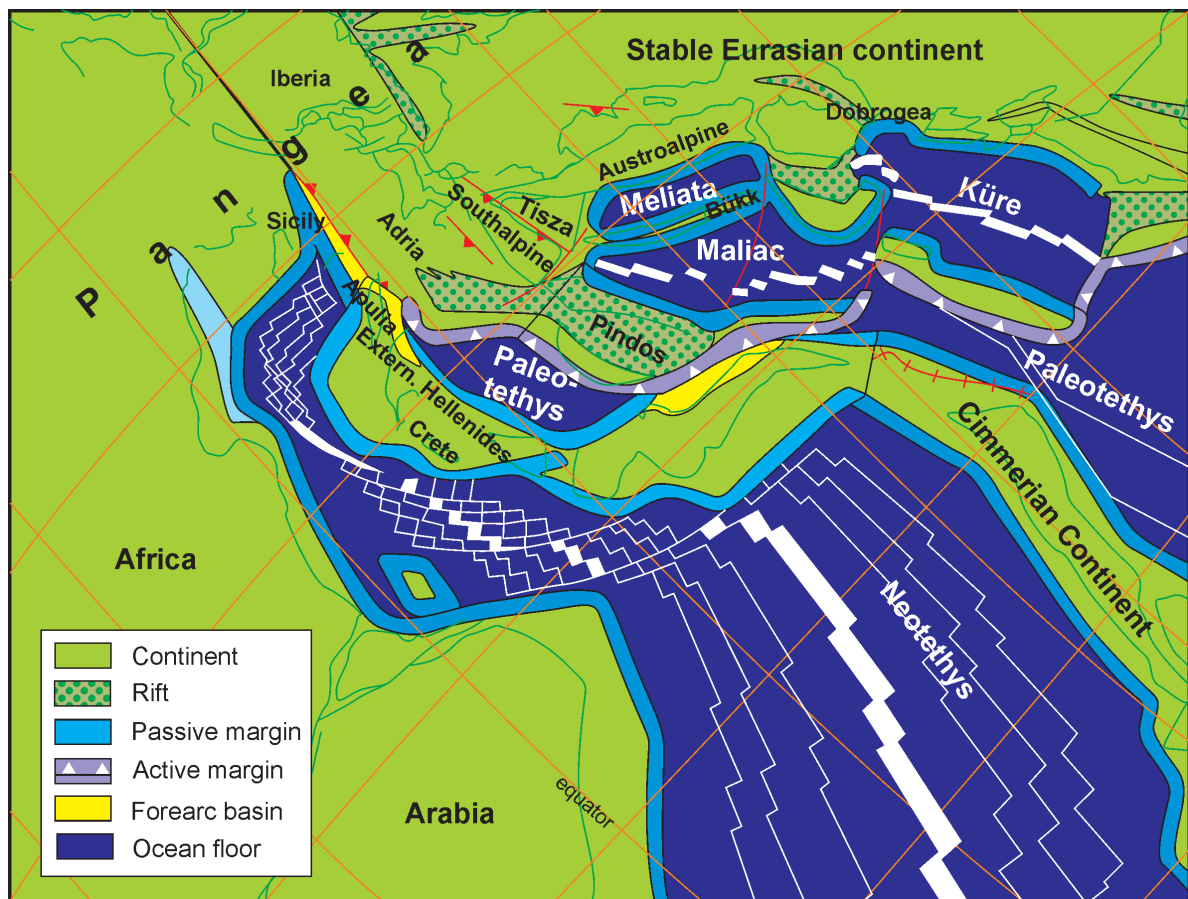


**Fig. 1.** Middle Carnian tectonic reconstruction for the western Tethyan realm (modified after Stampfli & Kozur 2006). Note the assumed Tethys rotation pole near Sicily implying increasing plate velocities towards E/SE. Note that it remains difficult, with this model, to explain subduction-related magmatic arcs.

garnet-micaschist as a matrix and plagioclase-rich biotite schist, within which hectometer-sized lenses of marble, Mn-rich quartzite, amphibolite and ultramafic rocks occur (Neubauer & Frisch 1993 and references therein). The marble was the host of a Mn-rich iron mineralization mined until ca. four decades ago. The amphibolites have a MOR-basalt geochemical signature (Neubauer et al. 1989). No protolith age were known up to now.

Metasedimentary rocks like the garnet-biotite-micaschist show a large population of Early–Middle Triassic, partly euhedral zircons implying an age of the sedimentary precursor rocks not older than Middle Triassic, and a significant Middle Triassic volcanic component. Zircons from the Mn-quartzites show a large Early Triassic volcanic component. The Mn-quartzite is interpreted to result from deep-sea Mn-rich cherts. Two amphibolites show late Permian/Early Triassic protolith ages.

As a whole, the dating results are entirely unexpected and require re-evaluation of the tectonic history of the Austroalpine units. Based on dating results, we conclude

that the Plankogel Complex represents a Triassic ophiolite-bearing tectonic mélangé with oceanic trench sediments and components from a deep-sea environment. The rich Permian to Middle Triassic volcanic components indicate, when calcalkaline, subduction of the Paleotethyan Ocean, and oceanic lithospheric elements were incorporated into the suspected trench sediments.

### Western termination of Tethys

Here, we review the Triassic geodynamic setting of the western termination Tethys which is considered as an eastward opening huge bay of Panthalassa within Pangea (Fig. 1). All reconstructions since Şengör (1979, 1984) assume that the western termination of Tethys is represented by a northern Paleotethys Ocean subducting underneath Laurasia and a southern, new formed Neotethys Ocean separated by the Cimmerian continent (Fig. 1). For demonstrating these processes and paleogeography, we use the currently popular model of

Stampfli & Kozur (2006) (Fig. 1). As Pangea is stable from Permian to Triassic times, a rotation pole for Tethyan plate motion is postulated at the western tip of Tethys embayment close to Sicily. This peculiar geodynamic setting implies slow motion in the west and rapid motion in the east caused by a rotation at the western termination of Tethys Oceans near Sicily in the future Mediterranean. Geological relicts, e.g., potential arc magmatism, and ophiolite suites, mélanges, oceanic basalts, radiolarian-bearing silicalites related to the Triassic Paleotethyan evolution are preserved in southeastern Europe of the Western Paleotethyan domain (Bortolotti et al. 2013). However, the Triassic tectonic history of that area is largely unclear and disputed. E.g., few potential Paleotethys Ocean remnants appear in different mountain belts of southeastern Europe, and their relationship to Neotethys are under discussion. Open key questions are: (i) the existence of potential Middle–Upper Triassic arc magmatism, back-arc opening (Meliata Ocean), formation of microcontinents (e.g., Apulia, Adria as part of the Western Cimmerian microcontinent) as well as on back-arc ophiolite formation; (ii) temporal–spatial evolutionary and patterns of the different microcontinents/ or blocks and their tectonic setting in the Southeast European mountain belts; (iii) Triassic tectonic processes and geodynamics of the Southeast European (eastern Mediterranean) mountain belts at the western termination of the convergent Paleotethys Ocean with the main open question, rift vs. magmatic arcs.

### Triassic tectonic processes at western termination of Tethys

In the following, models are discussed showing the interrelationships between Paleotethys and Neotethys and of intervening oceans (Fig. 2).

- Model 1 is the classical model as proposed by Şengör (1979, 1984): Paleotethys is subducting underneath the Eurasian continental margin. This implies there the presence of subduction magmatism, which was not identified in southeastern Europe.
- Model 2 (Stampfli & Kozur 2006) is similar but implies the rifting and short opening of a back-arc basin, in this case, the Dobrogea rift (Fig. 2).
- Model 3 (Bortolotti et al., 2013) separates Paleotethys and another ocean (TOFO=Vardar ocean), which is potentially a branch of Paleotethys. Note that this model does not exclude the Triassic opening and closure of the Dobrogea rift on the Eurasian margin. This model explains the magmatism in Dinarides/

Hellenides as rift magmatism in an overall extensional setting. Furthermore, the model does not include a subduction zone-related magmatism.

- Model 4 (Zulauf et al. 2018) explain magmatism in External Hellenides (e.g. Crete, and its extension in External Dinarides) as subduction-related magmatism of the Paleotethys Ocean and includes the Dobrogean rift as a sort of back-arc basin.
- Model 5, our own working hypothesis, implies two Paleotethyan branches, which were subducted during Triassic times underneath microcontinents.

As a major conclusion from all these models, revealing the nature of Triassic magmatism within the continental blocks is the key to understand the overall setting and to resolve the geodynamic setting. We tentatively assume, therefore, that the Triassic Dinaric–Hellenic magmatic belts representing supra-subduction magmatism. However, this model must be supplemented by future structural and paleomagnetic studies showing the kinematics of opening and closure of the oceanic systems (e.g. Muttoni et al. 2013), as well as the exact timing of these processes.

### Discussion and open questions

We argue that the Plankogel Complex is a tectonic mélange containing significant remnants of the Paleotethys Ocean likely related to TOFO. Consequently, the location within the Austroalpine nappe stack needs explanation. We suggest, that the preservation is in immediate hangingwall of the Cretaceous-aged high-pressure wedge (Froitzheim et al. 2008) is due to a strong rheological contrasts between upper and lower plate allowing to indent subducted lower plate succession into the upper plate (Vogt et al. 2018)

The reconstructions and models result in several key questions, which need more detailed work in the future:

- What is the significance of Middle to early Upper Triassic linear magmatic belts like in Dinarides, Southern Alps and Bükk Mts. (Köber et al. 2019). Does they represent rift magmatism as now often postulated or does they result from subduction? Although these show a calcalkaline to shoshonitic affinity, these are even interpreted as related to continental rifting (Lustrino et al. 2019 for Southern Alps; Pe-Piper 1998 for External Hellenides).
- Did the remnants of Triassic Paleotethys Ocean subduct during Triassic times and is there any further evidence for Triassic trench deposits?

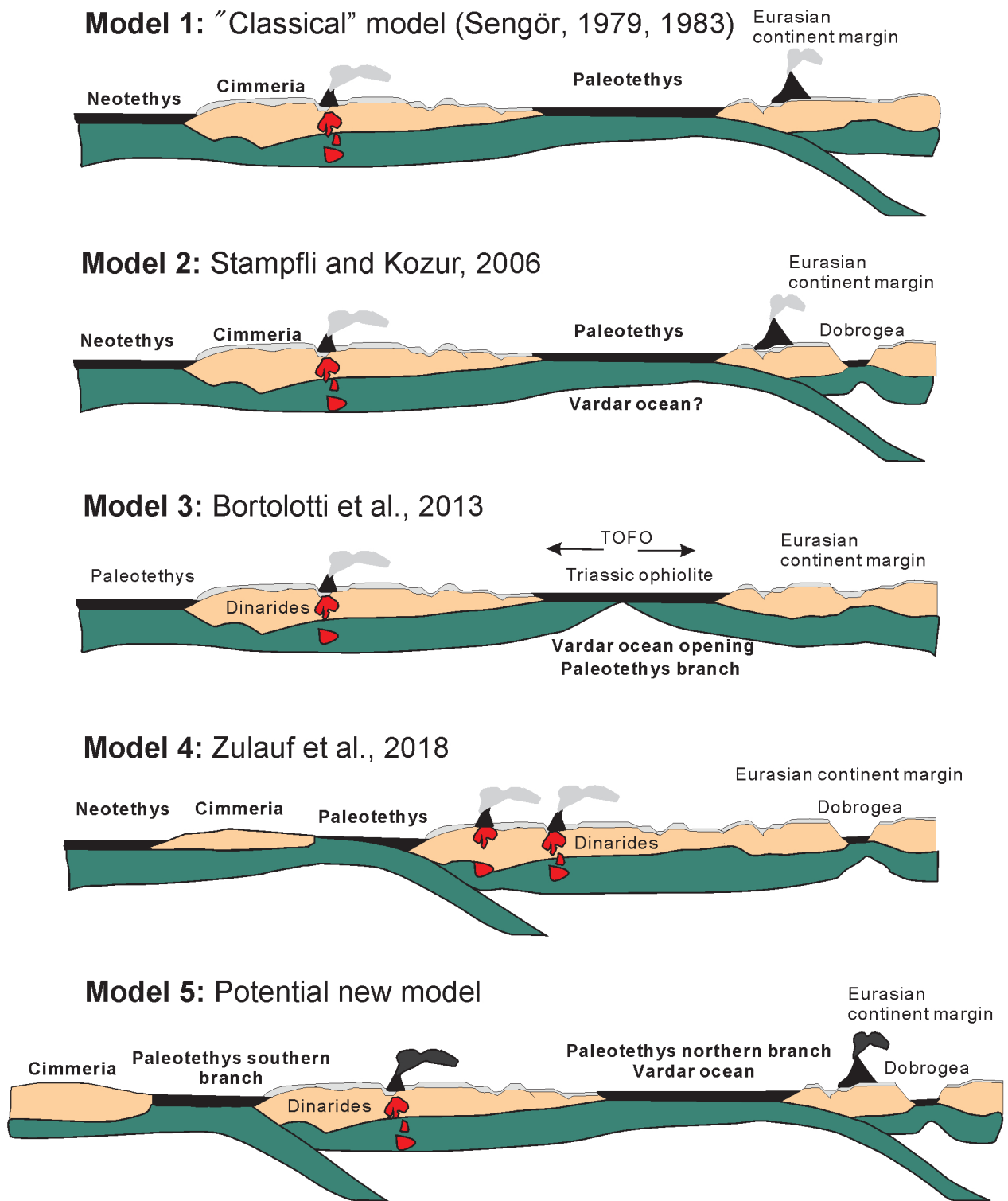


**Fig. 2.** Models of the Triassic tectonic evolution of Tethys. In all figures, the left side is S to SSW, the right side N and close to the Eurasian margin. For discussion, see text. TOFO=Triassic ocean-floor ophiolites (after Bortolotti et al. 2013).

- What is the relationship between TOFO/Vardar and other Triassic oceanic relics in southeastern Europe to the Meliata Ocean, which could be interpreted as a back-arc basin behind a continental pieces, which should carry linear subduction-related magmatic belts.
- Taking the currently popular tectonic model (e.g., Stampfli & Kozur 2006; Fig. 1), it seems impossible to explain Paleotethys closure and opening of Meliata Ocean in this sort of model when the Austroalpine mega-unit is separated from the potential Paleotethys

suture. Consequently, a new model is currently under development, which simplifies the ocean realms and explains the linear magmatic belts of the Southalpine, Dinaric and External Hellenides as magmatic arcs.

**Acknowledgements:** Analytical work on Plankogel Complex is supported by grant no. 91755212 of the NSF of China and Qingdao Leading innovation talents (no. 19-3-2-19-zhc) to Y. Liu.

## References

- Bortolotti V., Chiari M., Marroni M., Pandolfi L., Principi G. & Saccani E. 2013: Geodynamic evolution of ophiolites from Albania and Greece (Dinaric–Hellenic belt): one, two, or more oceanic basins? *Int. J. Earth Sci.* 102, 783–811.
- Froitzheim N., Plašienka D. & Schuster R. 2008: Alpine tectonics of the Alps and Western Carpathians. In: McCann T. (Ed.): The geology of central Europe, Mesozoic and Cenozoic. Vol. 2. *Geological Society Publishing House*, London, 1141–1232.
- Kövér S., Fodor L., Kovács Z., Klötzli U., Haas J., Zajzon N. & Szabó Cs. 2019: Late Triassic acidic volcanic clasts in different Neotethyan sedimentary mélanges: paleogeographic and geodynamic implications. *Int. J. Earth Sci.* 107, 2975–2998.
- Lustrino M., Abbas H., Agostini S., Caggiati M., Carminati E. & Gianolla P. 2019: Origin of Triassic magmatism of the Southern Alps (Italy): Constraints from geochemistry and Sr–Nd–Pb isotopic ratios. *Gondwana Res.*, <https://doi.org/10.1016/j.gr.2019.04.011>
- Muttoni G., Dallanave E. & Channell J.E.T. 2013: The drift history of Adria and Africa from 280 Ma to Present, Jurassic true polar wander, and zonal climate control on Tethyan sedimentary facies. *Palaeogeogr. Palaeoclimatol. Palaeoecol.* 386, 415–435.
- Neubauer F. & Frisch W. 1993: The Austroalpine metamorphic basement east of the Tauern window. In: von Raumer J. & Neubauer F. (Eds.): Pre-Mesozoic Geology in the Alps. *Springer*, Berlin, 515–536.
- Neubauer F., Frisch W., Schmerold R. & Schlöser H. 1989: Metamorphosed and dismembered ophiolite suites in the basement units of the Eastern Alps. *Tectonophysics* 164, 49–62.
- Pe-Piper G. 1998: The nature of Triassic extension-related magmatism in Greece: evidence from Nd and Pb isotope geochemistry. *Geol. Mag.* 135, 331–348.
- Plašienka D. 2018: Continuity and episodicity in the early Alpine tectonic evolution of the Western Carpathians: How large-scale processes are expressed by the orogenic architecture and rock record data. *Tectonics* 37, <https://doi.org/10.1029/2017TC004779>.
- Schmid S.M., Bernoulli D., Fügenschuh B., Matenco L., Schefer S., Schuster R., Tischler M. & Ustaszewski K. 2008: The Alpine–Carpathian–Dinaric orogenic system: correlation and evolution of tectonic units. *Swiss J. Geosci.* 101, 139–183.
- Schuster R. & Stüwe K. 2008: Permian metamorphic event in the Alps. *Geology* 36, 603–606.
- Şengör A.M.C. 1979: Mid-Mesozoic closure of Permo–Triassic Tethys and its implications. *Nature* 279, 590–593.
- Şengör A.M.C. 1984: The Cimmeride orogenic system and the tectonics of Eurasia. *Geol. Soc. Amer. Spec. Pap.* 195, 1–82.
- Stampfli G.M. & Kozur H. 2006: Europe from the Variscan to the Alpine cycles. In: Gee D.G. & Stephenson R.A. (Eds.), *European Lithosphere Dynamics. Geol. Soc. (London) Mem.* 32, 57–82.
- Thöni M. & Miller C. 2009: The “Permian event” in the Eastern European Alps: Sm–Nd and P–T data recorded by multi-stage garnet from the Plankogel unit. *Chem. Geol.* 260, 20–36.
- Vogt K., Willingshofer E., Matenco L., Sokoutis D., Gerya T. & Cloetingh S. 2018: The role of lateral strength contrasts in orogenesis: A 2D numerical study. *Tectonophysics* 746, 549–561.
- Zulauf G., Dörr W., Marko L. & Krahl J. 2018: The late Eo-Cimmerian evolution of the external Hellenides: constraints from microfabrics and U–Pb detrital zircon ages of Upper Triassic (meta)sediments (Crete, Greece). *Int. J. Earth Sci.* 107, 2859–2894.

# The Western Carpathians — record of 180 Myr lasting orogenic progradation and its drivers

DUŠAN PLAŠIENKA

Department of Geology and Palaeontology, Faculty of Natural Sciences, Comenius University in Bratislava, Mlynská dolina, Ilkovičova 6, 842 15 Bratislava, Slovakia; dusan.plasienka@uniba.sk

**Abstract:** The Meso–Cenozoic Western Carpathian orogenic wedge nucleated by development of the Meliatic–Turnaic accretionary complex in the course of subduction and suturing of the Tethys-related Meliata Ocean during the Middle–Late Jurassic. This Tethyan orogenic cycle passed gradually into the Cretaceous Austroalpine cycle with stacking of the Central Carpathian basement and cover nappe systems, whereby shortening was driven by the subcrustal subduction of the lower Austroalpine lithosphere pulled by the downgoing Meliatic slab. The subsequent Pennine cycle (Senonian–Eocene) generated the forward propagating accretionary wedge of the Pieniny Klippen and Flysch belts by subduction of the two branches of Pennine oceans and intervening Oravic continental fragment. The ongoing Oligocene–Neogene convergence was related to NE-ward extrusion of the Western Carpathian domain from the Alpine collision enhanced by the subduction retreat of the remnant oceanic lithosphere in the Carpathian embayment.

## Introduction

Traditionally, the Alpidic orogenic processes in the Eastern Alps and Western Carpathians have been attributed to two principal periods — the Eo-Alpine (Palaeo-Alpine, pre-Gosauian; mid-Cretaceous) and the (Neo-)Alpine (Senonian–Neogene). Several authors distinguished also the intermediate Meso-Alpine stage (Senonian–Eocene). However, this classification reflects the time constraints of the main tectonic events only and does not take into account the driving geodynamic processes. Moreover, it disregards the Late Jurassic to Early Cretaceous compressional orogenic processes that have been thoroughly documented in both the Eastern Alps and Western Carpathians during the last two decades. Hereafter, a conceptual categorization of the Alpidic tectonic evolution into the Tethyan, Austroalpine and Pennine cycles is proposed to account for the long-term convergence triggered by elimination of two major oceanic zones. Some controversies of the palaeotectonic models are briefly discussed, too.

## Tethyan cycle

The Tethyan (or Neotethyan) cycle embraces orogenic shortening processes connected with the elimination of the Tethys-related Meliata Ocean from the onset of its subduction ca 180 Ma ago up to the final collision of its former continental margins around the Jurassic/Cretaceous boundary (ca. 145 Ma). However, the

character and position of these margins remain among the most controversial issues of the Western Carpathian geology. According to the generally accepted palaeogeographical model, the Triassic Tethyan shelves and slopes showed a uniform facies zonation of the continent/ocean transition from the Dinarides–Hellenides, through Southern and Northern Calcareous Alps and Transdanubia up to the Western Carpathians and Tisia (e.g. Haas et al. 1995; Mandl 2000). This facies symmetry is verified also by the structural position of the previous facies zones in the resulting post-collision or post-obduction thrust stacks — ophiolitic mélanges on top, continental rise and slope below (Meliata and Hallstatt facies), and the carbonate outer and inner shelf facies (like the Wetterstein and Dachstein carbonate platforms) in the lowermost position (e.g., Missoni & Gawlick 2011). This scheme seems to be valid everywhere — except of the Western Carpathians, where this tectonic succession is upside down (Silicic carbonate platforms on top, Turnaic slope facies below and the Meliatic oceanic rocks underneath). Possible solutions of this discrepancy are fairly speculative — such as the wedging-in model of Meliatic complexes between the continental margin units proposed by Schmid et al. (2008), or the collisional suture concept of Plašienka (2018). According to the latter view, the close lithological relations of the Upper Paleozoic rocks of the Meliatic blueschist-facies Bôrka Nappe to the underlying Gemeric complexes of the same age (e.g., Vozárová et al. 2019) reveal an involvement of the distal passive Gemeric (Bôrka) continental margin into the subduction

process of the Meliata Ocean, hence the overlying Meliatic–Turnaic accretionary complexes should have represented the upper plate of the convergence system, i.e. the Jurassic active margin (Plašienka et al. 2019). In consequence, could all the structurally higher units (Silica–Aggtelek, Turňa–Torna, Bükk, or even the Transdanubian; collectively known also as the Pelso block — Fig. 1 represent “the other side of the Meliata Ocean”? This question is presently far from an answer consistent with all the controversial data.

The present knowledge about the composition, structure and tectonic evolution of all units that are structurally higher than the highest Austroalpine unit Gemicum was recently reviewed in detail by Plašienka (2018). These uppermost Carpathian units were united as the Internal Western Carpathian (IWC) tectonic system distinguished by several first-order characteristics: (i) Anisian (Pelsonian) rifting and breakup of the carbonate shelf and ensuing spreading of the Meliata Ocean; (ii) early Late Jurassic closing of the Neotethys-related oceanic domains, including the Meliata Ocean. However, modes of this closing seem to have been different along-strike the Neotethyan Belt (term coined by Missoni & Gawlick 2011). Intraoceanic subduction followed by obduction and prograding thrust stacking with sequential development of the late Middle–early Late Jurassic synorogenic basins in the lower (Austroalpine, Adriatic–Dinaridic) plate position was reconstructed e.g., for the Northern Calcareous Alps (NCA; Frisch &

Gawlick 2003; Missoni & Gawlick 2011), whereas the Wilsonian-type collision with development of the upper-plate Meliatic–Turnaic (+Silicic?) Jurassic accretionary wedge composed of pre- and synorogenic complexes is inferred for the Western Carpathians (Plašienka et al. 2019).

Considering the Tethyan relationships of the Meliata Ocean, in view of its opening and closure, tectonostratigraphic data and evolutionary trends, the IWC can be referred to as the Tethyan Carpathians (as a part of the Neotethyan Belt), too (Plašienka 2017). Thus all the Meliatic and structurally higher units would represent the Tethyan tectonic system of the Western Carpathians (Fig. 1). The corresponding tectonic processes comply with a closed Wilson-type orogenic cycle, so the term Tethyan cycle is suggested for this time period.

### Austroalpine cycle

The Central Western Carpathians (CWC) between the inferred Meliatic suture and the Pieniny Klippen Belt (PKB; Fig. 1) represent the eastern segment of the Cretaceous Austroalpine (AA) thrust system (e.g., Frotzheim et al. 2008; Schmid et al. 2008), thus the alias name Austroalpine Carpathians may be used as a synonym to the CWC. Unlike NCA, where the structures of the Neotethyan Belt were sealed by the carbonate platform from the Kimmeridgian onward and the

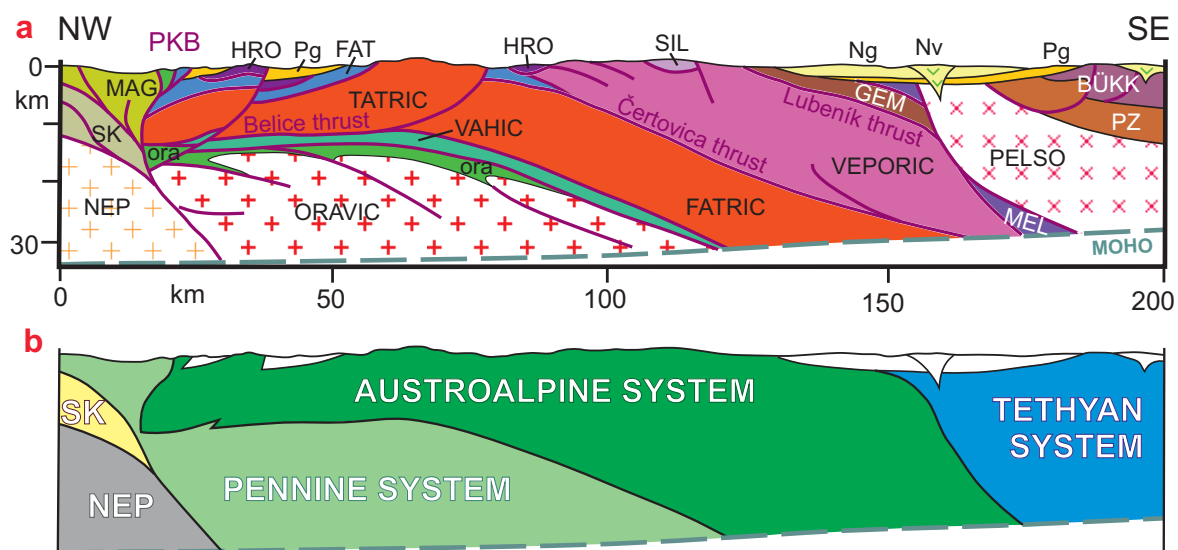


**Fig. 1.** A conceptual cross-section through the Western Carpathians. **a:** NEP — North European Platform; SK — Silesian–Krosno units of the EWC; MAG — Magura Superunit; ora — Oravic cover rocks; HRO — Hronic nappe system; SIL — Silicic nappes; GEM — Gemic Superunit; PZ — IWC Paleozoic complexes; Pg — Paleogene overstepping sediments; Ng — Neogene deposits; Nv — Neogene volcanics. **b:** outline of the major Carpathian tectonic systems.

thrust system became inactive for a longer time (Missoni & Gawlick 2011), the continuous, though episodic northward thrust propagation is documented in the CWC (Plašienka 2018 and references therein). Firstly, the Meliatic Bôrka Nappe overrode the Gemericum during the earliest Cretaceous, then the Gemeric basement-cover sheet was thrust over the Veporicum (130–120 Ma). Afterwards, shortening relocated to a wide basinal zone between the present northern Veporic and southern Tatric margins, from where the Fatric cover nappe system was detached and thrust over the Tatric foreland by 90 Ma. Frontal Fatric elements glided beyond the outer Tatric margin and overrode the Vahic oceanic domain. Finally, the Pennine realm was seized by the contractional tectonics by transformation of the northern AA (Tatric) boundary from the passive to the active margin and subduction of the South Pennine Piemont–Váh Ocean from the 90 Ma onward.

The Carpathian AA thick-skinned thrust sheets Tatric, Veporic and Gemeric are about 10–20 km thick (Fig. 1), which means that their lower crustal portions must have been subducted into the mantle. Supposedly, this subcrustal subduction was triggered by the pull force of the descending Meliatic oceanic slab still attached to the lower AA plate (Plašienka 2018; see also Handy et al. 2010). This mechanism could explain the problem of the driving force for the Cretaceous Austroalpine orogeny. During the Early Cretaceous, the IWC units were affected by widespread backthrusting to form a transient retro-wedge that developed contemporaneously with the expanding CWC pro-wedge.

However, among others there is one important, but still unresolved problem with the CWC nappe structure. The highest thin-skinned Hronic and Silicic cover nappe systems do not respect the thrusting polarity, they were emplaced late in the structural development of the area and overlie various, in part exhumed and deeply eroded CWC units with a pronounced structural and metamorphic discordance at their base — but probably still in the latest Cretaceous. Their palaeogeographic provenance and emplacement directions are therefore questionable.

### Pennine cycle

In the author's view, the Western Carpathian Penninic units include the Magura and Biele Karpaty superunits of the External Carpathian Flysch Belt (connected with the Alpine Lower Penninic Valaisan and Rhenodanubian units), the PKB Oravic units (Middle Penninic) and the problematic and ambiguously interpreted Belice Unit of

the Vahic (Upper Penninic) affiliation (Pennine system in Fig. 1). The latter unit was likely derived from an oceanic domain identified with the South Pennine Piemont–Váh Ocean (Plašienka 2012), which originated by the Middle Jurassic breakup and was eliminated by subduction under the outer AA margin. Subduction terminated by collision of the AA nappe stack in a backstop position with the Oravic continental ribbon by the end of Cretaceous. Subsequently, the Carpathian orogenic wedge annexed the Oravic and Biele Karpaty domains during the Paleocene–Middle Eocene and after that also the Magura realm in the Oligocene.

Interpretation of the structural and sedimentary development of the PKB units plays a crucial role in the tectonic models of the entire Western Carpathians. The PKB involves a heterogeneous group of units. The Oravic units (PKB proper) are composed of Jurassic to Eocene sedimentary successions that were sequentially detached from a narrow continental domain in the Middle Pennine position (Czorsztyn Ridge). It collided with the CWC wedge after subduction of the South Pennine Piemont–Váh Ocean during the latest Cretaceous, whereby the outermost CWC nappe units (like the Manín and Klape; cf. Plašienka 2019 and references therein) were partly incorporated into the PKB structure. Senonian through Eocene processes of incorporation of the PKB units into the growing Carpathian orogenic wedge were accompanied by linked synorogenic sedimentation in the wedge-top (Gosau-type) and in the foredeep trench-type basins in the Oravic units (Plašienka & Soták 2015).

Summing up, the Pennine cycle was governed by subduction of the Pennine (Alpine Atlantic) oceanic zones initiated some 90 Ma ago. In the Alps, subduction culminated by collision of the AA–Penninic thrust stack with the foreland European plate by approximately 35 Ma, but the convergence continued by additional shortening and mountain building due to the northward Adria push. The 35 Ma would be also the upper time limit of the Pennine cycle.

The Western Carpathian domain escaped this collision by its eastward extrusion, which was enhanced by the subduction retreat of the remnant Magura oceanic basin and probably also of the oceanic and/or transitional crust of the Silesian–Krosno basins connected with the Moldavian domains eastwards (Kováč et al. 2016, 2017 and references therein). Convergence continued until the Late Miocene in the NE part of the Carpathians and as late as to the sub-recent times in the Eastern Carpathians. However, the Oligocene–Neogene time period would represent a new orogenic cycle subsequent

to the Pennine cycle, which has lasted from 35 Ma till present.

## Conclusions

The Western Carpathians is a long-living convergent orogenic system that was driven by different geodynamic mechanisms in several cycles: (i) the Tethyan cycle (180–145 Ma) was governed by lithospheric subduction of the Tethys-related Meliata Ocean; (ii) the Austroalpine cycle (145–90 Ma) created a collisional stack of thick- and thin-skinned CWC units by subcrustal subduction of the lower AA lithosphere attached to the sinking Meliata slab; (iii) the Pennine cycle (90–35 Ma) was jointly driven by subduction of Pennine oceans and the northward push of the Adriatic microcontinent with accreted AA units; (iv) the terminal cycle (35–0 Ma) concerns the outermost Carpathian zones thrust over the European passive margin.

**Acknowledgements.** Financial support from the Slovak Research and Development Agency (project APVV-17-0170) is gratefully appreciated.

## References

- Frisch W. & Gawlick H.-J. 2003: The nappe structure of the Northern Calcareous Alps and its disintegration during Miocene tectonic extrusion – a contribution to understanding the orogenic evolution of the Eastern Alps. *Internat. J. Earth Sci.* 92, 712–727.
- Froitzheim N., Plašienka D. & Schuster R. 2008: Alpine tectonics of the Alps and Western Carpathians. In: McCann T. (ed.): *The Geology of Central Europe. Volume 2: Mesozoic and Cenozoic. Geol. Soc. Publ. House London*, 1141–1232.
- Haas J., Kovács S., Krystyn L. & Lein R. 1995: Significance of Late Permian-Triassic facies zones in terrane reconstruction in the Alpine-Nord Pannonian domain. *Tectonophysics* 242, 19–40.
- Handy M.R., Schmid S.M., Bousquet R., Kissling E. & Bernoulli D. 2010: Reconciling plate-tectonic reconstructions of Alpine Tethys with the geological–geophysical record of spreading and subduction in the Alps. *Earth-Sci. Rev.* 102, 121–158.
- Kováč M., Plašienka D., Soták J., Vojtko R., Oszczytko N., Less Gy., Čosović V., Fügenschuh B. & Králiková S. 2016: Paleogene palaeogeography and basin evolution of the Western Carpathians, Northern Pannonian domain and adjoining areas. *Global Planet. Change*, 140, 9–27.
- Kováč M., Márton E., Oszczytko N., Vojtko R., Hók J., Králiková S., Plašienka D., Klučiar T., Hudáčková N. & Oszczytko-Clowes M., 2017: Neogene palaeogeography and basin evolution of the Western Carpathians, Northern Pannonian domain and adjoining areas. *Global Planet. Change*, 155, 133–154.
- Mandl G.W. 2000: The Alpine sector of the Tethyan shelf – Examples of Triassic to Jurassic sedimentation and deformation from the Northern Calcareous Alps. *Mitt. Österr. Geol. Ges.* 92 (1999), 61–77.
- Missoni S. & Gawlick H.-J. 2011: Evidence for Jurassic subduction from the Northern Calcareous Alps (Berchtesgaden Alps; Austroalpine, Germany). *Internat. J. Earth Sci.* 100, 1605–1631.
- Plašienka D. 2012: Jurassic syn-rift and Cretaceous syn-orogenic, coarse-grained deposits related to opening and closure of the Vahic (South Penninic) Ocean in the Western Carpathians – an overview. *Geol. Quart.* 56, 601–628.
- Plašienka D. 2017: Tethyan, Austroalpine and Pennine Western Carpathians – how do they relate? EGU Series – Émile Argand Conf., 13<sup>th</sup> Workshop Alpine Geol. Stud., Sept. 7–18 2017, Zlatibor Mts, Serbia, Abstr. Vol., p. 83.
- Plašienka D. 2018: Continuity and episodicity in the early Alpine tectonic evolution of the Western Carpathians: How large-scale processes are expressed by the orogenic architecture and rock record data. *Tectonics* 37, 2029–2079.
- Plašienka D. 2019: Linkage of the Manín and Klape units with the Pieniny Klippen Belt and Central Western Carpathians: balancing the ambiguity. *Geol. Carpath.* 70, 35–61.
- Plašienka D. & Soták J. 2015: Evolution of Late Cretaceous–Palaeogene synorogenic basins in the Pieniny Klippen Belt and adjacent zones (Western Carpathians, Slovakia): tectonic controls over a growing orogenic wedge. *Ann. Soc. Geol. Polon.* 85, 43–76.
- Plašienka D., Méres Š., Ivan P., Sýkora M., Soták J., Lačný A., Aubrecht R., Bellová S. & Potočný T. 2019: Meliatic blueschists and their detritus in Cretaceous sediments: New data constraining tectonic evolution of the West Carpathians. *Swiss J. Geosci.* 112, 55–81.
- Schmid S.M., Bernoulli D., Fügenschuh B., Matenco L., Schefer S., Schuster R., Tischler M. & Ustaszewski K. 2008: The Alpine-Carpathian-Dinaridic orogenic system: correlation and evolution of tectonic units. *Swiss J. Geosci.* 101, 139–183.
- Vozárová A., Rodionov N., Šarinová K., Lepekhina E., Vozár J. & Paderin I. 2019: Detrital zircon U–Pb geochronology of Pennsylvanian–Permian sandstones from the Turnaicum and Meliaticum (Western Carpathians, Slovakia): provenance and tectonic implications. *Internat. J. Earth Sci.* <https://doi.org/10.1007/s00531-019-01733-7>

# Neogene exhumation and denudation of the Central Western Carpathian nappe units in the Danube Basin

TAMÁS CSIBRI, MICHAL KOVÁČ and SAMUEL RYBÁR

Department of Geology and Paleontology, Faculty of Natural Sciences, Comenius University in Bratislava, Mlynská dolina, Ilkovičova 6, 842 15 Bratislava, Slovakia; [tamas.csibri@gmail.com](mailto:tamas.csibri@gmail.com)

**Abstract:** The Blatné Depression located in the NW part of the Danube Basin represents the northernmost sub-basins of the Pannonian Basin System. Its subsidence is associated with oblique collision of the Central Western Carpathians with the European platform, followed by the back-arc basin rifting stage in the Pannonian domain. The Cífer conglomerate Fm. documents the latest Burdigalian–early Langhian deposition in fan delta lobes situated above the footwall and hanging wall of a WSW–ENE trending fault system. The activity of this fault preceded the opening of the late Langhian–Serravallian accommodation space with a NE–SW direction. During the thermal subsidence of the synrift stadium, the main direction of the extension was NW–SE. The imbrication of the Doľany conglomerates is oriented in the SE direction, towards the basin depocenter. The provenance of conglomerates points to the Central Western Carpathian source, especially when similar rocks occurs today in the Malé Karpaty Mts.

## Introduction

The Danube Basin, located at the junction of the Eastern Alps, Western Carpathians and Transdanubian Range represents the NW part of the Pannonian Basin System. It is bordered by the Malé Karpaty Mts. in NW and by the Považský Inovec Mts. in the NE and passes into the Gabčíkovo–Győr Depression in the south (Fig. 1).

The basin fill consists of marine to freshwater deposits reaching up to 3 000 m (Adam & Dłabač 1969). The main part of the basin fill is represented by the middle Miocene marine deposits of the Central Paratethys Sea, which are overlain by sequences of the late Miocene Lake Pannon, and by the late Miocene to Pliocene alluvial to fluvial sediments (e.g., Kováč et al. 2011). The primarily fine-grained sedimentary fill is intercalated with sandy to gravely facies, often at the base of Transgression–Regression (T–R) cycles (e.g., Kováč 2000).

The aim of this work is to revise the conglomerates from the Blatné depression (Danube Basin) in respect to their age, petrography and provenance. The definition of transport mechanisms and the character of depositional paleoenvironment will be derived from facies analysis, well-logs study, and seismic facies interpretation. The acquired knowledge should contribute to confirmations of the geodynamic development model of the area at the Eastern Alpine–Western Carpathian junction during the rifting phase of the Danube Basin (Kováč et

al. 2018). It should also contribute to paleogeographic models before and during the maximal flooding of the Central Paratethys Sea in the back-arc basin system (e.g. Kováč et al. 2017a).

## Material and methods

During the research, well cores (Cífer-2, Vištuk-1, Suchá nad Parnou-3, Trakovice-1, Ratkovce-1 and Bučany-2) and also outcrops were studied (Fig. 1). The well core samples were obtained from the repository of Nafta a.s. — Oil and Gas Company (Gbely town). The clast composition was confirmed by thin sections studied under a polarizing microscope. Abbreviations of minerals follow Whitney and Evans (2010). Grain size classification of clast follows Wentworth (1922) and the shape classification of clast follows Powers (1953). The sedimentary structures of the individual well cores and outcrops were evaluated in sense of Boggs (2006) and Nichols (2009). The conglomerates classification follows the work of Pettijohn (1975). Carbonate classification follows the work of Flügel (2010).

One reflection seismic line (554/77) was used for the purposes of seismic facies analysis. Interpretation was made in the Schlumberger Petrel software using the standard methods described by Mitchum & Vail (1977). The well logs data were evaluated based on Rider & Kennedy (2011).

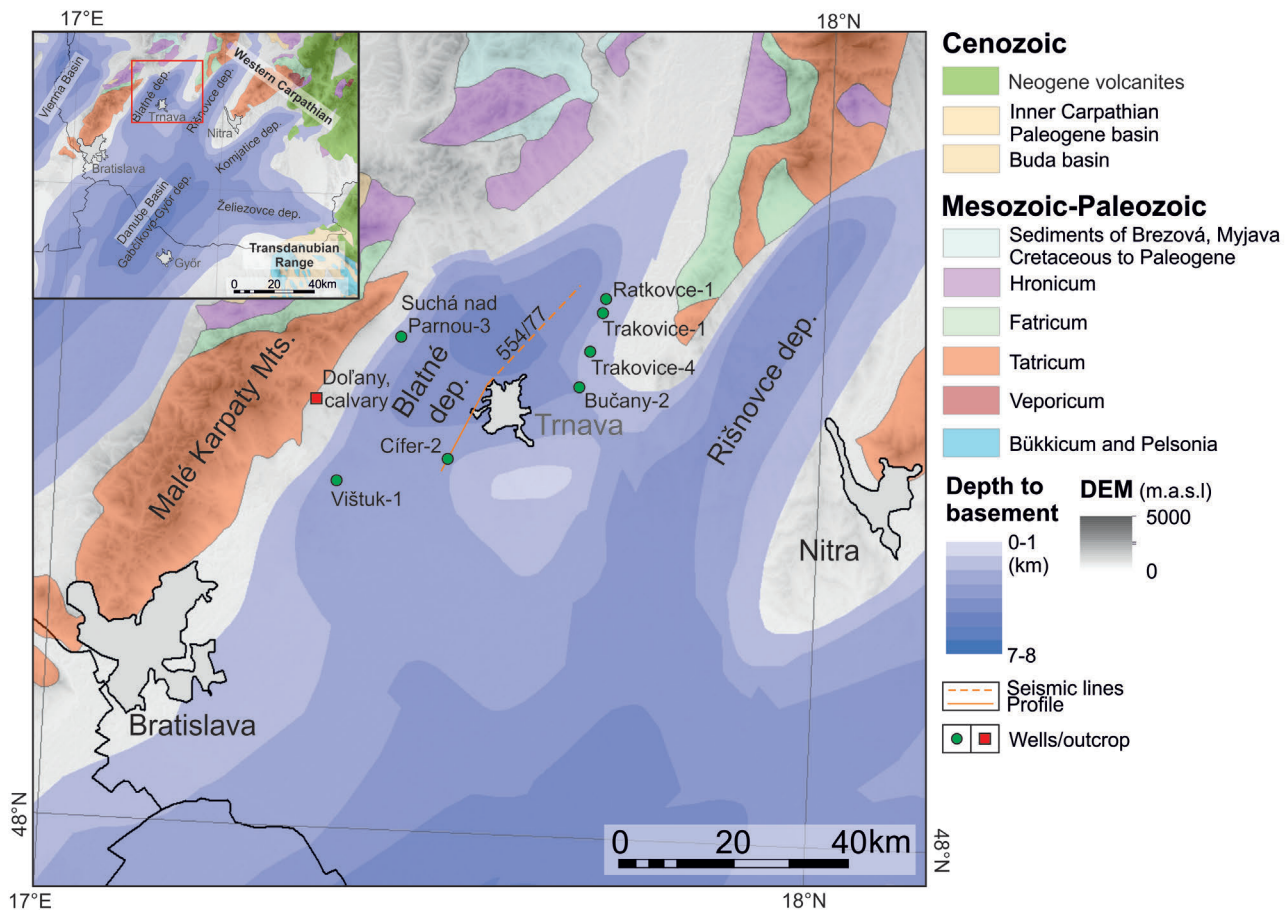


Fig. 1. Localization of the studied wells and outcrop in the Danube Basin.

### Coarse-grained sediments of the Blatné depression

In the Blatné depression are two types of conglomerates, different in age and petrographical composition.

#### *The Cifer conglomerate Formation (Karpatian/Lower Badenian)*

The Cifer conglomerate Formation is named after the well Cifer-2, where the stratotype section was described by Csibri et al. (2018). The base of the formation is created by older, resedimented blocks of monomict conglomerates and breccias (Paleogene?). These coarse-grained sediments consists clasts only from the Pre-Cenozoic crystalline basement of the Danube Basin. The monomict blocks are overlapped by clast supported polymict orthoconglomerates with sparitic matrix. In the clast composition, the carbonate rocks dominates. The deposition area was linked in to the proximal part of the fan delta. The overlying

conglomerate strata is separated by 40 meter thick siltstone layer. These conglomerates have higher portion of the granitoid clasts. They have higher proportions of matrix, even they are matrix supported. Therefore, the depositional environment is linked in to the distal part of fan delta. The fan delta character of both aforementioned conglomerate layer can be backed up by the sigmoid clinoform visible on the seismic line 554/77 (Csibri et al. 2018).

As a part of the Cifer conglomerate Formation are interpreted the conglomerates from the wells Suchá nad Parnou-3, Trakovice-1, Ratkovce-1 and Bučany-2.

#### *Provenance of the “Cifer conglomerates”*

The provenance of all processed conglomerates points to the Central Western Carpathian source. The source of granitoids can be associated with biotitic granodiorites exposed in the Modra Massif of the Malé Karpaty Mts. The metamorphic rocks (chloritic–sericitic schists, graphitic schists and biotitic paragneisses) are exposed in

the upper part of the crystalline complexes of the Pezinok Group in the Malé Karpaty Mts. The Lower Triassic is represented by quartz arenites, which source may be in the Lúžna Fm. which represents the sedimentary cover of the Tatric Unit. Similarly, the dark carbonates may belong to the Gutenstein Fm. (Middle Triassic). The wells, oriented in the northern part of the Blatné depression consist also sericitic fylites and chloritic schists derived from the Infratatric Orešany Unit. The source of the crinoidal limestone (Middle Jurassic) may be in the Vilská Fm. of the Vysoká nappe (Fatric Unit). From the Hronic Unit were derived the paleo-basalt of Malužiná Fm. (Permian) and oolitic limestones of Dachstein Fm. (Upper Triassic).

### *The Dol'any conglomerates (Špačince Fm., Lower Badenian)*

The Dol'any conglomerates are named after the village Dol'any, which is situated nearby the Malé Karpaty Mts. The type section is situated in the calvary of Saint Lenhard. It overlies the pre-Neogene basement discordantly and transgressively. The thickness of these conglomerates reached several tens meters and is spread only in the eastern margin of the Malé Karpaty Mts. The outcrop conditions of the Dol'any conglomerate are poor. During the field research, only fragments of clasts from the conglomerates was found. The only one outcrop is situated on the type locality.

The Dol'any conglomerates consists from two part. The lower part is represented by fine to medium-grained breccias with calcareous–sandy matrix. The composition of the clast is nearly monomict. The carbonate rocks (crinoidal limestones and grey, spotted limestones) represents the 94 % of the composition, the rest is created by metamorphic rocks (fylites and chloritic schists) and quartz arenites. The upper part continuous by coarse-grained polymict conglomerates. The clasts are well rounded and moderately sorted. The gradation is inverted and the conglomerates are imbricated (35° to the SE). The matrix is calcareous sand. The composition is still similar, but the portion of carbonates are lower.

Similar conglomerates according to the position were found in the well Vištuk-1. The base of the well is created by well sorted polymict medium-grained conglomerates with calcareous matrix. The composition in this case is different. The main lithological elements are the metamorphic rocks (chloritic schists, fylites and biotitic paragneisses). Minor clasts of granitoids and carbonates were observed.

### *Provenance of the Dol'any conglomerates*

The source of the individual clasts is explicitly local — from eastern part of the Malé Karpaty Mts. The source of the metamorphic rocks (chloritic schists and fylites) is in the Orešany Unit, with the exception of the biotitic paragneisse. The Biotitic paragneisses were derived from the crystalline complexes of the Pezinok Group. The quartz arenites may belong to the Lúžna Fm. The source of the carbonatic rocks may be in the Fatric Unit — the Lower Jurassic grey, spotted limestones (“fleckenmergel” Allgäu Fm.) and the Middle Jurassic crinoidic limestones (Vilské Fm.).

### **Tectonic context**

The sedimentation of the coarse clastic facies is generally influenced by tectonic activity (Vail et al. 1977). From the paleogeographical point of view, the accommodation space of the “Cífer conglomerate” was connected with the early Miocene WSW–ENE oriented fault system, active until the earliest-middle Miocene (Marko et al. 1991; Marko & Kováč 1996; Hók et al. 2016;). This process in a transtensional/extensional tectonic regime, associated with the lateral extrusion of the ALCAPA lithosphere eastward (Ratschbacher et al. 1991), which led to the opening of new depocenters situated between the Eastern Alps and Western Carpathians (e.g., lower Miocene terrestrial to marine deposits of the Styrian, Eisenstadt and Danube basins; Kováč et al. 2003). The Danube Basin pre-Cenozoic basement is built up in its central part by crystalline complexes of the Tatric Super-unit (Fusán et al. 1987). Gradual Oligocene–early Miocene uplift of these complexes is documented in the Malé Karpaty Mts. by AFT (Apatite Fission Track) cooling ages ~52 to 20 Ma (Králiková et al. 2016). The initial rifting at the western border of the Pannonian domain led to development of horsts and grabens within the pre-Cenozoic basement (Hók et al. 2016). This may have led to erosion and deposition of coarse clastics on the southern margin of the Middle Miocene Blatné depression in the form of the “Cífer conglomerate” during the synrift phase of the Danube Basin (Kováč et al. 2011; Rybár et al. 2016). The transport direction can be deduced from dip of the clinofolds, which seems to be prograding from S-SW to N-NE. This is in accordance with the above presented results of the provenance analyses. Later, in the middle–late Langhian, the accommodation space was enlarged (Kováč et al. 1999). The opening of

the Blatné Depression in its present form was a result of the oblique collision of the Central Western Carpathians, with a spur of the Bohemian Massif, representing the margin of the European platform (e.g., Hók et al. 2016; Kováč et al. 2017b). During the thermal subsidence of the synrift stadium, the main direction of the extension was NW–SE. The imbrication of the Doľany conglomerates are bending to the SE direction, towards to the basin depocenter.

**Acknowledgements:** Our appreciation goes to Nafta a.s. — Oil and Gas Company management for allowing access to their well core repositories. This work was supported by APVV agency under the contract No. APVV-16-0121, APVV-15-0575, APVV-14-0118 and by UK Grant 9/2018.

## References

- Adam Z. & Dlabáč M. 1969: Erklärungen zur Mächtigkeitkarte und zur lithofaziellen Entwicklung der Donau-Niederung. *Západné Karpaty* 11, 156–171.
- Boggs S. 2006: Principles of sedimentology and stratigraphy. *Upper Saddle River*, New Jersey, 1–655.
- Csibri T., Rybár S., Šarinová K., Jamrich M., Sliva L. & Kováč M. 2018: Miocene fan delta conglomerates in the north-western part of the Danube Basin: provenance, paleoenvironment, paleotransport and depositional mechanisms. *Geol. Carpath.* 69, 5, 467–482.
- Hók J., Kováč M., Pelech O., Pešková I., Vojtko R. & Králiková S. 2016: The Alpine tectonic evolution of the Danube Basin and its northern periphery (southwestern Slovakia). *Geol. Carpath.* 67, 5, 495–505.
- Kováč M. 2000: Geodynamic, paleogeographic and structural evolution of the Carpathian-Pannonian region in Miocene — A new view on the Neogene basins of Slovakia. *Veda*, Bratislava, 1–204 (in Slovak).
- Kováč M., Holcová K. & Nagymarosy A. 1999: Paleogeography, paleobathymetry and relative sea-level changes in the Danube Basin and adjacent areas. *Geol. Carpath.* 50, 4, 325–338.
- Kováč M., Grigorovič A.A., Brzobohatý R., Fodor L., Harzhauser M., Oszczytko N., Pavelič D., Rögl F., Saftič B., Sliva L. & Stráňák Z. 2003: Karpatian Paleogeography, Tectonics and Eustatic Changes. In: *The Karpatian — a Lower Miocene Stage of the Central Paratethys*. Masaryk University, Brno, 49–72.
- Kováč M., Synak R., Fordinál K., Joniak P., Tóth C., Vojtko R., Nagy A., Baráth I., Maglay J. & Minár J. 2011: Late Miocene and Pliocene history of the Danube Basin: inferred from development of depositional systems and timing of sedimentary facies changes. *Geol. Carpath.* 62, 6, 519–534.
- Kováč M., Márton E., Oszczytko N., Vojtko R., Hók J., Králiková S., Plašienka D., Klučiar T., Hudáčková N. & Oszczytko-Clowes M. 2017a: Neogene palaeogeography and basin evolution on of the Western Carpathians, Northern Pannonian domain and adjoining areas. *Global Planet. Change* 155, 133–154.
- Kováč M., Hudáčková N., Halásová E., Kováčová M., Holcová K., Oszczytko-Clowes M., Báldi K., Less Gy., Nagymarosy A., Ruman A., Klučiar T. & Jamrich M. 2017b: The Central Paratethys palaeoceanography: a water circulation model based on microfossil proxies, climate, and changes of depositional environment. *Acta Geologica Slovaca* 9, 2, 75–114.
- Kováč M., Halásová E., Hudáčková N., Holcová K., Hyžný M., Jamrich M. & Ruman A. 2018: Towards better correlation of the Central Paratethys regional time scale with the standard geological time scale of the Miocene Epoch. *Geol. Carpath.* 69, 3, 283–300.
- Králiková S., Vojtko R., Hók J., Fügenschuh B. & Kováč M. 2016: Low-temperature constraints on the Alpine thermal evolution of the Western Carpathian basement rock complexes. *J. Struct. Geol.* 91, 144–160.
- Marko F. & Kováč M. 1996: Reconstruction of the Miocene tectonic evolution of the Vadovce depression based on the analysis of structural and sedimentary record. *Mineralia Slovaca* 28, 81–91.
- Marko F., Fodor L. & Kováč M. 1991: Miocene strike-slip faulting and block rotation in Brezovské Karpaty Mts. (Western Carpathians). *Mineralia Slovaca*, 23, 3, 89–200.
- Mitchum R.M. Jr. & Vail P.R. 1977: Seismic stratigraphy and global changes of sea-level. Part 6: Stratigraphic interpretation of seismic reflection patterns in depositional sequences: In: Payton C.E. (Ed.): *Seismic Stratigraphy — Applications to Hydrocarbon Exploration*. American Association of Petroleum Geologists, *Memoir* 26, 135–144.
- Nichols G. 2009: *Sedimentology and Stratigraphy*. Blackwell Science Ltd., London, 1–335.
- Pettijohn F.J. 1975: *Sedimentary rocks*. Third edition. Harper & Row, New York, 1–628.
- Powers M.C. 1953: A new roundness scale for sedimentary particles. *J. Sediment. Petrol.* 23, 117–119.
- Rider M.H. & Kennedy M. 2011: *The geological interpretation of well logs*. 3<sup>rd</sup> Revised edition. Rider-French Consulting Limited, 1–440.
- Rybár S., Kováč M., Šarinová K., Halásová E., Hudáčková N., Šujan M., Kováčová M., Ruman A. & Klučiar T. 2016: Neogene changes in palaeogeography, palaeoenvironment and the provenance of sediment in the Northern Danube Basin. *Bull. Geosci.* 91, 2, 367–398.
- Vail P.E., Mitchum R.M. Jr. & Thompson S. III. 1977: Relative changes of sea level from coastal onlap. In: Payton C.E. (Ed.): *Seismic Stratigraphy: Applications to Hydrocarbon Exploration*. American Association of Petroleum Geologists, *Memoir* 26, 63–82.
- Wentworth Ch.K. 1922: A Scale of Grade and Class Terms for Clastic Sediments. *J. Geol.* 30, 5, 377–392.
- Whitney D.L. & Evans B.W. 2010: Abbreviations for names of rock-forming minerals. *Am. Mineral.* 95, 185–187.

# Lithology and tectonic structure of the HP/LT metamorphosed composite Bôrka Nappe: An important clue to the Meliata Ocean geological history

PETER IVAN<sup>1</sup>, ŠTEFAN MĚRES<sup>1</sup> and DUŠAN PLAŠIENKA<sup>2</sup>

<sup>1</sup>Comenius University, Faculty of Sciences, Department of Geochemistry, Ilkovičova 6, 842 15 Bratislava, Slovakia; peter.ivan@uniba.sk; stefan.meres@uniba.sk

<sup>2</sup>Comenius University, Faculty of Sciences, Department of Geology and Palaeontology, Ilkovičova 6, 842 15 Bratislava, Slovakia; dusan.plasienka@uniba.sk

**Abstract:** The composite Bôrka Nappe (Meliatic Superunit) is built up by a stack of partial nappes representing the lithotectonic formations of oceanic and continental affinity which underwent of the HP/LT subduction zone metamorphism but differ in metamorphic paths. Oceanic formations of the Mesozoic age are formed by sedimentary mélanges containing mostly igneous and sedimentary rocks of the intraoceanic suprasubduction origin, in lesser amount only basalts and deep-sea sediments of the ocean floor. Mélanges were originated as components of an accretionary prism during Late Jurassic subduction of the Meliata Ocean slab. Volcano-sedimentary formations of the continental provenance are the Early Palaeozoic and Permian in age and were involved in the subduction zone in the final collisional stage of the Meliata Ocean closing.

## Introduction

Although most geologists are familiar with the idea, that the HP/LT metamorphosed rock complexes are former components of oceanic plates involved in subduction zones, the reality could be quite different and variable rocks complexes including those of the continental provenance can be present there. The aim of this work is to introduce a new scheme of lithological division of the HP/LT metamorphosed composite Bôrka Nappe and to decode the complex geological history of individual lithotectonic units connected with the final stages of evolution of the Mesozoic Meliata Ocean basin.

## Geological background

Eu-alpine orogeny in the Western Carpathians is supposed to be related to the closing and further tectonic history of the Triassic–Jurassic Meliata Ocean. Relics of rocks complexes directly related to this ocean are preserved in inner Western Carpathians southward of the Lubeník–Margecany line and are denoted as the Meliatic Superunit. The composite Bôrka Nappe is a one of sub-units of the Meliatic Superunit and it is positioned between the Palaeozoic volcano-sedimentary units of the Gemeric Superunit (the Gelnica and Gočaltovo Groups) and carbonate complexes of the Triassic Silica Superunit. Unlike other part of the Meliatic Superunit, the Bôrka

Nappe is built up exclusively by HP/LT metamorphosed rocks of a wide age interval from the Early Palaeozoic to Mesozoic (Mello et al. 1998; Faryad & Frank 2011). The Bôrka Nappe is a nappe stack composed of several partial nappes (or slices) where every nappe is represented by the individual lithostratigraphic (lithotectonic) formation. Tectonic structure seems to be a product of several nappe-forming events finally modified during the Upper Cretaceous.

## Lithotectonic division of the Bôrka Nappe

Our proposal of a new scheme of lithotectonic units composing of the Bôrka Nappe is improved and modified version of the older preliminary concept developed by Ivan (2007). Based on the present-day state of knowledge six following lithotectonic formations can be discerned in the Bôrka Nappe: (1) Nižná Slaná Fm., (2) Jasov Fm., (3) Bučina Fm., (4) Hačava Fm., (5) Kobeliarovo Fm., and (6) Steinberg Fm. Up to now still remain questionable definition of further (7) Rudník Fm. due to paucity of necessary data. According to their age, these formations can be classified into three groups: (1) Early Palaeozoic units (Nižná Slaná and Rudník Fms.), (2) Permian units (Jasov and Bučina Fms.) and Mesozoic units (Hačava, Kobeliarovo and Steinberg Fms.). Only Mesozoic units are directly related to the oceanic environment and contain rocks originated as components of an oceanic basement, whereas

the Paleozoic formations display continental provenance. More or less preserved original stratigraphy is typical for continental units unlike formations of oceanic origin representing sedimentary ophiolite mélanges. All discerned units experienced HP/LT metamorphic alteration but they display marked differences in the metamorphic paths.

## Lithotectonic units in the Bôrka Nappe

### *Hačava Formation*

Hačava Fm. is a HP/LT metamorphosed sedimentary ophiolite mélange containing blocks of ophiolitic and also non-ophiolitic rocks various in size (typically first metres or first tens metres) embedded in matrix composed of mostly pelitic, rarely also psammitic clastic sediments metamorphosed as a whole in the blueschist facies conditions. Ophiolitic rocks are represented by metabasalts and metadolerites, less frequently also by strongly serpentized ultramafics and rare metagabbros. Metamorphosed black or red deep-sea silicic sediments are present as well. Group of non-ophiolitic rocks forms blocks of white or grey marbles, rarely metamorphosed marls. Some of basalts are directly connected with marbles originally extruding in the lime mud, whereas other ones are closely associated with deep-sea sediments. Matrix of mélange is composed of by the redeposited mostly basic volcanic material transformed to banded blueschists or sericite, chlorite-sericite and quartz-albite phyllites. Blueschist facies mineral association in mafic rocks reflects only progressive metamorphic path. Magmatic clinopyroxene is sometime preserved, while Na-pyroxene, Na-amphibole, (glaucophane), epidote, garnet, white mica, albite, chloritoid, titanite, magnetite/haematite or pyrite are newly-formed phases. Pumpellyite, actinolite and chlorite can be present as relics of previous low-grade metamorphic alteration. Zonal Na-amphiboles, Na-pyroxene, spessartite, tremolite iron oxides and apatite in fine-grained quartz are typical for metacherts. Local retrogression connected with transformation paragonite to white mica can be observed in phyllites from matrix (Plašienka et al. 2019). Serpentized ultramafics with typical mesh texture are composed mostly lizardite and chryzotile with less amount of magnetite, accessory crystals of brown chromian spinel, Mg-chlorite and rare Na-amphibole. At some places also primary pyroxenes and olivine have been found. Age of the Hačava Fm. is still unknown, its upper limit 150–160 Ma (Late Jurassic) follows from the

age of HP/LT metamorphism (Faryad & Henjes-Kunst 1997; Dallmeyer et al. 2008).

### *Kobeliarovo Formation*

Geological structure of the Kobeliarovo Fm. is similar to the Hačava Group — it is also ophiolite mélange but with blocks of marbles, metabasalts and metadolerites only. Also matrix of mélange is similar — sericite and chlorite-sericite phyllites combined with metamorphosed redeposited basic volcanic material. Some of metabasalts erupted directly in the unconsolidated carbonate environment. Most pronounced difference is the complete areal retrogression to the greenschist facies conditions. Albite, epidote, Na-actinolite and chlorite together with some carbonate, white mica and very conspicuous magnetite octahedrons up to 1 mm in size are typical mineral association here. Teeny relics of magnesioriebeckite are important witness of the former HP/LT metamorphic event. Exact data of age of this formation are still missing.

### *Steinberg Formation*

Steinberg Fm. is located in the immediate neighbourhood of the Dobšiná town. Previously it was mapped as part of various Palaeozoic units of the Gemic Superunit. Steinberg Fm. is represented by ophiolite mélange with blocks of metabasalts with relatively well-preserved original magmatic textures occurring in association with red deep-sea metacherts and metamorphosed sediments composed of disintegrated basaltic material. Blocks are embedded in the matrix built up by the dark sericite-albite-quartz phyllites or sericite phyllites. The mélange as a whole was metamorphosed in the blueschist facies and retrogressed to the greenschist facies conditions. Typical mineral association in the metabasalts is represented by albite, Na-actinolite, chlorite, epidote, leucogenized ilmenite, rarely also white mica is present. Presence of magnetite octahedrons (up to 1 mm) is a good attribute for identification of these rocks. Relics of glaucophane and winchite as indications of the HP/LT metamorphic stage are relatively frequently preserved. Quartz, Fe-oxides, chlorite, Na-actinolite, epidote and white mica are more widespread mineral components of the metamorphosed cherts and related mafic sediments, but also relic riebeckite, ferroglaucophane and Na-Ca pyroxene have been identified. Data on age of the Steinberg Fm. are fully missing, but based on close lithological similarity to the Jaklovce Group of the Meliatic Superunit it can be

speculate about Late Triassic age for ophiolite blocks and Middle Jurassic age for matrix sediments.

### ***Nižná Slaná Formation***

Despite its relative spatial extension the Nižná Slaná Fm. has not yet been recognized and was mapped as the Hačava Fm. The Nižná Slaná Fm. is the polymetamorphosed volcano-sedimentary complex with locally preserved original stratification, but mylonitized and tectonized in some parts. Metamorphosed basaltic volcanoclastic rocks locally intercalated by various types of pelitic sediments including those rich in organic matter are most widespread here. Bodies of metamorphosed basalts, dolerites and gabbros are also components of this formation. The Nižná Slaná Fm. underwent a multi-stage metamorphic alteration with the oldest stage in the epidote-amphibolite facies conditions. Association of magnesiohornblende, plagioclase, clinozoisite/epidote, Mg-chlorite, white mica, garnet (in sediments) and typically rutile sometime rimmed by ilmenite are characteristic for this stage. Overprint in the blueschist facies conditions is connected with formation of glaucophane, winchite, jadeite, garnet and titanite, clinozoisite is transformed to epidote. Local retrogression to greenschist facies conditions led to final association of Na-actinolite, albite, and chlorite together with white mica, carbonate and some titanite. Age of the Nižná Slaná Fm. is not exactly known, its upper limit is age of the oldest metamorphic phase (ca. 370 Ma, Late Devonian). Age of HP/LT metamorphic overprint seems to be the same like in the Hačava Fm. (Faryad & Frank 2011).

### ***Jasov Formation***

Volcano-sedimentary Jasov Fm. is composed dominantly by metamorphosed psammitic sediments with small lenses of metaconglomerates in the lower part of formation. Metasiltstones and metapelites occur mostly in its upper part (Mello et al. 1998). Small bodies or thin layers of metamorphosed rhyolites and their volcanoclastics sporadically occur the lower part of rock complex. Quartz and plagioclase (albite) phenocrysts are preserved in metarhyolites, typical mineral association for acid volcanic is quartz, muscovite and sometime albite. The same minerals associated with paragonite, chlorite and chloritoid can be observed in metamorphosed sediments. The Permian age of the Jasov Fm. was determined by U-Pb SHRIMP dating on zircons from metarhyolites (266±1.8 Ma Guadalupian; Vozárová et al. 2012).

### ***Bučina Formation***

Complex of metamorphosed acid volcanics and volcanoclastic rocks with lesser admixture of clastic components was denoted as Bučina Fm. (Mello et al. 1998). Original granularities of sediments vary from fine-grained pelitic sediments up to conglomerates with pebbles several cm in size. Clasts in conglomerates are represented exclusively by quartz and lesser amount of felsic volcanics. Widespread hydrothermal silicification and turmalinization is typical in all rock types of this formation. Quartz and white mica are highly prevailing mineral components here. The Permian age for the Bučina Fm. is supposed based on lithological similarity with the surrounding Permian units as Jasov Fm. or Gočaltovo Fm. in the Gemic Superunit.

### ***Rudník Formation***

Rudník Fm. is recently defined only conditionally based on two isolated findings of high-grade metamorphic rocks (amphibolites, amphibolite gneisses) overprinted in HP/LT metamorphic conditions (cf. Faryad 1988). Cover of younger geological formations disables to assess extent and details of geological position of these rocks. Analogues to these rocks occur in the Klátov Group (Gemic Superunit) of the Early Palaeozoic age.

## **Plate tectonic setting of volcanic rocks in the Bôrka Nappe lithotectonic units**

Close relations of the HP/LT metamorphosed Mesozoic mafic volcanic rocks of the Bôrka Nappe to subduction of the Meliata Ocean are generally accepted (e.g. Mello et al. 1998; Plašienka et al. 2019). However geochemical studies of these rocks surprisingly indicate that only metabasalts of the Steinberg Fm. associated with deep-sea sediments display signature close to typical oceanic N-MORB or back-arc basalts. Metabasalts of the Hačava Fm. erupting in the carbonate or marl environment display similarity to arc basalts (island arc tholeiites — IAT or calc-alkaline basalts — CAB) whereas metabasalts associated with radiolarian chert and pelitic sediment have strongly depleted N-MORB signature usually related to forearc settings. Blocks of metagabbro show surprisingly E-MORB affinity. Trace element distribution in metabasalt from the Kobeliarovo Fm. indicates also similarity to IAT.

In the Early Paleozoic Nižná Slaná Fm. two types of metabasalts have been identified: one type is geochemically similar to E-MORB, but the second type with trace element distribution pointing to the subduction related CAB is dominantly present. In the Permian formations mafic volcanics have not been found, but composition of metarhyolite from the Jasov Fm. indicates its calc–alkaline affinity (Vozárová et al. 2012).

### Lithology of the Bôrka Nappe and geological history of the Meliata Ocean

The composite Bôrka Nappe represents specific segment of the Meliatic Superunit which experienced as a whole HP/LT metamorphism in the subduction zone and so records specific information concerning of late stages of the Meliata Ocean evolution. The Bôrka Nappe consists of strongly imbricated partial nappes or slices, each formed by specific lithotectonic units differing not only in lithologies and tectonic settings, but also in paths of their metamorphic alteration and exhumation. Two groups of lithotectonic units can be discerned according to their position in the former Meliata Ocean basin: (1) Mesozoic units (Hačava, Kobeliarovo and Steinberg Fms.) more or less related to the basin floor and (2) Palaeozoic units representing continental margin of this basin. All oceanic units are metamorphosed sedimentary ophiolite mélanges formed during Late Jurassic subduction of the Triassic–Jurassic Meliata Ocean and consists of blocks of various igneous and sedimentary rocks embedded in the former trench sediments. It is noteworthy that the Steinberg Fm. only contains blocks of metabasalts and metamorphosed deep-sea cherts and pelitic sediments geochemically and lithologically reminding of relics of a typical ocean floor. Blocks of marbles originally probably representing platform limestones together with arc-related metabasalts frequently with evidence of eruption in the shallow carbonate environment dominate in the Hačava and Kobeliarovo Fms. and might point to a suprasubduction setting of the intraoceanic arc or forearc. Existence of such setting is supported also by findings of the ultradepleted oceanic metabasalts in the Hačava Fm. generated by repeated melting of the depleted oceanic mantle source during forearc or backarc extension (cf. Hickey-Vargas et al. 2018). It can be speculated that presence of light non-oceanic rocks (marbles) and/or larger thickness of crust are the cause of preserving and exhumation just

this parts of the subducting Meliata Ocean crust. The Palaeozoic Nižná Slaná, Jasov and Bučina Fms. generated in continental settings display many similarities in lithology and type of volcanism with some parts of the Gelnica or Gočaltovo Groups — their analogues in age from the Gemic Superunit. Based on this fact it could be supposed that the Meliata Ocean was opened inside lithospheric plate with geological structure remind in principle of the present-day Gemic Superunit. It cannot be excluded, that this opening developed in parallel direction with the Variscan oceanic suture which relicts has been identified on the northern margin of the Gemic Superunit (Ivan & Méres 2012).

**Acknowledgements:** this research was supported by the VEGA grant 1/0085/17.

### References

- Dallmeyer R.D., Neubauer F. & Fritz H. 2008: The Meliata suture in the Carpathians: regional significance and implications for the evolution of high-pressure wedges within collisional orogens. In: Siegesmund S., Fügenschuh B. & Froitzheim N. (Eds.): Tectonic aspects of the Alpine-Dinaride-Carpathian system. London, *Geol. Soc. Spec. Publ.* 298, 101–115.
- Faryad S.W. 1988: Glaucophanized amphibolites and gneisses near Rudník (Slovenské rudohorie Mts.). *Geol. Zbor. Geol. Carpath.* 39, 747–763.
- Faryad S.W. & Frank W. 2011: Textural and age relations of polymetamorphic rocks in the HP Meliata Unit (Western Carpathians). *J. Asian Earth Sci.* 42, 111–122.
- Hickey-Vargas R., Yogodzinski G., Ishizuka O., McCarthy A., Bizimis M., Kusano Y., Savov I.P. & Arculus R. 2018: Origin of depleted basalts during subduction initiation and early development of the Izu-Bonin-Mariana island arc: Evidence from IODP expedition 351 site U1438, Amami-Sankaku basin. *Geochim. Cosmochim. Acta* 229, 85–111.
- Ivan P. 2007: Lithostratigraphic units of the Bôrka Nappe: brief characteristic and possible genesis. In: L. Jurkovič (Ed.): Gechemistry in the present-day Earth sciences. Cambel's days, 2007. Bratislava, *Comenius University*, 42–48 (in Slovak).
- Ivan P. & Méres Š. 2012: The Zlatník Group — Variscan ophiolites on the northern border of the Gemic Superunit (Western Carpathians). *Mineralia Slov.* 44, 39–56
- Mello J., Reichwalder P. & Vozárová A. 1998: Bôrka Nappe: high-pressure relic from the subduction-accretion prism of the Meliata ocean (Inner Western Carpathians, Slovakia). *Slovak Geol. Mag.* 4, 261–273.
- Plašienka D., Méres S., Ivan P., Sýkora M., Soták J., Lačný A., Aubrecht R., Bellová S. & Potočný T. 2019: Meliatic blueschists and their detritus in Cretaceous sediments: new data constraining tectonic evolution of the West Carpathians. *Swiss J. Geosci.* 112, 55–81.
- Vozárová A., Šmelko M., Paderin I. & Larionov A. 2012: Permian volcanics in the Northern Gemicum and Bôrka Nappe system: U–Pb zircon dating and implications for geodynamic evolution (Western Carpathians, Slovakia). *Geol. Carpath.* 63, 191–200.

# A new era of the paleomagnetic research in the pre-Cenozoic of the Central Western Carpathians: Concepts, first results and ongoing studies

EMŐ MÁRTON<sup>1</sup>, DUŠAN PLAŠIENKA<sup>2</sup>, JOZEF MADZIN<sup>3</sup>, JACEK GRABOWSKI<sup>4</sup>,  
JANA BUČOVÁ<sup>3,5</sup>, ROMAN AUBRECHT<sup>2,3</sup> and MARIÁN PUTIŠ<sup>6</sup>

<sup>1</sup>Mining and Geological Survey of Hungary, Paleomagnetic Laboratory, Columbus 17-23, H-1145 Budapest, Hungary; paleo@mbfsz.gov.hu

<sup>2</sup>Comenius University, Faculty of Natural Sciences, Department of Geology and Paleontology, Ilkovičova 6, 842 15 Bratislava, Slovakia; dusan.plasienka@uniba.sk

<sup>3</sup>Slovak Academy of Sciences, Earth Science Institute, Ďumbierska 1, 974 11, Banská Bystrica, Slovakia; jozef.madzin@savba.sk

<sup>4</sup>Polish Geological Institute — National Research Institute, Paleomagnetic Laboratory, Rakowiecka 4, 00-975 Warsaw, Poland; jgra@pgi.gov.pl

<sup>5</sup>DPP Žilina Ltd, Legionárska 8203, 010 01 Žilina, Slovakia; jana.bucova@gmail.com

<sup>6</sup>Comenius University, Faculty of Natural Sciences, Department of Mineralogy and Petrology, Ilkovičova 6, 842 15 Bratislava, Slovakia; marian.putis@uniba.sk

**Abstract:** As a result of the critical revision of pre-Cenozoic paleomagnetic data from the Central Western Carpathians a team of Slovak, Hungarian and Polish researchers agreed to start systematic paleomagnetic investigations of the three nappe systems of this area. The new studies would improve the previous ones by using up-to date field, laboratory and statistical methods, as well as focus on formations which are widespread in the respective nappe units. The research started in the Hronic Unit, which is the topmost one, therefore less exposed to re-heating than the Fatric or Tatric nappe stacks. The so far obtained results suggest that during the Permian, the Hronicum was in near equatorial position in the northern hemisphere and at some distance from the European continent. Concerning the studied Triassic carbonates we conclude that they were remagnetized during the Late Cretaceous, basically before or in early stage of the deformation and transportation of the nappe unit. The Hronicum must have rotated about 35° in the CW sense after the Permian during a so far non-constrained period. A second, even larger (about 95°, taking into account the 60°CCW rotation measured on the Central Carpathian Paleogene flysch) general CW rotation can be connected to the closing of the Penninic Ocean. The ongoing studies in the Hronicum would aim at testing the oroclinal bending model by obtaining a robust data set for the area W of the Nízke Tatry Mts, on one hand, and start the systematic research on the Fatricum and Tatricum.

## Introduction

In a review paper Márton et al. (2015) compiled a paleomagnetic data base for the Western Carpathians. The tabulated data for the Central Western Carpathians were published between the 1970s and 2010 and are of very different quality. The typical problems, mostly handicapping the older results are:

- The often poor documentation (e.g. for the studied localities neither the local tectonic positions nor the paleomagnetic directions before tectonic corrections have been published). Thus the acquisition of the remanence in relation to the geological age of the rock cannot be checked.
- Sometimes oriented hand samples were collected in the field from which several specimens were drilled in the laboratory. This method does not guarantee that the best material is sampled. Moreover, it introduces a systematic error in the orientation of the cores by transferring the nearly always present uncertainty of the orientation of a hand sample.

- Incomplete laboratory analysis of the natural remanent magnetizations (this aspect will be explained in the next chapter)
- “Spotlike” distribution of the paleomagnetic data, in time and even more in geographical sense.

## The concepts of the “new era”

Of the nappe systems of the Central Western Carpathians, the uppermost one, and least affected by re-heating during nappe stacking (therefore most likely to preserve original magnetization) is the Hronic Unit. For this reason, a team of Slovak, Hungarian and Polish researchers decided to start the systematic study on the two most widespread age groups of the Hronicum, the Permian red beds and igneous rocks and the Triassic carbonates. The deeper buried rocks of the Fatricum and Tatricum would be subjects of the next stage of our study.

It was also agreed that the field and laboratory methods of the paleomagnetic processing should be harmonized.

Concerning field methods, the samples should be drilled and oriented in situ in all cases with magnetic compass. In special conditions, like strong susceptibility and/or remanence of some igneous rocks, in the vicinity of high power lines or in outcrops protected by metal nets, orientation with sun compass is also necessary. It goes without saying that the sampled object should be devoid of any sign of recent or ancient slumping.

In the laboratory, the remanent magnetization (NRM) in natural state as well as the anisotropy of magnetic susceptibility (AMS) is measured before the laboratory analysis of the paleomagnetic signal. Some specimens (the number of them depends on the degree of uniformity of the NRM), from each outcrop are demagnetized in several steps with alternating field or with thermal method, till the NRM signal is lost. Referring to item 3 of the previous chapter, this is very important, since the NRM can be composite (e.g. a primary magnetization can be overprinted during regional or local heating as well as by geological processes in an uplifted position). During thermal demagnetization, the magnetic susceptibility is monitored in order to follow possible changes in magnetic mineralogy, as heating can produce a new magnetic phase either with lower (e.g. magnetite or maghemite converted to hematite) or higher (e.g. pyrite converted to magnetite) susceptibilities. The magnetic mineral(s) originally present in the rock must be identified with magnetic methods, like Curie-point measurement or the thermal demagnetization of laboratory induced remanence.

As a result of demagnetization and re-measurement of the remaining NRM after each step so called demagnetization curves are produced, which can be analyzed for linear segments. Sometimes the NRM is single component, more often it is composite (Fig. 1). In the latter case, it is usual, that the component which is more resistant to

the respective demagnetization method is interpreted as the more ancient. Based on the experiments with the selected pilot specimens, the rest of the collection from the same group is demagnetized with either AF or thermal method.

The paleomagnetic direction for each locality is computed from the more resistant (or the only) magnetic component using standard statistical methods in two co-ordinate systems. One is the geographical, i.e. before tectonic correction, the other is the paleogeographical i.e., after tectonic correction. In case of geological objects, which are monoclinally tilted, typical of the outcrops suitable for paleomagnetic study in the Hronicum, decision about the pre- or post-deformation age of the remanence is made on an assemblage of localities, which are geographically distributed and are of similar ages.

It was also agreed on that in the case of the nappe systems of the Central Western Carpathians the sampling localities should be distributed as much as possible in E–W directions, so that the model of oroclinal bending can be tested.

## Summary of the results so far obtained for the Hronic Unit

### *Permian red beds and volcanic rocks*

Both types of rocks were studied from the Nízke Tatry Mts. (18 localities/sites, Fig. 2C) and only lava flows from the Malé Karpaty Mts. (four sites, Fig. 2B). Except one locality of the red beds, all the studied rocks had reversed polarity magnetizations. The majority is characterized by shallow inclinations, suggesting near-equatorial position in the northern hemisphere of the Hronicum during the Permian ( $8.2^\circ$ ) and suggesting a net rotation (summary of the rotations taking place after the Permian) of about  $70^\circ$  in the CW sense. Rocks collected from the area of the Malužiná valley have steeper inclinations (corresponding to a paleolatitude of  $23.3^\circ$ , similar to the expected Late Triassic latitude for a position between Europe and Africa) and about  $35^\circ$  of CW net rotation, after the acquisition of the paleomagnetic signal.

### *Anisian–Norian carbonates*

Of the 14 localities studied one is from the Strážovské vrchy Mts., the rest from the Nízke Tatry Mts. (Fig. 2A). They have magnetizations of pre-deformation age.

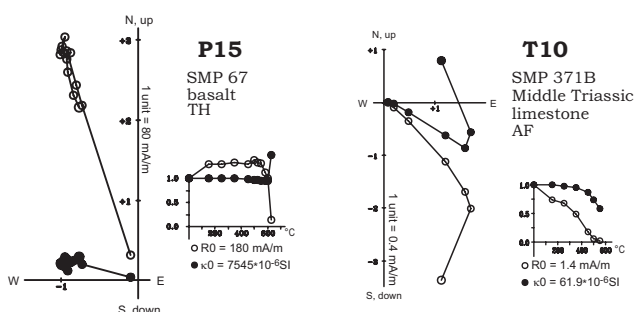


**Fig. 1.** Examples of a single component (P15) and a composite (T10) magnetization, respectively. Both specimens were thermally demagnetized in several steps, till the NRM (hollow circles on the right-side diagrams) was destroyed, while the susceptibility monitored (full circles on the right-side diagrams).

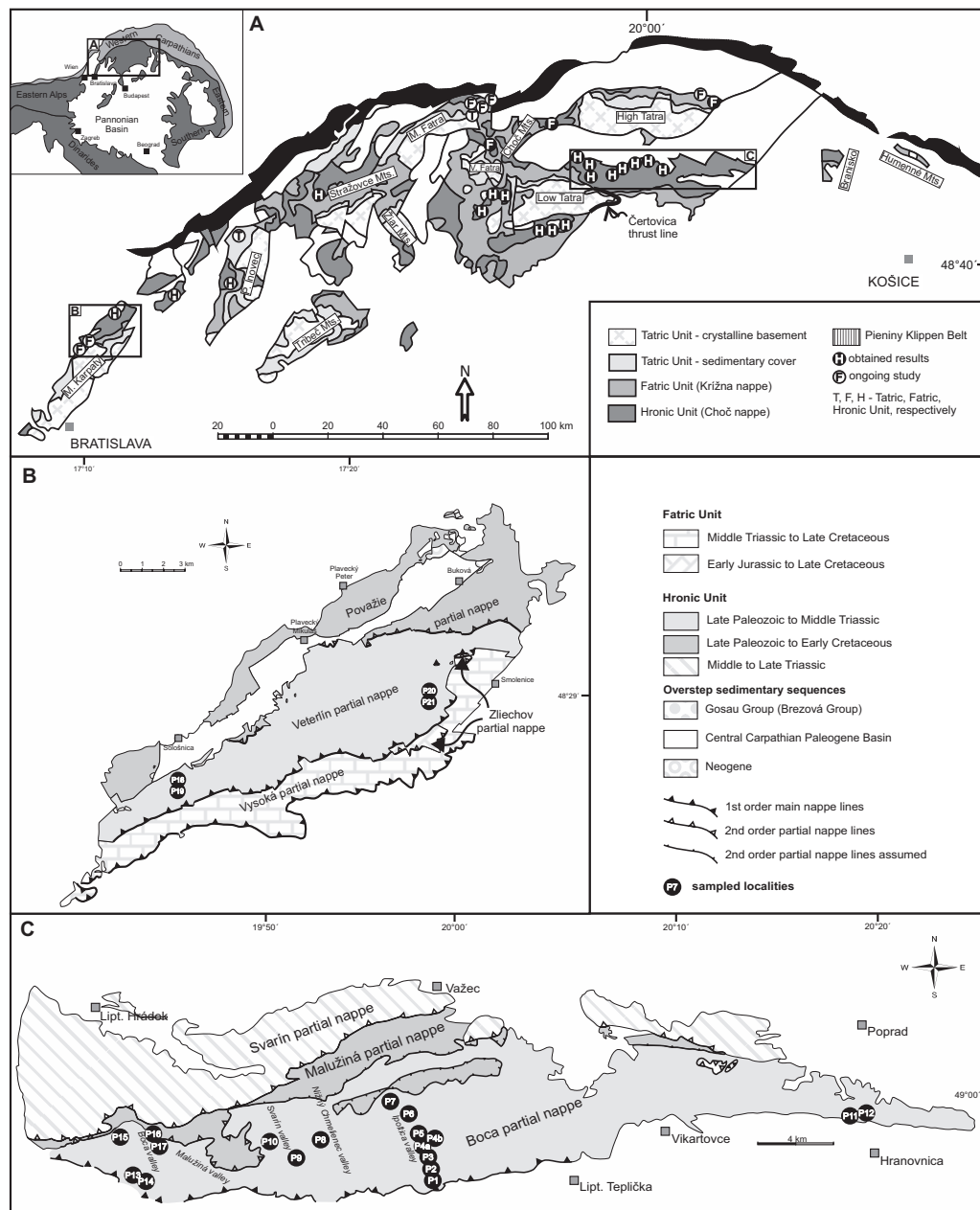


**Fig. 2.** Position of the studied area. **A** — Tectonic sketch map of the Central Western Carpathians with the position of the Mesozoic paleomagnetic localities. **B** — Simplified geological map of the northern part of the Malé Karpaty Mts. with the position of the Permian paleomagnetic localities. **C** — Simplified geological map of the northern part of the Nízke Tatry Mts. with the position of the Permian paleomagnetic localities.

However, the magnetizations are not interpreted as of Triassic age. The reason is that during the Triassic the polarity changes were frequent, while all the studied localities have normal polarity magnetizations and the inclinations are expected to show a trend towards steeper values during the Triassic, which is not the case in the studied material. Based on these features, we interpret the paleomagnetic signal as of Late Cretaceous age, acquired just before or during early phases of deformation and thrusting of the Hronicum above the deeper

nappe units at a latitude of  $34.7^\circ$ . The post-Turonian net rotation suggested is  $35^\circ$  CW. The conclusions support previous estimations of Grabowski (2000) that Hronic units in the Tatra Mts were remagnetized during Late Cretaceous thrusting.

### General implications

The above observations suggest that the Hronic Unit was at a considerable distance from stable Europe during

the Permian and close to it during the Late Cretaceous. While the estimated paleolatitudes are not influenced by later displacements, the observed declinations must be interpreted in the context of the post-Paleogene, about 60° CCW rotation of the Central Western Carpathians (Márton et al. 1999, 2009). Thus, the net rotation observed on the Triassic means about 95° of CW rotation after the Turonian, probably connected to the closing of the Penninic Ocean. In addition, a CW rotation of about 35° must have affected the Hronicum after the Permian. The age of this rotation is an open question, since there is no constraint on the acquisition of the paleomagnetic signal in the rocks of the Malužiná area, which exhibit exactly the same net rotation as the Triassic rocks, with most probably Cretaceous (pre-Turonian) remanence.

Reflecting to the possible oroclinal bending of the Hronicum, there seems to be no evidence for such tectonic process in the data we so far obtained.

### Work in progress

We have already collected oriented cores from several additional localities of the Mesozoic of the Hronicum, focusing on the area W of the Nízke Tatry Mts. (Fig. 2A).

At the same time, we sampled mostly Triassic sediments from deeper nappe systems (Fig. 2A), in order to gain information about the supposedly different “paleomagnetic history” of the respective systems.

**Acknowledgements:** This study was supported by the projects APVV-0212-12, APVV-17-0170, VEGA 2/0028/17 and NKFI K128625.

### References

- Grabowski J. 2000: Palaeo- and rock magnetism of Mesozoic carbonate rocks in the Sub-Tatric series (Central West Carpathians) — palaeotectonic implications. *Polish Geological Institute, Special Papers* 5, 1–88.
- Márton E., Grabowski J., Tokarski A.K. & Túnyi I. 2016: Palaeomagnetic results from the fold and thrust belt of the Western Carpathians: an overview. In: Pueyo E.L., Cifelli F., Sussman A.J. & Oliva-Urcia, B. (Eds.): *Palaeomagnetism in Fold and Thrust Belts: New Perspectives. Geological Society, London, Special Publications* 425, 7–36.
- Márton E., Mastella L. & Tokarski A.K. 1999: Large counter-clockwise rotation of the Inner West Carpathian Paleogene Flysch – evidence from paleomagnetic investigation of the Podhale Flysch (Poland). *Physics and Chemistry of the Earth* A24, 645–649.
- Márton E., Jeleńska M., Tokarski A.K., Soták J., Kováč M. & Spišiak J. 2009: Current-independent paleomagnetic declinations in flysch basins: a case study from the Inner Carpathians. *Geodinamica Acta* 22, 73–82.

# The Wechsel Gneiss Complex of Eastern Alps: A Cambrian continental arc and its Early Proterozoic hinterland

FRANZ NEUBAUER<sup>1</sup>, YONGJIANG LIU<sup>2,3</sup>, SIHUA YUAN<sup>1,4</sup>, SHENGYAO YU<sup>2,3</sup>, JOHANN GENSER<sup>1</sup>, BORAN LIU<sup>1</sup> and QINGBIN GUAN<sup>2,3</sup>

<sup>1</sup> Paris-Lodron-University of Salzburg, Department of Geography and Geology, Geology Division, Hellbrunnerstraße 34, 5020 Salzburg, Austria; franz.neubauer@sbg.ac.at; johann.genser@sbg.ac.at; sihua.yuan@sbg.ac.at; boran.liu@stud.sbg.ac.at

<sup>2</sup> Key Lab of Submarine Geoscience and Prospecting Techniques, MOE, Institute for Advanced Ocean Study, College of Marine Geosciences, Ocean University of China, Qingdao 266100, China; liuyongjiang@ouc.edu.cn; yushengyao@ouc.edu.cn; 642598908@qq.com; 1901386894@qq.com; 664106296@qq.com

<sup>3</sup> Laboratory for Marine Mineral Resources, Qingdao National Laboratory for Marine Science and Technology, Qingdao 266237, China

<sup>4</sup> College of Earth Science, Institute of Disaster Prevention, Sanhe, 065201, Hebei Province, China

**Abstract:** The Lower Austroalpine Wechsel Gneiss and Wechsel Phyllite units are known to have been overprinted by Devonian and Late Cretaceous metamorphism within greenschist facies conditions. For the first time, new U–Pb zircon reveal evidence for two stages of continental arc-like magmatism at 500–520 Ma and 550–570 Ma. We speculate on potential relationships of the continental arc-type magmatism and potential oceanic lithosphere (Speik complex) of Proto-Tethyan affinity, which is also preserved in the Austroalpine nappe complex. Abundant, nearly uniform 2.1 Ga-age signature of detrital zircons in metasediments (paragneiss, quartzite) calls for Lower Proterozoic continental crust in the nearby source showing the close relationship to northern Gondwana prominent in West Africa and Amazonia.

## Introduction

As known since a long time, the Austroalpine nappe complex of Eastern Alps and Western Carpathians contains two major basement units, which collided during the Variscan orogeny (e.g., Neubauer & Frisch 1993). These include (1) a nearly unmetamorphic Gondwana-derived fossil-rich unit, which represents an Ordovician back-arc unit and a Devonian passive margin (Neubauer & Sassi 1993); and (2) an amphibolite-grade metamorphic unit, which was fully affected by Variscan amphibolite-grade metamorphism including Devonian, early Variscan high-pressure metamorphism, and which is considered representing, in major portions, a poorly dated magmatic arc system with intermediary and acidic orthogneisses. Among these, the Lower Austroalpine Wechsel Gneiss unit of the Wechsel window shows Devonian pressure-dominated metamorphism in upper greenschist (Müller et al. 1999).

## Regional geological setting

The basement within the Wechsel window comprises three units from base to top (Fig. 1): (1) the Monotonous Wechsel Gneiss unit, (2) the Variegated Wechsel Gneiss Unit, and (3) the Wechsel Phyllite unit. In the field, albite porphyroblasts represent the most pronounced

feature of both Monotonous and Variegated Wechsel Gneiss units (Neubauer & Frisch 1993). The nature of the boundary between Wechsel Gneiss Units and Wechsel Phyllite Unit, tectonic or primary, remains unclear. In the variegated and Monotonous Wechsel Gneiss Units, Müller et al. (1999) found evidence for a Devonian high-pressure dominated metamorphism

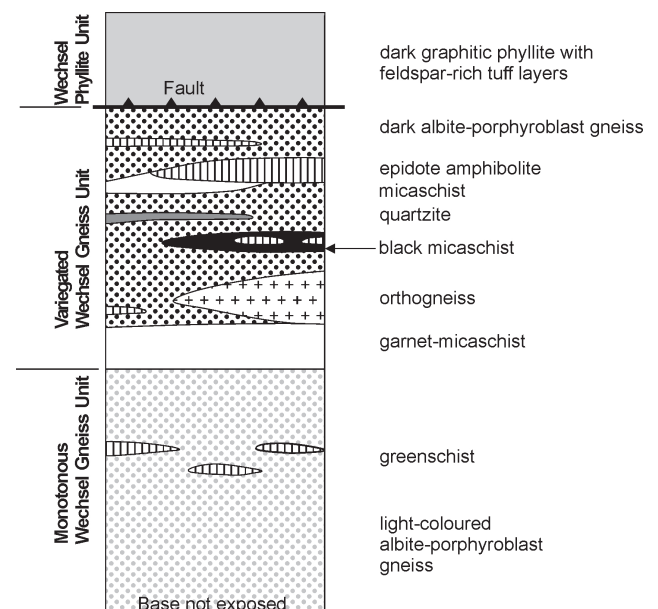


**Fig. 1.** Lithostratigraphic section of basement units within the Wechsel window, For explanation, see text.

and a low-grade (<350 °C) metamorphic overprint (70–80 Ma), the latter directly related to Early Alpidic nappe stacking of the deep structural level contemporaneous with Gosau basin at top of the Upper Austroalpine within the Austroalpine nappe complex.

## Results

### *Protolith ages of the Variegated Wechsel Gneiss Complex*

The Variegated Wechsel Gneiss Unit contains magmatic rocks (hornblende-gneiss, greenschist, acidic orthogneiss) with U–Pb zircon ages between 500 and 523 Ma. In paragneisses and quartzite, the detritus is dominated by several age groups that include euhedral zircons of ca. 490–500 Ma, 550 Ma and detrital components of ca. 1.9–3.2 Ga, with a pronounced maximum of ca. 2.1 Ga. In one samples only, the detritus is dominated by Devonian–Carboniferous ages (380–300 Ma) and its significance remains unclear.

### *Protolith ages of the Wechsel Phyllite Unit*

The Wechsel Phyllite Unit includes feldspar-rich tuffs, which gives latest Neoproterozoic ages (e.g.,  $556.5 \pm 2.3$  Ma and  $556.5 \pm 9.7$  Ma), whereas other samples bear a significant detrital component with dominant age populations of 450–550 Ma and 2.5–2.9 Ma

## Discussion

In consequence, the new age data gives evidence for two stages of continental arc-like magmatism at 500–520 Ma and 550–570 Ma. We speculate on potential

relationships of the continental arc-type magmatism and potential oceanic lithosphere (Speik complex) of Proto-Tethyan affinity, which is also preserved in the Austroalpine nappe complex (Neubauer 2002 and references therein). We argue, therefore, for long-lasing Late Neoproterozoic to Cambrian subduction of potentially Proto-Tethyan origin along margins of Gondwana.

The abundant, nearly uniform 2.1 Ga-age signatures calls for Lower Proterozoic continental crust in the nearby source showing the close relationship to northern Gondwana prominent in West Africa and Amazonia (Stephan et al. 2018).

**Acknowledgements:** The analytical work is supported by grant no. 91755212 of the NSF of China and Qingdao Leading innovation talents (no. 19-3-2-19-zhc) to Y. Liu.

## References

- Müller W., Dallmeyer R.D., Neubauer F. & Thöni M. 1999: Deformation-induced resetting of Rb/Sr and  $40\text{Ar}/39\text{Ar}$  mineral systems in a low-grade, polymetamorphic terrane (eastern Alps, Austria). *J. Geol. Soc. (London)* 156, 261–278.
- Neubauer F. 2002: Evolution of late Neoproterozoic to early Paleozoic tectonic elements in central and southeast European Alpine mountain belts: review and synthesis. *Tectonophysics* 352, 87–103.
- Neubauer F. & Frisch W. 1993: The Austroalpine metamorphic basement east of the Tauern window. In: von Raumer J. & Neubauer F. (Eds.): Pre-Mesozoic Geology in the Alps. *Springer*, Berlin, 515–536.
- Neubauer F. & Sassi F.P. 1993: The quartzphyllite and related units of the Austro-Alpine domain. In: von Raumer J. & Neubauer F. (Eds.): Pre-Mesozoic Geology in the Alps. *Springer*, Berlin, 423–439.
- Stephan T., Kroner U. & Romer R.L. 2019: The pre-orogenic detrital zircon record of the Peri-Gondwanan crust. *Geol. Mag.* 156, 2, 281–307.

# Succession of tectonometamorphic processes in the Veporic–Gemic contact zone revealed by monazite age data (Western Carpathians, Slovakia)

TOMÁŠ POTOČNÝ<sup>1</sup>, ŠTEFAN MÉRES<sup>2</sup> and DUŠAN PLAŠIENKA<sup>1</sup>

<sup>1</sup>Department of Geology and Palaeontology, Faculty of Natural Sciences, Comenius University, Mlynská dolina, Ilkovičova 6, 842 15 Bratislava, Slovakia; potocny9@uniba.sk, dusan.plasienka@uniba.sk

<sup>2</sup>Department of Geochemistry, Faculty of Natural Sciences, Comenius University, Mlynská dolina, Ilkovičova 6, 842 15 Bratislava, Slovakia; stefan.meres@uniba.sk

**Abstract:** The Veporic–Gemic contiguous zone is characterized by the presence of several major tectonic units exhibiting differing structural–metamorphic histories. Relying on the detailed structural, petrologic and geochronologic (EMPA dating of monazites) investigations, three main metamorphic stages have been distinguished. The first event (ca 360–355 Ma) is restricted to the Veporic basement and relates to the Variscan regional metamorphism and granitoid intrusions, the others two are Alpine in age. Ages around 145–140 Ma occur in the Meliatic HP Bôrka Nappe only and associate with its exhumation and thrust emplacement; while the mid-Cretaceous data (100–90 Ma) are found in all units and are likely connected with the main phase of the Western Carpathian nappe stacking and onset of the extension-related exhumation of the Veporic metamorphic dome.

## Introduction

The contact zone of the Veporic and Gemic basement-involved superunits in central Slovakia follows the Lubeník fault zone, which was the thrust plane of the latter over the former originally, later affected by significant transpressional and extensional reactivation. The deformation processes in this structurally complicated area resulted in a superposition and/or juxtaposition of several units that exhibit complex tectonic and metamorphic relationships. We present the structural, metamorphic and geochronologic data which constrain their tectonothermal evolution into three distinct stages.

## Geological setting

Three superposed major Western Carpathian tectonic units in the investigated area between Čierna Lehota and Štítnik villages in central Slovakia occur (Fig. 1). The Veporic Superunit in the lowermost structural position includes the pre-Alpine crystalline basement and the post-Variscan Upper Paleozoic–Triassic sedimentary cover (Foederata Unit). The Veporic basement is composed of polymetamorphic (Variscan and Alpine) metasediments and scarce metavolcanics (Hladomorná dolina Complex; HDC) intruded by Variscan granitoids (Kráľova hoľa Complex; KHC — Klinec 1966, 1971). The HDC is discordantly overlain by clastic deposits of the Permian Rimava Formation as a part of the South

Veporic sedimentary cover. In addition to the polyphase regional metamorphism, the HDC bears also superimposed contact metamorphic associations related to the hidden Upper Cretaceous granitic intrusion (Rochovce granite; Korikovský et al. 1986; Poller et al. 2001; Kohút et al. 2013) which was drilled in its underlier (e.g., Klinec 1980).

Along the SW–NE trending Lubeník fault zone, which turns to the N–S direction in the investigated area, rocks of Veporic Rimava Fm. are juxtaposed to the Paleozoic complexes of the Gemic Superunit. In the direct contact with the Veporic units, the Mississippian rocks of the Gemicum are represented by the Ochtiná Group overlain by the Pennsylvanian clastics of the Hámor Fm. (e.g., Vozárová 1996). The Ochtiná Unit is overthrust by the main Gemic basement and cover thrust sheet represented by the Lower Paleozoic low-grade poly-metamorphic volcano-sedimentary formations (Gelnica Group) and the Pennsylvanian–Permian cover clastics (Permian Gočaltovo Group in the area concerned).

The Gemic rock complexes are overridden by the Meliatic Superunit. The Meliaticum is formed by the Bôrka Nappe (Mello et al. 1998) composed of the Permian to Jurassic HP/LT metamorphosed sedimentary and volcanic rocks, and very low-grade Jurassic syn-orogenic sedimentary formations with huge olistostrome bodies (Meliata Unit s.s.; Mock et al. 1998). Rocks of the Bôrka Nappe underwent Upper Jurassic blueschist-facies metamorphism and were subsequently affected by the Early Cretaceous greenschist-facies

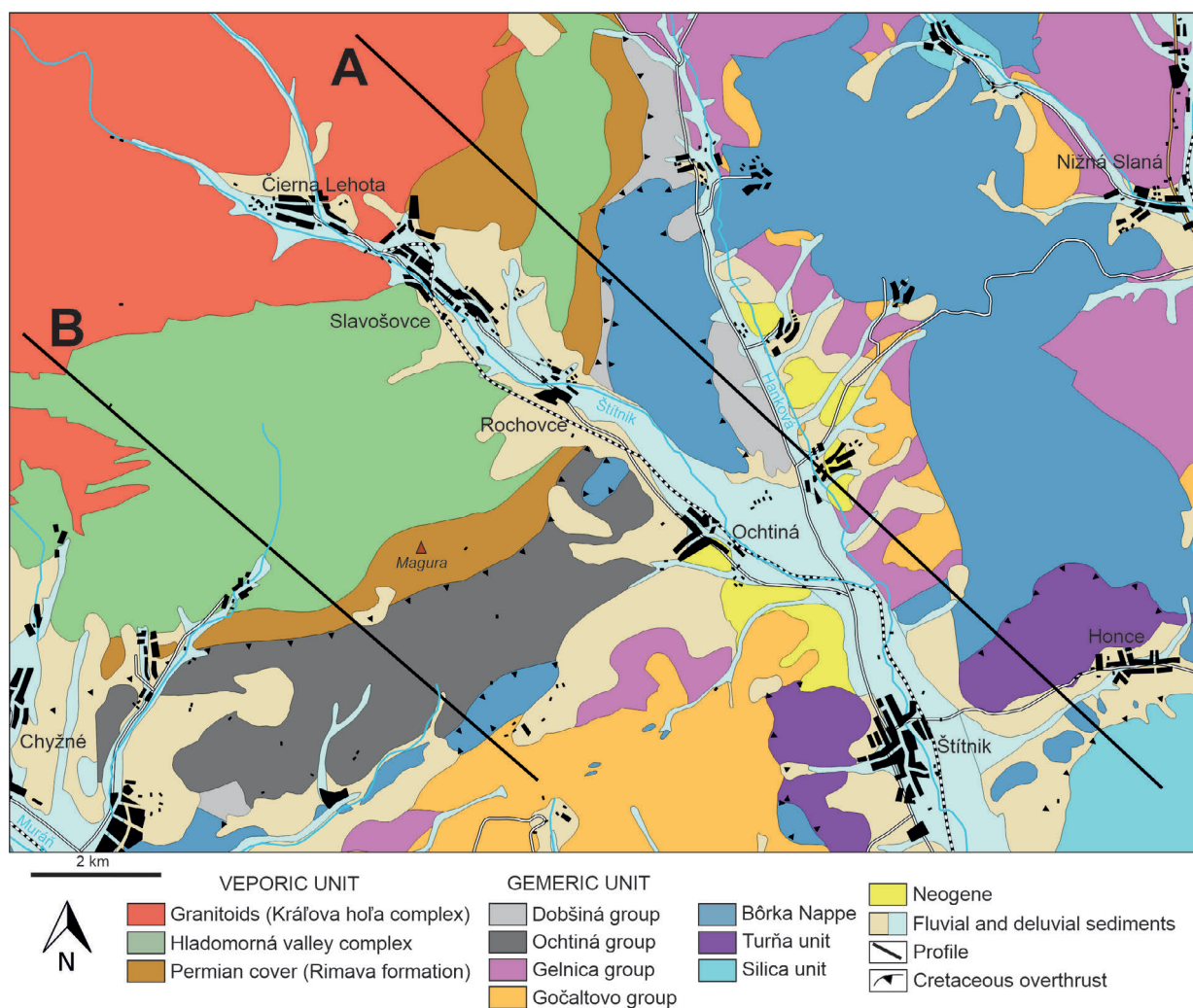


Fig. 1. Geological sketch map of the investigated area with indicated profile lines.

retrogression (e.g., Plašienka et al. 2019 and references therein). Meliaticum is tightly imbricated and forms a combined accretionary complex with the overlying Turňa Unit represented by a system of partial nappes and duplexes consisting of low-grade Carboniferous to Triassic metasediments (Lačný et al. 2016). The structurally highest unit is the Silica Nappe, which overlies the Meliatic-Turnaic accretionary complex with a pronounced structural and metamorphic discordance (Reichwalder 1982).

The structural relationships of the Veporic–Gemic–Turnaic–Meliatic thrust stack are described along two subparallel, NW–SE trending profile lines in the studied area (Fig. 1). The first profile A is located between the mountain ridges NW and SE of the Štítik River valley. It crosses units of the Veporicum (KHC, HDC, Rimava Fm.), Gemicum (Ochtiná, Gelnica and Gočaltovo groups), Meliaticum (Bôrka Nappe), Turnaicum and Silicicum. The second profile (B in Fig. 1)

follows the mountain ridge between valleys of the Štítik and Muráň rivers and includes from NW to SE the Veporic (KHC, HDC, Rimava Formation), Gemic (Ochtiná and Gočaltovo groups) and Meliatic units (Bôrka Nappe).

We investigated a number of samples, in part oriented, from all these units. Thin-sections were subjected to petrological study under the polarized microscope and electronic microanalyzer to obtain data about the lithology, metamorphism and microstructures. Several samples that contain metamorphic monazites were dated by the EMPA method providing ages that can be grouped into three main stages — one Variscan and two Alpine.

### Petrology, metamorphism and structures

First representative of the Veporic basement is a skarnoid body occurring within the Variscan granitoids near

Čierna Lehota village. The mineral composition of the skarnoid is dominated by garnet, biotite and ore minerals. The HDC includes different types of metasediments (phyllites and gneisses) and metavolcanic rocks in the study area. Characteristic feature of metasediments is very fine-grained matrix composed of chlorite, biotite, muscovite, quartz and plagioclase. Contact metamorphism related to the underlying Rochovce granite intrusion produced porphyroblasts of garnet, biotite, cordierite and andalusite. Metabasites from HDC consist of amphibole, epidote, chlorite and plagioclase with biotitization due to the mentioned Alpine contact metamorphism. The cover Rimava Fm. involves metasandstones, metavolcanics and metavolcanoclastics with mainly fine-grained matrix formed by sericite, quartz, albite and biotite. The Ochtiná group is represented by metaconglomerates, different types of phyllites and metabasalts. The mineral composition of phyllites includes chlorite, sericite, albite, quartz and organic matter. The main minerals of metabasalts are amphibole, chlorite and epidote. Occurrence of two types of amphibole is characteristic for these metavolcanic rocks. Rock composition of the Bôrka Nappe comprises different types of metabasalts in association with metacarbonates, phyllites and radiolarites. Chlorite, amphibole and epidote dominate in metavolcanics. Sericite, chlorite, albite and quartz are the main components of phyllites. Besides the contact metamorphism, we observed mineral associations characteristic for the greenschist facies conditions in all rock complexes.

Majority of the measured metamorphic foliation planes show moderate dips to SE, which is correlated with the main Alpine tectonic stages. The HDC is an exception, showing dip direction to the SW or S. These different attitudes are considered to be inherited from the pre-Alpine period, as it is indicated by the same orientation the Variscan granitoid sills near Chyžné village.

### Monazite ages

The first set of monazite age data come from rock complexes occurring along the A profile line (Fig. 1). Two generations of monazites were encountered in skarnoid body occurring within the Variscan granitoids. The older monazites Mnz1 show a rounded habitus, dimensions from 10  $\mu\text{m}$  to 30  $\mu\text{m}$  and always as inclusions in garnets occur. EMPA dating of Mnz1 revealed the Devonian/Carboniferous boundary ages ( $359 \pm 4.2$  Ma). The younger monazite generation (Mnz2) always occurs

out of the garnets, most commonly in biotite or quartz. Mnz2 has a dendritic, strongly irregular habitus and is present in layers 30  $\mu\text{m}$  to 100  $\mu\text{m}$  thick along with older allanite. Mnz2 has the early Late Cretaceous age  $92 \pm 7.2$  Ma.

Two generations of monazites were identified in a mylonitic granite (Zlatná valley, NE of Slavošovce) located between the Variscan granitoids and Permian Rimava Fm. The older monazites (age around 355 Ma) are located in a massive fabric and they have dimensions from 100  $\mu\text{m}$  to 50  $\mu\text{m}$ . The younger monazites (ages around 100 Ma) are restricted to the Alpine foliation planes.

Numerous post-kinematic idiomorphic porphyroblasts of monazites (30–500  $\mu\text{m}$  in size) were observed in the sericite-chlorite phyllites of the Bôrka Nappe (locality Honce, 10 km SE of Slavošovce). Monazites show a typical oscillation zonation which is reflected in their chemical composition. The EMPA dating of these monazites provided again two age groups: (1)  $147 \pm 17$  Ma and (2)  $89 \pm 18$  Ma.

We obtained other two distinct monazite age groups from the mylonitic granite and from garnet–biotite gneiss (NE of Chyžné village) located between the Variscan granitoid and HDC (profile line B in Fig. 1). Older monazite ages (around 355 Ma) were obtained from the mylonitic granite, while younger monazite ages (around 88 Ma) were identified from the garnet–biotite gneiss. Analogous monazite age 88 Ma was provided on the contact of the metamorphosed cordierite–biotite gneiss from the HDC near the contact with the Permian Rimava Fm. (NE of Magura Hill).

Further on, two monazite ages were acquired from sericite–chlorite phyllites of the Bôrka Nappe (locality Hrádok, 5 km S of Slavošovce). These monazites are very fine-grained (below 30  $\mu\text{m}$ , frequently below 15  $\mu\text{m}$ ). Dating provided two different age groups: older (1) monazites  $139 \pm 13$  Ma, and younger (2) monazites  $97 \pm 5$  Ma. Older monazites occur in the coarser-grained domains and younger monazites are always present as elongated grains aligned within the very fine-grained foliation domains. Microscopic observations indicate shearing along the foliation planes.

### Conclusions

Three principal tectono-metamorphic events can be discerned based on our petrologic and structural investigations and monazite age data: (1) the oldest monazite ages from the skarnoid body and from the mylonitic

granites indicate the Variscan regional metamorphosis tacking from intrusion of granitoids into the Lower Paleozoic pelitic protolith of HDC; (2) the monazites age group around 145–140 Ma from sericite–chlorite phyllites of the Bôrka Nappe likely indicates exhumation related to thrusting of the Meliatic accretionary wedge over the lower-plate Veporic and Gemic units, following subduction of the Meliata Ocean; (3) the youngest monazite age group from all analysed rocks records the Alpine overprint of the Veporic basement simultaneously with recrystallization of the Meliatic complexes during the main phase of the Western Carpathian nappe stacking and commencement of the extension-related exhumation of the Veporic metamorphic dome.

**Acknowledgements:** Financial support from the Grant Agency for Science, Slovakia (project VEGA 1/0085/17) and from the Slovak Research and Development Agency (project APVV-17-0170) is gratefully appreciated.

## References

- Klinec A. 1966: Zum Bau und Bildung des Veporiden-Kristallin. *Sbor. Geol. vied, rad ZK* 6, 7–28 (in Slovak with German summary).
- Klinec A. 1971: The main tectonic elements in the eastern Veporides. *Geol. práce, Správy* 57, 105–109 (in Slovak with English summary).
- Klinec A. 1980: Contiguous zone of Gemicides and Veporides enlightened by well near Rochovce. *Geol. Zbor. — Geol. Carpath.* 31, 537–540.
- Kohút M., Stein H., Uher P., Zimmerman A. & Hraško Ľ. 2013: Re–Os and U–Th–Pb dating of the Rochovce granite and its mineralization (Western Carpathians, Slovakia). *Geol. Carpath.* 64, 71–79.
- Korikovsky S.P., Janák M. & Boronichin V.A. 1986: Geothermometry and mineral equilibria during recrystallization of garnet mica schists and cordierite-bearing hornfelses in the Rochovce granite aureole (Slovak Ore Mts., Rochovce–Chyžné district). *Geol. zbor. — Geol. Carpath.* 37, 607–633.
- Lačný A., Plašienka D. & Vojtko R. 2016: Structural evolution of the Turňa Unit constrained by fold and cleavage analyses and its consequences for the regional tectonic models of the Western Carpathians. *Geol. Carpath.* 67, 177–193.
- Mello J., Reichwalder P. & Vozárová A. 1998: Bôrka nappe: high-pressure relic from the subduction-accretion prism of the Meliata ocean (Inner Western Carpathians, Slovakia). *Slovak Geol. Mag.* 4, 261–273.
- Mock R., Sýkora M., Aubrecht R., Ožvoldová L., Kronome B., Reichwalder P. & Jablonský J. 1998: Petrology and stratigraphy of the Meliaticum near the Meliata and Jaklovce Villages, Slovakia. *Slovak Geol. Mag.* 4, 223–260.
- Plašienka D., Méres Š., Ivan P., Sýkora M., Soták J., Lačný A., Aubrecht R., Bellová S. & Potočný T. 2019: Meliatic blueschists and their detritus in Cretaceous sediments: New data constraining tectonic evolution of the West Carpathians. *Swiss J. Geosci.* 112, 55–81.
- Poller U., Uher P., Janák M., Plašienka D. & Kohút M. 2001: Late Cretaceous age of the Rochovce granite, Western Carpathians, constrained by U–Pb single-zircon dating in combination with cathodoluminescence imaging. *Geol. Carpath.* 52, 41–47.
- Reichwalder P. 1982: Structural characteristic of root zones of some nappes in innermost parts of West Carpathians. In: Maheľ M. (Ed.): Alpine structural elements: Carpathian–Balkan–Caucasus–Pamir orogene zone. *Veda Publ.*, Bratislava, 43–56.
- Vozárová A. 1996: Tectono-sedimentary evolution of late Paleozoic basins based on interpretation of lithostratigraphic data (Western Carpathians, Slovakia). *Slovak Geol. Mag.* 3–4, 251–271.

# Orogenic wedging and basin formation in the Central Western Carpathians: New insights from Súľov–Domaníža and Žilina–Rajec basins

JÁN SOTÁK<sup>1,2</sup>, MICHAL KOVÁČ<sup>2</sup>, DUŠAN PLAŠIENKA<sup>2</sup> and RASTISLAV VOJTKO<sup>2</sup>

<sup>1</sup>Earth Science Institute, Slovak Academy of Sciences, Ďumbierska 1, 974 11 Banská Bystrica, Slovakia; sotak@savbb.sk

<sup>2</sup>Department of Geology and Paleontology, Faculty of Natural Sciences, Comenius University, Mlynská dolina, Ilkovičová 6, 845 15 Bratislava, Slovakia

The Súľov–Domaníža Basin (SDB) belongs to wedge-top basins developed on the CWC orogenic wedge. Late Paleocene–Early Eocene transgression of the SDB led to development of thrust-top carbonate platforms (Kambühel Fm, Alveolina Lms) and calciclastic fans, which unconformably overlapped frontal CWC nappes and Peri-Klippen units. Synsedimentary tectonics of the SDB started in the late Thanetian–early Ypresian by normal faulting and disintegration of the orogenic wedge margin. The basin was supplied by continental margin deposystems, and filled with submarine landslides, fault-scarp breccias, base-of-slope aprons, cohesive debris flows and finally also diluted-flow deposits. Thick conglomerate lithosomes were accumulated from late Thanetian to early Lutetian. They are intercalated by claystone interbeds with rich planktonic and agglutinated microfauna, implying deep-water environments of gravity-flow deposition. The rapid subsidence was accelerated by gravitational collapse and subcrustal tectonic erosion of the CWC plate, which probably resulted from a super-critical taper of orogenic wedge due to subduction and underthrusting of the Oravic ribbon continent.

During the late Ypresian–Lutetian, the SDB merged with adjoining Paleogene basins of the Mid-Slovakian weakness zone (MSWZ) under conditions of bathyal up to abyssal deposition. Lutetian formations are formed by hemipelagic marls and turbiditic sequences, non-calcareous red claystones with *Reticulophragmium amplexens* and various deep-water deposits (Domaníža Fm., Žilina Fm., Hájik Mb., etc.).

Basin deepening was enhanced by Lutetian transgression, which

enabled a marine connection with the Magura Ocean. Southern basin of MSWZ in the Horná Nitra Depression is akin to the Krappfeld-type succession with basal reddish terrestrial sediments followed by Late Paleocene/Early Eocene shallow-marine formations and Lutetian deep-water marls. This implies a southward connection of MSWZ with the Carinthian embayment of the Mediterranean Tethys and northward connection with Alpine Tethys. Lutetian sea also flooded the Central-Carpathian Paleogene fore-arc basin (CCPB) by accommodation of carbonate ramps (Borové Fm).

Since the Lutetian, a deep-water basins were accommodated a weakening zone (MSWZ) between north-westward growing orogenic wedge and the north-eastward moving crustal fragments of the CWC (Fig. 1). Therefore, the common feature of the MSWZ is a superposition of wedge-top and fore-arc basins like this in Žilina, Rajec, Domaníža, Pružina, Horná Nitra, and Turiec depressions (Fig. 2).

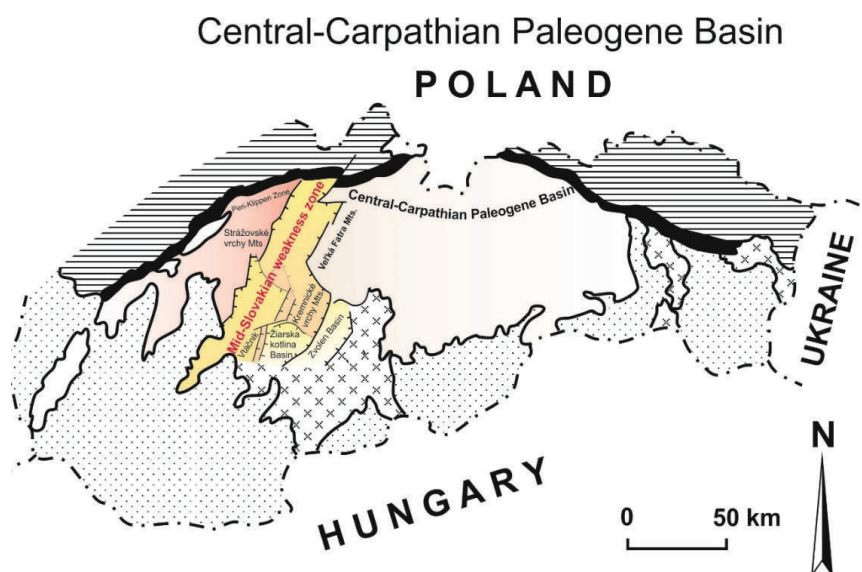


**Fig.1.** Mid-Slovakian weakness zone between wedge-top and fore-arc basins of the Central Western Carpathians.

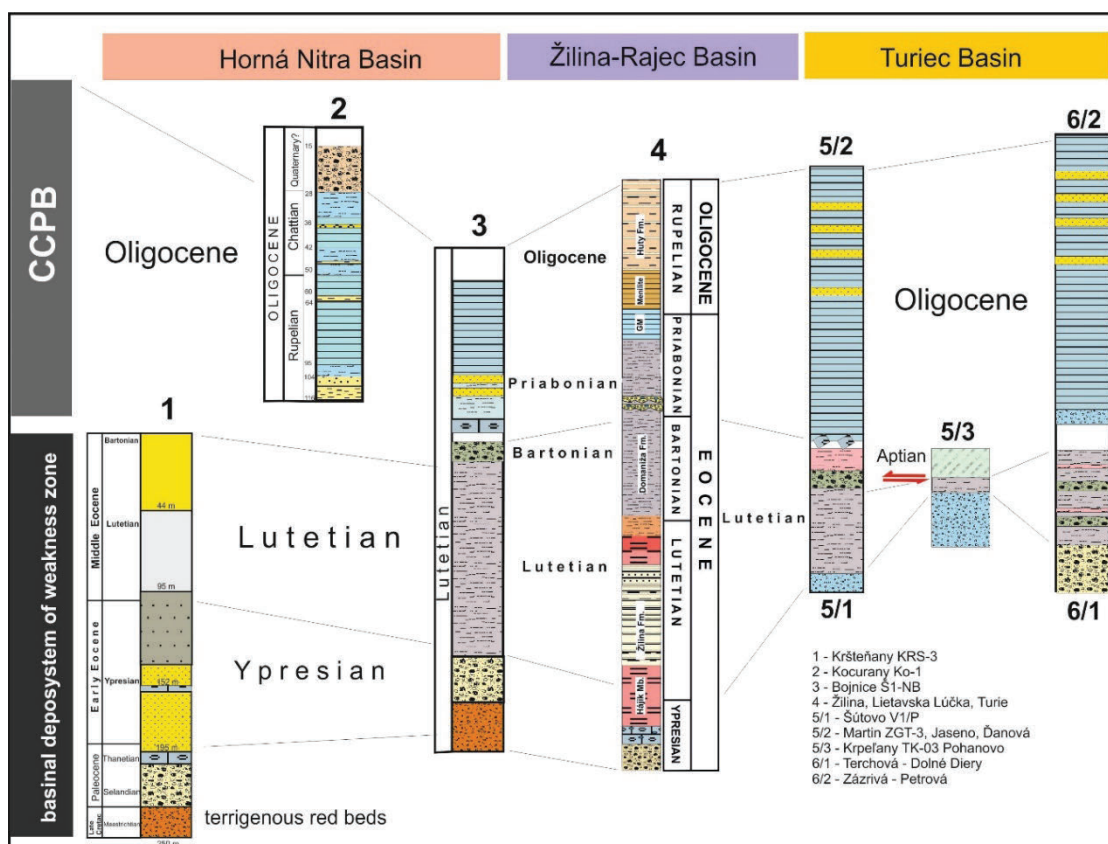


**Fig. 2.** Correlation scheme of the Paleogene formations within the Mid-Slovakian weakness zone (Horná Nitra, Žilina–Rajec and Turiec basins).

Post-Lutetian basin inversion and orogenic wedging in western part of the CWC was accompanied by eastward lateral migration of the Late Eocene–Oligocene depocentres of the Central Carpathian Paleogene Basin (CCPB). Late Eocene formations of the MSWZ are composed of gray and dark-grey weakly calcareous claystones. They still reveal a deep-water deposition with agglutinated and planktonic foraminifers, which differ from coeval claystone formations of the CCPB (Huty Fm.). Early Oligocene claystones and menilite

shales of the MWZ progressed from Late Eocene formation with correlative conformity to highstand formations of Globigerina Marls in the CCPB. Late Oligocene formations of the MSWZ are formed by turbiditic and sandy-rich facies of submarine fan deposystems of the CCPB.

**Acknowledgement:** The research was supported by project APVV-14-0118, APVV-17-0170 and grant VEGA 2/0034/16.

# Structural control of the Banská Hodruša ore deposit (Štiavnica Stratovolcano)

RASTISLAV VOJTKO<sup>1</sup>, PETER ŽITŇAN<sup>2</sup>, JÁN PRCÚCH<sup>3</sup>, JAROSLAV LEXA<sup>4</sup>,  
PETER KODĚRA<sup>5</sup>, MARTIN CHOVAN<sup>6</sup> and ALEXANDER KUBAČ<sup>5</sup>

<sup>1</sup>Department of Geology and Palaeontology, Faculty of Natural Sciences, Comenius University in Bratislava, Mlynská dolina, Ilkovičova 6, SK-842 15 Bratislava, Slovakia; rastislav.vojtko@uniba.sk

<sup>2</sup>Prospech Slovakia, Ltd., Kammerhofská 8, SK-969 01 Banská Štiavnica, Slovakia; pzitnan@gmail.com

<sup>3</sup>Slovenská Banská Ltd., SK-966 61 Hodruša-Hámre, Slovakia; janoprcuch@gmail.com

<sup>4</sup>Earth Science Institute, Slovak Academy of Sciences, Dúbravská cesta 9, SK-840 05 Bratislava, Slovakia; geoljalx@savba.sk

<sup>5</sup>Department of Economic Geology, Faculty of Natural Sciences, Comenius University in Bratislava, Mlynská dolina, Ilkovičova 6, SK-842 15 Bratislava, Slovakia; peter.kodera@uniba.sk, alexander.kubac@uniba.sk

<sup>6</sup>Department of Mineralogy and Petrology, Faculty of Natural Sciences, Comenius University in Bratislava, Mlynská dolina, Ilkovičova 6, SK-842 15 Bratislava, Slovakia; martin.chovan@uniba.sk

**Abstract:** The Banská Hodruša deposit is located in the central zone of the Štiavnica Stratovolcano of Miocene age. The mineralisation is placed in the low-angle normal fault zone with the dip direction of 125° and generally flat dip (5–30°). This zone was formed at the lithological boundary between the Miocene granodiorite pluton and hanging wall units consisting of fragments of sediments (mainly limestones) and the pre-caldera stage andesites further up in the sequence. The mineralisation consists of stockwork and individual veins of various dips (10–90°) in the low-angle normal fault zone with very strict geometric characteristics, which are conform to the geometry of the shear zone.

## Introduction

Neogene volcanism and back-arc related extension is the important area of epithermal deposits of low (intermediate)-sulphidation types in the Carpathian arc. Banská Štiavnica and Kremnica are the most famous mining regions in Slovakia of such type of ore mineralization (cf. Lexa 2005). The studied epithermal precious/base metal mineralization occurs within the Štiavnica–Hodruša ore district in the central zone of the large Štiavnica Stratovolcano of Miocene age.

Mineralogy and geochemistry of the mineralization was recently described in the paper of Kubač et al. (2018). The mineralisation controls were poorly understood yet; however, the study presented in this paper, revealed several unique characteristics. Main goal of the study was to describe geometrical characteristics, structural controls, and tectonic evolution of the Au±Ag, Pb, Zn, Cu epithermal mineralisation in the central zone of the Štiavnica Stratovolcano.

## Geological setting

The studied area is located in the central zone of the middle to upper Miocene Štiavnica Stratovolcano in the internal portion of the Western Carpathians.

The Štiavnica Stratovolcano has markedly developed an extensive caldera (some 20 km in diameter), a late stage resurgent horst in the caldera centre and an extensive complex of subvolcanic intrusions. The structure of the Štiavnica Stratovolcano can be roughly divided into pre-caldera stage, caldera stage, and post-caldera stage (Konečný et al. 1995).

The deposit is located between Hodruša–Hámre and Banská Štiavnica municipalities in the middle of the central zone of the stratovolcano. The gold mineralization is known to occur between the 10<sup>th</sup> and 19<sup>th</sup> levels of the Rozália Mine in ~160–300 m a.s.l. The mineralization is hosted mainly by intensively altered pyroxenic andesites of the pre-caldera stage and rarely by thin, relatively older quartz-diorite porphyry sills. The thickness of the mineralized zone is typically tens of metres. The deposit has a tabular shape and is gently dipping (5–30°) south-eastward. The epithermal mineralisation is hosted in intensive stockwork with veinlets from several centimetres to metres wide. The mineralised zone is disrupted/dismembered by a post-mineral set of quartz-diorite porphyry sills.

Both, the mineralization and the quartz-diorite porphyry sills were later disrupted by late steeply dipping strike-slip to normal faults, base metal veins and subparallel structures (Koděra et al. 2005, 2014; Kubač et al. 2018).

## Methods

Faults and striae on the fault surfaces are very often present in rock masses and therefore kinematic and dynamic analyses of fault-slip data is very popular tool for reconstruction of the palaeostress fields. Slickenside lineations are formed on fault planes during the motion of the two walls. These lineations are measured in the field so as to provide information on the direction of fault movement. Standard procedures for brittle fault-slip analysis and palaeostress reconstruction are now well established (Angelier 1990, 1994; Michael 1984).

The standard runtime techniques provide a determination of four parameters of the reduced stress tensor. The software applications utilize an inversion method which is based on the assumption of Bott (1959) that slip on a plane occurs in the direction of the maximum resolved shear stress. Fault data were inverted to obtain the four parameters of the reduced stress tensor:  $\sigma_1$  (maximum principal stress axis),  $\sigma_2$  (intermediate principal stress axis), and  $\sigma_3$  (least principal stress axis) and the ratio ( $\Phi$ ) of principal stress differences is expressed by the formula  $\Phi = (\sigma_2 - \sigma_3) / (\sigma_1 - \sigma_3)$  (e.g., Angelier 1994).

## Results

The structural analysis was carried out predominantly in the eastern sector of the Rozália Mine. A heterogeneous population of fault-slips was collected and separated into homogeneous fault-slip groups using the inversion method.

Structurally, the youngest deformational stage was controlled by extensional tectonic regime with the orientation of the principal tension axis in WNW–ESE direction. During this stage NE–SW normal faults were formed with moderate inclination predominantly in SE. These faults are related to the late extensional event in the Štiavnica area.

Based on cross-cutting criteria, a strike-slip tectonic regime with NNE–SSW dextral strike-slip faults and ENE–WSW sinistral strike slip faults were identified as older than the aforementioned normal faults and  $\sigma_1$  operated in the NE–SW direction while  $\sigma_3$  in the NW–SE direction. It is assumed that this deformation was responsible for initial stage of the Štiavnica type dislocations.

The most distinct structure hosting Au±Ag, Pb, Zn, Cu mineralisation at the Rozalia Mine is the low-angle normal fault zone. The zone is characterised by normal

faulting with the NE–SW strike of fault planes and complex structures in between the fault zone. As described above, this zone has well developed internal structure. Tension gashes, predominantly oriented in the NNE–SSW direction with moderate dip to the ESE are filled by the Krištof type veins. To the contrary a gentle dipping releasing bends predominantly at the roof are filled by the Agnesa type veins, having the same age as the Krištof type veins. These veins are typically shallow dipping (less than 30°) with the dip direction SE-wards (cf. Kubač et al. 2018).

Most probably, the slightly older kinematics is responsible for the formation of the Karolína stockwork (The Central Stockwork), which was controlled by a NNW–SSE oriented  $\sigma_3$ . It is important to note that this deformation was observed only along the Karolína zone and has practically the same deformation as the low-angle normal fault zone. However, the general strike of the zone is in the WNW–ESE direction. This zone represents the initial phase of Au±Ag, Pb, Zn, Cu mineralisation on the low-angle normal fault zone and understanding of its structural evolution is crucial for the discovery of additional ore bodies within this zone.

The pre-low-angle normal fault deformational stage is controlled by extensional tectonic regime with the orientation of  $\sigma_3$  axis in a NE–SW direction. During this stage, the NW–SE normal faults were activated with moderate to steep dip on both sides. These faults are considered to be related to pre-granodiorite intrusion phase, because these faults were not observed in the granodiorite pluton yet.

Probably the oldest known deformation is represented by NW–SE dextral strike-slip faults. This homogeneous fault set is weak and some additional information is still missing.

## Interpretation and discussion

Geological model of the studied area is based mainly on structural measurements with respect to the mineralisation in the central zone of the Štiavnica Stratovolcano.

During the Early Badenian, a large andesite stratovolcano was formed also known as “the pre-caldera stage”. The Štiavnica Stratovolcano has multistage evolution and the formation of the large andesite stratovolcano was followed by denudation and emplacement of granodiorite pluton (Lexa et al. 1999). The granodiorite intrusion was accompanied by disseminated base metal mineralization and intensive advanced argillic alteration in overlying complex of andesites.

Subsequent uplift of the granodiorite intrusion caused evolution of the sector collapse related low-angle normal fault zone, which was newly identified during our research. A Central Stockwork at the deposit originated in the early stage of the exhumation process. Geometrically, the stockwork can be characterized as an E–W and ESE–WNW structures with the 40–60° inclination to the south. Typically, the stockwork is composed of a quartz–carbonate gangue rich in Mn-bearing minerals, base metal sulphides, gold, and Ag-tellurides (Kubač et al. 2018). The stockwork has trishear geometry with typical upside down triangular shape with the base of triangle at the subhorizontal roof of the low-angle normal fault shear zone. This structure is interpreted as a result of southward movement of the hanging wall in the low-angle normal fault shear zone. The inclination of the fault zone in a deeper part is less than 30° southward with the slickenside lineations at azimuth of 170° and can be characterized as the low-angle normal fault. It is important to note, the initial stage with randomly-oriented hydrothermal cracks indicate that differences between principal palaeostress axes were relatively small. Randomly directed veinlets were later replaced by slightly younger the NE–SW directed veinlets inside the Central Stockwork trishear zone in the central area.

Exhumation of the granodiorite intrusion caused unroofing, which was carried out by evolution of the low-angle normal fault shear zone. This shear zone is located at the boundary between the Miocene granodiorite and andesite of the lower stratovolcanic structure. In general, low-angle normal fault zone (dip <30°) accommodate much extension of the continental crust and such faults are common in areas of high extensional strain (e.g., Axen 1990). They apparently move under low resolved shear stress and are anomalously weak. Mechanical analysis shows that fault weakening may preclude equality of the regional and fault zone stress tensors, and predicts reorientation and increase of principal stresses in weak fault zones. These changes suppress hydraulic fracturing, which were firstly identified by Nemčok et al. (2000) in the brittle detachment zone and allow slip under frictional sliding conditions typical of upper crustal rocks (Axen, 1992). The low-angle normal fault is weak, partly or totally due to elevated pore fluid pressure. The zone is related to exhumation of the granodiorite pluton and related sector collapse during the pre-caldera stage of the Štiavnica Stratovolcano. The low-angle normal fault zone has complex internal structure with evolution of R and R' Riedel's shears, tension gashes, restraining bends, releasing bends etc.

According to recent structural data, these structures correspond to the well-developed low-angle normal fault zone. All these structures have uniform kinematics characterized by hanging wall general displacement vector ESE-wards as it is evidenced by the slickenside lineation on faults. The fluids responsible for Au–Ag mineralization used the extensional internal structures during the unroofing of hanging wall andesite complex.

The Krištof type veins are hosted predominantly by the NNE–SSW striking tension gashes with moderate dip to the ESE. The vein system typically contains stockworks of thin veins or occurs as individual veinlets. The thickness of individual veins is usually 4–40 cm in average, rarely up to 200 cm. Quartz is the dominant gangue mineral accompanied by native gold and infrequent base metal sulphides and carbonates in predominantly banded structures.

The Agnesa-type veins, typically shallow dipping (dip <30°) with dip direction ESE-ward, are usually located in the roof of the low-angle normal fault zone. High pore pressure in such zones may be contained by upper plate strata with mineral precipitation in their hanging walls (Axen 1992). This is also the case of the Agnesa-type of veins. Structurally, the veins were formed in shallow dipping releasing bends in the roof of low-angle normal fault zone or in the local extensional structures in the middle of the zone. The formation of the veins is associated with the normal movement of the hanging wall during continual exhumation of the granodiorite pluton. It is represented by several individual veins with up to 3 m thickness, predominantly rich in base metals accompanied by gold. Quartz is the main gangue mineral in this vein type and carbonates are very rare (Kubač et al. 2018).

The final stage of the granodiorite exhumation is accompanied by emplacement of quartz-diorite porphyry in and around of the low-angle normal fault zone in andesites of the pre-caldera stage of the Štiavnica Stratovolcano evolution. The Au±Ag, Pb, Zn, Cu mineralisation was dismembered by this set of quartz-diorite porphyry sills, which were emplaced along the contact zone of the granodiorite pluton and along individual faults of the low-angle normal fault zone. Generally, the quartz-diorite porphyry sills post-date the Au ± Ag, Pb, Zn, Cu mineralisation in this zone. However, there is at least one older type of quartz–diorite porphyry, which is mineralized by the Au ± Ag, Pb, Zn, Cu veins and it is also affected by brecciation, irregular fracturing, mylonitization or by pervasive alteration, which are features typical for mineralized andesites (Koděra et al. 2005).

## Conclusions

Identification of the low-angle normal fault zone is the main new discovery that has remained unrecognized until recently. The studied Au±Ag, Pb, Zn, Cu Banská Hodruša deposit was developed in the pre-caldera stage units of the Štiavnica Stratovolcano and exhibits structures for syntectonic epithermal deposits including structural association with polyphase faulting related to exhumation of the granodiorite intrusion.

The E–W striking Central Stockwork has trishear geometry with a typical triangular shape with the base of triangle at the subhorizontal roof of the low-angle normal fault zone. This structure is interpreted as a result of southward movement of the hanging wall in the earliest stage of shear zone formation. Veinlets forming the stockwork were later disrupted by younger NE–SW oriented epithermal veinlets inside the trishear zone, which are arranged in the formed low-angle normal fault zone. The zone has general dip direction in 120° with the inclination from 5–30°

The low-angle normal fault zone produced generally two types of vein systems: (i) The Agnesa-type veins are typically shallow dipping (less than 30°) with dip direction ESE-wards. Structurally, the veins were formed in releasing bends in the roof of the low-angle normal fault zone. (ii) The Krištof-type veins, having the same age as the Agnesa-type veins, are hosted predominantly by the NNE–SSW oriented tension gashes with moderate dip to the ESE.

The precious/base metal mineralisation is disrupted by quartz–diorite porphyry sills, which were emplaced mostly parallel to the low-angle normal fault zone, hence the quartz–diorite porphyry sills generally post-date the mineralisation in this zone. However, at least one older type of quartz–diorite porphyry predates the Au±Ag, Pb, Zn, Cu mineralisation.

The quartz–diorite porphyries together with the precious metal mineralization were later displaced by normal faults and epithermal vein mineralization of the Štiavnica type.

Understanding the kinematics and spatial distribution of the low-angle normal fault zone is crucial for future exploration due to its significant economic potential to

host high grade Au±Ag, Pb, Zn, Cu mineralization in the central part of the Štiavnica Stratovolcano.

**Acknowledgements:** This work was supported by Slovak Research and Development Agency under the contracts Nos. APVV-15-0083 and APVV-0315-12. The authors thank all the staff from the Slovenská Banská Ltd. especially from the Rozália Mine for their fruitful insight and discussions.

## References

- Angelier J. 1990: Inversion of field data in fault tectonics to obtain the regional stress – III. A new rapid direct inversion method by analytical means. *Geoph. J. Int.* 103, 363–376.
- Angelier J. 1994: Fault slip analysis and paleostress reconstruction. In: Hancock P.L. (Ed.): *Continental deformation*. Pergamon Press, University of Bristol (U.K.), London, 53–100.
- Axen G.J. 1992: Pore pressure, stress increase, and fault weakening in low-angle normal faulting. *J. Geoph. Res.* 97, B6, 8979–8991.
- Bott M.H.P., 1959: The mechanics of oblique slip faulting. *Geological Magazine* 96, 109–117.
- Koděra P., Lexa J. & Rankin A.H. 2005: Epithermal gold veins in a caldera setting: Banská Hodruša, Slovakia. *Mineralium Deposita* 39, 921–943.
- Koděra P., Lexa J., Fallick A.E., Wälle M. & Biroň A. 2014: Hydrothermal fluids in epithermal and porphyry Au deposits in the Central Slovakia Volcanic Field. *Geological Society London, Special Publications* 402, 177–206.
- Konečný V., Lexa J. & Hojstříčová V. 1995: The Central Slovakia Neogene Volcanic Field: a review. *Acta Vulcanologica* 7, 63–78.
- Kubač A., Chovan M., Koděra P., Kyle J.R., Žitňan P., Lexa J. & Vojtko R. 2018: Mineralogy of the epithermal precious and base metal deposit Banská Hodruša at the Rozália Mine (Slovakia). *Mineralogy and Petrology* 112, 5, 705–731.
- Lexa J. 2005: 1–3: Epithermal Au–Ag and Pb–Zn–Cu–Ag–Au deposits of the Central Slovakia Neogene volcanic field: Kremnica and Banská Štiavnica–Hodruša mining districts: Lat. 48°28' N, Long. 19°00' E. *Ore Geology Review* 27, 1, 50–51.
- Lexa J., Štohl J. & Konečný V. 1999: Banská Štiavnica ore district: relationship among metallogenetic processes and the geological evolution of a stratovolcano. *Mineralium Deposita* 34, 639–665.
- Michael A.J. 1984: Determination of stress from slip data: faults and folds. *J. Geoph. Res.* 89, B13, 11517–11526.
- Nemčok M., Lexa O. & Konečný P., 2000: Calculations of tectonic, magmatic and residual stress in the Štiavnica Stratovolcano, Western Carpathians: implications for mineral precipitation paths. *Geol. Carpath.* 51, 19–36.

**Theme 2:**

Petrology and geochemistry: Towards geodynamics and metallogeny

# Variscan odyssey of the Bohemian Massif and the related plutonic activity

VOJTĚCH JANOUŠEK<sup>1,2</sup>

<sup>1</sup>Czech Geological Survey, Klárov 3, 118 21 Prague 1, Czech Republic; vojtech.janousek@geology.cz

<sup>2</sup>Institute of Petrology and Structural Geology, Faculty of Science, Charles University, Albertov 6, 128 43 Prague 2, Czech Republic

**Abstract:** The voluminous Variscan granitic plutonism in the heart of the Bohemian Massif (Teplá–Barrandian and Moldanubian domains) episodically accompanied the complete orogenic cycle from the Late Devonian Andean-type subduction, through Early Carboniferous collision, deep subduction and relamination of the Saxothuringian continental crust and massive late syn-/post-collisional anatexis of the Moldanubian crust to the Late Carboniferous orogenic collapse. The granites were generated both from crustal sources, dominated by fertile metasediments with much Neoproterozoic arc-derived and Eburnean-age detritus, and mantle, variably contaminated by oceanic subduction-related fluids and deeply subducted felsic crustal material. The latter process finally resulted in the unusual and eye-catching spatial–temporal association of ultrapotassic intrusions and high-pressure, felsic Grt–Ky granulites.

## Variscan Bohemian Massif — a deeply dissected ‘hot’ orogen

The Variscan Bohemian Massif, an archetypal example of a large hot orogen in Central Europe, was intruded by voluminous and compositionally diverse, mostly broadly granitic plutons. They yield unique insight into the composition of the orogenic lower/middle crust and its development in both space and time (Žák et al. 2014 for review).

From the NW to the SE, the Variscan tectonic sequence in the core of the Bohemian Massif is as follows (Franke 2000; Schulmann et al. 2009): Saxothuringian Neoproterozoic basement with Palaeozoic metasedimentary/metagneous cover, the Teplá suture and the supra-crustal Teplá–Barrandian Unit (TBU). Crossing the Central Bohemian Plutonic Complex (CBPC), the Moldanubian Zone represents the orogen’s ‘root’ locally containing, besides mid-crustal units, abundant lower crustal or upper mantle bodies. It suffered a strong anatexis, producing the enormous Moldanubian Plutonic Complex (MPC). To the E the Moldanubian Zone is bounded by Brunia microplate, little affected by the Variscan tectonometamorphism.

Many authors (but for alternative views see e.g., Franke 2000, Finger et al. 2007 or Kroner & Romer 2013) assumed that the Variscan Orogeny in the Bohemian Massif was driven by oceanic subduction passing into deep underthrusting of the attenuated Saxothuringian continental crust (O’Brien 2000; Janoušek et al. 2004b; Schulmann et al. 2009, 2014). This is in line with the occurrence of Variscan blueschists (Faryad & Kachlík 2013), diamond- and/or

coesite-bearing gneisses, high-pressure (HP) granulites, eclogites, garnet pyroxenites and mantle peridotites in the Saxothuringian Zone (e.g., Massonne 2001; O’Brien & Rötzler 2003; Schmädicke et al. 2010; Kotková et al. 2011).

These observations, together with geochemical affinity and matching protolith ages between Saxothuringian orthogneisses and felsic Moldanubian granulites (Janoušek et al. 2004b; Janoušek & Holub 2007) with HP–HT metamorphic imprint: (>2 GPa and >1000 °C: O’Brien & Rötzler 2003; Kotková & Harley 2010; Vrána et al. 2013; Perraki & Faryad 2014) led to the model of relamination of felsic Saxothuringian crust under the Moldanubian back-arc (Schulmann et al. 2014; Maierová et al. 2014; Kusbach et al. 2015). If true, this model would have grave consequences for mechanism and magmatic evolution of the whole orogen, as examined below.

## Variscan plutonic activity

This contribution does not aim to paint a complete picture of evolving Variscan magmatism over the entire Bohemian Massif. Instead it focusses on the key region of the TBU, Moldanubian Zone and the CBPC in between — interpreted as the forearc, backarc (future orogenic root) and magmatic arc, respectively (Schulmann et al. 2009). In the following text, when useful, petrology and geochemistry of granitoids is characterized in terms of the I/S-type classification (Chappell & White 1974) or the synthetic Barbarin (1999) scheme.

### *I — Normal-K calc-alkaline suite (I, ACG)*

Initial stage of arc-related magmatism in the TBU marked minor **Čistá** and **Štěnovice plutons** (~375 Ma; Venera et al. 2000; Žák et al. 2011a). Chemically similar was contemporaneous protolith to the tonalite–granodiorite **Staré Sedlo** and **Mirotice orthogneisses** in the roof of the CBPC (Košler et al. 1993). In the CBPC itself, the unmetamorphosed Amp-bearing gabbros and quartz diorites–trondhjemites of the c. 355 Ma **Sázava suite** (Janoušek et al. 2004a) were emplaced during regional transpression (Žák et al. 2005). Characteristic is a metaluminous chemistry, CHUR-like Sr–Nd isotopic composition, subduction-related LILE/HFSE enrichment and ample evidence for magma hybridization (Janoušek et al. 1995, 2004a).

### *II — High-K calc-alkaline suite (I/S, KCG)*

The mainly (Amp) Bt granodioritic c. 345 Ma **Blatná suite** (Dörr & Zulauf 2010; Janoušek et al. 2010) recorded a transpression along the NW contact of the CBPC, while the southern margin was pervasively overprinted by deformation marking the onset of the Moldanubian exhumation (Žák et al. 2012). The felsic magmas originated by melting of greywackes rich in Neoproterozoic to Early Palaeozoic volcanogenic detritus (Janoušek et al. 2010). The granitoids enclose numerous mafic enclaves or Qtz monzonitic bodies with evidence for interaction with moderately enriched mantle melts ( $\epsilon_{\text{Nd}_i}^{\text{Nd}} \sim -3$ ) (Janoušek et al. 2000).

### *III — (Ultra-) potassic suite (ultra-K)*

Characteristic Moldanubian feature are ~343–335 Ma syn- or post-tectonic ultra-K intrusions and dyke swarms (Holub 1997; Kotková et al. 2010; Kubínová et al. 2017). Strongly Kfs-phyric **durbachite suite** of Amph–Bt quartz syenitic–melagranitic plutons (e.g., Milevsko, Třebíč) is rich in mafic enclaves. Equigranular **Bt–two-Px syenitoids** of the late (337–335 Ma) Tábor and Jihlava plutons are less voluminous (Janoušek et al. 2019).

Both suites are characterized by high Cr, Ni and Mg# as well as low HFSE and high Pb, LREE, LILE, U and Th (Holub 1997; Becker et al. 1999; Janoušek & Holub 2007). The crust-like isotopic compositions ( $^{87}\text{Sr}/^{86}\text{Sr}_i \sim 0.713$ ,  $\epsilon_{\text{Nd}_i}^{\text{Nd}} \sim -8$ ) of the basic members cannot reflect shallow-level assimilation of the local crust (Janoušek et al. 1995). Instead, the spatial/temporal association with felsic HP granulites and complementary geochemical

signatures suggest that primary ultra-K magmas came from mantle contaminated by felsic crust during the ~340 Ma HP metamorphism (Janoušek & Holub 2007; Schulmann et al. 2014). The compositional range reflects ensuing mixing with leucogranitic melts (Holub 1997; Wenzel et al. 1997; Gerdes et al. 2000). The cessation of ductile deformation along the TBU/Moldanubian boundary is bracketed by c. 338–337 Ma Tábor syenite and reversely-zoned Říčany granite (Trubač et al. 2017).

### *IV — Porphyritic biotite granite suite (I/S)*

In southern part of MPC dominate ~331–323 Ma strongly Kfs-megacrystic **Weinsberg-type** biotite granites probably generated by partial melting of heterogeneous lower crust (Liew et al. 1989; Friedl et al. 1993; Gerdes 2001; Gerdes et al. 2003).

### *V — Peraluminous two-mica granites (S, MPG/CPG)*

Two-mica granites, some with Crd or magmatic And, are the main component of the MPC. The main types include Eisgarn, Čiměř, Lipnice, Kouty–Světlá or Deštná (see Matějka & Janoušek 1998; Breiter 2010 for details). U–Pb ages on monazite cluster at c. 328–326 Ma (Friedl et al. 1996; Gerdes et al. 2003; Žák et al. 2011b; Janoušek et al. 2015). All are peraluminous, having originated by the biotite ( $\pm$  muscovite) dehydration melting of metasediments (René et al. 2008). The eastern branch of the MPC occurs in the middle of a large elongated migmatitic complex that probably formed during diapir-like upwelling in the front of the underthrusting Brunia indenter (Verner et al. 2014).

### *VI — Post-tectonic tonalite–granite plutons (I)*

The late medium-grained (Amp–) Bt tonalites to granites (e.g., ~316–315 Ma Altenberg and Mauthausen, ~310–300 Ma Freistadt — Gerdes et al. 2003) intruded mostly the older granitoids of the Weinsberg suite in the southern MPC. These are metaluminous, high-K calc-alkaline rocks with CHUR-like Sr–Nd isotopic signatures that were interpreted in terms of partial melting of metatonalitic lower crust (Gerdes 1997).

## Concluding remarks

The so-far available Nd model ages and (scarce) U–Pb ages of inherited zircons indicate that the bulk of the Variscan granitoids in the Moldanubian Zone and at its

contact with TBU were generated from fertile Cadomian to Early Palaeozoic metasediments dominated by the Neoproterozoic arc and Eburnean (~2.1 Ga) basement-derived detritus. Variably important was a contribution from mantle, at the arc stage characterized by an evolution from CHUR-like to strongly enriched (yielding ultrapotassic magmas). This reflected probably the progressive contamination of the orogenic mantle by deeply subducted felsic crust of presumed Saxothuringian provenance.

**Acknowledgements:** The author is thankful to the organizers for invitation to present this review. D.R. Bowes, V. Erban, F. Finger, A. Gerdes, F.V. Holub†, J. Hora, J. Kočergina, T. Magna, M. René, G. Rogers, J. Trubač, K. Verner, S. Vrána†, J. Žák and many others are acknowledged for enlightening discussions and/or invaluable data. This research was supported by the GAČR project 18–24378S.

## References

- Barbarin B. 1999: A review of the relationships between granitoid types, their origins and their geodynamic environments. *Lithos* 46, 605–626.
- Becker H., Wenzel T. & Volker F. 1999: Geochemistry of glimmerite veins in peridotites from Lower Austria — implications for the origin of K-rich magmas in collision zones. *J. Petrol.* 40, 315–338.
- Breiter K. 2010: Geochemical classification of Variscan granitoids in the Moldanubicum (Czech Republic, Austria). *Abh. Geol. B.–A.* 65, 19–25.
- Chappell B.W. & White A.J.R. 1974: Two contrasting granite types. *Pacific Geol.* 8, 173–174.
- Dörr W. & Zulauf G. 2010: Elevator tectonics and orogenic collapse of a Tibetan-style plateau in the European Variscides: the role of the Bohemian shear zone. *Int. J. Earth Sci.* 99, 299–325.
- Faryad S.W. & Kachlík V. 2013: New evidence of blueschist facies rocks and their geotectonic implication for Variscan suture(s) in the Bohemian Massif. *J. Metamorph. Geol.* 31, 63–82.
- Finger F., Gerdes A., Janoušek V., René M. & Riegler G. 2007: Resolving the Variscan evolution of the Moldanubian sector of the Bohemian Massif: the significance of the Bavarian and the Moravo–Moldanubian tectonometamorphic phases. *J. Geosci.* 52, 9–28.
- Franke W. 2000: The mid-European segment of the Variscides: tectonostratigraphic units, terrane boundaries and plate tectonic evolution. In: Franke W., Haak V., Oncken O. & Tanner D. (Eds.): *Orogenic Processes: Quantification and Modelling in the Variscan Belt*. *Geol. Soc. London Spec. Pub.* 179, 35–61.
- Friedl G., von Quadt A., Ochsner A. & Finger F. 1993: Timing of the Variscan Orogeny in the southern Bohemian Massif (NE-Austria) deduced from new U–Pb zircon and monazite dating. *Terra Abstracts* 5, 235–236.
- Friedl G., von Quadt A. & Finger F. 1996: Timing der Intrusionstätigkeit im Südböhmischen Batholith. Symposium, Tektonik–Strukturgeologie–Kristallingeologie, Salzburg, 10–15 April 1996, book of abstracts. *Fakultas Universitätsverlag*, Vienna, 127–130.
- Gerdes A. 1997: Geochemische und thermische Modelle zur Frage der spätorogenen Granitgenese am Beispiel des Südböhmischen Batholiths: Basaltisches Underplating oder Krustenstapelung? *Unpublished PhD. thesis, Georg-August-Universität, Göttingen*, 1–113.
- Gerdes A. 2001: Magma homogenization during anatexis, ascent and/or emplacement? Constraints from the Variscan Weinsberg granites. *Terra Nova* 13, 305–312.
- Gerdes A., Wörner G. & Finger F. 2000: Hybrids, magma mixing and enriched mantle melts in post-collisional Variscan granitoids: the Rastenberg Pluton, Austria. In: Franke W., Haak V., Oncken O. & Tanner D. (Eds.): *Orogenic Processes: Quantification and Modelling in the Variscan Fold Belt*. *Geol. Soc. London Spec. Pub.* 179, 415–431.
- Gerdes A., Friedl G., Parrish R.R. & Finger F. 2003: High-resolution geochronology of Variscan granite emplacement – the South Bohemian Batholith. *J. Czech Geol. Soc.* 48, 53–54.
- Holub F.V. 1997: Ultrapotassic plutonic rocks of the durbachite series in the Bohemian Massif: petrology, geochemistry and petrogenetic interpretation. *Sbor. geol. Věd, ložisk. Geol. Mineral.* 31, 5–26.
- Janoušek V. & Holub F.V. 2007: The causal link between HP–HT metamorphism and ultrapotassic magmatism in collisional orogens: case study from the Moldanubian Zone of the Bohemian Massif. *Proc. Geol. Assoc.* 118, 75–86.
- Janoušek V., Rogers G. & Bowes D.R. 1995: Sr–Nd isotopic constraints on the petrogenesis of the Central Bohemian Pluton, Czech Republic. *Geol. Rundsch.* 84, 520–534.
- Janoušek V., Bowes D.R., Braithwaite C.J.R. & Rogers G. 2000: Microstructural and mineralogical evidence for limited involvement of magma mixing in the petrogenesis of a Hercynian high-K calc-alkaline intrusion: the Kozárovce granodiorite, Central Bohemian Pluton, Czech Republic. *Trans. Roy. Soc. Edinb., Earth Sci.* 91, 15–26.
- Janoušek V., Braithwaite C.J.R., Bowes D.R. & Gerdes A. 2004a: Magma-mixing in the genesis of Hercynian calc-alkaline granitoids: an integrated petrographic and geochemical study of the Sázava intrusion, Central Bohemian Pluton, Czech Republic. *Lithos* 78, 67–99.
- Janoušek V., Finger F., Roberts M.P., Frýda J., Pin C. & Dolejš D. 2004b: Deciphering the petrogenesis of deeply buried granites: whole-rock geochemical constraints on the origin of largely undepleted felsic granulites from the Moldanubian Zone of the Bohemian Massif. *Trans. Roy. Soc. Edinb., Earth Sci.* 95, 141–159.
- Janoušek V., Wiegand B. & Žák J. 2010: Dating the onset of Variscan crustal exhumation in the core of the Bohemian Massif: new U–Pb single zircon ages from the high-K calc-alkaline granodiorites of the Blatná suite, Central Bohemian Plutonic Complex. *J. Geol. Soc.* 167, 347–360.
- Janoušek V., Trubač J., Dörr W., Gerdes A., Moyen J.F., Žák J. & Matějka D. 2015: Extensive post-collisional melting in a mid-crustal gneiss dome — case of the Variscan Melechov Pluton, Moldanubian Batholith. *Goldsch. Abstr.* 1421.
- Janoušek V., Holub F.V., Verner K., Čopjaková R., Gerdes A., Hora J. M., Košler J. & Tyrrell S. 2019: Two-pyroxene syenitoids from the Moldanubian Zone of the Bohemian Massif: peculiar magmas derived from a strongly enriched lithospheric mantle source. *Lithos* 342–343, 239–262.
- Košler J., Aftalion M. & Bowes D.R. 1993: Mid-late Devonian plutonic activity in the Bohemian Massif: U–Pb zircon isotopic evidence from the Staré Sedlo and Mirovice gneiss complexes, Czech Republic. *Neu. Jb. Mineral., Mh.* 1993, 417–431.
- Kotková J. & Harley S.L. 2010: Anatexis during high-pressure crustal metamorphism: evidence from garnet–whole-rock REE

- relationships and zircon–rutile Ti–Zr thermometry in leucogranulites from the Bohemian Massif. *J. Petrol.* 51, 1967–2001.
- Kotková J., O'Brien P.J. & Ziemann M.A. 2011: Diamond and coesite discovered in Saxony-type granulite: solution to the Variscan garnet peridotite enigma. *Geology* 39, 667–670.
- Kotková J., Schaltegger U. & Leichmann J. 2010: Two types of ultrapotassic plutonic rocks in the Bohemian Massif — coeval intrusions at different crustal levels. *Lithos* 115, 163–176.
- Kroner U. & Romer R.L. 2013: Two plates — many subduction zones: the Variscan Orogeny reconsidered. *Gondwana Res.* 24, 298–329.
- Kubínová Š., Faryad S.W., Verner K., Schmitz M.D. & Holub F.V. 2017: Ultrapotassic dykes in the Moldanubian Zone and their significance for understanding of the post-collisional mantle dynamics during Variscan Orogeny in the Bohemian Massif. *Lithos* 272–273, 205–221.
- Kusbach V., Janoušek V., Hasalová P., Schulmann K., Fanning C.M., Erban V. & Ulrich S. 2015: Importance of crustal relaxation in origin of the orogenic mantle peridotite–high-pressure granulite association: example from the Náměšť Granulite Massif (Bohemian Massif, Czech Republic). *J. Geol. Soc.* 172, 479–490.
- Liew T.C., Finger F. & Höck V. 1989: The Moldanubian granitoid plutons in Austria: chemical and isotopic studies bearing on their environmental setting. *Chem. Geol.* 76, 41–55.
- Maierová P., Lexa O., Schulmann K. & Štípská P. 2014: Contrasting tectono-metamorphic evolution of orogenic lower crust in the Bohemian Massif: a numerical model. *Gondwana Res.* 25, 509–521.
- Massonne H.J. 2001: First find of coesite in the ultrahigh-pressure metamorphic area of the central Erzgebirge, Germany. *Eur. J. Mineral.* 13, 565–570.
- Matějka D. & Janoušek V. 1998: Whole-rock geochemistry and petrogenesis of granites from the northern part of the Moldanubian Batholith (Czech Republic). *Acta Univ. Carol., Geol.* 42, 73–79.
- O'Brien P.J. 2000: The fundamental Variscan problem: high-temperature metamorphism at different depths and high-pressure metamorphism at different temperatures. In: Franke W., Haak V., Oncken O. & Tanner D. (Eds.): *Orogenic Processes: Quantification and Modelling in the Variscan Belt*. *Geol. Soc. London Spec. Pub.* 179, 369–386.
- O'Brien P.J. & Rötzler J. 2003: High-pressure granulites: formation, recovery of peak conditions and implications for tectonics. *J. Metamorph. Geol.* 21, 3–20.
- Perraki M. & Faryad S.W. 2014: First finding of microdiamond, coesite and other UHP phases in felsic granulites in the Moldanubian Zone: implications for deep subduction and a revised geodynamic model for Variscan Orogeny in the Bohemian Massif. *Lithos* 202–203, 157–166.
- René M., Holtz F., Luo C., Beermann O. & Stelling J. 2008: Biotite stability in peraluminous granitic melts: compositional dependence and application to the generation of two-mica granites in the South Bohemian batholith (Bohemian Massif, Czech Republic). *Lithos* 102, 538–553.
- Schmädicke E., Gose J. & Will T.M. 2010: The P–T evolution of ultrahigh temperature garnet-bearing ultramafic rocks from the Saxonian Granulitgebirge Core Complex, Bohemian Massif. *J. Metamorph. Geol.* 28, 489–508.
- Schulmann K., Konopásek J., Janoušek V., Lexa O., Lardeaux J.M., Edel J.B., Štípská P. & Ulrich S. 2009: An Andean type Palaeozoic convergence in the Bohemian Massif. *C. R. Geosci.* 341, 266–286.
- Schulmann K., Lexa O., Janoušek V., Lardeaux J.M. & Edel J.B. 2014: Anatomy of a diffuse cryptic suture zone: an example from the Bohemian Massif, European Variscides. *Geology* 42, 275–278.
- Trubač J., Janoušek V., Žák J., Somr M., Kabele P., Švancara J., Gerdes A. & Žáčková E. 2017: Origin of reverse compositional and textural zoning in granite plutons by localized thermal overturn of stratified magma chambers. *Lithos* 277, 315–336.
- Venera Z., Schulmann K. & Kröner A. 2000: Intrusion within a transtensional tectonic domain: the Čistá granodiorite (Bohemian Massif) — structure and rheological modelling. *J. Struct. Geol.* 22, 1437–1454.
- Verner K., Žák J., Šrámek J., Paclíková J., Zavřelová A., Machek M., Finger F. & Johnson K. 2014: Formation of elongated granite–migmatite domes as isostatic accommodation structures in collisional orogens. *J. Geodyn.* 73, 100–117.
- Vrána S., Janoušek V. & Franěk J. 2013: Contrasting mafic to felsic HP–HT granulites of the Blanský les Massif (Moldanubian Zone of southern Bohemia): complexity of mineral assemblages and metamorphic reactions. *J. Geosci.* 58, 347–378.
- Wenzel T., Mertz D.F., Oberhänsli R., Becker T. & Renne P.R. 1997: Age, geodynamic setting, and mantle enrichment processes of a K-rich intrusion from the Meissen Massif (northern Bohemian Massif) and implications for related occurrences from the mid-European Hercynian. *Geol. Rundsch.* 86, 556–570.
- Žák J., Holub F.V. & Verner K. 2005: Tectonic evolution of a continental magmatic arc from transpression in the upper crust to exhumation of mid-crustal orogenic root recorded by episodically emplaced plutons: the Central Bohemian Plutonic Complex (Bohemian Massif). *Int. J. Earth Sci.* 94, 385–400.
- Žák J., Kratinová Z., Trubač J., Janoušek V., Sláma J. & Mrlina J. 2011a: Structure, emplacement, and tectonic setting of Late Devonian granitoid plutons in the Teplá–Barrandian Unit, Bohemian Massif. *Int. J. Earth Sci.* 100, 1477–1495.
- Žák J., Verner K., Finger F., Faryad S.W., Chlupáčová M. & Veselovský F. 2011b: The generation of voluminous S-type granites in the Moldanubian Unit, Bohemian Massif, by rapid isothermal exhumation of the metapelitic middle crust. *Lithos* 121, 25–40.
- Žák J., Verner K., Holub F.V., Kabele P., Chlupáčová M. & Halodová P. 2012: Magmatic to solid state fabrics in syntectonic granitoids recording early Carboniferous orogenic collapse in the Bohemian Massif. *J. Struct. Geol.* 36, 27–42.
- Žák J., Verner K., Janoušek V., Holub F.V., Kachlík V., Finger F., Hajná J., Tomek F., Vondrovic L. & Trubač J. 2014: A plate-tectonic model for the assembly of the Bohemian Massif constrained by structural relationships around granitoid plutons. In: Schulmann K., Martínez Catalán J.R., Lardeaux J.M., Janoušek V. & Oggiano G. (Eds.): *The Variscan Orogeny: Extent, Timescale and the Formation of the European Crust*. *Geol. Soc. London Spec. Pub.* 405, 169–196.

# How long does it take to make a giant porphyry copper deposit? Advances in high-precision geochronology and modelling of magmatic–hydrothermal processes

ALBRECHT VON QUADT<sup>1</sup>, SIMON J.E. LARGE<sup>2</sup>, YANNICK BURET<sup>2</sup>,  
IRENA PEYTCHEVA<sup>1,3</sup> and CHRISTOPH A. HEINRICH<sup>1</sup>

<sup>1</sup>ETH Zurich, Dept. Earth Sciences, Switzerland; vonquadt@erdw.ethz.ch

<sup>2</sup>Natural History Museum, London, United Kingdom

<sup>3</sup>Bulgarian Academy of Science, Geological Institute, Sofia, Bulgaria

## Introduction

Porphyry copper deposits are characterized by multiple phases of magma emplacement alternating with hydrothermal veining, alteration and copper deposition. This geological complexity has contributed to the notion that the formation of the best deposits is a complex process drawn out over an extended time period. Combining the most precise geochronological constraints with microchemical evidence from zircon concur with physical models that the formation of even the biggest deposits is a rapid process lasting a few 10<sup>4</sup>–10<sup>5</sup> years.

and efficiency of data gathering (by LA-ICPMS). Single crystals of magmatic zircon preserve a record of crystallization age and trace-element content (Szymanowski et al. 2017). Samples of igneous rock typically contain zircon populations with resolvable variations in age and degree of chemical differentiation preceding emplacement and final solidification of the sample. Assuming that the youngest zircon crystals in successively emplaced pre-, inter- and post-mineralization porphyries date the time of emplacement, reliable age brackets on vein and sulfide mineralization ages have been obtained.

## Methods

A workflow of field documentation, zircon petrography using SEM-CL imaging, LA-ICPMS microchemistry including Hf isotopes, and final recovery of the same crystals for chemical-abrasion isotope-dilution thermal-ionization mass spectrometry (CA-ID-TIMS) provides time calibrated information about the evolution of mineralizing magma chambers. These data may be complemented by Re–Os geochronology of molybdenite, whereas in-situ LA-ICPMS U–Pb geochronology and Ar–Ar dating are useful for regional age determination but not for measuring the duration of deposit formation.

## Petrochronology

Zircon petrochronology (the combination of U–Pb geochronology with the trace-element geochemistry of zircons, including the estimation of crystallization temperatures from trace-level Ti in solid solution has experienced huge progress over the last decade with regard to analytical precision, accuracy (notably by CA-ID-TIMS)

## Results and discussion

Combining the most decisive case studies carried out at different scales and locations, four major conclusions regarding magma evolution and time scales in porphyry-mineralizing magmatic systems have emerged (Ok Tedi, Papua New Guinea; Koloula, Solomon Island; Batu Hijau, Indonesia; Bajo de la Alumbrera, Argentina; Large et al. 2018; Tapster et al. 2016; Buret et al. 2016, 2017).

(1) The magmatic history of ore-producing districts, typically kilometers to tens of kilometers in scale, is long-lived and typically evolves magma emplacement over several millions of years or more. This long-lived magmatism is driven by lower-crustal magmatic differentiation, fractional crystallization and crustal assimilation, enhancing the initial volatile content of mantle melts. Extrusive volcanism typically stops before porphyry ore formation, but major eruptions may immediately follow and possibly terminate the process of porphyry copper ore formation by catastrophic magma and volatile release.

(2) Hydrothermal ore emplacement in quartz vein stockworks, cutting typically composite porphyry

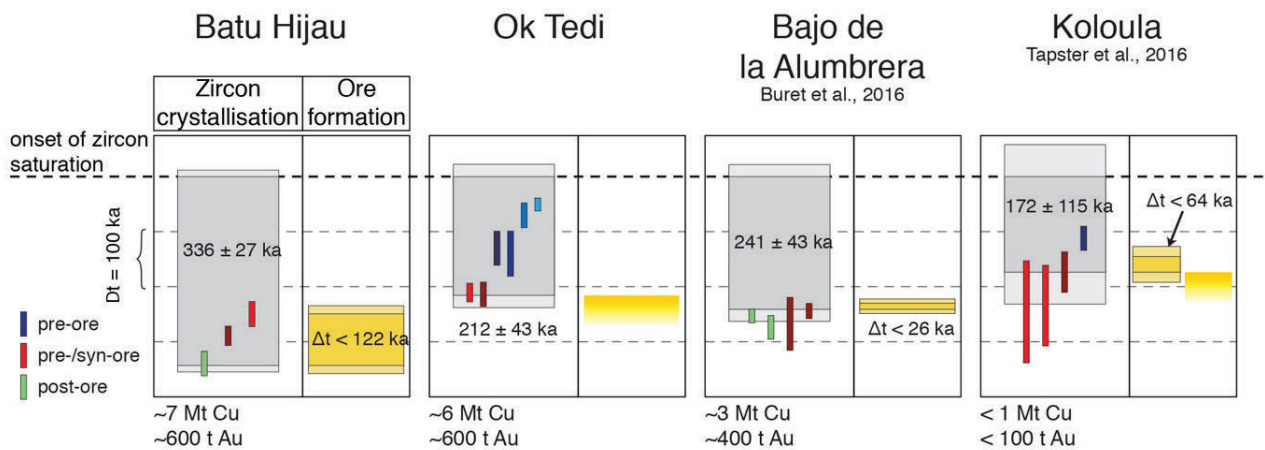


**Fig. 1.** Summary data comparing deposits of different size, Batu Hijau (Indonesia), Ok Tedi (Papua New Guinea; Large et al. 2018), Bajo de la Alumbraera (Argentina) and Koloula (Solomon Island).

stocks, is bracketed that this process extends over 10'000 to 100'000 years for world-class to giant ore, but not millions of years, by multiple pulses of alternating porphyry emplacement and vein formation documented by contact intersections in the field.

(3) Zircon trace-element compositions show that successive porphyries in a stock are derived from the same magma source and follow a common trend of fractional crystallisation of plagioclase, amphibole and titanite.

(4) Results are consistent with the interpretation that a single upper-crustal magma reservoir at 5–10 km depth acts as the source of fluid making one ore deposit. Antecrysts with geochemical signatures recording upper-crustal fractionation indicate life-times of large crystallizing magma chambers in the upper crust lasting several 100'000 years.

### Summary

In summary, economic porphyry copper deposits are not assisted by complexity or by extended duration of superimposed processes. Rather, the largest and richest deposits result from fine-tuning the balance of concurrent processes of fluid production, fluid focussing and heat transfer from the magmatic fluid plume to convecting meteoric water. The thermal lifetime of large upper crustal magma reservoirs as the source of ore fluids and all ore forming components typically lasts a few hundred thousand years, determined by the rate of cooling

of the magma chamber. The duration of one or several events of porphyry emplacement and hydrothermal Au–Cu mineralization is much shorter, spanning a range of tens of thousands of years in total, with even shorter durations of individual magma and fluid pulses determined by the rate of fluid extraction from the magma chamber.

### References

- Buret Y., von Quadt A., Heinrich C.A., Selby D., Wälle M. & Peytcheva I. 2016: From a long-lived upper-crustal magma chamber to rapid porphyry copper emplacement: Reading the geochemistry of zircon crystals at Bajo de la Alumbraera (NW Argentina). *Earth Planet. Sci. Lett.* 450, 120–131.
- Buret Y., Wotzlaw J.F., Roozen St., Guillong M., von Quadt A. & Heinrich C.A. 2017: Zircon petro-chronological evidence for a plutonic-volcanic connection in porphyry copper deposits. *Geology* 45, 7, 1–4, Data Repository item 2017203, doi:10.1130/G38994.1
- Large S.J.E., von Quadt A., Wotzlaw J.F., Guillong M. & Heinrich C.A. 2018: Magma Evolution Leading to Porphyry Au–Cu Mineralization at the Ok Tedi Deposit, Papua New Guinea: Trace Element Geochemistry and High-Precision Geochronology of Igneous Zircon. *Econ. Geol.* 113, 39–61.
- Szymanowski D., Wotzlaw J.-F., Ellis B., Bachmann O., Guillong M. & von Quadt A. 2017: Protracted low-temperature storage of supereruptive magma reservoirs. *Nature Geoscience* 10, doi: 10.1038/NGEO3020.
- Tapster S., Condon D.J., Naden J., Noble S.R., Petterson M.G., Roberts N.M.W., Saunders A.D. & Smith D.J. 2016: Rapid thermal rejuvenation of high-crystallinity magma linked to porphyry copper deposit formation; evidence from the Koloula Porphyry Prospect, Solomon Islands. *Earth Planet. Sci. Lett.* 442, 206–217.

# The influence of cationic partitioning among crystallographic sites based on bond-valence constraints and the genetic environment geochemistry on the composition of tourmaline-supergroup minerals

PETER BAČÍK<sup>1,2</sup>

<sup>1</sup>Comenius University in Bratislava, Faculty of Natural Sciences, Department of Mineralogy and Petrology, Ilkovičova 6, 842 15 Bratislava, Slovakia; peter.bacik@uniba.sk

<sup>2</sup>Earth Science Institute of the Slovak Academy of Sciences, Dúbravská cesta 9, 840 05 Bratislava, Slovakia

**Abstract:** Theoretical bond-length calculation from ideal bond valences for each ion and coordination can predict ion site preference in the structure. It revealed that the *B*-site occupancy is strictly limited to  $B^{3+}$ , *T* site can freely accommodate  $Si^{4+}$  and  $Be^{2+}$ ,  $B^{3+}$  and  $Al^{3+}$  substitution requires compression or expansion of  $TO_4$  tetrahedron. Proper bond lengths for octahedral sites were calculated for  $Al^{3+}$  (*Z*-site preference),  $Ti^{4+}$ ,  $Mn^{3+}$ ,  $Ga^{3+}$ ,  $V^{3+}$ ,  $Fe^{3+}$  (mixed preference),  $Mg^{2+}$ ,  $Fe^{2+}$ ,  $Li^+$ ,  $Mn^{2+}$ ,  $Ni^{2+}$ ,  $Zn^{2+}$ ,  $Cu^{2+}$ ,  $Sc^{3+}$  and  $Zr^{4+}$  (*Y*-site preference). Another group of cations including  $U^{4+}$ ,  $Th^{4+}$ ,  $Y^{3+}$ , lanthanoids from  $Tb^{3+}$  to  $Lu^{3+}$  and  $Ce^{4+}$  have significantly longer bonds than typical *Y*-O but form too short bonds for the *X* site. Therefore, they probably prefer octahedron. The usual empirical bond length for the *X* site is met with  $Na^+$ ,  $Ca^{2+}$ ,  $Sr^{2+}$ ,  $Pb^{2+}$  and lanthanoids from  $La^{3+}$  to  $Gd^{3+}$ , while  $K^+$ ,  $Rb^+$  and  $Cs^+$  are too big. However, the tourmaline composition results from interaction of structure with the genetic environment. The proportion of REE,  $U^{4+}$  and  $Th^{4+}$  in tourmaline is structurally limited, while e.g.  $Zr^{4+}$ ,  $Sc^{3+}$ ,  $Sr^{2+}$ ,  $Pb^{2+}$  have only geochemical limits with no obvious structural constraints. Moreover, environmental properties such as pressure or specific local structural arrangements can overcome structural constraints.

## Introduction

Tourmaline supergroup minerals belong to cyclosilicates with a relatively complex structure. It contains 5 different cationic crystallographic sites at different coordination – one tetrahedral *T* site, two octahedral *Z* and *Y* sites, polyhedral *X* site, triangular *B* site, and 8 different anionic sites — O1–O8 (Donnay & Buerger 1950). This structural complexity results in large variability of chemical elements which can be incorporated in the tourmaline structure. The major elements include small Si and B, slightly larger Al, Mg, Fe, Li, Mn, Cr, V, and Ti, and also the largest Na, Ca and K. Anionic sites comprise dominant O (as  $O^{2-}$  and  $OH^-$  anions) and minor F (Henry et al. 2011). However, many other elements can occupy tourmaline structure in minor to trace amounts.

Although the site occupancy usually follows Goldschmidt rules, local structural and bond-valence requirements may result in various disorder. Moreover, the tourmaline structure can accommodate cations which usually should be improper for specific structural site. Although it is usually not possible to analytically determine the position of each ion, mainly for trace elements,

some predictions can be made based on bond-valence constraints for each ion at each site. Bond lengths can be derived from structural data, but it can be applied only on ions which are abundant in the structure. However, theoretical bond-length calculation from ideal bond valences for each ion with various coordination can predict the ion site preference in the structure. It could also help to identify internal crystal-chemical and external genetical and geochemical factors influencing tourmaline composition.

## Topology of tourmaline crystal structure

Tourmaline group minerals has a relatively complex structure. The main structural element is built from the 3D framework of edge-connected  $ZO_6$  octahedra, interconnected by regularly distributed structural “islands”. These comprise six-member rings of  $TO_4$  tetrahedra, triplets of  $YO_6$  octahedra, large 9-coordinated *X* sites and  $BO_3$  triangles (Bosi 2017). Chains of  $ZO_6$  octahedra are oriented in the *c* direction and provide support for the structure but also sufficient flexibility for any local or long-distance structural distortion.

Moreover, their direction manifests in long-prismatic tourmaline crystal habitus (Bačík et al. 2015a).

### Site occupancy based on bond-valence constraints

#### *TO<sub>4</sub> tetrahedron*

The most prominent feature of the tourmaline structure, which defines it as cyclosilicate, is represented by the ring of six *TO<sub>4</sub>* tetrahedra, which are connected by the pairs of O<sup>2-</sup> anions. The apical atoms O (O6) are directed to the same (–c) pole of crystal (Donnay & Buerger 1950). Each *TO<sub>4</sub>* tetrahedron shares O anions with the *X* (2×), *Y* and *Z* (2×) sites.

The most abundant cation at the *T* site is Si<sup>4+</sup>. The calculated Si–O distance of 1.624 Å is very similar to the empirical bond length of 1.621 Å. There are two typical substituents for Si<sup>4+</sup> — Al<sup>3+</sup> and B<sup>3+</sup>. Tetrahedral Al have longer bonds (1.746 Å) and B shorter bonds (1.475 Å calculated, 1.482 Å empirical) than Si<sup>4+</sup>. Consequently, B<sup>3+</sup> causes compression and Al<sup>3+</sup> expansion of tetrahedron. If any Be<sup>2+</sup> is present in tourmaline structure, it likely prefers the *T* site with 1.635 Å calculated bond length. Other cations form very long bonds (Ti<sup>4+</sup> 1.819 Å, Fe<sup>3+</sup> 1.870 Å), therefore, their presence at the *T* site is unlikely.

#### *BO<sub>3</sub> site*

Triangular BO<sub>3</sub> groups lie parallel to the (0001) plane and connect to the vertices of ZO<sub>6</sub> and YO<sub>6</sub> octahedra. The BO<sub>3</sub> group shares O with *Z* (2×), *Y* (2×), and *X* (3×) sites.

Boron is the only cation occupying the B site. The calculated B–O bond length of 1.372 Å is similar to empirical average bond length. This indicates that B–O bond length in tourmaline is almost ideal allowing only minute variations. Other possible cations have much larger calculated bond lengths (Si<sup>4+</sup> 1.512 Å, Be<sup>2+</sup> 1.594 Å) excluding their possible substitution.

The presence of vacancies at *B* site was presumed but with no spectroscopic or structural evidence (Grice & Ercit 1993; Hawthorne 1996). Substitution mechanism that would result in vacancies at *B* produces unacceptably short H–*Y* and H–*Z* distances (Hawthorne 1996).

#### *ZO<sub>6</sub> and YO<sub>6</sub> octahedron*

The rings of tetrahedra are connected to two types of octahedra — ZO<sub>6</sub> and YO<sub>6</sub>, which combined form brucite

layer. The ZO<sub>6</sub> octahedron is smaller than YO<sub>6</sub> octahedron and is more distorted. It is connected to the *T* (3×), *Y* (2×), and *B* (2×) sites. The *Y* site is relatively regular octahedron with larger size than *Z*. The YO<sub>6</sub> octahedron is connected by O atoms with *X* (2×), *T* (2×), *Z* (3×), and *B* (2×) sites.

The *Z* site is usually dominated by Al<sup>3+</sup> with calculated Al–O bond length of 1.904 Å and empirical distance of 1.868 Å. Smaller empirical bond length results from angular and bond-length distortion of the ZO<sub>6</sub> octahedron. Smaller bond lengths were calculated only for Si<sup>4+</sup> (1.782 Å) and Be<sup>2+</sup> (1.755 Å) which were never evidenced in octahedral coordination in tourmaline. All other cations have larger octahedral bond lengths; Ti<sup>4+</sup>, Mn<sup>3+</sup>, Ga<sup>3+</sup> and Cr<sup>3+</sup> below 2.00 Å, V<sup>3+</sup> and Fe<sup>3+</sup> slightly larger than 2.00 Å, Mg<sup>2+</sup>, Fe<sup>2+</sup>, Li<sup>+</sup>, Mn<sup>2+</sup>, Ni<sup>2+</sup>, Zn<sup>2+</sup>, Cu<sup>2+</sup>, Sc<sup>3+</sup> and Zr<sup>4+</sup> between 2.09 and 2.20 Å. These are proper values for the *Y* site in tourmaline evidenced in comparison to empirical data. Empirical bond lengths are always smaller due to octahedral distortions influencing bond valences in real structure.

The last group of cations which could occupy octahedral sites include cations with bond lengths between 2.20 and 2.30 Å. These are usually only in trace amounts and include U<sup>4+</sup>, Th<sup>4+</sup>, Y<sup>3+</sup> and lanthanoids from Tb to Lu (HREE). Moreover, Ce<sup>4+</sup> has bond length of 2.217 Å. These cations are not excluded but their proportion is very limited and would cause large distortion of the YO<sub>6</sub> octahedra, if present. Those with bond length larger than 2.30 Å (LREE from La<sup>3+</sup> to Gd<sup>3+</sup>, Pb<sup>4+</sup>) are highly unlikely to occupy octahedra in tourmaline.

#### *XO<sub>9</sub> polyhedron*

The *X* site with coordination number of 9 is the trigonal antiprism located along threefold symmetry axis. The XO<sub>9</sub> polyhedron is connected through O atoms to *T* (6×), *Y* (3×), and *B* (3×) sites.

Based on the empirical data, the bond lengths at this site varies between 2.609 (Ca<sup>2+</sup>) and 2.692 (Na<sup>+</sup>). This can be considered the “Goldilocks zone” (similar to astronomical term, the zone of structurally stable bond lengths with minimal induced distortion) of the *X* site; cations with larger or smaller bond lengths have a limited occupancy. The perfect match with the “Goldilocks” bond lengths was calculated for Na<sup>+</sup> (2.618 Å), Sr<sup>2+</sup> (2.678 Å) and Pb<sup>2+</sup> (2.697 Å). The calculated Ca–O bond length of 2.522 Å is, similarly to Na–O, significantly shorter than empirical. This results from the contraction of neighbouring octahedral Y–O bonds leaving smaller bond valence for the *X*-site cations.

Other monovalent cations including  $K^+$ ,  $Rb^+$  and  $Cs^+$  have much larger bond lengths ( $>2.90 \text{ \AA}$ ) limiting their presence at tourmaline structure almost entirely. Barium has also relatively large bond length ( $2.834 \text{ \AA}$ ). In contrast,  $U^{4+}$ ,  $Th^{4+}$ ,  $Y^{3+}$ , lanthanoids from  $Tb^{3+}$  to  $Lu^{3+}$  (HREE) and  $Ce^{4+}$  have significantly smaller bond lengths ( $<2.45 \text{ \AA}$ ), probably too small for the  $X$  site. Only trivalent lanthanoids from  $La^{3+}$  to  $Gd^{3+}$  with bond lengths similar to  $Ca^+$  are likely occupying the  $X$  site.

### Crystal chemistry vs. genetic environment

For the understanding crystal-chemical properties and prediction of the site occupancy and substitutions in any mineral, Goldschmidt rules are usually used. However, the bond-length calculation provides a few advantages. It can be used for various coordination and cation charges very flexibly, only requiring a proper calculation of the bond valence. Moreover, it can be easily compared to empirical analytical data from structural refinement as evidenced here.

For every structural site, the “Goldilocks zone” of bond lengths can be assumed. This defines the range of bond length, which does not induce large structural tension and distortion. It is quite narrow in small sites such as  $B$  and  $T$  in tourmaline, but larger in sites with higher coordination number. This is one of limits for the site occupancy. Cations with larger deviation from the “Goldilocks zone” can still be accommodated at the respective site but their substitution is limited. This is the case of  $Al$  and  $B$  at  $T$  site — they substitute for  $Si$  but only in a limited proportion. Similarly, the proportion of REE in tourmaline is limited, although these can be abundant in the environment. It results from the deviation from the “Goldilocks zone” for both  $X$  and  $Y$  site and also relatively high charge for the  $X$  site. However, based on the present data, if present, REE likely divide between the  $Y$  (HREE) and  $X$  (LREE) site.

In contrast, some cations are straight in the “Goldilocks zone” but are usually absent or only in trace amounts. This can be only explained by external geochemical properties of the genetic environment. Such elements can be fractionated into different minerals with better structural properties for their accommodation. This is the case of  $Be^{2+}$  at  $T$  site, which, due to small charge, prefers other minerals such as beryl, chrysoberyl, etc. Some other elements are usually only in trace amounts in tourmaline environment or are already bound in other minerals —  $Zr^{4+}$ ,  $Sn^{4+}$ ,  $Sc^{3+}$ ,  $Zn^{2+}$ ,  $Ni^{2+}$ ,  $Sr^{2+}$ . However,

some of these can accumulate in tourmaline in specific conditions although usually also only in trace amounts —  $Cr^{3+}$ ,  $V^{3+}$ ,  $Cu^{2+}$ , and  $Pb^{2+}$ .

However, elasticity of the tourmaline structure can allow incorporation of elements from the outside of the “Goldilocks zone”. The compression of the tourmaline structure at UHP conditions allowed the incorporation of  $K$  into the structure of maruyamaite (Hawthorne et al. 2016). However,  $K$  can be introduced at the  $X$  site also in  $Fe^{3+}$ -rich tourmalines with properly expanded structure (Žáček et al. 2000). In contrast,  $Al$ -rich environment in Detva-Biely vrch deposit resulted in composition with high proportion of  $VO^{2-}$ . This resulted in the compression of  $Y-O$  bond and subsequent incorporation of the disproportionately large  $Cl^-$  anion at  $W$  site (Bačík et al. 2015b). And although never observed in natural samples or in experiments, octahedral  $Si$  at  $Z$  site could be present in tourmaline at UHP conditions (Broska et al. 2019).

However, there is a limit for a simple bond-length prediction of the site preference because the local and long-distance structural requirements also influence the cationic distribution. It is manifested in various cationic disorder reactions at octahedral sites. Along with the  $Al-Mg$  disorder (Hawthorne et al. 1993), the  $Cr$  and  $V$  disorder between  $Y$  and  $Z$  sites was documented (Bosi et al. 2004, 2017; Cempírek et al. 2013). These were explained by several external factors: the  $Fe/(Fe+Mg)$  ratio (Grice & Ercit 1993), influence of the  $X$ -site occupancy (Ertl et al. 2010a), structural deformations (Foit 1989; Bosi & Lucchesi 2007), pressure (Ertl et al. 2010b) and temperature (Bosi 2011). However, none of them was proved to be decisive. Nevertheless, more complex bond-valence calculations have shown possible mechanisms allowing disorder (Bačík 2015, 2018).

**Acknowledgement:** This work was supported by the Slovak Research and Development Agency under the Contract no. APVV-18-0065

### References

- Bačík P. 2015: Cation ordering in octahedral sites in tourmalines of schorl-dravite series. *Can. Mineral.* 53, 571–590.
- Bačík P. 2018: The crystal-chemical autopsy of octahedral sites in Na-dominant tourmalines: octahedral metrics model unconstrained by the  $Y$ ,  $Z$ -site disorder assignment. *J. Geosci.* 63, 137–154.
- Bačík P., Ertl A., Števkó M., Sečkář P. & Giester G. 2015a: Acicular zoned tourmaline (magnesi-foitite to foitite) from a quartz vein near Tisovec, Slovakia: The relationship between crystal chemistry and acicular habitus. *Can. Mineral.* 53, 221–234.

- Bačík P., Koděra P., Uher P., Ozdín D. & Jánošík M. 2015b: Chlorine-enriched tourmalines in hydrothermally altered diorite porphyry from the Detva, Biely Vrch porphyry gold deposit (Slovakia). *Can. Mineral.* 53, 673–691.
- Bosi F. 2011: Stereochemical constraints in tourmaline: from a short-range to a long-range structure. *Can. Mineral.* 49, 17–27.
- Bosi F. 2017: Tourmaline structure and crystal chemistry. In: Tourmaline 2017. International symposium. Book of abstracts, 12–13.
- Bosi F. & Lucchesi S. 2007: Crystal chemical relationships in the tourmaline group: Structural constraints on chemical variability. *Am. Mineral.* 92, 1050–1063.
- Bosi F., Lucchesi S. & Reznitskii L. 2004: Crystal chemistry of the dravite-chromdravite series. *Eur. J. Mineral.* 16, 345–352.
- Bosi F., Reznitskii L., Hålenius U. & Skogby H. 2017: Crystal chemistry of Al–V–Cr oxy-tourmalines from Sludyanka complex, Lake Baikal, Russia. *Eur. J. Mineral.* 29, 457–472.
- Broska I., Bačík P., Kumar S., Janák M., Kurylo S., Filip J., Bazarník J. & Mikuš T. 2019: Myrmekitic intergrowth of tourmaline and quartz in eclogite-hosting gneisses of the Tso Moriri UHP metamorphic terrane (Eastern Ladakh, India). *Geol. Soc. London, Spec. Publ.* 481, <https://doi.org/10.1144/SP481-2017-167>.
- Cempírek J., Houzar S., Novák M., Groat L.A., Selway J.B. & Šrein V. 2013: Crystal structure and compositional evolution of vanadium-rich oxy dravite from graphite quartzite at Bítoványky, Czech Republic. *J. Geosci.* 58, 149–162.
- Donnay G. & Buerger M.J. 1950: The determination of the crystal structure of tourmaline. *Acta Cryst.* 3, 5–12.
- Ertl A., Mali H., Schuster R., Körner W., Hughes J.M., Brandstätter F. & Tillmanns E. 2010a: Li-bearing, disordered Mg-rich tourmalines from the pegmatite-marble contact from the Austroalpine basement units (Styria, Austria). *Mineral. Petrol.* 99, 89–104.
- Ertl A., Marschall H.R., Giester G., Henry D.J., Schertl H.-P., Ntaflos T., Luvizotto G.L., Nasdala L. & Tillmanns E. 2010b: Metamorphic ultra high-pressure tourmalines: Structure, chemistry, and correlations to PT conditions. *Am. Mineral.* 95, 1–10.
- Foit F.F. Jr. 1989: Crystal chemistry of alkali-deficient schorl and tourmaline structural relationships. *Am. Mineral.* 74, 422–431.
- Grice J.D. & Ercit T.S. 1993: Ordering of Fe and Mg in the tourmaline crystal structure: The correct formula. *Neues Jahrb. Miner. Abh.* 165, 245–266.
- Hawthorne F.C. 1996: Structural mechanisms for light-element variations in tourmaline. *Can. Mineral.* 34, 123–132.
- Hawthorne F.C., Macdonald D.J. & Burns P.C. 1993: Reassignment of cation site-occupancies in tourmaline: Al–Mg disorder in the crystal structure of dravite. *Am. Mineral.* 78, 265–270.
- Hawthorne F.C., Lussier A.J., Ball N.A., Henry D.J., Shimizu R., Ogasawara Y. & Ota T. 2016: Maruyamaite,  $K(\text{MgAl}_2)(\text{Al}_5\text{Mg})\text{Si}_6\text{O}_{18}(\text{BO}_3)_3(\text{OH})_3\text{O}$ , from the ultrahigh-pressure Kókchetav massif, northern Kazakhstan: Description and crystal structure. *Am. Mineral.* 101, 355–361.
- Henry D., Novák M., Hawthorne F.C., Ertl A., Dutrow B.L., Uher P. & Pezzotta F. 2011: Nomenclature of the tourmaline-super-group minerals. *Am. Mineral.* 96, 895–913.
- Žáček V., Frýda J., Petrov A. & Hyršl J. 2000: Tourmalines of the povondraite–(oxy)dravite series from the cap rock of meta-evaporite in Alto Chapare, Cochabamba, Bolivia. *J. Czech Geol. Soc.* 45, 3–12.

# Mylonitic Late Variscan granites from the central Balkan fold-thrust belt, Bulgaria

ELEONORA BALKANSKA<sup>1</sup>, IANKO GERDJIKOV<sup>1</sup>, STOYAN GEORGIEV<sup>2</sup>,  
ANNA LAZAROVA<sup>2</sup> and ALEXANDRE KOUNOV<sup>3</sup>

<sup>1</sup>Faculty of Geology and Geography, Sofia University, 1504 Sofia, Bulgaria; balkanska@gea.uni-sofia.bg

<sup>2</sup>Geological Institute, Bulgarian Academy of Sciences, 1113 Sofia, Bulgaria

<sup>3</sup>Department of Environmental Sciences, Basel University, 4056 Basel, Switzerland

**Abstract:** New structural and U–Pb zircon data from central Balkan fold-thrust belt reveal the existence of a zone of localized deformation confined mainly in the sheet-like Late Variscan Ambaritsa metagranites with crystallization age of  $307.8 \pm 3.9$  Ma. It is not well-established yet what were the relationships between the deformation and emplacement of the Ambaritsa intrusion. However, it could be suggested that both processes were tightly related and probably coeval, taking place during the latest stages of the Variscan compression as the deformation rests confined mainly in the Ambaritsa pluton and the later magmatic plutons in the study area are not affected by this specific deformation phase.

## Introduction

The Balkan fold-thrust belt is considered as a retro-wedge in respect to the south-vergent internal units (i.e. Rhodope) of the Balkanide orogen confined between the Moesian platform to the north and the Vardar suture to the southwest (Fig. 1, e.g. Gochev 1991; Vangelov et al. 2013). Formed during the Mesozoic and Cenozoic, the belt preserves some vestiges of the Variscan orogen. The pre-Permian rocks, largely exposed in the western part of the Balkan fold-thrust belt, were more extensively studied (e.g. Haydoutov 1989; Plissart et al. 2017) in contrast to those in the central part of the belt, which have attracted less attention. Here we present structural and U–Pb LA-ICP-MS zircon data for a specific magmatic unit within the pre-Permian basement of the central parts of the Balkan fold-thrust belt revealing the development of a Late Variscan zone of localized deformation confined mainly in probably contemporaneous sheet-like intrusion.

## Geological setting

In the central part of the Balkan fold-thrust belt two Variscan lithotectonic units (terranes) differing by its metamorphic grade as well as the lithologies and protolithic ages (Stara Planina low-grade metamorphic complex and Sredna Gora high-grade metamorphic complex) are juxtaposed. Their boundary is considered as a suture (Thracian and Balkan terrane, according to Haydoutov 1989 and Sredna Gora and Balkan terrane, according to Carrigan et al. 2005). More recent studies described this

contact as a major ductile shear zone (Gerdjikov et al. 2007), often intruded by Late Variscan plutons (Gerdjikov & Balkanska 2013) and in places reactivated by an Alpine brittle thrust (e.g. Milanov et al. 1971; Balkanska & Gerdjikov 2010). This major boundary is cropping out in the western parts of the central Balkan fold-thrust belt (in Zlatitsa area) where the thrusting is dated at  $333.9 \pm 0.2$  Ma (D1 on Fig. 2, Gerdjikov et al. 2010a), shortly after the thermal peak of the metamorphism in the Sredna Gora metamorphic complex dated at about 337 Ma (Carrigan et al. 2006). However, in the study area, the thrust boundary is obscured by the voluminous Variscan granitoid magmatism (Gerdjikov et al. 2010b) and the later Alpine brittle to brittle-ductile compressional events, the most prominent of which is related to the formation of Botev Vrah thrust (Balkanska & Gerdjikov 2010). Common feature of the Stara Planina low-grade and Sredna Gora high-grade metamorphic complexes is the presence of abundant intrusive rocks ranging in composition from diorites to leucogranites. They are strongly deformed to undeformed and could be used as time markers delimiting different tectonic events. The Cambrian Karlovo granites (Fig. 2), representing the largest pluton intruding the Stara Planina low-grade metamorphic complex, are exposed in the southern parts of the study area.

## Ambaritsa metagranites — main structural features and emplacement age

The Ambaritsa metagranites are largely exposed in the allochthon of the Late Alpine Botev Vrah thrust which

occupies the Stara Planina Mountains crest. However, relatively large and elongated (up to 4 km) to small bodies intruded both the low-grade metamorphic complex and the Karlovo granites in the autochthon of the thrust.

These rocks represent a suite dominated by leucocratic fine-grained granites and minor diorites and granodiorites. The Ambaritsa metagranites are entirely recrystallized and overprinted by a strong fluid-assisted mylonitization. They are transformed in sericite or sericite-chlorite schists with a foliation defined by elongated quartz aggregates and align chlorite and sericite flakes. A greenschist facies deformation is well

evidenced by the mineral association of sericite, chlorite, clay minerals, epidote, quartz and Fe-hydroxides, bulging recrystallization of quartz, feldspars replaced by sericite and clay minerals, “flame-shaped” perthites, etc.

Within the autochthon of the Botev Vrah thrust as well as in the allochthon relicts exposed along the footsteps of the Stara Planina Mountains the foliation is moderately dipping (30–60°) to the S and SW while the lineation, defined by chlorite, quartz and sericite is predominantly plunging towards SW or SE. The rocks form mainly S-type tectonites. At the Stara Planina Mountains crest, within Botev Vrah allochthon, the Ambaritsa metagranites form subhorizontal about 350 m

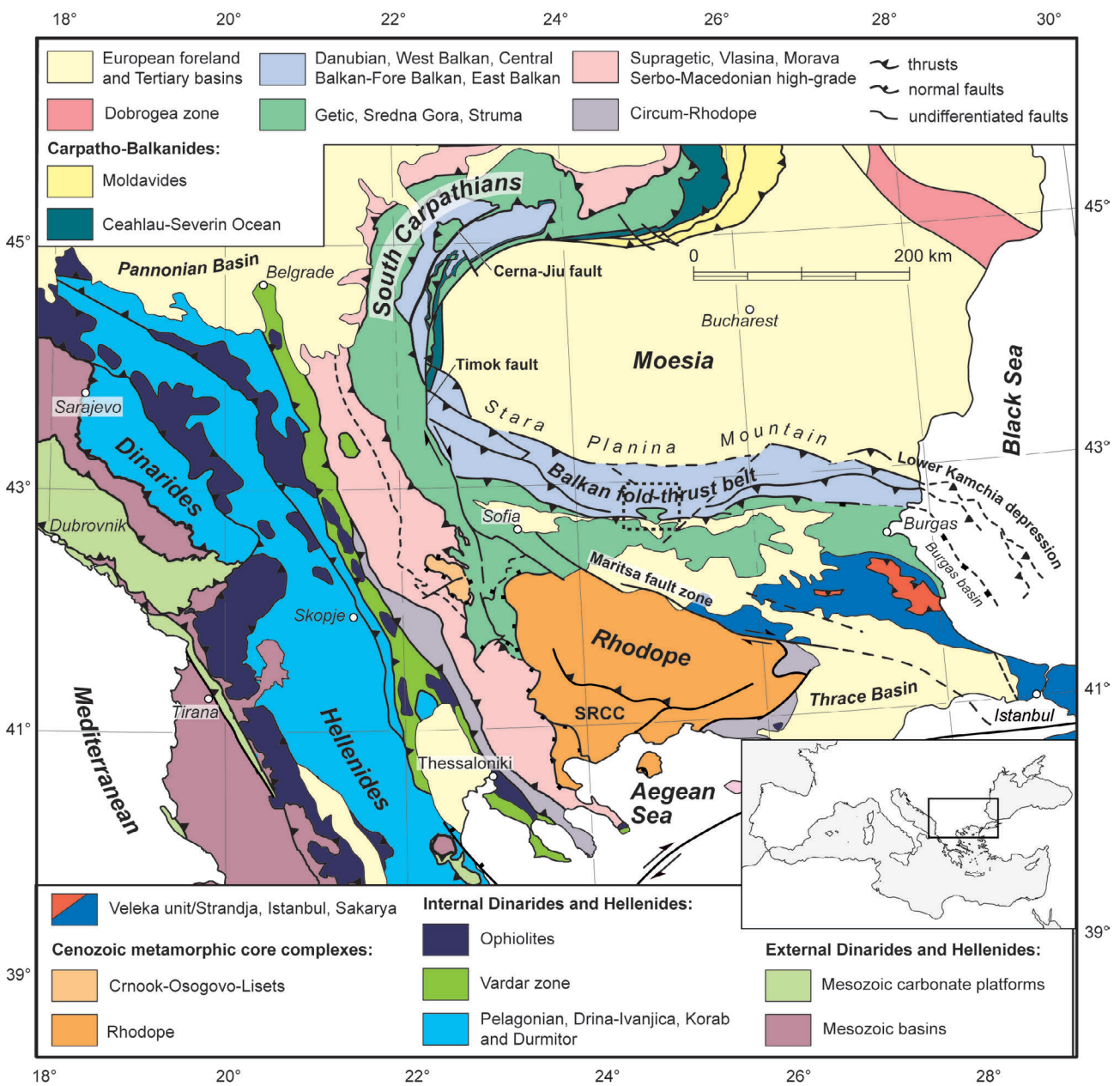


Fig. 1. Tectonic map of the Balkan Peninsula (modified after Schmid et al. 2008; Bernoulli 2001). Box outlines studied area.

thick planar body. Here the foliation planes dip virtually in all directions at mainly shallow angles (20–45°). Hence, the orientation of the generally down-dip lineation is also very variable. These tightly foliated rocks are affected by meso- and micro-scale folds with various morphologies: open to less frequently tight or isoclinal, often chevron-like folds with shallow plunging axes in all directions. No consistent shear sense has been documented within the Ambaritsa metagranites.

The sample for U–Pb LA-ICP-MS dating was taken from the allochthon of the Botev Vrah thrust. 25 spot analyses were made preferentially from the rims, but also from the cores of the zircons. The zircons exhibit well expressed oscillatory zonation typical for growth in igneous conditions of acid to intermediate magmas.

Some of the crystals show cores with ages close to that of the rims, suggesting for some magmatic dynamics in the chamber during their formation. The magmatic ages are determined using the eight most concordant analyses and yield an age of  $307.8 \pm 3.9$  Ma (Fig. 3, with weighted average  $^{206}\text{Pb}/^{238}\text{U}$  of  $307.8 \pm 1.4$  Ma). No xenocrystic component has been found.

### Localized deformation in the domain occupied by the Ambaritsa metagranites

The Ambaritsa metagranites most probably initially built up a large sheet-like body, later dismembered during the Alpine orogeny. The granite emplacement

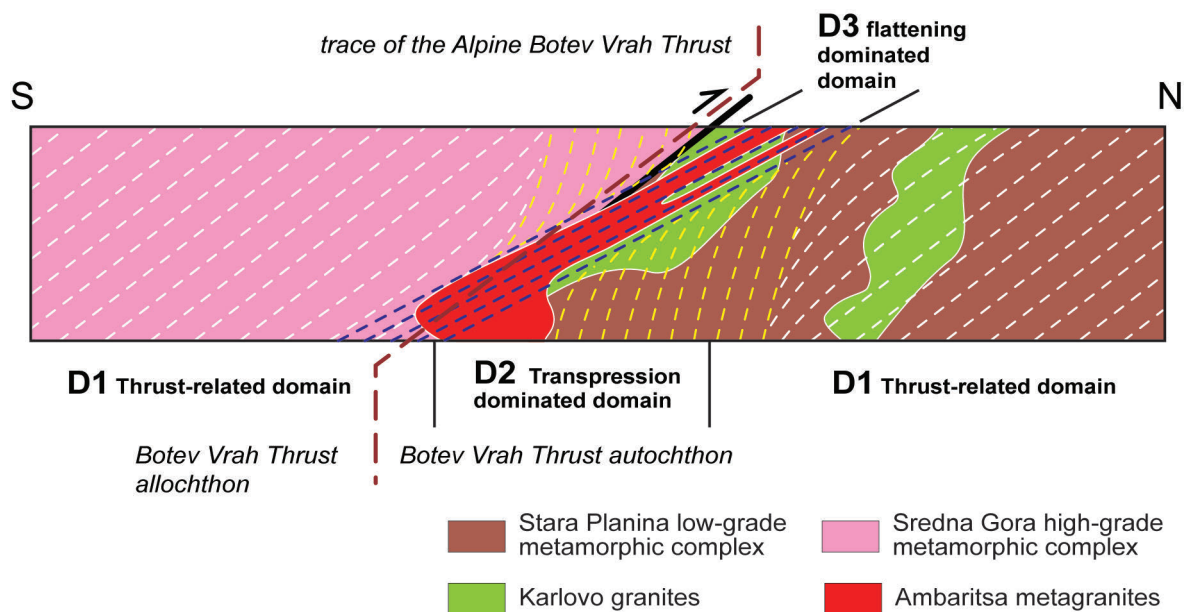


Fig. 2. Scheme for the tectonic evolution of the study area.

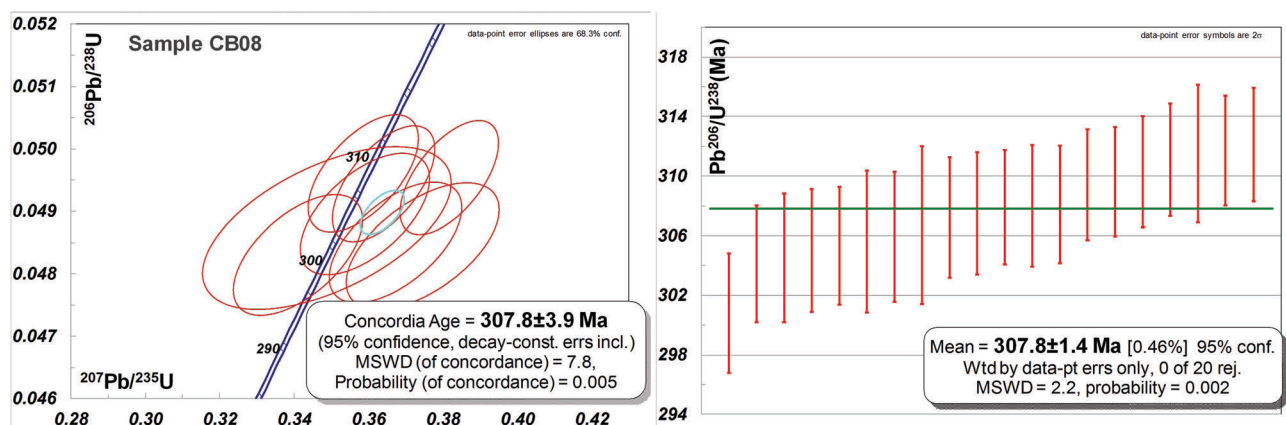


Fig. 3. LA-ICP-MS U–Pb zircon dating of the Ambaritsa metagranites. Concordia diagram (left) and Weighted average  $^{206}\text{Pb}/^{238}\text{U}$  diagram (right).

and deformation postdate an earlier transpressional stage documented in the Karlovo granites and the Stara Planina low-grade metamorphic complex (D2 on Fig. 2) evidenced by a steep foliation and sub-horizontal lineation which were not observed in the Ambaritsa metagranites. Additionally, field data and 3D analysis of the satellite imagery clearly indicate that the steep foliation within their host rocks is rotated to much shallow dips in the vicinities of Ambaritsa granite bodies. The fact that the deformation in the Ambaritsa metagranites took place at a relatively lower temperature (~300–400 °C) than in the host rocks (Karlovo granites and part of Stara Planina low-grade metamorphic complex) suggests that probably at the end of the transpressional phase the rocks from the studied area were exhumed to relatively shallower crustal levels. This lower-temperature overprint is also observed in their immediate host rocks as well as in the enclosed meter to decameter xenoliths.

The deformation of the Ambaritsa metagranites was restricted to a rather narrow zone (up to 400 metres thick) along which they were intruded (D3 on Fig. 2). However, it could not be clearly established what were the relationships between the Ambaritsa intrusion emplacement and the deformation. Though, it could be suggested that both processes were tightly related and probably coeval as the deformation rests confined mainly in the sheet-like Ambaritsa pluton and the later magmatic plutons in the study area are not affected by this specific deformation. Therefore, it could be suggested that the deformation was related to the latest stages of the magmatic activities in a fluid-rich environment.

Generally south plunging lineation observed in the Ambaritsa metagranites and the fact that the foliation is tightly folded suggests that the deformation was probably taken place in a renewed pulse of Variscan compression. The lack of distinct shear sense criteria and rotational features suggests that the deformation was characterised by a significant flattening component in the absence of major displacements.

The differences in the dips and plunges of the foliation and lineation from the Ambaritsa metagranites at the mountain crest and those from the southern slope are probably due to rotations of the former during later Alpine events (e.g. Botev Vrah thrust emplacement). Once restoring the Alpine thrusting along the Botev Vrah thrust it could be assumed that both segments of these metagranites, cropping out now on both sides of

the thrust, are parts of the same relatively narrow (not more than 400 m thick) shallow dipping zone of strain localization. Additionally, the fact that later magmatic plutons were not affected by this specific deformation suggests that it has taken place during the latest pulses of the Variscan compression.

**Acknowledgements:** This study was financed by the Bulgarian National Science Fund Grant (DMU 03/41) and Sofia University Science Fund Grant (180/2009).

## References

- Balkanska E. & Gerdjikov I. 2010: New data on the structure of Botev Vrah thrust along the southern foot of Central Stara Planina Mountain. *Compt. Rend. Acad. Sci. Bulg.* 63, 1485–1492.
- Carrigan C.W., Mukasa S.W., Haydoutov I. & Kolcheva K. 2005: Age of Variscan magmatism from the Balkan sector of the orogen, central Bulgaria. *Lithos* 82, 125–147.
- Carrigan C.W., Mukasa S.W., Haydoutov I. & Kolcheva K. 2006: Neoproterozoic magmatism and Carboniferous high-grade metamorphism in the Sredna Gora Zone, Bulgaria: An extension of the Gondwana-derived Avalonian-Cadomian belt? *Precamb. Res.* 147, 404–416.
- Gerdjikov I. & Balkanska E. 2013: Kalofer granitoid suite. A Late Variscan stitching pluton. *Compt. Rend. Acad. Sci. Bulg.* 66, 709–716.
- Gerdjikov I., Georgiev N., Dimov D. & Lazarova A. 2007: The different faces of supposedly single thrust: a reevaluation of the Vezhen thrust, Central Balkanides. *Proc. Geosc. Bulg. Geol. Soc.*, 24–26.
- Gerdjikov I., Ruffet G., Lazarova A., Vangelov D., Balkanska E. & Bonev K. 2010a: <sup>40</sup>Ar/<sup>39</sup>Ar geochronological constrains of a Variscan transpression in Central Stara Planina Mountain. *Proc. Geosc. Bulg. Geol. Soc.*, 109–110.
- Gerdjikov I., Lazarova A., Balkanska E., Bonev K., Vangelov D., Dimov D. & Kounov A. 2010b: A new model for the pre-Permian basement of the Central Stara Planina Mountain. *Compt. Rend. Acad. Sci. Bulg.* 63, 1169–1176.
- Gochev P. 1991: The Alpine orogen in the Balkans — a polyphase collisional structure. *Geotect. Tectonophys. Geodynam.* 22, 3–44 (in Bulgarian).
- Haydoutov I. 1989: Precambrian ophiolites, Cambrian island arc and Variscan suture in the South Carpathian-Balkan region. *Geology* 17, 905–908.
- Milanov L., Kuikin S., Gercheva Y., Christov S. & Chuneva V. 1971: Geology of East Troyan Stara Planina Mountain. *Bull. Commit. Geol.* 18, 199–222 (in Bulgarian).
- Plissart G., Monnier C., Diot H., Maruntiu M., Berger J. & Triantafyllou A. 2017: Petrology, geochemistry and Sm–Nd analyses on the Balkn–Carpathian Ophiolite (BCO — Romania, Serbia, Bulgaria): Remnants of a Devonian back-arc basin in the easternmost part of the variscan domain. *Journal of Geodynamics* 105, 27–50.
- Vangelov D., Gerdjikov I., Kounov A. & Lazarova A. 2013: The Balkan Fold-Thrust Belt: an overview of the main features. *Geol. Balc.* 42, 29–47.

# Variscan I-type granitoids in the Eastern Alps and their geodynamic setting: An updated discussion based on new geochronological results

FRITZ FINGER<sup>1</sup>, HARALD FRITZ<sup>2</sup>, CHRISTOPH HAUZENBERGER<sup>2</sup>, EWALD HEJL<sup>1</sup>,  
WALTER KURZ<sup>2</sup> and MARTIN LINDNER<sup>1</sup>

<sup>1</sup>University of Salzburg, Jakob Haringer Straße 2a, 5020 Salzburg, Austria;  
Friedrich.Finger@sbg.ac.at; Ewald.Hejl@sbg.ac.at; Martin.Lindner@stud.sbg.ac.at

<sup>2</sup>University of Graz, Universitätsplatz 2, 8010 Graz, Austria;  
Harald.Fritz@uni-graz.at; Christoph.Hauzenberger@uni-graz.at; Walter.Kurz@uni-graz.at

Variably deformed granitoids with Devonian, Carboniferous and Permian formation ages, commonly termed “Variscan granitoids”, are widespread in the basement units of the eastern Alps. Many of them are I-type (volcanic-arc-type) tonalites and granodiorites and were, thus, considered to be related to the Palaeotethys subduction system located along the southern Variscan fold belt flank (Finger et al. 1997). However, the issue could be more complicated. New geochronological and geochemical research over the past twenty years has shown that the Variscan I-type granitoids in the Eastern Alps are not cogenetic but form separate plutonic provinces, that were magmatically active at different times. Single granite-forming events likely reflect different tectonic/geodynamic stages during the evolution of the Variscan orogen.

An early generation of Late Devonian to Lower Carboniferous I-type granitoids (370–330 Ma) comprises the dioritic–tonalitic–granodioritic Cetic granitoids of the Helvetic unit (Frasl & Finger 1988; Thöni 1991), the mainly granodioritic Seckau–Bösenstein granitoids (Mandl et al. 2018), and distinct deformed tonalite gneisses in the eastern Tauern Window (“Altkristalline Tonalitgneise” — Schmidt 2017).

A second generation of I-type granitoids with Upper Carboniferous ages (330–300 Ma) occurs in the Eastern Tauern Window (Malta Tonalite, Hochalm Granite, Kölnbrein Granite).

A third, early Permian generation of I-type granitoids (ca. 290–300 Ma) is prominent in the central and western Tauern Window (Venediger Tonalite) and in the Southern Alps.

The following questions must be asked, considering the recent tectonic models for the Variscan orogen (Von Raumer et al. 2013):

- Which of the intra-Alpine Variscan I-type granitoids are directly subduction-related, i.e., formed above an active subduction zone?
- Is it possible that some of the intra-Alpine Variscan I-type granitoids belong to the Rheic and not to the Palaeotethys subduction system?
- Alternatively, is it possible that parts of the intra-Alpine Variscan granitoids have inherited their I-type characteristics from the remelting of significantly older volcanic-arc-type crust, thus being not subduction related in the strict sense.

## References

- Finger F., Roberts M.P., Haunschmid B., Schermaier A. & Steyrer H.P. 1997: Variscan granites of central Europe: their typology, potential sources and tectonothermal relations. *Mineralogy and Petrology* 61, 67–96.
- Frasl G. & Finger F. 1988: The Cetic Massif below the Eastern Alps — characterized by its granitoids. *Schweiz. Mineral. Petrogr. Mitt.* 68, 433–439.
- Mandl M., Kurz W., Hauzenberger C., Fritz H., Klötzli U. & Schuster R. 2018: Pre-Alpine evolution of the Seckau Complex (Austroalpine basement/Eastern Alps): Constraints from in-situ LA-ICP-MS U–Pb zircon geochronology. *Lithos* 296–299, 412–430.
- Schmidt R. 2017: Geologisch–petrographische Untersuchungen im Komplex der Alten Gneise im östlichen Tauernfenster (Maltatal). *MSc. Thesis, Salzburg University*, 1–88.
- Thöni M. 1991: Neue Rb/Sr-Daten an Mineralien und Gesteinen des Leopold von Buch-Denkmales und am Tonalit von Schaitten. *Mitt. Gesell. Geol. Bergbaust. Österr.* 37, 157–162.
- von Raumer J.F., Bussy F., Schaltegger U., Schulz B. & Stampfli G.M. 2013: Pre-Mesozoic Alpine basements — their place in the European Paleozoic framework. *Geological Society of America Bulletin* 125, 89–108.

# Hydrothermal amphiboles from Na–Ca and Na–Ca–K-silicate alterations: An example from Elatsite porphyry copper–gold deposit, Bulgaria

HRISTIANA GEORGIEVA, ROSSEN NEDIALKOV and IVAN KRUMOV

University of Sofia “St. Kliment Ohridski”, bul. “Tsar Osvoboditel” 15, 1504 Sofia, Bulgaria;  
hristiana.georgieva@abv.bg; med@gea.uni-sofia.bg; ivan.d.krumov@gmail.com

**Abstract:** The progression of exploitation and new prospecting get to the discovery of Na–Ca and transitional Na–Ca–K-silicate alterations (transitional between Na–Ca and K-silicate alteration) in the deeper parts of the Elatsite porphyry copper–gold deposit (PCGD). The study of these new for the deposit alterations reveal the presence of different in morphology, distribution and chemistry hydrothermal amphiboles.

## Introduction

The Elatsite PCGD is one of the biggest deposits of this type in Europe. It is operating since 1983–1984 and is the best studied in Bulgaria. Nevertheless, with the progressing exploitation and new prospecting drillings in deeper parts of the hydrothermal system are discovered new alteration types. Sodic–calcic (Na–Ca) alteration and the transition between Na–Ca and K-silicate alterations are characterised for the first time. These alterations are not frequently established in PCGDs and the information about them enrich the knowledge about the deposits and present the possibility to build up a more exhaustive model of the hydrothermal system of Elatsite PCGD.

## Samples and methods of investigation

The studied alterations are established during several years of sampling and field observations on the constantly changing benches of the open pit mine and on some interesting drill cores samples conceded gentility by the mining company.

The petrography of the alterations is characterised under the microscope. The mineral chemistry is obtained with microprobe analyses (47 analyses) accomplished on JEOL JSM 35 CF at “Eurotest-Control” EAD, Sofia, Bulgaria (EDS analysis, 100 seconds for spectra acquisition, at 15 KEV acceleration voltage, using natural and synthetic standards, EDX – TRACOR NORTHERN TN-2000). Mineral trace elements (22 analyses) are made on LA-ICPMS at the Geological institute of the Bulgarian academy of sciences on a Perkin Elmer – ELAN DRC spectrometer with New Wave UP193FX

LA device. The internal standard ( $\text{SiO}_2$ ) is from the microprobe analyses of the respective minerals. The laser system operated at constant 8 Hz pulse rate and laser energy 1.80–2.60 J/cm<sup>2</sup> on the sample surface for 25 to 35  $\mu\text{m}$  spot size.

## Geological setting

The Elatsite porphyry copper–gold deposit is situated at the most northern part of the Panagyurishte–Etropole ore region which is part of the Apuseni–Banat–Timok–Srednogorie Late Cretaceous copper belt (Popov 1996; Popov & Popov 2000; von Quadt et al. 2005). The magmatism of the belt is predominantly calc-alkaline to shoshonitic and it is subduction related (Kamenov et al. 2002, 2007).

The geology of the Elatsite deposit consists of a basement, intruded by the Late Cretaceous magmatic subvolcanic to hypabyssal complex, composed by dikes and dike-like, east-west elongated intrusive bodies. The main porphyritic rocks are presented by quartz-monzodiorites and granodiorites as well as quartz-diorites (von Quadt et al. 2002). The basement comprises low-grade Paleozoic variegated schists (anchymetamorphic to greenschist metamorphic degree) intruded by the Variscan Vezhen granitoid (mainly granodiorite) pluton (Kalaidziev et al. 1984; Kamenov et al. 2002). At the contact of the Vezhen pluton with the metamorphic rocks are formed sillimanite (observed in xenoliths in the magmatic rocks) and andalusite hornfelses, knotted schists with andalusite and/or rare biotite porphyroblasts and rare amphibole hornfelses.

The hydrothermal alteration products, related with the porphyritic magmatism, are represented by propylitic,

K-silicate, K-silicate–sericitic, sericitic (Kanazirski et al. 2002; Strashimirov et al. 2002; Georgiev 2005), phillite–argillic (Tarkian et al. 2003), argillic (Kehayov 2005) and quartz–adularia–carbonate alterations (Ivanov et al. 2014). Indications for supposed mixed sodium–potassic alteration with summarized mineral association — richterite, paragonite (determined by X-ray spectroscopy) and pyroxene (diopside) were first reported in the PhD thesis of Georgiev 2005 (communication from Kanazirski).

Our recent studies ascertain the presence of Na–Ca alteration (rare in the deposit), the more common Na–Ca–K-silicate (transitional between Na–Ca and K-silicate alteration) and skarn formation (related with local disclosure of Ca alteration in the hornfelse sequence) affecting calc-schists.

## Petrography

Na–Ca alteration is well preserved mainly in veins and veinlets and relatively rarely observed as affecting all the volume of the rock. The mineral composition of the Na–Ca alteration is represented dominantly by amphibole, epidote, plagioclase, albite, rarely clinopyroxene, rutile, magnetite, apatite, small amount of hematite and quartz. This type of alteration affects mostly the Late Cretaceous magmatic subvolcanic to hypabyssal porphyritic complex and less the granodiorites of the Vezhen pluton.

The amphibole veins with up to several tens of centimetres thickness are the most astonishing manifestations of the Na–Ca alteration (Fig. 1). They are hosted in



**Fig. 1.** Amphibole veins (black in colour) from Na–Ca alteration (1) in the granodiorites of the Vezhen pluton, with superimposed K-silicate alteration (2).

the granodiorites of the Vezhen pluton and are superimposed by the K-silicate alteration. The mineral assemblage includes dominantly amphibole (Hb-1) and small quantity of quartz and magnetite.

When Na–Ca alteration is disseminated uniformly in the volume of the host rocks, it is composed mainly of amphibole (Hb-2), rutile, apatite, magnetite and small quantity of quartz and clinopyroxene. Usually the magmatic texture is preserved, and the secondary amphiboles replace primary mafic minerals and form clusters or occurs in thin veinlets.

The transitional Na–Ca–K-silicate alteration is characteristic by the presence of amphibole, titanite, magnetite, apatite, secondary biotite and small amount of K-feldspar, quartz and rutile. Amphibole (Hb-3) has green colour and is typically replacing magmatic porphyroblasts, and/or occurs as veinlets and nests grown up with secondary biotite.

## Discussion

### *Chemical composition of hydrothermal amphibole*

The classification of the hydrothermal amphiboles was made using the equations of Locock et al. 2014 after Hawthorne et al. 2012.

The Hb-1 occurs as euhedral crystals up to few millimetres (rare 1 cm), black in colour. Hb-1 is determined as hornblende to actinolite, with  $Mg^{\#}$  ratio ( $Mg/Mg+Fe$ ) between 0.75–0.87 and high contents of Ti,  $Fe^{+3}$ , Mn and Cl (Fig. 2). The higher Cl values (0.11–0.42 wt. %) define Hb-1 as a Cl-rich amphibole (Kullerud 2000). Hb-1 has high concentration of Cr, Co, Ni, Cu, Pb and rare earth elements ( $\Sigma REE=160.74$ ) compared to the other types of amphibole. It is showing deep Eu negative anomaly ( $Eu/Eu^*=0.30$ ) on the chondrite normalized patterns and a relatively flat distribution of light and heavy REE with La/Yb ratio 0.25–0.63.

Hb-2 occurs as euhedral to anhedral, green coloured crystals (under the microscope), up to few tens of  $\mu m$ . It is characterised by two morphological types of reparation: in veinlets (Hb-2.1.) or uniformly distributed (Hb-2.2.) in the rocks. Hb-2.1. is determined as magnesio-hornblende while Hb-2.2. is defined as magnesio-hornblende to actinolite. Hb-2.1. has  $Mg^{\#}=0.70-0.71$  and higher values for  $Fe^{+2}$ , Al and Ti compared to Hb-2.2 ( $Mg^{\#}=0.71-0.78$ ; Fig.2).

Hb-3 is determined as magnesio-ferri-hornblende to actinolite, with  $Mg^{\#}=0.72-0.83$ . Their chondrite-normalized patterns have the lowest content of REE

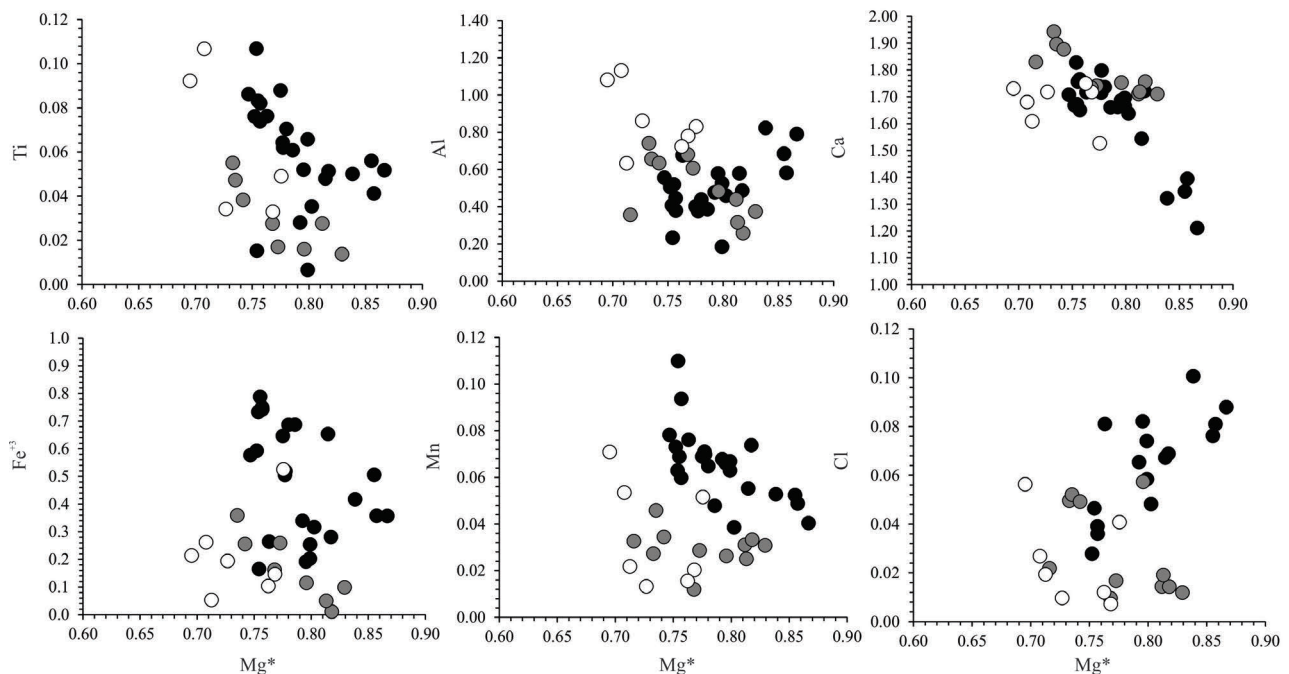


**Fig. 2.** Plots show compositional variations  $Mg^*$  ( $Mg/Mg+Fe$ )/element (apfu) in hydrothermal amphiboles: Hb-1 (with black); Hb-2 (with white) and Hb-3 (with grey).

( $\sum REE=96.62$ ) and a deep negative Eu anomaly ( $Eu/Eu^*=0.38$ ). In Hb-3 are determined the lowest contents of trace elements from the all amphiboles.

### Pressure

The pressure of the hydrothermal amphiboles crystallization was determined after Mutch et al. 2016.

The estimated pressure for Hb-1 is between 0.59 to 1.18 kbar. For Hb-2.1., the results are 2.02–2.15 kbar, and for Hb-2.1., estimated pressure is around 1.11–1.52 kbar. For Hb-3 from the transitional alteration, estimated values are between 0.65–1.29 kbar. These results correlate with the pressure estimations of Stefanova (2009) obtained fluid inclusions associated with the K-silicate alteration (0.916 kbars).

### Conclusions

During the transition of Na–Ca to Na–Ca–K-silicate alteration, the contents of Mg, Ti, Mn, Cl, trace and REE elements are decreasing. The Mg and Ti decrease (in Hb-3) is probably related to the appearance of secondary biotite.

The deep negative Eu anomaly of Hb-1 (indicating probably the presence of  $Eu^{+3}$ ) and the high  $Fe^{+3}$  content in Hb-1 compared to Hb-2 and Hb-3 may indicate

a higher oxygen fugacity during their formation. The higher values of Cl in Hb-1 allows us to assume that in the early stage of Na-Ca alteration the fluid was Cl-rich. The decrease in rare and REE elements during the transition between Na-Ca to Na-Ca-K-silicate alteration is related to their preference to stay in the Cl-rich fluid.

**Acknowledgements:** We greatly appreciate the assistance of the Elatsite mining company and the group of colleagues from the Scientific Research Centre, Sofia University “St. Kliment Ohridski” working at the Elatsite PCGD.

### References

- Georgiev G. 2005: Geological model of the Elatsite deposit. *PhD thesis, University of Mining and geology, Sofia*, 1–162 (in Bulgarian).
- Hawthorne F.C., Oberti R, Harlow G., Maresch W.V. et al. 2012: Nomenclature of the amphibole supergroup. *Am. Mineral.* 97, 2031–2048.
- Ivanov Z., Nedialkov R. & Bogdanov K. 2014: Magmatic and ore-related breccias in the Elatsite porphyry-copper deposit (PCD), Bulgaria. *Proceedings of XX CBGA Congress*, Tirana, Special issue, 158–161.
- Kalaidziev S., Hadziiski G. & Angelkov K. 1984: Structural conditions for localization of the copper-porphyry deposit Elatsite. *Bulg. Geol. D* 45, 189–196 (in Bulgarian).

- Kamenov B.K., von Quadt A. & Peytcheva I. 2002: New insight into petrology, geochemistry and dating of the Vezhen pluton, Bulgaria. *Geochem. Mineral. Petrol.* 39, 3–25.
- Kamenov B., Yanev Y., Nedialkov R., Moritz R. et al. 2007: Petrology of Upper Cretaceous island-arc ore-magmatic centers from Central Srednogorie, Bulgaria: Magma evolution and paths. *Geochem. Mineral. Petrol.* 45, 39–77.
- Kanazirski M., Chipchakova S., Gorova M. & Arnaudova R. 2002: Wallrock alterations in the porphyry copper deposits of the Panagyurishte ore district and formation–facial belonging of the metasomatites. *Geol. Balk.* 32, 77–80.
- Kehayov R.M. 2005: Mineral association of gold and conditions of their formation in copper-porphyry deposit Elatsite. *PhD thesis, University of Sofia*, 1–208 (in Bulgarian).
- Kullerud K. 2000: Occurrence and origin of Cl-rich amphibole and biotite in the Earth's crust — implications for fluid composition and evolution. In: Stober I. & Bucher K. (Eds.): *Hydrogeology of Crystalline Rocks. Water Science and Technology Library 34, Springer, Dordrecht*, 205–225.
- Locock A. 2014: An Excel spread sheet to classify chemical analyses of amphiboles following the IMA 2012 recommendations. *Comput. & Geosci.* 62, 1–11.
- Mutch E.J.F., Blundy J.D., Tattitch B.C., Cooper F.J. & Brooker R.A. 2016: An experimental study of amphibole stability in low-pressure granitic magmas and a revised Al-in-hornblende geobarometer. *Contrib. Mineral. Petrol.* 171, 85.
- Popov P. 1996: Characteristic features of the Banat-Srednogorie metallogenic zone: plate tectonic aspects of the Alpine metallogeny in the Carpatho-Balkan region. Proceedings of the Annual Meeting, Sofia, 1996. UNESCO, IGCP Project 1, 137–154.
- Popov P & Popov 2000: General geologic and metallogenic features of the Panagyurishte ore region. In: Strashimirov S. & Popov P. (Eds.): *Geology and metallogeny of the Panagyurishte ore region (Srednogorie zone, Bulgaria). Guide to Excursions, ABCD-Geode 2000, Borovets, Bulgaria*, 1–7.
- Stefanova E. 2009: Genetic features of quartz from copper-porphyry deposit Elatsite. *PhD thesis, University of Sofia*, 1–157 (in Bulgarian).
- Strashimirov S., Petrunov R. & Kanazirski M. 2002: Porphyry-copper mineralization in the Central Srednogorie zone, Bulgaria. *Miner. Deposita* 37, 587–598.
- Tarkian M., Hünken U., Tokmakchieva M. & Bogdanov K. 2003: Precious-metal distribution and fluid-inclusion petrography of the Elatsite porphyry copper deposit, Bulgaria. *Miner. Deposita* 38, 261–281.
- Von Quadt A., Peytcheva I., Kamenov B., Fanger L., Heinrich C.A. & Frank M. 2002: The Elatsite porphyry copper deposit in the Panagyurishte ore district, Srednogorie zone, Bulgaria: U–Pb zircon geochronology and isotope-geochemical investigation of magmatism and ore genesis. In: Blundell, Neubauer & von Quadt (Eds): *The timing and location of major ore deposits in an evolving orogen. Geol. Society, London*, 204, 119–135.
- Von Quadt A., Moritz R., Peytcheva I. & Heinrich Ch. 2005: Geochronology and geodynamics of Late Cretaceous magmatism and Cu–Au mineralization in the Panagyurishte region of the Apuseni–Banat–Srednogorie belt, Bulgaria. *Ore Geol. Rev.* 27, 95–126.

# Eclogites of the Western Carpathians revisited

MARIAN JANÁK

Earth Science Institute, Slovak Academy of Sciences, Dúbravská cesta 9, 840 05 Bratislava, Slovakia; marian.janak@savba.sk

**Abstract:** An overview and new investigations of eclogites from the crystalline basement of the Western Carpathians are presented. On examples from the Low Tatra Mts. (Veporic Unit) and the Western Tatra Mts. (Tatric Unit) thermodynamic modelling of pseudosections constrained the stability of the observed mineral assemblages in terms of compositions and P–T conditions. The new data show that these rocks, in spite of strong retrogression, reached eclogite facies conditions thus supporting previous investigations.

## Introduction

Eclogite facies rocks are vestige of deep crustal subduction during an orogenic cycle, providing important information about the depth of subduction. The term *eclogite* as a petrographic rock name is restricted to rocks of broadly basaltic composition which lack primary plagioclase and have a predominant assemblage of jadeite-bearing clinopyroxene (omphacite) and garnet. True eclogites have previously been unknown in the Western Carpathians. However, microtextures indicating former eclogite facies stage have been observed in the amphibolite facies metabasites (garnet–clinopyroxene amphibolites) in several places of the pre-Mesozoic basement of the Central Western Carpathians, mainly in the core mountains of the Tatric Unit, e.g. Tribeč Mts. (Hovorka & Méres 1990), Malá Fatra Mts. (Hovorka et al. 1992 ; Janák & Lupták 1997), Western Tatra Mts. (Janák et al. 1996), Low Tatra Mts. (Méres et al. 2008; Janák et al. 2009) and Branisko Mts. (Faryad et al. 2005). In these rocks a high-pressure stage is indicated by symplectite textures characteristic for breakdown of omphacite to diopside and plagioclase.

## Low Tatra Mts. eclogite (Veporic Unit)

First finding of omphacite-bearing eclogite (Fig. 1) in the Western Carpathians was reported from the Low Tatra Mts. in the Veporic Unit near Heľpa village (Janák et al. 2007). Here, eclogites together with garnet-bearing ultramafic rocks (Grt+Ol+Opx+Sp) occur as lenses and boudins in the kyanite-bearing ortho- and paragneisses derived from Cambro–Ordovician protoliths. Omphacite with the highest jadeite content (~40 mol. %) occurs as inclusions in the garnet whereas omphacite with lower jadeite content (20–30 mol. %) occurs in the matrix. Most of clinopyroxene has jadeite content below 19 mol. %, forming the symplectites with plagioclase,

amphibole and quartz. Conventional geothermobarometry on eclogite facies assemblage garnet+omphacite+phengite+quartz (Ravna & Terry 2004) constrained the maximum pressure and temperature conditions of around 2.5 GPa and 700 °C (Janák et al. 2007).

## Western Tatra Mts. eclogite (Tatric Unit)

In the Western Tatra, strongly retrogressed eclogites form lenses in banded amphibolites being accommodated in a hangingwall (Upper unit) of an inverted metamorphic sequence, above the micaschists in the footwall (Lower unit). Exhumation of eclogites was facilitated by ductile extrusion and mid-crustal thrusting during the Variscan orogeny. In eclogites, primary omphacite (Cpx I) has been wholly converted to symplectites of diopside (Cpx II) and plagioclase and therefore these rocks have been described as garnet–clinopyroxene amphibolites (Janák et al. 1996). The attainment of the eclogite facies stability field was inferred from the composition of a “reconstructed” omphacite

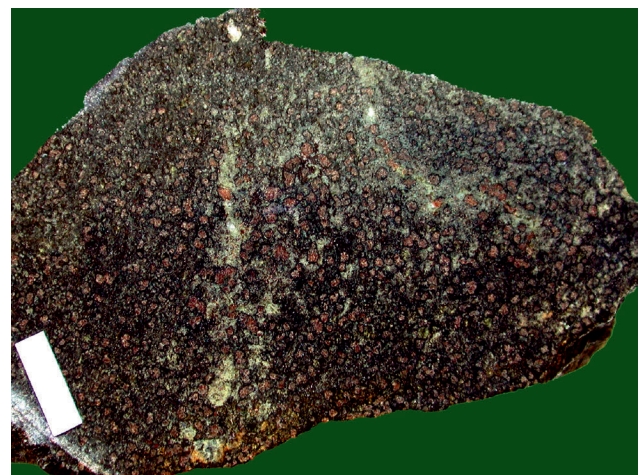


**Fig. 1.** Eclogite from the Low Tatra Mts. (Veporic Unit). Scale bar (white rectangle) is 1 cm (Janák et al. 2007).

(Jd36 mol. %), implying a minimum peak-pressure of 15–16 kbar. The Sm/Nd dating of garnet from eclogite in the Western Tatra yields 342 Ma age, which likely records cooling during exhumation (Moussallam et al. 2012).

### Thermodynamic modelling

Isochemical phase diagrams (P–T pseudosections) have been calculated using the *Perple\_X* thermodynamic software (Connolly 1990, 2005: version 6.8.6) with the internally consistent thermodynamic dataset (hp11 version) of Holland & Powell (2011). Solid-solution models for garnet, white mica (White et al. 2014), omphacite (Green et al. 2007), plagioclase (Holland & Powell 2003), amphibole (Dale et al. 2005) were used. The bulk rock composition was determined from the whole-rock XRF analysis.

The pseudosection for Helpa eclogite (VV-40) from the Veporic unit of the Low Tatra Mts. shows that the calculated isopleths of clinopyroxene and white mica match the measured compositions of omphacite and phengite in the stability field of garnet+omphacite+phengite+rutile+quartz, in spite of partial re-equilibration of garnet due to retrogression. The compositions of omphacite (Jd  $\geq$  30 mol. %) and phengitic white mica ( $\geq$  3.45 Si a.p.f.u) thus constrain the pressure values to 2.2–2.4 GPa at 650–700 °C. These conditions are consistent with previous P–T estimates obtained from conventional geothermobarometry) implying subduction to depths of around 80 km (Janák et al. 2007).

The pseudosection for Baranec eclogite (ZT-17) from the Western Tatra Mts. (Tatric Unit) shows that model compositional isopleths of clinopyroxene corresponding to composition of “reconstructed” omphacite (Jd36 mol. %) and measured clinopyroxene (Jd10 mol. %) constrain the pressure conditions from 1.7–1.0 GPa during exhumation. The peak-pressure assemblage stable at  $\geq$ 17 GPa would be garnet+omphacite+rutile+quartz. These results are in agreement with the previous P–T estimates and interpretations that the garnet–clinopyroxene amphibolites of the Western Tatra Mts. are in fact retrogressed eclogites (Janák et al. 1996).

**Acknowledgements:** This work was supported by the Slovak Research and Development Agency projects under the Contract no. APVV-18-0107 and the Slovak Scientific Grant Agency VEGA (grant no. 2/0060/16).

### References

- Connolly J.A.D. 2005: Computation of phase-equilibria by linear programming: A tool for geodynamic modeling and its application to subduction zone decarbonation. *Earth and Planetary Science Letters* 236, 524–541.
- Dale J., Powell R., White R.W., Elmer F.L. & Holland T.J.B. 2005: A thermodynamic model for Ca–Na clinopyroxenes in Na<sub>2</sub>O–CaO–FeO–MgO–Al<sub>2</sub>O<sub>3</sub>–SiO<sub>2</sub>–H<sub>2</sub>O–O for petrological calculations. *Journal of Metamorphic Geology* 23, 771–791.
- Green E., Holland T. & Powell R. 2007: An order-disorder model for omphacitic pyroxenes in the system jadeite-diopside-hedenbergite-acmite, with applications to eclogitic rocks. *American Mineralogist* 92, 1181–1189.
- Faryad S.W., Ivan P. & Jacko S. 2005: Metamorphic petrology of metabasites from the Branisko and Čierna hora mountains (Western Carpathians Slovakia). *Geologica Carpathica*, 56, 3–16.
- Holland T.J.B. & Powell R. 2003: Activity–composition relations for phases in petrological calculations: An asymmetric multi-component formulation. *Contributions to Mineralogy and Petrology* 145, 4, 492–501.
- Holland T.J.B. & Powell R. 2011: An improved and extended internally consistent thermodynamic dataset for phases of petrological interest, involving a new equation of state for solids. *Journal of Metamorphic Geology* 29, 3, 333–383.
- Hovorka D. & Méres Š. 1990: Clinopyroxene-garnet metabasites from the Tribeč Mts. (Central Slovakia). *Mineralia Slovaca* 22, 533–538.
- Hovorka D., Méres Š. & Caño F. 1992: Petrology of the garnet-clinopyroxene metabasites from the Malá Fatra Mts. *Mineralia Slovaca* 24, 45–52.
- Janák M. & Lupták B. 1997: Pressure-temperature conditions of high-grade metamorphism and migmatization in the Malá Fatra crystalline complex, the Western Carpathians. *Geologica Carpathica* 48, 287–302.
- Janák M., O’Brien P.J., Hurai V. & Reutel C. 1996: Metamorphic evolution and fluid composition of garnet-clinopyroxene amphibolites from the Tatra Mountains, Western Carpathians. *Lithos* 39, 57–79.
- Janák M., Méres Š. & Ivan P. 2007: Petrology and metamorphic P–T conditions of eclogites from the northern Veporic unit, Western Carpathians, Slovakia. *Geologica Carpathica* 58, 2, 121–131.
- Janák M., Mikuš T., Pitoňák P. & Spišiak J. 2009: Eclogites overprinted in the granulite facies from the Ďumbier crystalline complex (Low Tatra Mountains, Western Carpathians). *Geologica Carpathica* 60, 193–204.
- Méres Š., Janák M., Ivan P. & Konečný P. 2008: Omphacite – metamorphic index mineral of the eclogite facies in the crystalline basement of the Western Carpathians. *Mineralia Slovaca* 40, 89–102 (in Slovak with English abstract and resume).
- Moussallam Y., Schneider D.A., Janák M., Thöni M. & Holm D.K. 2012: Heterogeneous extrusion and exhumation of deep-crustal Variscan assembly: Geochronology of the Western Tatra Mountains, northern Slovakia. *Lithos* 144, 88–108.
- Ravna E.J.K. & Terry M.P. 2004: Geothermobarometry of UHP and HP eclogites and schists — an evaluation of equilibria among garnet-clinopyroxene-kyanite-phengite-coesite/quartz. *Journal of Metamorphic Geology* 22, 579–592.
- White R.W., Powell R., Holland T.J.B., Johnson T.E. & Green E.C.R. 2014: New mineral activity–composition relations for thermodynamic calculations in metapelitic systems. *Journal of Metamorphic Geology* 32, 3, 261–286.

# The geochemical characteristics of the Menilite Formation in the Czech Carpathians: A short review

PETR JIRMAN<sup>1,2</sup>, EVA GERŠLOVÁ<sup>1</sup> and LUJZA MEDVECKÁ<sup>1</sup>

<sup>1</sup>Department of Geological Sciences, Faculty of Science, Masaryk University, Kotlářská 2, 611 37, Brno, Czech Republic; p.jirman@seznam.cz

<sup>2</sup>Czech Geological Survey, branch Brno, Leitnerova 22, 602 00 Brno, Czech Republic

**Abstract:** The Paratethys area contains a significant number of petroleum provinces. Most of the accumulations within the Carpathians are sourced by the Oligocene organic-rich Menilite Formation and its equivalents. The vertical variations in lithology within the formation reflect different depositional environment which strongly influences the source rock potential. The Menilite Formation has mostly “good” to “very good” source rock potential based on the Rock-Eval and TOC data, respectively. The Chert Member represents the most prolific member and reaches the HI up to 725 mg HC/g TOC. Significantly lower source rock potential was evaluated within the Šitbořice and partly Subchert members. The organic matter within the Menilite Formation is based on the organic petrography observations predominantly composed by the kerogen type I, while the kerogen type III macerals are typically very rare. The Rock-Eval interpretations indicating presence of kerogen type II and III were inaccurate due to higher amount of non-pyrolyzable organic carbon portion which underestimated the HI.

## Introduction

The occurrence of the Menilite Formation in the Czech Republic is described from the Ždánice, Subsilesian, Silesian and Fore-Magura Units. The Menilite Formation is there according to Stráník et al. (1974) and Stráník (1981) subdivided into the Subchert Member (NP22), Chert Member (upper NP22 to lower NP23), Dynów Marlstone (NP23) and Šitbořice Member (upper NP23 to lower NP25) and comprises non-calcareous shales, marlstones and cherts (Bubík et al. 2016). The overall thickness of the formation is up to 200 meters within the Ždánice Unit and up to about 100 m in the Silesian Unit.

## Material and methods

A total of 118 samples were analysed using ELTRA S/C Elemental Analyser. A subset of 77 samples was evaluated by Rock-Eval pyrolysis. The data was previously partly published by Jirman et al. (2018, 2019).

The Rock-Eval 6 instrument was used to determine the free hydrocarbons content  $S_1$  [mg HC/g rock], residual hydrocarbon potential  $S_2$  [mg HC/g rock] and temperature of the maximum of the  $S_2$  peak  $T_{max}$  [°C]. The hydrogen index (HI) was calculated following Lafargue et al. (1998) as  $100 \cdot S_2/TOC$  [mg HC/g TOC].

Determination of  $HI_{true}$  is based on the same formula but using the pyrolyzable portion ( $TOC_{live}$ ) which was determined according to Dahl et al. (2004) based on the  $S_2$  versus TOC cross-plot. Samples with oxygen index (OI) data were analysed on Rock-Eval 6 instrument (Turbo version). The OI was calculated as  $100 \cdot S_3/TOC$  [mg  $CO_2/g$  TOC], where  $S_3$  represents the amount of  $CO_2$  [mg  $CO_2/g$  rock] generated in the pyrolytic oven during decomposition of organic matter. Contents of total carbon (TC) and total organic carbon (TOC) were analysed using ELTRA S/C Elemental Analyser. TOC was measured after de-carbonization of the samples with concentrated phosphoric acid.

An Olympus BX51 microscope including a Zeiss Photomultiplier MK3 system with fluorescence light and a lens of 40× magnification was used to quantitative maceral analysis using polished blocks. Macerals were determined following Taylor et al. (1998) and ICCP (1998, 2001).

## The source rock potential

The source rock potential was evaluated by the genetic potential (Rock-Eval  $S_1+S_2$  peaks) and the TOC according to Peters and Cassa (1994).

The Menilite Formation has mostly “good” source rock potential according to the genetic potential and “very good” potential according to the TOC

(Fig. 1). The Chert Member has the highest source rock potential among the members with the average genetic potential of 45 mg HC/g rock and TOC of 5.9 %<sub>wt.</sub>. The lowest potential has been observed within the Šitbořice Member and partly within the Subchert Member. On the other hand, the Šitbořice Member represents most of the Menilite Formation thickness while the Chert Member is typically only several meters thin.

The thermal immaturity of the organic matter was confirmed by Rock-Eval  $T_{max}$  (up to 433 °C). Higher thermal maturity is expected below the Magura Group of Nappes due to deeper burial.

### Comparison to the Jurassic Mikulov Marls

The Upper Jurassic Mikulov Marls have been identified as the major source rock in the Vienna Basin (e.g., Bližkovský et al. 1994; Geršlová et al. 2015). The Menilite Formation evaluated by Jirman et al. (2018, 2019) has higher source rock potential (Fig. 1) according to the genetic potential (average 15 versus 4.6 mg HC/g rock) and TOC (average 3.6 versus 1.4 %<sub>wt.</sub>) compared to the Mikulov Marls.

However, the key factors affecting the amount of the oil generation are thermal maturity, strata thickness and facial stability. These parameters are much favourable for the Mikulov Marls compared to the Menilite Formation.

### The Menilite Formation kerogen genetic type

The kerogen genetic type was evaluated based on the (1) Rock-Eval pyrolysis data represented by the HI,  $T_{max}$  and OI and (2) maceral analysis.

### The Rock-Eval interpretations

Based on the Rock-Eval data (Fig. 2), the organic matter within the Menilite Formation represents mostly kerogen type II with high amount of kerogen type III. Rare type I admixtures occurs in the Chert Member. The HI versus OI data generally confirms described kerogen distribution even the type III within the Šitbořice Member was not observed.

### The organic petrography interpretations

The organic matter of all Menilite Formation samples is based on the organic petrography dominated by lipinitic macerals representing the kerogen type I. In contrast, vitrinite and inertinite macerals (kerogen type III) are typically very rare or virtually absent, respectively.

The Subchert Member contains abundant liptodetrinite accompanied by bituminite and alginite all belonging to the kerogen type I. The organic matter within the Chert Member is characterized by prevailing alginite macerals (kerogen type I). The dominant maceral within the Dynów Marlstone is liptodetrinite and rare bituminite

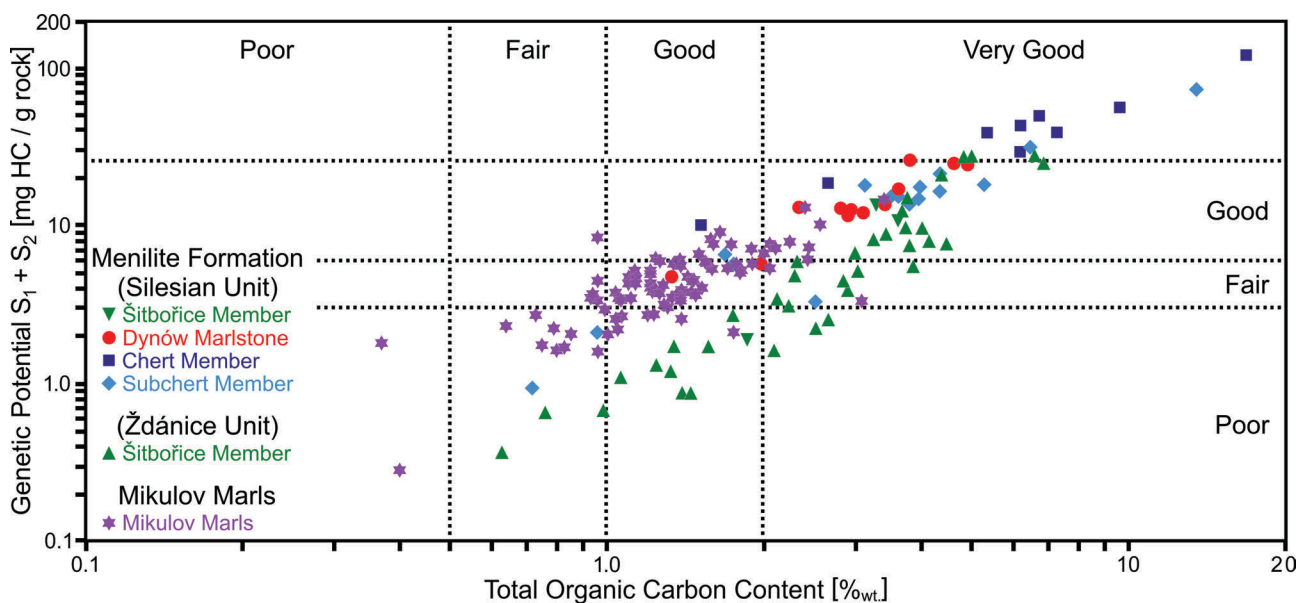


**Fig. 1.** Comparison of the source rock potential of the Menilite Formation from Silesian and Ždánice units and the Mikulov Marls. The data after Jirman et al. (2018, 2019) and Geršlová et al. (2015).

both again representing the kerogen type I. Within the Šitbořice Member, the organic matter is represented by the liptinite group (kerogen type I) with admixtures of vitrinite group (kerogen type III). However, the prevailing kerogen type may be classified as type II due to the admixtures of spores, pollens and plant particles (type III).

### Kerogen genetic type interpretations comparison

As evident from the kerogen genetic type interpretations of both the Rock-Eval and Organic petrography data, the results are not in agreement. The kerogen genetic type evaluation based on raw HI versus  $T_{max}$  and/or versus OI data (Fig. 2) generally underestimate the kerogen type towards the type III.

However, the HI can be according to Dahl et al. (2004) simply re-calculated to the so-called  $HI_{true}$ . The  $HI_{true}$  as a HI based on the pyrolyzable portion of the organic carbon only rectifies errors caused by the non-pyrolyzable organic carbon content which is determined by the TOC versus  $S_2$  cross-plot (Fig. 3).

The  $HI_{true}$  reaches ~570 mg HC/g TOC in the Subchert Member, ~750 in the Chert Member, ~730 in the Dynów Marlstone and ~590 mg HC/g TOC in the Šitbořice Member. The kerogen genetic type evaluation based on the  $HI_{true}$  is in agreement to the maceral analysis in this study.

### Conclusions

The Menilite Formation has “good” to “very good” source rock potential based on the Rock-Eval and TOC data. Both the parameters reach higher values within the Menilite Formation compared to the Mikulov Marls. The hydrocarbon potential of the Menilite Formation strongly reflects changing conditions during its deposition and diagenesis.

The Menilite Formation contains predominantly kerogen type I even the HI values indicate kerogen type II and III. This is caused by the presence of non-pyrolyzable organic carbon portion within the overall TOC which underestimates the HI.

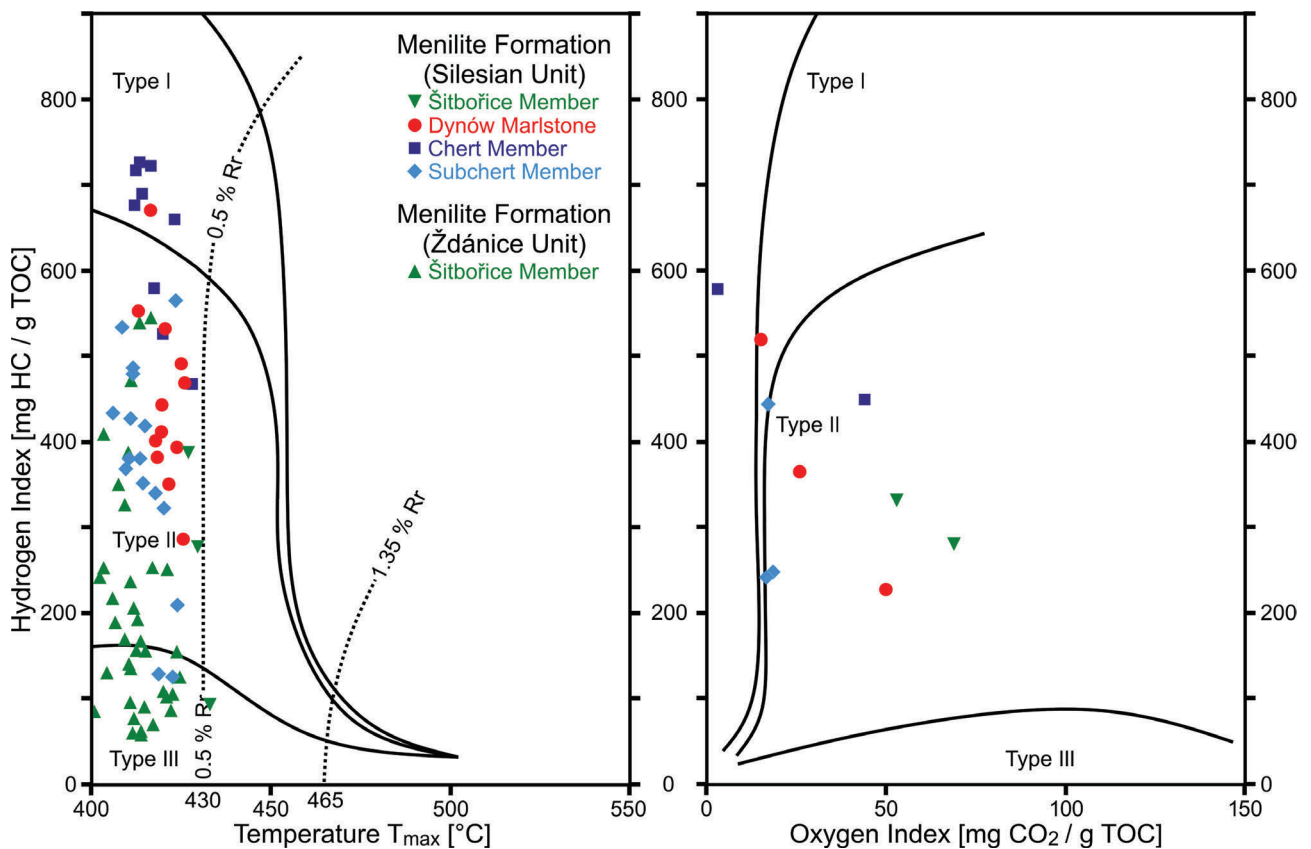


**Fig. 2.** Comparison of the Menilite Formation from Silesian and Ždánice units with respect to the prevailing kerogen type based on the HI versus  $T_{max}$  or OI, respectively. Kerogen type maturation paths according to Espitalié et al. (1985). The data after Jirman et al. (2018, 2019).

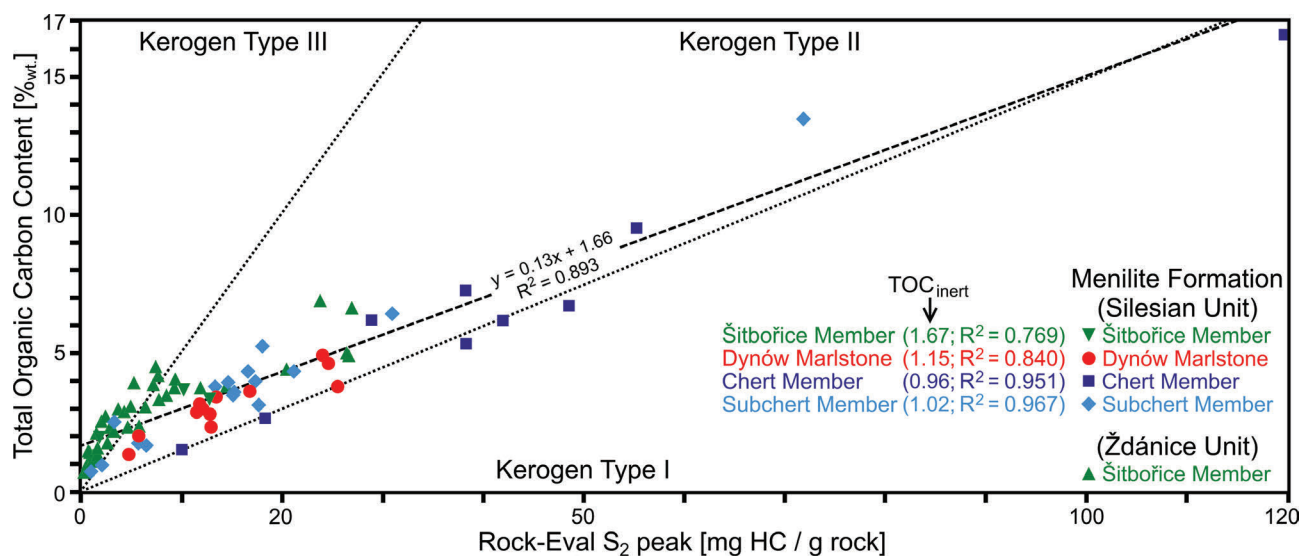


**Fig. 3.** Cross-plot of TOC versus residual hydrocarbon potential (Rock-Eval S<sub>2</sub> peak). The amount of non-pyrolizable organic carbon necessary for the HI<sub>true</sub> calculation was determined based on this diagram. Modified according to Dahl et al. (2004); genetic boundaries of kerogen types according to Langford and Blanc-Valleron (1990). The data after Jirman et al. (2018, 2019).

The Menilite Formation is one of the potential source rocks with less yield in the Czech Republic. Therefore, oil can be expected to have mixed geochemical features.

**Acknowledgements:** The authors thank to MND, a.s. for the samples and ERASMUS+ programme for supporting the Ph.D. student Petr Jirman. Special thanks go to M. Bubík and R.F. Sachsenhofer. The research has been financially supported by the institutional funds of Masaryk University.

## References

- Blížkovský M., Kocák A., Mořkovský M., Novotný A., Gaža B., Kostelníček P., Hlavatý V., Lunga S., Vass D., Franců J. & Müller P. 1994: Exploration History, Geology and Hydrocarbon Potential in the Czech Republic and Slovakia. In: Popescu B.M. (Ed.): Hydrocarbons of Eastern Central Europe, Habitat. Exploration and Production History. Springer-Verlag, Berlin, 71–117.
- Bubík M., Franců J., Gilíková H., Otava J. & Švábenická L. 2016: Upper Cretaceous to lower Miocene of the Subsilesian Unit (western Carpathians, Czech Republic): stratotypes of formations revised. *Geol. Carpath.* 67, 3, 239–256.
- Dahl B., Bojesen-Koefoed J., Holm A., Justwan H., Rasmussen E. & Thomsen E. 2004: A new approach to interpreting Rock-Eval S<sub>2</sub> and TOC data for kerogen quality assessment. *Organic Geochemistry* 35, 1461–1477.
- Espitalié J., Deroo G. & Marquis F. 1985: La pyrolyse Rock-Eval et ses applications. Première partie. *Revue de l'Institut Français du Pétrole* 40, 563–579.
- Geršlová E., Opletal V., Sýkorová I., Sedláková I. & Geršl M. 2015: A geochemical and petrographical characterization of organic matter in the Jurassic Mikulov Marls from the Czech Republic. *International Journal of Coal Geology* 141–142, 42–50.
- International Committee for Coal and Organic Petrology 1998: The new vitrinite classification (ICCP system 1994). *Fuel* 77, 349–358.
- International Committee for Coal and Organic Petrology 2001: The new inertinite classification (ICCP system 1994). *Fuel* 80, 459–471.
- Jirman P., Geršlová E., Pupp M. & Bubík M. 2018: Geochemical characteristic, thermal maturity and source rock potential of the Oligocene Šitbořice member of the Menilite Formation in the Ždánice Unit (Czech Republic). *Geol. Quarterly* 62, 858–872.
- Jirman P., Geršlová E., Bubík M., Sachsenhofer R.F., Bechtel A. & Więclaw D. 2019: Depositional environment and hydrocarbon potential of the Oligocene Menilite Formation in the Western Carpathians: A case study from the Loučka section (Czech Republic). *Mar. Petrol. Geol.* 107, 334–350.
- Lafargue E., Marquis F. & Pillot D. 1998: Rock-Eval 6 applications in hydrocarbon exploration, production, and soil contamination studies. *Revue de l'Institut Français du Pétrole* 53, 421–437.
- Langford F.F. & Blanc-Valleron M.M. 1990: Interpreting Rock-Eval pyrolysis data using graphs of pyrolizable hydrocarbons vs. total organic carbon. *AAPG Bulletin* 74, 799–804.
- Peters K.E. & Cassa M.R. 1994: Applied source rock geochemistry. *AAPG Memoir* 60, 93–102.
- Stráňák Z. 1981: Lithofacies and correlation of the Menilitic Formation in the Carpathian Flysch belt of Moravia. *Zemní Plyn a Nafta* 26, 9–18 (in Czech with English summary).
- Stráňák Z., Benešová E., Cicha I., Gabriel M., Kolářová M. & Žůrková I. 1974: Vysvětlující text k základní geologické mapě 1:25 000 M-33-106-D-c (Šitbořice). MS, Ústřední Ústav Geologický, Brno (in Czech).
- Taylor G.H., Teichmüller M., Davis A., Diessel C.F.K., Littke R. & Robert P. 1998: Organic Petrology. *Gebrüder Borntraeger*, Berlin, 1–704.

# Genesis of the Carpathian obsidians

MILAN KOHÚT<sup>1</sup>, ROBERT ANCKIEWICZ<sup>2</sup>, ADRIÁN BIROŇ<sup>3</sup>, MARTIN DANIŠÍK<sup>4</sup>,  
VOJTĚCH ERBAN<sup>5</sup>, AXEL GERDES<sup>6</sup>, ALISON HALTON<sup>7</sup>, KAROL JESENÁK<sup>8</sup>,  
CHRIS KIRKLAND<sup>4</sup>, YULIA KOCHERGINA<sup>5</sup>, TOMÁŠ MAGNA<sup>5</sup>, TOMÁŠ MIKUŠ<sup>3</sup>,  
STANISLAVA MILOVSKÁ<sup>3</sup>, RASTISLAV MILOVSKÝ<sup>3</sup>, NICK PEARCE<sup>9</sup>, CLEMENTE RECIO<sup>10</sup>,  
SARAH SHERLOCK<sup>7</sup>, JURAJ ŠURKA<sup>3</sup>, JOHN WESTGATE<sup>11</sup> and PAVEL BAČO<sup>12</sup>

<sup>1</sup>Earth Science Institute, Slovak Academy of Sciences, Bratislava, Slovakia, milan.kohut@savba.sk

<sup>2</sup>Institute of Geological Sciences, Polish Academy of Sciences, Cracow, Poland

<sup>3</sup>Earth Science Institute, Slovak Academy of Sciences, Banská Bystrica, Slovakia

<sup>4</sup>John de Laeter Centre, Curtin University, Perth, Australia

<sup>5</sup>Czech Geological Survey, Praha, Czech Republic

<sup>6</sup>Institute of Earth Sciences, Goethe University, Frankfurt, Germany

<sup>7</sup>School of Physical Sciences, The Open University, Milton Keynes, United Kingdom

<sup>8</sup>Faculty of Science, Comenius University, Bratislava, Slovakia

<sup>9</sup>Institute of Geography and Earth Science, Aberystwyth University, United Kingdom

<sup>10</sup>University of Salamanca, Salamanca, Spain

<sup>11</sup>Department of Geology, University of Toronto, Toronto, Canada

<sup>12</sup>Dionýz Štúr State Institute of Geology, Košice, Slovakia

**Abstract:** Comprehensive study of the Carpathian obsidians reveals that these rocks as typical arc igneous products were derived by multistage processes with the primary basaltic magma formed due to melting of the lower crustal source at the mantle/crust border. Subsequent formation of melt reservoirs in the middle and upper crust, accompanied by secondary melting of the surrounding rocks with recurrent addition of an ascending melt, and repeated processes of assimilation and fractionation produced a suite of chemically variable lithology from basalt to rhyolites and obsidians before 12.0–11.4 Ma in the Carpathians.

## Introduction

Obsidian is instantaneously solidified (quenched) igneous–volcanic rock, originated mainly from the acid rhyolitic melt, often referred to as “*natural volcanic glass*” with typical glassy lustre and usually dark jet-black, grey or brown colour. Generally, it is dominantly composed of amorphous, dark (opaque ± locally translucent) volcanic glass (≥95 volume %), with addition of various minerals like biotite, plagioclase, alkali feldspar, quartz, pyroxenes, amphiboles, magnetite, Fe–Ti oxides, zircon, apatite, monazite, pyrrhotite, pyrite, chalcopyrite, olivine, uraninite, ilmenite, hercynite and garnet. Obsidian was widely used for tool-making (stone industry) during prehistoric times, and played significant role in the evolution of Humankind and civilization. Volcanic glass was geologically known since the end of the 18<sup>th</sup> Century on our territory. It was archeologically documented in the 19<sup>th</sup> Century in the Zemplín–Tokaj area (on the both sides of present boundary between SE Slovakia and NE Hungary), the only natural volcanic glass region in Central Europe (see review: Biró 2006). The Carpathian obsidians (CO) were traded since the Aurignacien 28 000 yrs. BP.

## Geological setting

The Carpathian obsidians from the studied Zemplín–Tokaj area belong to the Eastern Slovakian Neovolcanic Field (ESNF) in the SE Slovakia/NE Hungary, where the isolated Sarmatian volcanos penetrate the Miocene strata and pre-Cenozoic basement. The complicated geological setting of the Zemplínske vrchy Mts (ZVM) and their surrounding includes the evolution from the Paleozoic up to recent. The ZVM form typical tectonic horst surrounded by the East Slovakian Basin with several elevated volcanic bodies. Present architecture is a consequence of the back-arc extension, associated with the asthenosphere updoming accompanied by calc-alkaline volcanism and pull-apart opening during the Miocene, followed by the Pannonian to Quaternary late stage regional uplift and erosion. The Paleozoic basement rock sequences encompass various sedimentary and volcanic rocks of the Carboniferous to Permian age, whereas the high-grade metamorphic rocks (gneisses, amphibolites, and metagranites) can be found in deeper horizon. The Mesozoic cover is composed of conglomerates, sandstones, calcareous shales, dolomites, rarely with the evaporite intercalations of the Lower

Triassic in age. The Middle Triassic is formed mainly by carbonates (limestones and dolomites). The oldest Cenozoic sediments in the studied area are the Lower Miocene–Karpatian in age (claystones and of sandstones), followed by the Badenian basal conglomerates, sandstones, and grey calcareous claystones, that were overlaid by extrusive rhyodacite lava flow bodies and their tuffites and tuffs of the Upper Badenian age. The Lower–Middle Sarmatian rhyolite tuffs and tuffites are intercalated by clays and sandy claystones. The Middle–Upper Sarmatian rhyolite volcanism is represented by the dyke bodies, and an extrusion body with associated volcanoclastics in the Viničský broader area. The margins of the bodies are formed by perlitized obsidian, often in breccia development. The Upper Sarmatian is formed by calcareous sands and sandstones with interbeds of clays, tuffitic clays and tuffites. The sequence finished by the Pannonian lacustrine and river clays, silts with intercalations of sands, river gravels (Kobulský et al. 2014).

### Mineralogy

Although the obsidians are dominated by the amorphous volcanic glass an important role play the rock-forming and accessory minerals from genetic point of view. The Carpathian obsidians consist of a broad association of minerals like plagioclase, biotite, alkali feldspar, quartz, pyroxenes, amphiboles, magnetite, Fe–Ti oxides, pyrrhotite, pyrite, olivine, zircon, apatite, monazite, uraninite, ilmenite, and garnet that are observable mainly under the microscope. These minerals can be present in the form of phenocrysts (having size 100–1000  $\mu\text{m}$ ), microlites (10–50  $\mu\text{m}$ ), and hair like trichites. Beside the autolithic origin of these minerals, sporadic xenoliths from the source and/or assimilated rocks can be also present. Commonly observed banded texture or alternation of dark and pale stripes is caused by minute microlites and trichites oriented in the direction of the melt flow. Although, the majority of described minerals have the primary magmatic origin, not all of them reflect their crystallization from a parent rhyolite melt. Plagioclases — most of the grains are subhedral microlites, although the phenocrysts in the size up to 450  $\mu\text{m}$  are present locally as well. Generally, they are zoned with broad chemical composition (andesine–bytownite  $\text{An}_{33-89}$ ) in the cores, whereas more acid oligoclase ( $\text{An}_{19-31}$ ) and scarcely albite compositions were identified in the rime. K-fs's — are less frequent than Pl; sporadic anhedral grains up to 100  $\mu\text{m}$  are mainly anorthoclases, while high-temperature sanidines were found as well as.

Biotites — form mainly larger laths 100–850  $\mu\text{m}$  in size, and/or smaller oval/anhedral flakes having brown pleochroic colour. Typical primary magmatic Fe-biotites have annite composition with  $\text{mg}^\# = 0.32\sim 0.43$  and/or high  $\text{TiO}_2$  content 3.2–4.6 wt. % indicating high-temperature origin. Elevated Fe content together with moderate Mg and Al contents show their peraluminous character influenced partly by calc-alkaline source. Generally, the low  $\text{Fe}^{3+}$  (ca 7 % from  $\text{FeO}$ ) suggests for their crystallization at QFM buffer. Pyroxenes — form essentially euhedral and subhedral microlites and trichites, and locally anhedral grains in aggregates. Commonly, all of them belong to Ca–Fe–Mg group of pyroxenes. Pyroxenes are dominantly orthopyroxenes; clinopyroxenes are rare. Opx's are of enstatite composition ( $\text{mg}^\# = 0.55\sim 0.76$ ), some of them have pigeonite and fersilite composition ( $\text{mg}^\# = 0.29\sim 0.35$ ). Cpx's have augitic composition ( $\text{mg}^\# = 0.60\sim 0.68$ ). Amphiboles — were identified as subhedral microlites, and/or anhedral grains in aggregates. They fit in to Mg–Fe–Mn group of amphiboles of grunerite and/or commingtonite composition ( $\text{Si}_{(\text{apfu})} = 7.02\sim 7.64$ ; and  $\text{mg}^\# = 0.31\sim 0.58$ ). Magnetite — form mostly small anhedral grains and trichites, and/or subhedral/anhedral xenocrystic grains up to 45  $\mu\text{m}$  with typical ilmenite lamellas in a few cases. Olivines — were locally found with pyroxene in xenocrystic aggregates as anhedral grains 5–100  $\mu\text{m}$  of forsterite composition ( $\text{mg}^\# = 0.55\sim 0.68$ , and  $\text{fe}^\# = 0.32\sim 0.49$ ), having tholeiitic character. Zircon — forms euhedral quadrangle and prismatic grains 10–50  $\mu\text{m}$  in size with low  $\text{HfO}_2 = 1.33\sim 1.88$  wt. % and low  $\text{Th/U} = 0.11\sim 0.46$  distinctive for felsic fractionated igneous rocks. Apatites — form mainly euhedral and subhedral prismatic microlites in size of 20–55  $\mu\text{m}$ . Typical fluor-apatites with increased fluorine content  $\text{F} = 2.02\sim 4.41$  wt. % indicate igneous origin from fractionated melt. Monazites — were commonly found as subhedral grains 15–100  $\mu\text{m}$  in size and/or oval grains with sign of magmatic corrosion. Studied monazites are commonly enriched in Th ( $\text{ThO}_2 \leq 10.63$  wt. %) and depleted in uranium ( $\text{UO}_2 \leq 0.75$  wt. %) or Si ( $\text{SiO}_2 \leq 2.65$  wt. %) with both cheralite and huttonite substitutions. Primary magmatic monazites (Ce) yield normally the Cenozoic–Miocene ages (CHIME), although the Variscan restite ones (age 330 Ma) were identified as well as.

### Geochemistry and dating

Geochemically studied samples of the Carpathian obsidians from ZVM belong to the volcanic peraluminous

rocks, and high potassium calc-alkaline rhyolite series (ASI=1.05~1.15). Their SiO<sub>2</sub> content varies in narrow interval from 76.4 to 77.5 wt. % reflecting their fractionation nature. Relatively elevated FeO<sup>t</sup> values with simultaneous declination in MgO (wt. %) indicate their overall ferroan character. The Rb/Sr ratio=2.13~3.46 points to the distinct differentiation of these volcanic rocks, however this does not appear in most of the surrounding rocks. Based on the classical I/S-typology for felsic magmatic rocks, studied obsidians belong to typical mixed (hybrid) I/S-type igneous rocks. Normalized REE patterns show uniform distribution trend with a pronounced negative Eu anomaly, La<sub>N</sub>/Yb<sub>N</sub>=3.43~7.17 and partially elevated HREE values compared to surrounding rhyolite and dacite rocks. Their C1 chondrite normalized REE patterns are falling on the boundary between “hot-dry-reduced” and “cold-wet-oxidized” magmas (Bachmann & Bergantz 2008) reflecting genesis of magma from mantle and crust sources. The binary plots of CaO/Na<sub>2</sub>O vs. Al<sub>2</sub>O<sub>3</sub>/TiO<sub>2</sub> respectively Rb/Ba vs. Rb/Sr clearly indicate that our samples fit the mixing trajectories with dominant crustal magma proportion and weak (30~10 %) contribution from mantle component. The Carpathian obsidians and their host rhyolite and dacite rocks represent a typical magmatic analogue of volcanic arc products from the geotectonic point of view (Kohút et al. 2018). Cl/F ratio of studied CO varies between 1~3.5 what is familiar to obsidians from the Mature Island Arcs and/or those originated at the Continental Margins (Macdonald et al. 1992).

WR Sr isotopic composition of studied obsidians with measured <sup>87</sup>Sr/<sup>86</sup>Sr values in narrow interval 0.7114~0.7122 and <sup>87</sup>Rb/<sup>86</sup>Sr=7.3129~8.8110 are considerably more radiogenic than values from basaltic to rhyolitic rocks of the Central Slovakian Neovolcanic Field (CSNF) see Kohút et al. (2012). Generally, Sr isotopic composition of the CO suggests a crustal source little affected by sub-continental lithospheric mantle (SCLM). The Nd isotopic composition of the CO with <sup>147</sup>Sm/<sup>144</sup>Nd=0.1172~0.1271 and <sup>143</sup>Nd/<sup>144</sup>Nd=0.51225~0.51227 is more radiogenic comparing volcanic rocks of the CSNF. Indeed these values resemble those of the Western Carpathians orthogneisses with mainly crustal origin (Kohút et al. 2012). WR lead isotopes of the CO with <sup>206</sup>Pb/<sup>204</sup>Pb=18.87~19.88; <sup>207</sup>Pb/<sup>204</sup>Pb=15.683~15.687 and <sup>208</sup>Pb/<sup>204</sup>Pb=38.91~38.93 are higher than MORB and gently lower than common upper crustal rocks. However, Pb isotopic picture of the CO is akin to the Western Carpathians amphibolites and/or indicates derivation in the Arc from SCLM that was influenced by less radiogenic crustal source. WR Hf isotopic signature

of the CO with <sup>176</sup>Hf/<sup>177</sup>Hf=0.28263~0.28265; <sup>176</sup>Lu/<sup>177</sup>Hf=2.023~2.026 and initial εHf<sub>(12)</sub>=-4.7~-5.2 is familiar to common continental magmas characteristics. Whereas zircon initial values εHf<sub>(0)</sub>=-1.4~-6.5 call for slight SCLM source contribution. The CO oxygen isotopic composition with δ<sup>18</sup>O<sub>(VSMOW)</sub>=8.6~9.3 ‰ indicates rather mixed crustal/mantle origin. Again, no simple explanation can be offered yet. Closed system fractionation of basaltic magma is precluded by the δ<sup>18</sup>O data of the CO, and also excluded simple crustal contamination with sedimentary rocks and/or granites+orthogneisses as an important mechanism in the formation of hosting rhyolites, but allows the possibility of magma mixing as a partial cause of the isotope variations. Hydrogen composition of studied samples with δ<sup>2</sup>H<sub>(VSMOW)</sub> varying in -103.2~-109.0 ‰ is within standard obsidian values of primary magmatic residual H<sub>2</sub>O remaining after volcanic degassing, and excluding exchange with meteoric water. Li isotope composition with δ<sup>7</sup>Li=0.3 to 0.6 ‰, underscored by elevated Li contents of 60~70 ppm is similar to S-type granitic and/or common supra-crustal rocks. On the other hand boron isotopic composition with δ<sup>11</sup>B=+0.6~-2.1 ‰ and low B contents B=21~26 ppm is rather indicative for volcanic products generated from altered oceanic crust and/or I-type granitic rocks.

Dating of the CO was mostly associated with dating of host rhyolitic rocks in the past. The first K–Ar dating of biotites and WR provided a broad age range of 13.5 ± 2.5 Ma to 10.8 ± 0.5 Ma (see review Kohút et al. 2017). Direct dating of the Carpathian obsidians was performed by the Uranium Fission tracks method (FT) with the ages 14.2 ± 0.5 and 11.1 ± 0.8 Ma (Repčok et al. 1988), as well as Bigazzi et al. (1990) with higher ages from 17.8 ± 1.1 Ma to 13.7 ± 0.8 Ma. Latterly studied obsidians were also dated by WR K–Ar method with ages 15.0 to 11.1 Ma (Bačo et al. 2017). Our new FT dating of the CO glasses using the isothermal plateau fission track (ITPFT) method provided slightly younger ages in a narrow time range of 12.0~11.2 Ma. Noteworthy, that four of the five WR Rb/Sr isotopic analyses of our CO samples form a pseudo-isochron with an age 13.5 Ma and initial Sr ratio 0.7103 what is a bit older age as brought the ITPFT dating, but still within the age interval of older dating methods. There was applied Ar/Ar isotopic dating (glass and biotites) from our CO samples due to more accurately determine the age of rhyolite magmatism. The obtained ages for glass varying from 12.0 to 11.4 Ma are comparable to those of the ITPFT method, whereas the biotites provided slightly older ages (14.4~12.4 Ma). Albeit studied obsidians contain

mostly tiny zircons (10~25 µm in size), enough larger zircon grains suitable for spot age dating of the rhyolite/obsidian magmatism in the high temperature domain were separated. Unfortunately, the use of SHRIMP failed to achieve a sufficient amount of radiogenic Pb to obtain meaningful ages and/or isotopic ratios, whereas the use of LA MC-ICPMS provided representative ages. However, rather than direct dating of the magma crystallization beginning, we obtained data on the source rocks. The most zircon grains were restitic ones with ages 490~478 Ma (originating from orthogneisses), 354~352 Ma (Variscan granites), 283~278 (Permian magmatites) and 88~83 Ma (Rochovce granite). This is consistent with the isotopic characteristics of the source rocks, and/or structure of the pre-Cenozoic basement in the Western Carpathians, suggesting recycling of the older crustal igneous rocks. Merely the rare zircons with ages 15 and 13 Ma have confirmed the CO's Miocene age.

### Conclusions

Summarizing the above presented like the high silica content of CO strictly suggesting their crustal affiliation; mineral composition with the presence of accessory minerals as olivine, pyroxene, amphibole and/or bytownite feldspar indicating their partial mantle-derived origin; isotopic characteristics with more radiogenic Sr–Nd isotopic composition, and elevated values of the stable isotopic O, H and Li signatures attesting their crustal-dominated source, in contrast their Pb, Hf and B isotopic systematics argumentative for a lower crustal metabasic source slightly influenced by sub-continental lithospheric mantle. Collectively, isotopic compositions of the Carpathian obsidians resemble the arc igneous products derived by multi-stage processes with the primary basaltic magma formed due to melting of the lower crustal source at the mantle/crust boundary. Subsequent formation of a melt reservoirs in the middle and upper crust, accompanied by secondary melting of the surrounding rocks, and recurrent mixing with an ascending lower crustal SCLM influenced melt, and/or repeated processes of assimilation and fractionation produced

a suite of chemically variable lithology from basalt to rhyolites and/or obsidians before 12.0~11.4 Ma in the Carpathians.

**Acknowledgements:** This work was supported by the Slovak Research and Development Agency under the Contract no. APVV-0549-07, APVV-18-0107; and VEGA grants: 0060/16 and 0084/17. The work was also supported by the projects: ITMS: 26220120064 and ITMS: 26210120013, which had been co-financed through the European Regional Development Fund.

### References

- Bachmann O. & Bergantz G.W. 2008: Rhyolites and their source mushes across tectonic settings. *Journal of Petrology* 49, 2277–2285.
- Bačo P., Kaminská L., Lexa J., Pécskay Z., Bačová Z. & Konečný V. 2017: Occurrences of Neogene volcanic glass in the Eastern Slovakia – raw material source for the stone industry. *Anthropologie* LV/1-2, 207–230.
- Bigazzi G., Marton P., Norelli P. & Rozložník L. 1990: Fission track dating of Carpathian obsidians and provenance identification, *Nucl. Tracks Radial. Meas.* 17, 3, 391–396.
- Biró K.T. 2006: Carpathian Obsidians: Myth and reality. In: Proceedings of the 34<sup>th</sup> Intern. Symp. on Archaeometry (3<sup>rd</sup>–7<sup>th</sup> May 2004, Zaragoza Spain). *Institución Fernando el Católico (C.S.I.C.)*, 267–278.
- Kobulský J., Žecová K., Gazdačko L., Bačo P., Bačová Z., Maglay J., Petro L. & Šesták P. 2014: Guidebook to Geological-Educational Map of the Zemplínske vrchy Mts. *ŠGÚDŠ Bratislava*, 1–84.
- Kohút M., Kollárová V., Mikuš T., Konečný P., Šurka J., Milovská S., Holický I. & Bačo P. 2018: The mineralogy and petrology of the Carpathian obsidians. *Conference CEMC-2018 Abstract book*, 50–52.
- Kohút M., Lexa J., Michalko J., Carl C., Huhma H. & Konečný P. 2012: Source of rocks and genesis of the Western Carpathians Neovolcanic rocks in the light of isotope study. Conference GEOCHÉMIA 2012, Bratislava. *Conferences, symposia and seminars ŠGÚDŠ Bratislava*, 71–75 (in Slovak).
- Kohút M., Westgate J., Pearce N. & Bačo P. 2017: Obsidians of the Eastern Slovakia – New results of FT dating in the context of the Western Carpathians Cenozoic Volcanism evolution. *Mente et Malleo* 2/1, 32 (in Slovak).
- Macdonald R., Smith R.L. & Thomas J.E. 1992: Chemistry of the Subalkalic Silicic Obsidians. *USGS Professional Paper* 1523, 1–214.
- Repčok I., Kaličiak M. & Bacsó Z. 1988: The age of some volcanites of the Eastern Slovakia, determined by the uranium Fission track method. *Záp. Karpaty, ser. miner., petrog., geoch., metalogenéza* 11, 75–88 (in Slovak).

# Regionally dependent metasomatism of orogenic mantle revealed by highly siderophile elements and Re–Os isotope geochemistry of Variscan lamproites: A pilot study from the Bohemian Massif

LUKÁŠ KRMÍČEK<sup>1,2</sup> and LUKÁŠ ACKERMAN<sup>1</sup>

<sup>1</sup>Institute of Geology of the Czech Academy of Sciences, Rozvojeová 269, CZ-165 02 Prague 6, Czech Republic; krmicek@gli.cas.cz

<sup>2</sup>Brno University of Technology, Faculty of Civil Engineering, AdMaS Centre, Veveří 95, CZ-602 00 Brno, Czech Republic; krmicek.l@fce.vutbr.cz

**Abstract:** Orogenic (high-silica) lamproites represent a group of post-collisional mantle-derived igneous rocks that hold the potential to sample components with extreme compositions from highly heterogeneous mantle. In our pilot study, we explore highly siderophile element (HSE) and Re–Os isotope systematics of Variscan orogenic lamproites sampled from the termination of the Moldanubian and Saxo–Thuringian zones of the Bohemian Massif. Orogenic lamproites of the Bohemian Massif are distinguished by variably high contents of SiO<sub>2</sub>, high Mg# and predominant mineral associations of K-rich amphibole and Fe-rich microcline. The HSE show (i) consistently very low contents in all investigated orogenic lamproites compared to the estimated concentrations in majority of mid-ocean ridge basalts, hotspot-related volcanic rocks and arc lavas, and (ii) marked differences in relative and absolute HSE abundances between the samples from the Moldanubian and Saxo-Thuringian Zone. Such a regional dependence in HSE from mantle-derived melts is exceptional. Orogenic lamproites have highly variable and high initial suprachondritic <sup>187</sup>Os/<sup>188</sup>Os values (up to 0.631) compared with rather chondritic to subchondritic Os isotope values of the young lithospheric mantle below the Bohemian Massif. The highly radiogenic Os isotope component in orogenic lamproites may be derived from preferential melting of metasomatised vein assemblages sitting in depleted peridotite mantle. This process appears to be valid generally in the petrogenesis of orogenic lamproites both from the Bohemian Massif (Variscan lamproites) and from the Mediterranean area (Alpine lamproites). As a specific feature of the orogenic lamproites from the Bohemian Massif, originally ultra-depleted mantle component correlative with remnants of the Rheic Ocean lithosphere in the Moldanubian Zone was metasomatised by a mixture of evolved and juvenile material, whereas the lithospheric mantle in the Saxo-Thuringian Zone was enriched through the subduction of evolved crustal material with highly radiogenic Sr isotope signature. As a result, this led to observed unique regionally dependent coupled HSE, Rb–Sr and Re–Os isotope systematics.

## Introduction

The platinum-group elements (PGE: Os, Ir, Ru, Rh, Pt and Pd), along with Re and Au, are grouped together as the highly siderophile elements (HSE), defined by their strong affinities for metals and sulphides relative to silicates. These elements have variable partitioning behaviour between highly compatible Os, Ir, Ru and Rh relative to mildly compatible Pt and Pd and moderately incompatible Re and Au during melting and mafic melt crystallization (e.g., Day et al. 2013). This exceptional geochemical behaviour serves HSE as a powerful tool for tracing different mantle processes such as partial melting, melt percolation and mantle metasomatism. However, the behaviour of HSE in orogenic mantle is not well constrained because of a limited amount of available HSE data of compositionally highly variable mantle-derived orogenic melts and mantle xenoliths. This is intriguing as orogenic lamproites hold a potential to sample mantle domains with extreme geochemical

(including isotope) composition from highly heterogeneous orogenic mantle. In spite of that, there are still only a few papers dealing with incomplete HSE systematics of lamproitic rocks till the present day (e.g., Conticelli et al. 2007; Prelević et al. 2015).

Lamproites are comparatively a rare group of peralkaline, ultrapotassic and perpotassic mantle-derived igneous rocks. Traditionally, lamproites can be found in both anorogenic and orogenic geodynamic settings, and it has been demonstrated that their mantle source can be enriched by interaction with different reservoirs within the lithospheric mantle, including subducted continental and oceanic material (e.g., Prelević et al. 2010, 2015; Krmíček et al. 2016).

## Orogenic lamproites in the Bohemian Massif

In the Bohemian Massif, the occurrences of peralkaline dykes of lamproitic composition are almost

exclusively restricted to the eastern margin of the Moldanubian Zone and to the West Sudetes Domain of the Saxo–Thuringian Zone (e.g., Krmíček et al. 2011, 2016 and references therein). These dykes are all orogenic in origin, being emplaced after their host geological units collided during the Variscan orogeny (Fig. 1). Spatial distribution of these lamproites in a belt at the eastern termination of the Moldanubian and Saxo–Thuringian zones is genetically connected with the closure of the Rheic Ocean followed by the subduction of the Bruno–vistulian Terrane (Krmíček et al. 2016).

Orogenic lamproites and their more evolved equivalents (leucolamproites) occur both in the Moldanubian and Saxo–Thuringian zones. Their compositions can be distinguished by predominant mineral associations of K-rich amphibole and Fe-rich microcline, which mineralogically correspond to a new variety of silica-rich lamproite (Krmíček et al. 2011).

The dykes have not been directly dated, however, based on  $^{40}\text{Ar}/^{39}\text{Ar}$  age determinations of other mafic intrusions with lamproitic affinity from the Bohemian Massif, their presumed emplacement age is  $\sim 330$  Ma (Awdankiewicz et al. 2009; Krmíček et al. 2011).

### Analytical methods

The concentrations of HSE and Re–Os isotope data were obtained at the Institute of Geology of the Czech Academy of Sciences in Prague following the methods described in detail by Krmíček et al., in review. Osmium

isotope measurements were determined using the Thermo Triton Plus multicollector thermal ionization mass spectrometer (TIMS), while Ir, Ru, Pt, Pd and Re concentrations were analysed by the sector-field ICP-MS (Element 2, Thermo).

### Results

Contents of HSE in all samples show consistently very low values ( $\Sigma\text{HSE}$  mostly below 1 ppb; Krmíček et al., in review) with respect to the estimated concentrations both in the primitive upper mantle (PUM; Becker et al. 2006) and in the mantle-derived rocks such as mid-ocean ridge basalts, hotspot-related volcanic rocks (ocean island basalts, continental flood basalts, komatiites, intraplate alkaline volcanic rocks such as kimberlites and anorogenic lamproites) and arc lavas (e.g., Day 2013; Gannoun et al. 2016 and references therein), with the Moldanubian lamproites being recognised by higher values on average than the samples from the Saxo–Thuringian Zone.

The primitive mantle-normalised HSE distributions exhibit fractionated patterns with progressive increase from iridium-PGE (I-PGE; Os, Ir, Ru, Rh) to platinum-PGE (P-PGE; Pt, Pd) with  $\text{Pt}_N/\text{Os}_N$  between 1.5 and 36, feature typical for mantle-derived melts (see Gannoun et al. 2016 and references therein), while Re is mostly similar to or lower than Pt.

The present-day  $^{187}\text{Os}/^{188}\text{Os}$  isotope ratios vary widely within the studied sample suite, ranging between 0.157 and 0.685, corresponding to variable radiogenic initial  $^{187}\text{Os}/^{188}\text{Os}_{(330)}$  values of 0.157–0.631. There is no significant difference between the samples from different zones as they oscillate between the  $^{187}\text{Os}/^{188}\text{Os}$  and  $^{187}\text{Re}/^{188}\text{Os}$  values close to the composition of PUM and a component with highly radiogenic  $^{187}\text{Os}/^{188}\text{Os}$  both at relatively low and high  $^{187}\text{Re}/^{188}\text{Os}$ .

### Discussion

Due to contrasting behaviour of Os and Re during partial melting, mantle-derived melts should be preferably enriched in Re over Os leaving the mantle residues with subchondritic Re/Os ratios. Indeed, arc lavas and melts derived by partial melting of MORB or OIB sources exhibit Re-enriched compositions (usually  $>100$  ppt of Re; Gannoun et al. 2016 and references therein). For the rest of HSE, during the mantle depletion caused by common partial melting degrees ( $<20\%$ ), low-melting

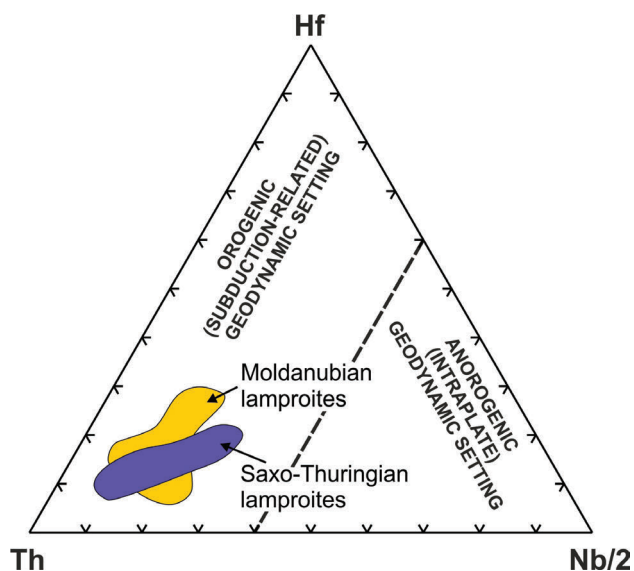


**Fig. 1.** Position of studied Variscan lamproites from the Bohemian Massif in the Th–Hf–Nb/2 discrimination diagram developed for potassic mantle-derived rocks by Krmíček et al. (2011).

point (e.g., Cu-bearing) sulphides represent a predominant host for P-PGE, while I-PGE are hosted by highly refractory phases such as alloys or high temperature sulphides leading to characteristic enrichment from Os through Pt to Re in mantle-derived melts (e.g., Day 2013; Gannoun et al. 2016). However, observed Re and other HSE abundances in orogenic lamproites from the Bohemian Massif require a mantle source overall largely replenished in all HSE, especially in Re (Fig. 2). The most possible explanation for these characteristics is a presence of large proportion of recycled, HSE-poor material (e.g., eclogite, pyroxenite; Ackerman et al. 2013; Aulbach et al. 2016) in the parental source of lamproitic magmas, which would be consistent with observed variable, but radiogenic  $^{187}\text{Os}/^{188}\text{Os}$  signatures. Moreover, there is a unique regional dependence between relatively Re-enriched Moldanubian lamproites and those from the Saxo-Thuringian Zone (Fig. 2). This difference can be primarily caused by the presence of regionally contrasting depleted/enriched mantle source and/or by variable oxygen fugacity during partial melting or metasomatism of depleted mantle source by regionally contrasting material. Additionally, Tertiary orogenic lamproites from the Mediterranean area display relative Re and Os enrichment compared to Variscan orogenic lamproites from the Bohemian Massif (Fig. 2). Such enrichment could be related to the interaction with a component derived from the convective mantle via volatile-rich carbonatite fluids (Prelević et al. 2010).

Studied orogenic lamproites have high and variable suprachondritic initial  $^{187}\text{Os}/^{188}\text{Os}$  values, much higher than predominantly only slightly superchondritic to subchondritic values found in the Bohemian upper mantle rocks (e.g., Ackerman et al. 2013; Kochergina et al.

2016) but similar to those found in pyroxenites (cf. Ackerman et al. 2016). The highly radiogenic  $^{187}\text{Os}/^{188}\text{Os}$  component is sampled both by lamproites (with high Mg#) and leucolamproites, which, together with absence of xenoliths, excludes the possibility that radiogenic  $^{187}\text{Os}/^{188}\text{Os}$  component is related to low-pressure contamination by continental crust with high  $^{187}\text{Os}/^{188}\text{Os}$ . The observed variability in  $^{187}\text{Os}/^{188}\text{Os}$  can be explained by binary mixing between clinopyroxenite and ambient mantle. This process seems to be valid generally in the petrogenesis of orogenic lamproites both from the Bohemian Massif and from the Mediterranean area. On the other hand,  $^{187}\text{Os}/^{188}\text{Os}$  variations in combination with Os abundances alone do not have sufficient sensitivity to distinguish possible variations in mantle sources (and thus the nature and extent of mantle metasomatism) of orogenic lamproites from the Moldanubian and Saxo-Thuringian zones. Therefore, we introduce the combination of  $^{187}\text{Os}/^{188}\text{Os}$  and  $^{87}\text{Sr}/^{86}\text{Sr}$  as the latter is very sensitive indicator of subduction-related (fluid-enhanced) metasomatism. Using this approach, the composition of Moldanubian and Saxo-Thuringian lamproites is best explained by vein/wall-rock melting model requiring 60–70 % contribution from the metasomatised mantle with different (regionally dependent) Sr-isotope composition. This is in agreement with assumption of Krmíček et al. (2016), that the originally ultra-depleted mantle component (correlative with subducted Rheic Ocean lithosphere) was metasomatised by a mixture of evolved and juvenile material (thinned continental crust?) in the Moldanubian Zone, whereas the lithospheric mantle in the Saxo-Thuringian Zone underwent subduction-related metasomatism by evolved (with pronounced negative Eu anomaly and highly radiogenic  $^{87}\text{Sr}/^{86}\text{Sr}$ ) crustal material.

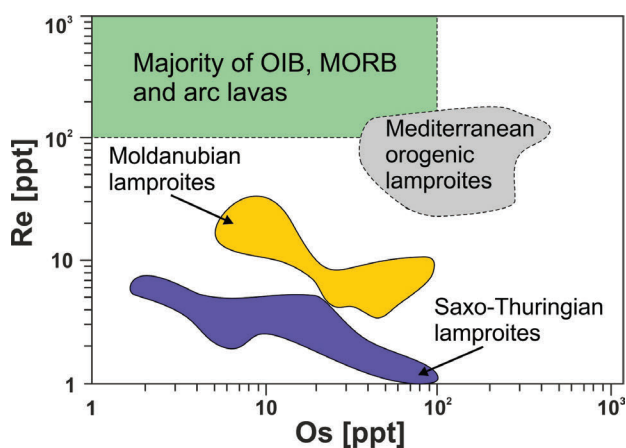


Fig. 2. Re and Os abundances (ppt) of the studied Variscan lamproites in comparison with the Mediterranean orogenic lamproites and majority of OIB, MORB and arc lavas (Krmíček et al., *in review* and references therein).

## Conclusions

Based on our pilot study of highly siderophile elements and Re–Os isotope geochemistry of orogenic lamproites from the Bohemian Massif, we present the following conclusions:

- All HSE show consistently very low contents in all samples compared to the other mantle-derived volcanic rocks as the result of high proportions of HSE-depleted material (e.g., pyroxenite, eclogite) in the source parental for orogenic lamproitic magmas.
- There are remarkable differences in relative and absolute HSE abundances between the samples from the Moldanubian and Saxo-Thuringian zones.

- Studied orogenic lamproites have highly variable and suprachondritic  $^{187}\text{Os}/^{188}\text{Os}$  values overlapping the values found in mantle pyroxenites from the Bohemian Massif. Therefore, the highly radiogenic Os isotope component in orogenic lamproites may be derived from preferential melting of metasomatised mantle rich in clinopyroxenite vein assemblages sitting in depleted peridotite mantle.
- Based on the combination of Os–Sr isotope signature, the composition of Moldanubian and Saxo–Thuringian lamproites can be best explained by vein/wall-rock melting model requiring 60–70 % contribution from the metasomatised mantle with different (regionally dependent)  $^{87}\text{Sr}/^{86}\text{Sr}$  composition.

**Acknowledgements:** This research was financially supported by the internal project of the Institute of Geology of the Czech Academy of Sciences (no. 9324) and the institutional project RVO 67985831 as well as by the BUT project LO1408 “AdMaS UP — Advanced Materials, Structures and Technologies”, supported by the Ministry of Education, Youth and Sports CR under the “National Sustainability Programme I”.

## References

- Ackerman L., Bizimis M., Haluzová E., Sláma J., Svojtka M., Hirajima T. & Erban V. 2016: Re–Os and Lu–Hf isotopic constraints on the formation and age of mantle pyroxenites from the Bohemian Massif. *Lithos* 256–257, 197–210.
- Ackerman L., Pitcher L., Strnad L., Puchtel I.S., Jelínek E., Walker R.J. & Rohovec J. 2013: Highly siderophile element geochemistry of peridotites and pyroxenites from Horní Bory, Bohemian Massif: implications for HSE behaviour in subduction-related upper mantle. *Geochim. Cosmochim. Acta* 100, 158–175.
- Aulbach S., Mungall J.E. & Pearson D.G. 2016: Distribution and processing of highly siderophile elements in cratonic mantle lithosphere. *Rev. Mineral. Geochem.* 81, 239–304.
- Awdankiewicz M., Awdankiewicz H., Kryza R., Rodionov N. & Timmerman M. 2009: Ar–Ar and SHRIMP constraints on the age of Late Palaeozoic intermediate and silicic dykes and sills in the Sudetes. *Mineral. Spec. Pap.* 34, 9.
- Becker H., Horan M.F., Walker R.J., Gao S., Lorand J.P. & Rudnick R.L. 2006: Highly siderophile element composition of the Earth’s primitive upper mantle: Constraints from new data on peridotite massifs and xenoliths. *Geochim. Cosmochim. Acta* 70, 4528–4550.
- Conticelli S., Carlson R.W., Widom E. & Serri G. 2007: Os, Sr, Nd and Pb Isotope Composition of Italian Quaternary Volcanism. In: Beccaluva L., Bianchini G. & Wilson M. (Eds.): *Cenozoic Volcanism in the Mediterranean Area. Geological Society of America*, Boulder, 171–202.
- Day J.M.D. 2013: Hotspot volcanism and highly siderophile elements. *Chem. Geol.* 341, 50–74.
- Gannoun A., Burton K.W., Day J.M.D., Harvey J., Schiano P. & Parkinson I. 2016: Highly siderophile element and Os isotope systematics of volcanic rocks at divergent and convergent plate boundaries and in intraplate settings. *Rev. Mineral. Geochem.* 81, 651–724.
- Kochergina Y.V., Ackerman L., Erban V., Matusiak-Małek M., Puziewicz J., Halodová P., Špaček P., Trubač J. & Magna T. 2016: Rhenium–osmium isotopes in pervasively metasomatized mantle xenoliths from the Bohemian Massif and implications for the reliability of Os model ages. *Chem. Geol.* 430, 90–107.
- Krmíček L., Ackerman L., Hrubý J. & Kynický J.: The highly siderophile elements and Re–Os isotope geochemistry of Variscan lamproites from the Bohemian Massif: implications for regionally dependent metasomatism of orogenic mantle. *Chem. Geol.*, in review.
- Krmíček L., Cempírek J., Havlín A., Přichystal A., Houzar S., Krmíčková M. & Gadas P. 2011: Mineralogy and petrogenesis of a Ba–Ti–Zr-rich peralkaline dyke from Šebkovice (Czech Republic): Recognition of the most lamproitic Variscan intrusion. *Lithos* 121, 74–86.
- Krmíček L., Romer R.L., Ulrych J., Glodny J. & Prelević D. 2016: Petrogenesis of orogenic lamproites of the Bohemian Massif: Sr–Nd–Pb–Li isotope constraints for Variscan enrichment of ultra-depleted mantle domains. *Gondwana Res.* 35, 198–216.
- Prelević D., Brüggmann G., Barth M., Božović M., Cvetković V., Foley S.F. & Maksimović Z. 2015: Os-isotope constraints on the dynamics of orogenic mantle: The case of the Central Balkans. *Gondwana Res.* 27, 1560–1573.
- Prelević D., Stracke A., Foley S.F., Romer R.L. & Conticelli S. 2010: Hf isotope compositions of Mediterranean lamproites: mixing of melts from asthenosphere and crustally contaminated mantle lithosphere. *Lithos* 119, 297–312.

# Magmatic evolution of the Štiavnica volcano

JAROSLAV LEXA<sup>1</sup>, BERTRAND ROTTIER<sup>2</sup>, KEEWOOK YI<sup>3</sup>, ANDREAS AUDÉTAT<sup>2</sup>,  
IGOR BROSKA<sup>1</sup>, PETER KODĚRA<sup>4</sup> and MILAN KOHÚT<sup>1</sup>

<sup>1</sup>Earth Science Institute, Slovak Academy of Sciences, Bratislava, Slovakia; geoljalx@savba.sk

<sup>2</sup>Bayerisches Geoinstitut, University of Bayreuth, Bayreuth, Germany

<sup>3</sup>Korea Basic Science Institute, Ochang, Republic of Korea

<sup>4</sup>Department of Economic Geology, Faculty of Natural Sciences, Comenius University, Bratislava, Slovakia

**Abstract:** The Štiavnica stratovolcano evolved in five stages: (1) construction of the extensive andesite strato-volcano during the interval 15.0–13.6 Ma, including diorite and diorite porphyry intrusions; (2) emplacement of subvolcanic intrusive rocks associated with a resurgent uplift, sector collapse and denudation of the volcano — with the granodiorite pluton showing the age around 13.6 Ma, quartz-diorite porphyry sills and dykes dated at 13.77–13.0 Ma and granodiorite porphyry stocks showing the age around 12.95 Ma, (3) subsidence of the caldera and its filling by differentiated andesites around 12.9 Ma, (4) renewed volcanic activity marked by post-caldera andesites between 12.8 and 12.2 Ma; (5) uplift of the resurgent horst in the central part of the caldera accompanied by rhyolite volcanic/intrusive activity between 12.2 and 11.4 Ma. Volcanic and intrusive rocks of the Štiavnica volcano were sourced from an upper crustal magmatic reservoir stored at a pressure between ~1 and ~3 kbar. The different phenocrysts (plagioclase, orthopyroxene, clinopyroxene, Mg-hornblende, and quartz) have crystallized from dacitic to rhyolitic melts at a temperature between ~960 to ~700 °C. A clear change in mineralogy from plagioclase–orthopyroxene–clinopyroxene, plagioclase–orthopyroxene, plagioclase–orthopyroxene–hornblende, plagioclase–hornblende–biotite, and then plagioclase–hornblende–biotite–quartz is observed with the decrease of temperature of the melts. Crystal mush in the upper-crustal magma chamber was repeatedly fed by magmas having an andesitic composition resulting from differentiation and crustal contamination of primitive mantle magmas in a lower and/or middle crustal reservoir. Eruption of volcanic rocks and emplacement of subvolcanic intrusions resulted from a mixing between the evolved magmas stored in the upper crustal reservoir and newly injected primitive magmas and/or due to fluid saturation and exsolution of the magmas. Late stage rhyolites represent a segregation of the interstitial silicic melt from the crystals mush in the upper crustal reservoir during its cooling at temperature <750 °C. The porphyry-skarn Cu–Au, Fe-skarn, disseminated base metal and epithermal mineralizations of the Štiavnica volcano associate genetically with those magmatic rocks that resulted from a prolonged cooling of magma in the upper crustal reservoir — cooling and perhaps magma mixing that provoked fluid exsolution from the long-lived crystal mush were the key factors in formation of ore deposits.

*We dedicate this contribution to the late RNDr. Vlastimil Konečný, CSc., who played a leading role in mapping of the Štiavnica volcano and along with J. Lexa has laid down essential aspects of its geology and evolution.*

## Introduction

Majority of the world's Cu, Au, Ag, and Mo are sourced from magmatic–hydrothermal and epithermal ore deposits. These deposits are generally formed during discrete short periods of times in long-lived magmatic systems and their formation results from an interplay between magmatic and hydrothermal factors (e.g., Sillitoe 2010; Richards 2011; Audétat & Simon 2012). The middle Miocene Štiavnica volcano provides a unique opportunity to study relationships among magmatic evolution and related metallogenetic processes. While preserved volcanic complexes allow a serious paleovolcanic reconstruction (Konečný et al. 1998; Chernyshev et al. 2013) a resurgent horst in the central part of its caldera exposes subvolcanic intrusive complexes with related ore mineralizations. Thanks to extensive past and ongoing mining works and exploration drilling as well as extensive labo-

ratory investigation of varied mineralizations, we have extensive data concerning their mineralogy and genesis. This opens a way to study one of the fundamental metallogenetic aspects — their relationship to the magmatic evolution of the volcano.

Previous studies on the magmatic evolution of the volcano (Lexa et al. 1997; Konečný P. et al. 2002; Kovalenker et al. 2006), based on petrography, major and trace elements geochemistry and a limited application of thermo-barometer, concluded that magma evolved first in a lower crustal reservoir probably up to an andesitic composition and then evolved further in an upper crustal magma chamber by assimilation–fractionation processes. Mixing due to repeated injections of andesitic magma was a common phenomenon in this shallow reservoir. Storage conditions in the upper crustal magma chamber were estimated to be 850–1050 °C, 1.7–2.5 kbar and 3–6 H<sub>2</sub>O wt. %.

Here, the magmatic evolution of the volcano is reconstructed in a greater detail by studying major and trace element compositions of minerals and silicate melt inclusions hosted in orthopyroxene, clinopyroxene, plagioclase, amphibole, and/or quartz from the pre-, syn-, and post-ore volcanic and subvolcanic rocks and using up-to-date methods of thermobarometry. This approach is coupled with U–Pb zircon dating of subvolcanic intrusive rocks that due to alterations could not be dated well enough by conventional K/Ar and Rb/Sr methods.

### Methods applied

We have selected 39 rock samples typical of different stages of the Štiavnica volcano. Textures and mutual relationships of mineral phases were documented by optical microscopy. Major and minor elements of selected samples were determined by ICP-ES and trace elements by ICP-MS in ACME laboratories. Phenocrysts and glassy silicate melt inclusions hosted in orthopyroxene, clinopyroxene, plagioclase, and quartz from samples of different stages were analyzed by EPMA for major elements, Cl and S concentrations. Using the LA-ICP-MS at the Bayerisches Geoinstitut we have analyzed in the selected rocks different silicates, oxides, rock matrixes and also un-exposed silicate melt inclusions hosted in different phenocrysts. The U–Th–Pb dating of separated accessory zircons by SHRIMP has been carried out in cooperation with Korea Basic Science Institute in its high resolution ion microprobe laboratory.

To determine oxygen fugacity, temperature and pressure at which the different minerals and matrixes were formed or at which they are in equilibrium we have variably used the opx-liquid (Putirka 2008) cpx-liquid (Neave & Putirka 2017), and amphibole thermobarometry (Ridolfi et al. 2012; Mutch et al. 2016; Putirka 2016) and Ti-in-quartz barometer (Huang & Audétat 2012; Audétat 2013), Fe–Ti oxides (Ghiorso & Evans 2008), Ti-in-zircon (Ferry & Watson 2007), and zircon saturation thermometry (Watson & Harrison 1983).

### Structure and evolution of the volcano and related mineralizations

K/Ar and Rb/Sr ages of the Štiavnica volcano rocks (Chernyshev et al. 2013) have been supplemented by new U–Th–Pb zircon dating of subvolcanic intrusions and caldera filling (Table 1).

**Table 1:** Results of new U–Th–Pb zircon dating.

Sample	Description	Age (Ma)
BLJ-1	Px andesite hosting a diorite porphyry stock	14.85±0.48
GD-1	Granodiorite bell-jar pluton, Hodruša – Mayer shaft	13.53±0.14
RB-1073	Granodiorite bell-jar pluton, Hodruša–Ravenstein	13.63±0.21
RB-1149	Granodiorite bell-jar pluton, Hodruša – All Saints mine	13.61±0.22
RB-350	Quartz-diorite porphyry sill, pre- Au mineralization	13.77±0.15
RB-349	Quartz-diorite porphyry sill, post- Au mineralization	13.46±0.19
RB-1148	Thick quartz-diorite porphyry sill above granodiorite	13.25±0.13
KDP-1	Quartz-diorite porphyry sill, Paradajz	13.73±0.20
KDP-3	Quartz-diorite porphyry ring dyke, Juraj štôľňa	12.99±0.18
R-8	Granodiorite porphyry stock; Zlatno, borehole R-8	12.92±0.11
R-12	Granodiorite porphyry stock; Zlatno, borehole R-12	12.98±0.08
ST-102	Glassy amph-bt andesite, early caldera fill, Ilija	12.85±0.15
ST-107	Amph-bt andesite; late cladera fill, south of Močiar	13.02±0.08

The scheme of the volcano evolution (Konečný et al. 1998; Chernyshev et al. 2013) has been updated as follows: (1) construction of an extensive pyroxene and amphibole–pyroxene andesite stratovolcano during the interval 15.0–13.6 Ma, including emplacement of diorite intrusion hosting a barren high sulfidation system at Šobov and a diorite porphyry stock at Beluj (1b) hosting the Au-porphyry type mineralization; (2) emplacement of subvolcanic intrusive rocks, mostly by the underground cauldron subsidence mechanism, associated with a resurgent uplift, sector collapse and denudation of the volcano following a granodiorite pluton emplacement (Kubač et al. 2018); the stage includes: (2a) emplacement of a granodiorite bell-jar pluton before the uplift in the depth 2–3 km, showing the age around 13.6 Ma; Fe-skarn and disseminated base metal mineralizations associate with the pluton; (2b) emplacement of quartz-diorite porphyry sills pre-dating the Hodruša epithermal Au mineralization related to the sector collapse (Kubač et al. 2018) around 13.75 Ma and sills that post-date the uplift and the epithermal Au mineralization in the interval 13.5–13.0 Ma; (2c) emplacement of granodiorite porphyry stocks and dyke clusters hosting the porphyry-skarn type Cu–Au mineralization around 12.95 Ma, (3) a subsidence of the caldera and its filling by evolved amphibole-biotite andesites and dacites around 12.9 Ma, including rare hot-spring siliceous deposits; (4) renewed activity of less evolved andesites during the interval 12.8–12.2 Ma, (5) an uplift of the resurgent horst in the central part of the caldera

accompanied by rhyolite volcanic/intrusive activity and an extensive system of epithermal precious and base metals veins during the interval 12.2–11.4 Ma.

### Magmatic evolution of the volcano

The Central Slovakia Volcanic Field, including the Štiavnica volcano, shows a close relationship to extension in a back-arc syn- to post-collision setting. The magmas were generated in association with tectonothermal rejuvenization related to extension induced asthenospheric upwelling. There are two concepts explaining the origin of andesitic magmas that were further subjected to evolution in the crust: (a) partial melting of metasomatized lithospheric mantle generated hydrous high-alumina basalts that evolved further at the base of the crust by a high-pressure fractionation and/or lower crustal assimilation (e.g. Harangi et al. 2007; Seghedi & Downes 2011); (b) radiogenic isotope data favor partial melting of the lower crustal metabasic source influenced by subcontinental lithospheric mantle and crustal assimilation (Kohút et al. 2019).

Essential P–T–X parameters of the investigated Štiavnica volcano rocks are summarized in Table 2. As evidenced by interpreted pressures between ~1 and ~3 kbar volcanic and intrusive rocks of the Štiavnica volcano had their source in an upper crustal magma reservoir at a depth of 4–12 km. Dominantly silicic composition of melt inclusions and thermometry indicate that the different phenocrysts (plagioclase, orthopyroxene, clinopyroxene, Mg-hornblende, and quartz) have crystallized from dacitic to rhyolitic residual melts at a temperature between ~960 and ~700 °C. A clear change of mineralogy from plagioclase–orthopyroxene–clinopyroxene, plagioclase–orthopyroxene, plagioclase–orthopyroxene–hornblende, plagioclase–hornblende–

biotite to a final plagioclase–hornblende–biotite–quartz is observed with the decrease of magma temperature. With exception of the most evolved rocks (subvolcanic intrusions 2a–2c, caldera fill (3) and late stage rhyolites (5)) matrix compositions of andesites are substantially less silicic than melt inclusions in phenocrysts. Along with the frequent presence of mafic enclaves, disequilibrium phenocrysts assemblages and resorbed cores of phenocrysts it indicates that the evolved crystal-rich magma was mixed with a more mafic magma. Apparently, the upper-crustal magma chamber was repeatedly fed by magmas having an andesitic composition. These magmas probably represent products of differentiation ( $\pm$ crustal contamination) of primitive magmas in lower and/or middle crustal reservoirs. A direct evidence for a magma evolution in the middle crustal reservoir is provided by the pressure and temperature of mafic Cr-rich clinopyroxene phenocrysts in the orthopyroxene–clinopyroxene andesites, indicating pressure and temperature conditions of 3.7–5.3 kbar and 1130 to 1170 °C, respectively. The crystal assemblage of the Beluj diorite porphyry (1b), hosting the Au-porphyry type mineralization, characterized by magmatic garnet, high-Al Mg-hornblende, Cr-rich clinopyroxene, orthopyroxene and plagioclase, suggests a mixing of magmas sourced from three levels of crystallization (lower-, middle-, and upper-crustal). Apparently, it was the extent of mafic magma input into the upper-crustal crystal mush that has governed the composition of erupting magmas — a larger input of mafic magma lead to eruptions of pyroxene and pyroxene–amphibole andesites with less silicic matrixes, while during periods of a lesser mafic magma input the erupting magmas composition was governed by magma differentiation towards more silicic and volatiles enriched composition.

Late stage rhyolites (5) show the same composition as silicate melt inclusions in phenocrysts of other rocks.

**Table 2:** Summarized P–T–X parameters of the Štiavnica volcano rocks.

Stage	SiO <sub>2</sub> (%) Whole rock Konečný et al. (1998)	SiO <sub>2</sub> (%) Dry rock ACME labs (2018)	SiO <sub>2</sub> (%) Matrix	SiO <sub>2</sub> (%) Melt inclusions	Pressure (kbar)	Temperature (°C)
5	72.2–77.7	74.30	76–77	71–80	2.9–3.2	700–760
4	56.1–63.5	–	66.5–78.1	70–78 (63–68)	1–3, ~ 4.2	770–860, ~ 910
3	58.8–64.4	61.85–66.63	74–78	70–78	1.7–2.9	730–820
2c	57.7–63.4	60.02–63.02	Eutectic Qtz–Kfs–Pl	73–79	1.5–3.0	720–810
2b	57.9–64.0	62.73–64.46	Eutectic Qtz–Kfs–Pl	73–81	~2.7	~770
2a	60.2–64.7	61.82–62.99	Eutectic Qtz–Kfs–Pl	71–81	2.0–3.3	740–820
1b	60.1–61.1	57.23–58.23	59–63	74–77	2.1–3.0, 3.7–6.1	795–880, ~1135
1	56.1–61.5	55.61–60.19	68.3–71.1	Mostly 70–80	0.7–2.2	750–860

Thus, they represent a segregation of the interstitial silicic melt from the crystal mush during its cooling at temperature  $<750$  °C, leading to the formation of erup-tible rhyolite magma pockets. Injection of mafic magma into the crystal mush and related thermal rejuvenization could be a relevant triggering mechanism. A similar conclusion has been reached by Demko in Demko et al. (2010) based on geochemical and radiogenic isotope data.

The eruption of volcanic rocks and emplacement of subvolcanic intrusions resulted from a mixing between the evolved crystal mush and injected new primitive magma and/or due to fluid saturation and exsolution of volatiles from magma. Both processes lead to a decrease in density and viscosity and thus to the magma mobiliza-tion and uprise.

Mineralizations of the Štiavnica volcano associate genetically with those magmatic rocks that resulted from a prolonged cooling of the upper crustal crystal mush and related fluid saturation (2a, 2b, 2c, 5) as well as a limited extent of magma mixing. Cooling and perhaps also magma mixing that led to the fluid saturation and exsolution from the long-lived crystal mush were the key factors in formation of the different ore deposits. In contrast, according to our observation the source magma of the Beluj Au porphyry systems resulted from a mixing between a deep and hydrous magma and an evolved, dry, upper crustal crystal mush.

**Acknowledgements:** This study was financed through a Swiss SNSF Early Postdoc Mobility Grant to B. Rottier (NJS; P2GEP2\_174895), through the Slovak grants APVV-15-0083 and VEGA 1/0560/15 to P. Koděra and J. Lexa and APVV-SK-KR-18-0008 to I. Broska and M. Kohút.

## References

- Audétat A., Simon A.C., Hedenquist J.W., Harris M. & Camus F. 2012: Magmatic controls on porphyry copper genesis. In: *Geology and genesis of major copper deposits and districts of the world — A tribute to Richard H. Sillitoe*, 553–572.
- Chernyshev I.V., Konečný V., Lexa J., Kovalenker V.A., Jeleň S., Lebedev V.A. & Goltsman Y.V. 2013: K–Ar and Rb–Sr geochronology and evolution of the Štiavnica stratovolcano (central Slovakia). *Geologica Carpathica* 64, 327–360.
- Demko R., Lexa J., Koděra P., Biroň A., Smolka J., Šesták P., Konečný P., Tuček L., Ferenc Š., Bačo P., Repčiak M., Kollárová V., Pipík-Kyška R. & Mikušová J. 2010: Maps of paleovolcanic reconstruction of Slovak rhyolite volcanic and analysis of magmatic and hydrothermal processes. *Open file report, Archive ŠGÚDŠ*, Bratislava, 1–689 (in Slovak).
- Harangi S., Downes H., Thirlwall M. & Gmeling K. 2007: Geochemistry, petrogenesis and geodynamic relationships of Miocene calc-alkaline volcanic rocks in the Western Carpathian Arc, eastern central Europe. *Journal of Petrology* 48, 2261–2287.
- Kohút M., Anczkiewicz R., Erban V., Kochergina Y.V., Magna T., Recio C., Yi K. & Broska I. 2019: The Miocene granitic rocks of the Central Slovakian Neovolcanic Field: Isotopic constraints. In: Hrdličková K. & Daňková L. (Eds.): *Abstract volume of the 17th Meeting of the Central European Tectonic Groups, CETEG 2019, Rozdrojovice*, 39.
- Konečný P., Lexa J. & Konečný V. 2002: Evolution of the Banská Štiavnica stratovolcano and corresponding magma chamber (Central Slovakia). *Proceedings of XVII. Congress of CBGA Bratislava, September 1-4, 2002. Geologica Carpathica* 53, special issue (CD).
- Konečný V., Lexa J., Halouzka R., Hók J., Vozár J., Dublan L., Nagy A., Šimon L., Havrila M., Ivanička J., Hojstričová V., Mihalíková A., Vozárová A., Konečný P., Kováčiková M., Filo M., Marcin D., Klukanová A., Liščák P. & Žáková E. 1998: Explanations to the geological map of the Štiavnické vrchy and Pohronský Inovec Mountains (Štiavnica stratovolcano) 1:50 000, I. and II. part. *Geological Survey of Slovak Republic, Bratislava*, 1–473 (In Slovak with English summary).
- Kovalenker V.A., Naumov V.B., Prokof'ev V.Yu., Jelen S. & Gaber M. 2006: Compositions of Magmatic Melts and Evolution of Mineral-Forming Fluids in the Banská Štiavnica Epithermal Au–Ag–Pb–Zn Deposit, Slovakia: A Study of Inclusions in Minerals. *Geochemistry International* 44, 2, 118–136.
- Kubač A., Chovan M., Koděra P., Kyle J.R., Žitňan P., Lexa J. & Vojtko R. 2018: Mineralogy of the epithermal precious and base metal deposit Banská Hodruša at the Rozália mine (Slovakia). *Mineralogy and Petrology* 112, 705–731.
- Lexa J., Konečný P., Kojstříčová V., Konečný V. & Köhlerová M. 1997: Petrologic model of the Štiavnica stratovolcano. *Open file report, Archive ŠGÚDŠ*, Bratislava, 1–52 (in Slovak).
- Lexa J., Štohl J. & Konečný V. 1999: Banská Štiavnica ore district: relationship among metallogenetic processes and the geological evolution of a stratovolcano. *Mineralium Deposita* 34, 639–665.
- Richards J.P. 2011: High Sr/Y arc magmas and porphyry Cu±Mo±Au deposits: just add water. *Economical Geology* 106, 1075–1081.
- Seghedi I. & Downes H. 2011: Geochemistry and tectonic development of Cenozoic magmatism in the Carpathian–Pannonian region. *Gondwana Research* 20, 655–672.
- Sillitoe R.H. 2010: Porphyry copper systems. *Economical Geology* 105, 3–41.

# Mineralogy of Nb–Ta bearing apatite–cordierite metasomatised metabasite from Mostovyi ore occurrence (Ukrainian Shield)

NATALIIA LYZHACHENKO<sup>1</sup>, SERGII KURYLO<sup>2,3</sup>, SERGII BONDARENKO<sup>3</sup>  
and VOLODYMYR SYOMKA<sup>3</sup>

<sup>1</sup>SE “Institute of Environmental Geochemistry NASU”, Kyiv, Ukraine; lyzhachenko@gmail.net

<sup>2</sup>Earth Science Institute, Slovak Academy of Sciences, Ďumbierska 1, 974 11 Banská Bystrica, Slovakia; kurylo.sergiy@gmail.com

<sup>3</sup>M.P. Semenenko Institute of Geochemistry, Mineralogy and Ore Formation, NASU, Kyiv, Ukraine

**Abstract:** The unique type of rare-metal metasomatite from the Mostovyi Ta–Nb–Au ore occurrence at the western margin of Korsun–Novomyrgorodskiy pluton is described. Nb–Ta-bearing metasomatite was formed in a result of alteration of metabasite rocks by P-, F-rich fluid from felsic magmas. The main characteristic and chemical compositions of main and secondary minerals in metasomatite and metabasite are shown.

## Introduction

The Mostovyi ore occurrence located in the northern part of the Bratsk–Zvenygorod tectonic structure at the western margin of Korsun–Novomyrgorodskiy pluton within the Ingul Megablock of the Ukrainian Shield (Kropyvnytskyi region, central part of Ukraine) (Fig. 1). The Mostovyi occurrence composed of Proterozoic gneisses of Ingul series intruded by granite and pegmatite of Kirovograd complex. The ore mineralization presented by Au and rare metal (Ta, Nb) elements. Gold is in relationship to graphite-bearing gneisses and rare metal- to aplitic-pegmatites and metasomatites (Bezvyunnyi 2005; Ivanov et al. 2011). The contribution describes the Nb–Ta-bearing apatite–cordierite metasomatite (ACM) from Mostovyi Au-rare metal occurrence.

All samples were selected from exploration borehole of the Mostovyi occurrence. Thin sections were studied in reflected light. The major-element has been analysed by JEOL JXA-8520F. Analytical results in empirical formulae of minerals from ACM and metabasite are given in Table 1.

## Petrography

Host metamorphic rocks are presented by graphite–cordierite–biotite, graphite–biotite, biotite–muscovite gneisses and mylonites. Magmatic rocks are represented by aplite, pegmatites and granite but graphite–cordierite–biotite gneisses dominate. They are grey, dark grey with schistosity structure, commonly equigranular, less porphyroblastic. Porphyroblasts are represented by cordierite and K-feldspar, 3–8 mm in size. Groundmass is

fine- to medium-grained. The main minerals: biotite, cordierite, plagioclase, quartz, K-feldspar, graphite; accessory minerals are zircon, monazite, apatite, sillimanite.

Rare metal apatite–cordierite metasomatite hosted by porphyroblastic biotite–cordierite gneisses and contain small relic of metabasite rocks. The wide of metasomatic zone is about 3 meters. The main minerals form two size group: first presented by tabular cordierite, 3 to 15 mm in size; second — grains groundmass in

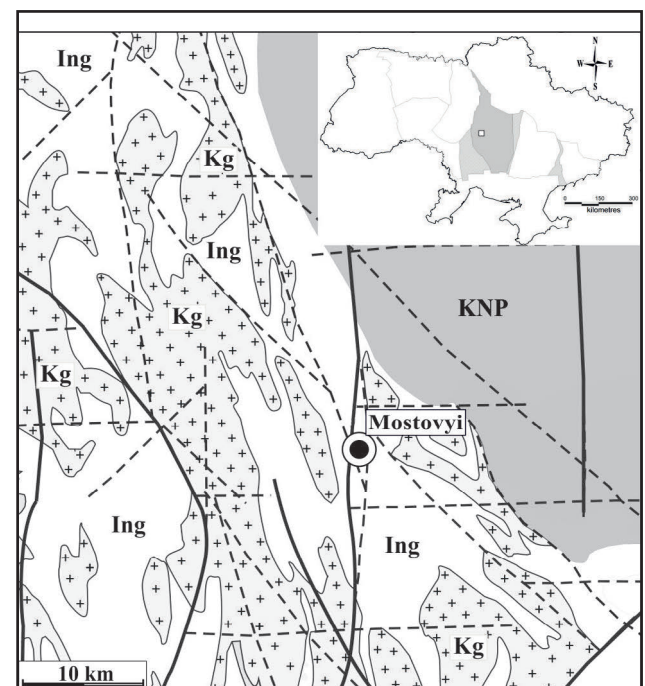


**Fig. 1.** Location of Mostovyi Nb–Au ore occurrence. KNP — Korsun–Novomyrgorodskiy pluton, Kg — granitoids of Kirovograd complex (S-type), Ing — gneisses of Ingul series.

interstitial of cordierite and consists of smaller cordierite, apatite, quartz, sulphides, graphite and biotite (0.4–1.3 mm). Mineral composition ACM in vol. %: cordierite 60–85, apatite 10–30, biotite 3–10, quartz 1–7, graphite 2–5, tourmaline (identified in thin-section) 0–2, small pyroxene relic. Sulphides and sulfosalts are represented by pyrrhotite (3–5 %), arsenopyrite, lollingite, pyrite, chalcopyrite and less molybdenite. Oxides are represented by Nb-rutile and relics of ilmenite. Group of orthophosphate is formed by graftonite, sarcopside, jahnsomervellite. Secondary minerals are chlorite, carbonate (sometimes up to wt. 3 %), hematite, and phosphate (arrojadite, ludlamite, laudite). Accessories: monazite, zircon, sillimanite, rarely uraninite.

Relics of metabasite bodies are represented by transitional rock type from gabrodiorite to gabbro–norite, groundmass is medium-grained (1.2–2.2 mm). Mineral composition in vol. %: hornblende 45–50, plagioclase 25–30, salite 10–15, biotite 5–6, orthopyroxene 2–3, titanite about 1, ilmenite <1 %. Among accessories is only apatite.

## Mineralogy

### Nb–Ta bearing apatite-cordierite metasomatite

Light-blue **cordierite** forms tabular grains from 0.5 to 15 mm in size, with numerous inclusions of apatite, quartz, biotite, graphite, Nb-rutile, sulphides, monazite, zircon. The chemical composition of the mineral phases is similar. Cordierite grains are mostly magnesian, Fe/(Fe+Mg) value is 0.3–0.4 and gradually increase from the core to rime. Al varies from 3.88 to 3.98 apfu. Cordierite is partly transformed to pinnite aggregates. In transitional phase cordierite is hydrated and enriched in iron. Brown **biotite** forms singular euhedral grains <2 mm in size, or small aggregates up to 4 mm. Chemical composition is homogeneous, average Fe/(Fe+Mg) value is 53.8 at. %, annite end-membership is dominant, TiO<sub>2</sub> varied in narrow range 2.14–2.88 wt. %, fluorine content is very low. **Sillimanite** is presented in very fine needles (0.1–0.5 mm) included in cordierite and prismatic crystals (<0.2 mm) in groundmass, poor at trace elements. **Graphite** occurs as non-oriented fine-flakes, less than 0.5 mm in size or aggregates included in quartz, forms intergrowth with biotite, sulfides and arrojadite. **Quartz** forms small rounded grains in groundmass, commonly with numerous graphite inclusions.

**Nb-rutile** commonly occurs as inclusions in cordierite and rarely in apatite, and singular grains in groundmass

**Table 1:** Empirical formulas of investigated minerals.

Apatite-cordierite metasomatite	
Silicate	
Cordierite	$(\text{Na}_{0.166-0.18} \text{K}_{0.001})_{0.174} (\text{Mn}_{0.049-0.053} \text{Fe}^{2+}_{0.58-0.652} \text{Mg}_{1.195-1.227})_{1.89-1.92} [(\text{Fe}^{3+})_{0.1-0.116} \text{Al}_{3.88-3.98} \text{Si}_{5.04-5.056} \text{O}_{18}]$
Titanite	$(\text{Ca}_{1.0} \text{LREEY}_{0.002} \text{Ti}_{1.0})_{0.95} (\text{Sn}_{0.003} \text{Al}_{0.16} \text{Ti}_{0.78})_{0.95} [\text{Al}_{0.01} \text{Si}_{0.99} \text{O}_4] (\text{F}_{0.16} \text{O}_{0.84})_{1.0}$
Biotite	$(\text{Na}_{0.026} \text{K}_{1.776} \text{Ca}_{1.802})_{1.802} (\text{Ti}_{0.291} \text{Cr}_{0.036} \text{Fe}_{2.44} \text{Mg}_{2.094} \text{Al}_{0.733})_{5.63} [(\text{Al}_{2.544} \text{Si}_{5.456})_2 \text{O}_{20}] (\text{OH})_2$
Sillimanite	$\text{Al}_{2.002}^{vi} [(\text{Al}_{0.011} \text{Si}_{0.989})_{1.0} \text{O}_5]$
Oxides	
Nb-Rutile	(1) $(\text{W}_{0.001} \text{V}_{0.011} \text{Cr}_{0.06} \text{Fe}_{0.035} \text{Ta}_{0.014} \text{Nb}_{0.074} \text{Ti}_{0.855})_{0.990} \text{O}_2$ (2) $(\text{W}_{0.0} \text{V}_{0.016} \text{Cr}_{0.008} \text{Fe}_{0.046} \text{Ta}_{0.03} \text{Nb}_{0.088} \text{Ti}_{0.809})_{0.998} \text{O}_2$ (3) $(\text{W}_{0.001} \text{V}_{0.016} \text{Cr}_{0.009} \text{Fe}_{0.064} \text{Ta}_{0.045} \text{Nb}_{0.108} \text{Ti}_{0.755})_{0.99} \text{O}_2$
Sulfide and sulfosalts	
Pyrrhotite	$\text{Fe}_{0.921} \text{Ni}_{0.003} \text{Co}_{0.002} \text{As}_{0.001} \text{S}_{1.073}$
Pyrite	$\text{Fe}_{0.999} \text{Ni}_{0.007} \text{Co}_{0.001} \text{S}_{1.993}$
Arsenopyrite	$\text{Fe}_{0.763-1.004} \text{Ni}_{0.01-0.167} \text{Co}_{0.006-0.075} \text{As}_{1.054-1.156} \text{S}_{0.827-0.911}$
Lollingite	$\text{Fe}_{0.747} \text{Ni}_{0.17} \text{Co}_{0.103} \text{As}_{1.934} \text{S}_{0.043}$
Molybdenite	$\text{MoS}_2$
Phosphate minerals	
Apatite	$(\text{Ca}_{4.681} \text{Mn}_{0.109} \text{Fe}_{0.042})_{4.832} (\text{PO}_4)_3 (\text{F}_{0.785} \text{OH}_{0.215})_{1.0}$
Monazite-(Ce)	$\text{Ca}_{0.081} \text{Th}_{0.017-0.104} \text{Ce}_{0.396} \text{La}_{0.212} \text{Nd}_{0.137} \text{Sm}_{0.013} \text{P}_{1.0} \text{O}_4$
Graftonite	$(\text{Mg}_{0.307} \text{Mn}_{0.700} \text{Ca}_{0.738} \text{Fe}_{1.152})_{2.903} (\text{PO}_4)_2$
Sarcopside	$(\text{Mn}_{0.239} \text{Mg}_{0.991} \text{Fe}_{1.607})_{2.853} (\text{PO}_4)_2$
Jahnsomervellite	$\text{Na}_{3.886} \text{Ca}_{3.247} \text{Al}_{0.065} \text{Ba}_{0.008} \text{Sr}_{0.004} \text{P}_{7.189} (\text{Mg}_{8.933} \text{Fe}_{7.577} \text{Mn}_{3.523} \text{Zn}_{0.076} \text{Sc}_{0.047} \text{Ta}_{0.209} (\text{P}_{17.88} \text{Si}_{0.11} \text{O}_{72}))$
Ludlamite	$(\text{Fe}_{3.608} \text{Mg}_{1.517} \text{Mn}_{0.222})_{2.781} (\text{PO}_4)_2 \cdot x \text{NH}_2 \text{O}$
Arrojadite?	$(\text{Ca}_{0.165} \text{Fe}_{0.092} \text{Mg}_{0.898} \text{Mn}_{0.008})_{2.835} \text{Al}_{1.821} (\text{P}_{11.987} \text{Si}_{0.11} \text{O}_{48}) (\text{OH}_{1.865} \text{F}_{0.13})_2$
Lazulite	$(\text{Na}_{3.679} \text{K}_{0.523} \text{Ca}_{0.294} \text{Ba}_{0.899} \text{Sr}_{0.016} \text{Pb}_{0.002})_{5.41} (\text{Fe}_{3.608} \text{Mg}_{4.567} \text{Mn}_{4.643})_{12.818} \text{Al}_{0.948} (\text{P}_{17.86} \text{Si}_{0.138} \text{O}_4)$
Metabasite	
Hornblende	$(\text{Ca}_{1.939} \text{Na}_{0.163} \text{K}_{0.054})_{2.161} (\text{Cr}_{0.006} \text{Ti}_{0.042} \text{Mn}_{0.124} \text{Fe}_{1.986} \text{Mg}_{2.58} \text{Al}^{vi}_{0.262})_{5.006} [(\text{Al}^{iv}_{0.863} \text{Si}_{7.137})_2 \text{O}_{22}] (\text{Cl}_{0.001} \text{F}_{0.238} \text{OH}_{1.761})_{2.0}$
Salite	$\text{Ca}_{0.967} (\text{Fe}_{0.44} \text{Mg}_{0.566} \text{Mn}_{0.013})_{1.029} \text{Al}_{0.024} (\text{Al}^{vi}_{0.032} \text{Si}_{1.976} \text{O}_6)$
Titanite	$(\text{Ca}_{1.0} \text{LREEY}_{0.002})_{1.0} (\text{Sn}_{0.003-0.012} \text{Al}_{0.17} \text{Ti}_{0.78})_{0.96} \text{Si}_{0.99} \text{O}_4 (\text{F}_{0.16} \text{O}_{0.84})_{1.0}$
Apatite	$(\text{Ca}_{4.743} \text{Mn}_{0.106} \text{Fe}_{0.043})_{4.892} (\text{PO}_4)_3 (\text{F}_{0.852} \text{OH}_{0.148})_{1.0}$
Ilmenite	$\text{Fe}^{2+}_{0.874} \text{Fe}^{3+}_{0.052} \text{Mn}_{0.075} \text{Ti}_{0.97} \text{O}_4$

(Fig. 2). The lowest Nb–Ta content shows rutile from apatite (Nb<sub>2</sub>O<sub>5</sub> 10.47–11.94 wt. %, Ta<sub>2</sub>O<sub>5</sub> 2.24–4.76 wt. %) (1). Ta–Nb content in rutile from groundmass is slightly higher (Nb<sub>2</sub>O<sub>5</sub> 12.09–13.20 wt. %, Ta<sub>2</sub>O<sub>5</sub> 6.28–8.56 wt. %) (2). The richest Nb–Ta content

exhibit rutiles included in cordierite ( $\text{Nb}_2\text{O}_5$  — 13.82–16.10 wt. %,  $\text{Ta}_2\text{O}_5$  — 9.45–11.49 wt. %) (3) (Fig. 3, Table 1). Also, rutile slightly enriched in  $\text{V}_2\text{O}_5$  2.03–3.35 wt. % and  $\text{Cr}_2\text{O}_3$  0.978–2.03 wt. %. The lowest content of these oxides is in rutile of type (1). Relic of **ilmenite** was identified on the very thin (<1  $\mu\text{m}$ ) rime of sulphides grains.

*Sulphides*

**Pyrrhotite** is the most common sulphide mineral in ACM. It was identified in groundmass in association with chalcopyrite and sphalerite. **Pyrite** replaces pyrrhotite, fills the thin fissure in groundmass and rarely is replaced by hematite. **Arsenopyrite** is in association

with pyrite, lollingite and graphite. Internal zoning of arsenopyrite is caused by uneven content of Co and Ni. **Lollingite** is closely associated with arsenopyrite. It forms anhedral grains in groundmass or prismatic grains included in cordierite. Replacement of lollingite by arsenopyrite was also observed. Lollingite shows high content of Co 2.79–3.17 wt. % and Ni 4.82–5.05 wt. %. **Molybdenite** is rare mineral occurring in intergrowth with graphite.

*Phosphates*

**Fluorapatite.** Greenish fluorapatite in ACM forms rounded grains 0.2–2 mm in size and situated in interstitial of cordierite grains. Colourless fluorapatite from

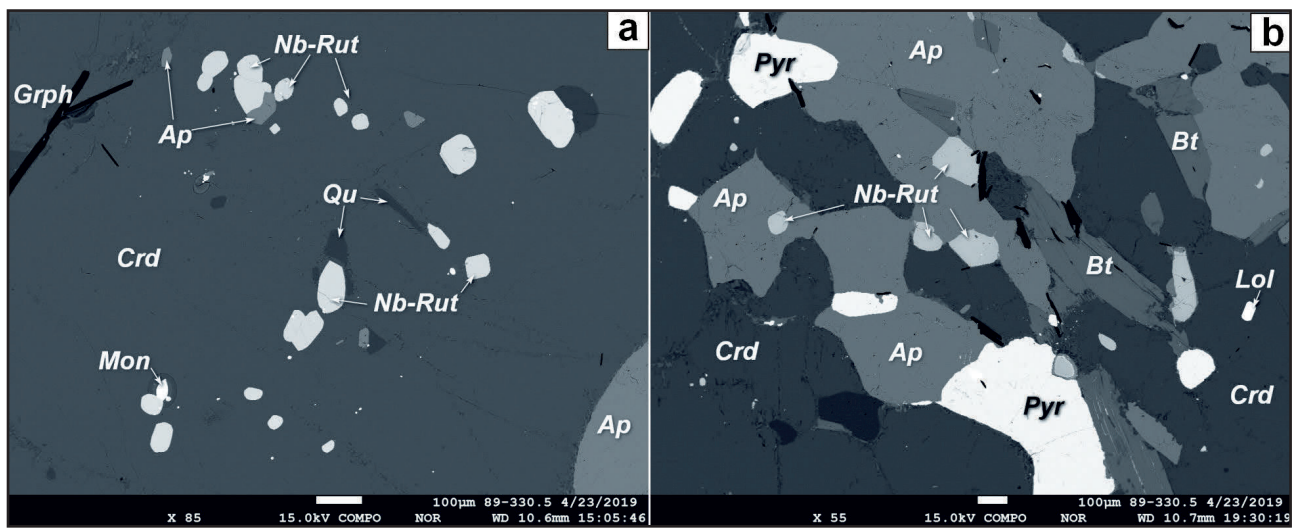


Fig. 2. BSE micrographs: a — Nb-rutile inclusions in cordierite; b — Nb-rutile in interstitial groundmass and as inclusions in apatite.

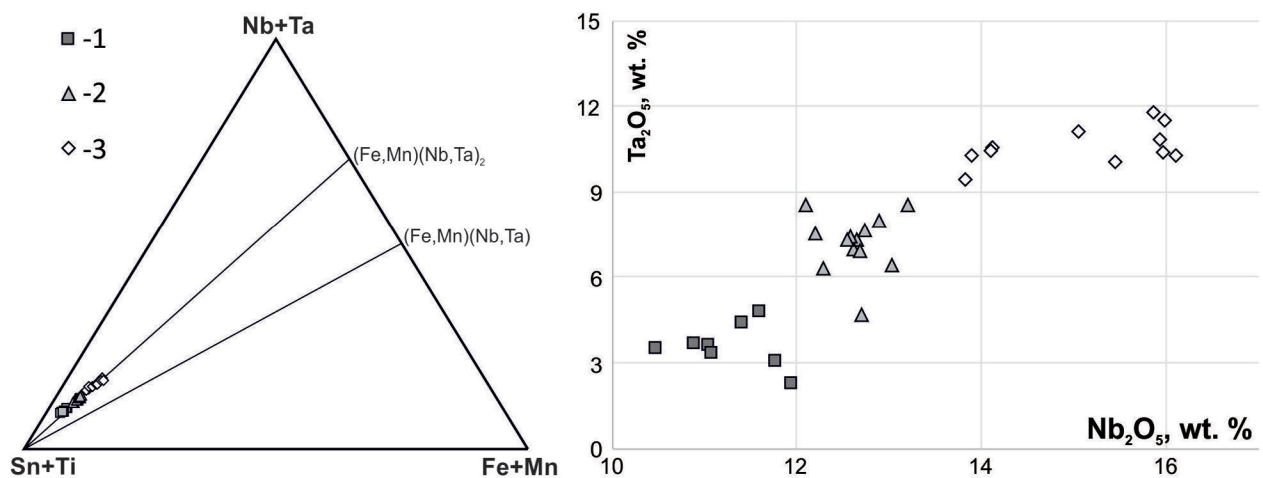


Fig. 3. Chemical composition of Nb-rutile from: 1 — inclusions in apatite, 2 — single grains in groundmass, 3 — inclusions in cordierite.

host gneisses forms very fine grains (<50–70  $\mu\text{m}$ ), shows the highest fluorine (up to 4.37 wt. %) and the lowest Mn, Fe (Mn/Fe<1) contents, and very low REE content. Apatite from ACM shows a bit lower content of fluorine (2.7 to 3.4 wt. %), and significantly higher MnO and FeO (Mn/Fe>2). Total content of LREE is <0.22 wt. %.

Secondary phosphates form aggregates, 0.4–2.0 mm in size, consist of graftonite, fine grains phosphates of fillowite group, arrojadite, lazulite and veins of ludlamite. **Graftonite** ( $X_{\text{Fe}}=0.54$ ) forms tabular grains <0.5 mm in size and it is the most common orthophosphate. Graftonite is Mn-enriched ( $X_{\text{Mn}}=0.32$ ) and Mg-rich ( $X_{\text{Mg}}=0.14$ ). **Sarcopside** occurs in intergrowth with apatite, where apatite in such case very similar to quartz myrmekite in plagioclase. The size of this aggregates very variable, but less than 0.5 mm. Sarcopside is distinctly Fe-dominant ( $X_{\text{Fe}}=0.57$ ), Mg-enriched ( $X_{\text{Mg}}=0.35$ ) and Mn-poor ( $X_{\text{Mn}}=0.08$ ). Orthophosphate of **fillowite** group is rare, form small single tabular grains, 5–30  $\mu\text{m}$  in size. According to classification diagram (Grew et al. 2010), plot points of fillowite group orthophosphate are placed on the border between jahnsomervellite and chladnite fields, but last membership is slightly predominant. They are slightly Mg-dominant ( $X_{\text{Mg}}=0.45$ ), Fe-enriched ( $X_{\text{Fe}}=0.38$ ) and Mn-rich ( $X_{\text{Mn}}=0.18$ ).

Arrojadite, lazulite and ludlamite occur within phosphate aggregate as well as the single grains but in accessory amount. **Ludlamite** is the most common of that group, forms very fine (up to 5–7  $\mu\text{m}$ ) alternating veins within sarcopside grains. **Arrojadite** (?) is rare mineral which occurs in intergrowth with graphite or on the rime of phosphate aggregate <15  $\mu\text{m}$  in size. **Lazulite** is in a small grain on the contact between graftonite and cordierite, formed as a result from cordierite alteration.

**Monazite-(Ce)** is present in a singular tabular grains (<200  $\mu\text{m}$  in size) or as intergrowth with apatite. The content of  $\text{ThO}_2$  and  $\text{UO}_2$  varies from 1.9 to 11.6 wt. % and from 1.5 to 3.5 wt. % respectively. Such distribution of Th and U caused patchy and zonal internal structure. The content of CaO is 1.25–2.25 wt. % in a Th poor grains, and up to 3.5 wt. % in Th rich. Introduction Th and Ca in structure monazite are provides by brabantite substitution scheme ( $X_{\text{brb}}$  — 0.1–0.3).

### Mineralogy of metabasite rocks

**Amphibole** occurs in prismatic grains (0.5–2.0 mm in size) and presented by magnesiohornblende (f — 44.6 at. %). Concentration of Zn, Ni, Sr is less than 0.05 wt. %. **Titanite** forms singular grains (<300  $\mu\text{m}$ ) or small aggregate. Heterogenic internal structure is caused by the different content of  $\text{SnO}_2$  (0.39–1.1 wt. %). **Salite** was identified as a relic anhedral grains, 100–150  $\mu\text{m}$  in size, included in hornblende. The Fe/(Fe+Mg) value is 42.9–44.7 at. %. Content of  $\text{Al}_2\text{O}_3$  less than 0.8 wt. % and content of Na, Zn is <0.07 wt. %. **Ilmenite** appears as a small inclusion in titanite, less than <10  $\mu\text{m}$  in size. Ilmenite enriched in MnO — 1.7–4.0 wt. %).

### Discussion and conclusion

The Nb–Ta-bearing apatite-cordierite metasomatite is a new type or rare metal mineralisation at the western margin of Korsun–Novomyrgorodskyi pluton. The origin of Nb–Ta mineralisation is still unclear. We can conclude that rare metal metasomatite was formed in a result of strong hydrothermal-metasomatic alteration of metabasite rocks by postmagmatic fluid enriched in F, P (and probably Ta–Nb) in conditions of amphibolite facies of regional metamorphism. The sources of postmagmatic fluids were numerous rare-metal granitoids dykes intruded gneisses.

**Acknowledgements:** Support from VEGA 0084/17 grant and Grant Project NAS of Ukraine (0118U006497) are greatly appreciated.

### References

- Bezvyunnyi V.P. 2005: Rare metal, gold mineralization and metasomatic processes of the Petroostrov ore field. *Scientific proceedings of UkrSGRI* 1, 82–84 (in Ukrainian).
- Ivanov B.N., Kosuga V.N. & Pogukai V.I. 2011: Areal and exocontact rare metal metasomatites Shpolano-Tashlyk ore region. *Geochem. and Ore Form.* 30, 10–17 (in Russian).
- Grew E., Yates M., Beane R., Floss C. & Gerbi C. 2010: Chopinite-sarcopside solid solution,  $[(\text{Mg},\text{Fe})_3\text{□}](\text{PO}_4)_2$ , in GRA95209, a transitional acapulcoite: Implications for phosphate genesis in meteorites. *American Mineralogist*, 95, 260–272.

# Hybrid I/S nature of Prašivá granite type, Low Tatra pluton: Evidence from mineralogical data

MARIA MARASZEWSKA, IGOR BROSKA and SERGYI KURYLO

Earth Science Institute, Slovak Academy of Sciences, Dúbravská cesta 9, 840 05 Bratislava; geolmara@savba.sk

**Abstract:** This study focuses on two facies of Prašivá granitoid: (1) Magurka settlement and (2) Liptovská Lužná village. The both facies are biotite monzogranites with porphyrocrysts of K-feldspar. Apart from textural and petrographic similarities, mineral assemblages show significant differences. In both facies rapakivi and anti-rapakivi intergrowths of feldspars and plagioclase are common but characteristic specific mineral assemblage from Magurka area represent annite and monazite-(Ce) on the other hand, from Liptovská Lužná shows presence of Mg-biotite and primary allanite-(Ce) with monazite relics. The mineral assemblage suggests mixing or different input and interaction of more mafic  $\text{Ca}^{2+}$  and  $\text{H}_2\text{O}$  rich melt portion into former magma batch resulted in compositional variability within the Prašivá granite body.

## Introduction

The mixing and mingling of magmas is regarded as one of the essential processes in magma evolution responsible for formation of the so-called hybrid granitoids. The interaction of mafic and felsic melts is mirrored in zonal structure of granite bodies, their fabrics and composition.

Meso-Variscan granitoids exposed in the Western Carpathians are subdivided into S- and I-types (e.g. Petrik et al. 1994): geochemical differences between S- and I- types are underlined by set of typological mineralogical phases, especially the ilmenite+monazite versus magnetite+allanite paragenesis, respectively. However, the several features, including Rb–Sr and Nd–Sm isotope systematics (Kohút & Nabělek 2008), or presence of mafic enclaves (Petrik & Broska 1989) indicates that I- type should be influenced by melt mixing.

This contribution focuses on distribution of selected tephromorphic accessory minerals suggesting the inhomogeneous nature of the parental granite.

## Geological Setting

The Low Tatra pluton includes two main granitoid types: Prašivá granodiorite to granite located on northwest from the Demänovská Dolina and Ďumbier tonalite to granodiorite occurring in more eastern part of the mountain range. Both are classified as calc-alkaline metaluminous granitoids with transition to peraluminous type, however the Prašivá type is richer in alkalis, especially  $\text{K}_2\text{O}$  (Putiš et al. 2003). Apart from these two major types, several distinct, predominantly peraluminous granite bodies occur within the granite pluton and roof metamorphic complexes (e.g. Dupej & Siegl 1981).

Nd–Sm, Rb–Sr and Pb–Pb isotope characteristics of Prašivá granite in contact zone with dioritic MME implies predominant role of mantle-derived mafic melt mixed with crustal one (Poller et al. 2005). Zircon U–Th–Pb dating yielded ages  $353 \pm 3$  Ma (Broska et al. 2013).

## Sample localities and methods

Investigated representatives of different facies of Prašivá granitoid were taken in area of Magurka settlement (on the trail to the Ďurková saddle) (NTM-7) and in valleys close to the Liptovská Lužná (NTM-12 and NTM-16).

The petrographical description is based on transmitted and reflected light microscopy. Mineral composition was carried out using SEM and microprobe at the Earth Science Institute SAS in Banská Bystrica.

## Results

### Petrography

The Prašivá granite type from both localities is porphyritic with heterogranular structure, medium to coarse grained. The composition varies from quartz monzonite (18 % Q, 31 % Fld, 49 % Pl) to monzogranite (25 % Q, 33 % Fld, 42 % Plg).

Presence of up to 1 cm large perthitic K-feldspar porphyrocrysts is very typical textural pattern of the Prašivá granite type. Kfs occurs as smaller microcline grains in interstitial position, and as rims on plg and older Kfs is often altered in various degree. Pl (An 38–41) is present in two generations: smaller, euhedral, highly sericitized and saussuritized crystals with corroded margins, often

enclosed in K-feldspar porphyrocrysts, and larger, polysynthetic twinning or normal zonational, rimmed by albite or orthoclase overgrowths. On the boundaries between feldspars, quartz and myrmekite intergrowths are widespread.

The dark-brown biotite (annite) is present often as aggregates or cloths. It shows variable effect of alternation (chloritisation), replacement along cleavage plains by fibrous prehnite (NTM-7) or by epidote, ilmenite and garnet (NTM-12, 16; Fig. 1a). Muscovite only as a secondary phase occurs.

The most widespread accessory phase is apatite occurring as relatively large, prismatic crystals in biotite.

Monazite is abundant in Mg granite, often as relatively large crystals enclosed in biotite and associated with apatite. Granites from Liptovská Lužná area contain much smaller and dispersed grains of monazite.

Zircons are present as inclusions in biotite or apatite and within feldspars. In all samples Zr/Hf ratios are between 20–33; it is typical value for Variscan granites in the Western Carpathians.

Magnetite is widespread as euhedral crystals, often with thin titanite rims in Liptovská Lužná but in Magurka is present in lower amount and partly replaced by hematite. Ilmenite was found as lensoidal inclusions in biotite and as a skeletal, strongly oxidised relicts with inclusions of rutile overgrown by titanite.

#### Apatite

Apatite in all samples forms euhedral, prismatic, in lesser extent stubby crystals and represents almost end-member fluorapatite. Some crystals are homogenous, when the other show well-developed concentric zonation.

In both facies of investigated granites apatite show generally low Mn and Fe content — 0.06–0.17 and 0.02–0.17 wt. %, however the NTM-7 apatite is slightly

richer in Mn (Fig. 2). The most distinguishing feature is elevated  $\text{SO}_2$ ,  $\text{REE}_2\text{O}_3$  and  $\text{Na}_2\text{O}$  contents in NTM-12 and NTM-16. The REE+Y content in some grains correlates with Na and with Si, what suggest two mechanisms of coupled substitution.

#### Monazite-(Ce)

Monazite-(Ce) is abundant in NTM-7, where it occurs as inclusions in biotite. It forms sub- to anhedral, cracked heterogenous crystals up to 250  $\mu\text{m}$ . The monazites show complex zonation, with patchy irregularly distributed lighter and darker patches (especially when they are located on biotite margins), or concentric zonation (Fig. 1b,c). The lighter patches or cores in monazites are generally enriched in Th and Y, what suggest higher degree of huttonite and xenotime substitution. The irregularly distributed Th-rich zones are thought to be a result of dissolution–reprecipitation of primary monazite causing secondary Th enrichment or depletion in distinct areas; a typical phenomenon of fluid-aided metasomatism (Poitrasson 1996).

In Liptovská Lužná samples, monazite was found only in sample NTM-12. It occurs as inclusions in apatite and skeletal relicts in allanite. All monazites are slightly depleted in P (28–29 wt. %) and REE and show enrichment in  $\text{SiO}_2$  (2–2.5 wt. %),  $\text{ThO}_2$  (11–14 wt. %) and CaO (0.8–1 wt. %). It suggests the advanced dissolution–reprecipitation process and/or their secondary origin.

#### Allanite-(Ce)

Allanite-(Ce) was found in NTM-12 and 16 (Liptovská Lužná), as fine crystalline aggregates in biotite and as a interstitial large euhedral- to subhedral grains rimmed by epidote.

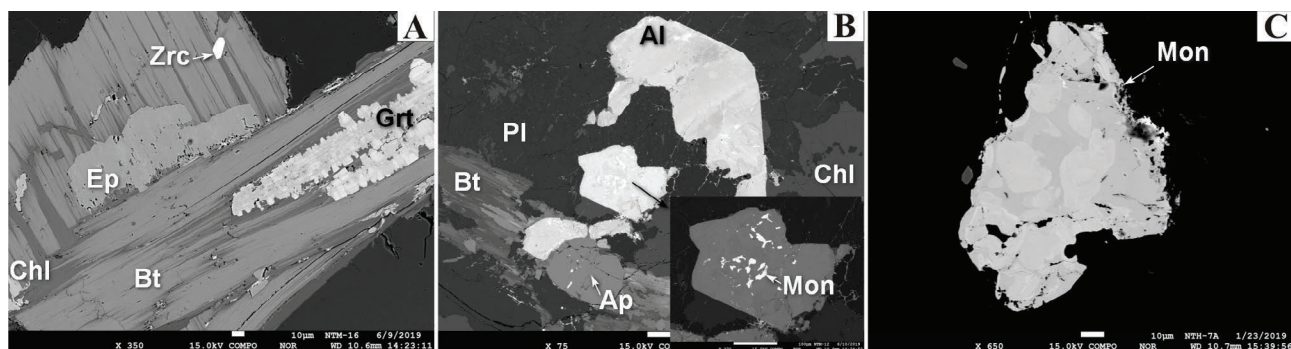


**Fig. 1.** Example of mineral assemblages in Prašivá granitoids: **A** — Garnet and epidote lenses in chloritised biotite NTM-12; **B** — Subhedral zoned allanite-(Ce) in plagioclase with enclosed relicts of monazite NTM-16 (Liptovská Lužná area); **C** — patchy monazite from NTM-7 (Magurka area)

Darker and brighter domains are distributed subordinately or the latter are developed along the cracks due to oxidation process. The  $\text{ThO}_2$  content is highly variable from 0.7 in darker zones to 1–2.7 wt. % in brighter and correlate with lower concentration of REE, higher oxidation state of iron and enrichment in Ca. The plot REE+Th+U vs  $\text{Al}_{\text{tot}}$  (Petřík et al. 1995) suggests that most of the allanites were formed in highly oxidised metaluminous melts during moderate-pressure conditions (Broska et al. 2021).

*Garnet*

Garnets were found only in Liptovská Lužná as an anhedral, streak or lens-like aggregates in chloritised biotite (Fig. 1a). Its composition correspond to andradite (91–68 mol. %) with variable grossular component (>30 to 13 mol. %). Depletion in silica and excess in  $\text{Fe}^{3+}$  suggests high degree of hydration and oxidation.

**Conclusions**

The mineral assemblages and rock textures suggest spatial compositional heterogeneity within Prašivá intrusion. They show features of both metaluminous and peraluminous magmas. It seems that the magmas before the mixing event intruded as a crystal mush containing phenocrysts of biotite with enclosed accessory apatite and REE phases as well as older populations of K-feldspar. The most important factors which governed the development of new mineral phases or modifications of accessory minerals content of volatiles and redox conditions. The fluctuations and changes in these parameters resulted in interaction of transferred phenocrysts and hybrid melt as well as growth of the new phases.

The facies in more eastward Magurka areas of the pluton, indicate larger input of felsic crustal magmas to existed metaluminous melt. The more reduced character of melt is recorded in lower ratio of  $\text{Mg}/(\text{Fe}+\text{Mg})$  in

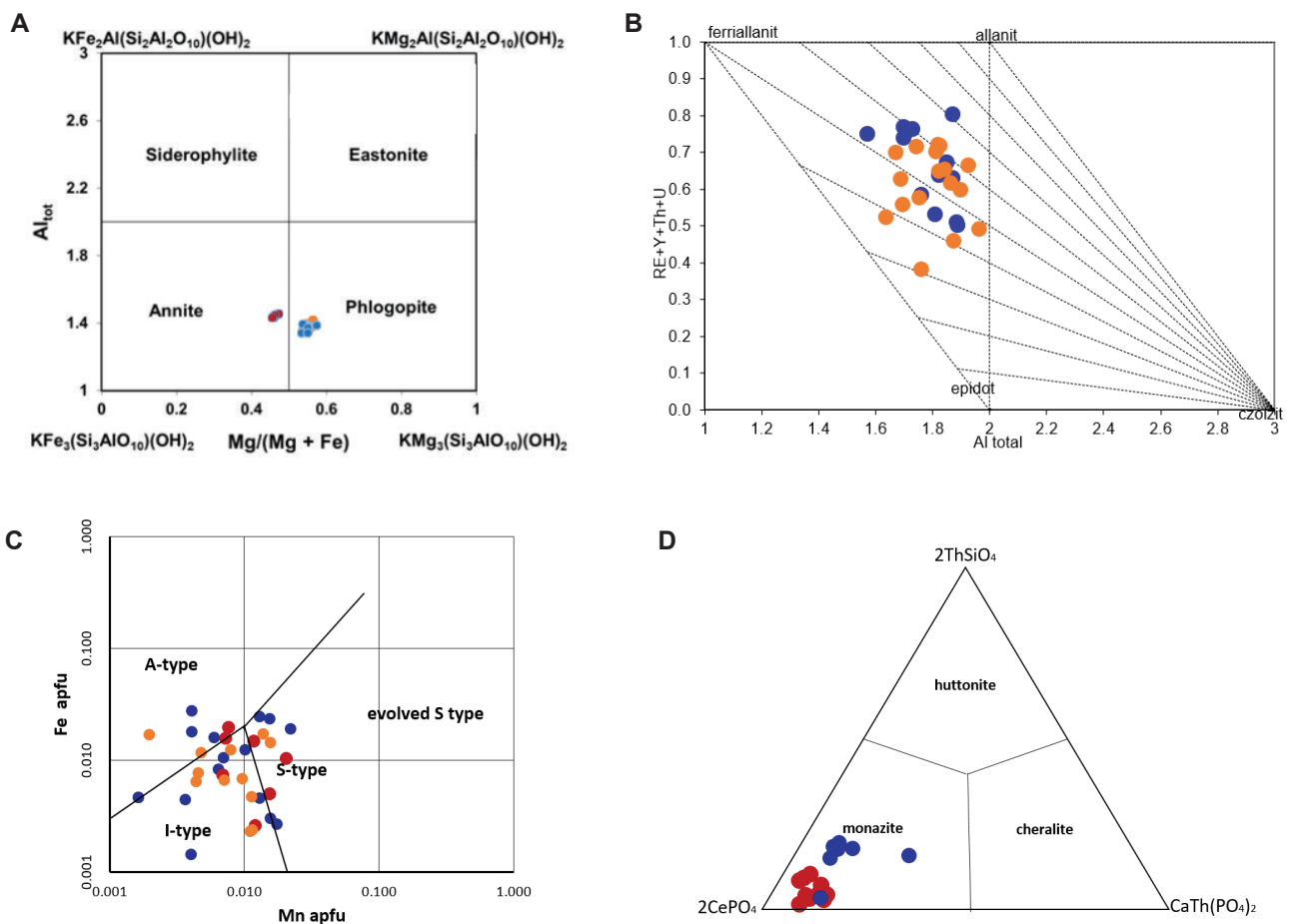


**Fig. 2.** Composition of main and accessory minerals in the Prašivá granite: **A** — Classification of biotites from Prašivá granitoids; **B** — REE+Y+Th+U vs  $\text{Al}_{\text{tot}}$  (apfu) diagram for NTM12 and NTM16 allanites (after Petřík et al. 1995); **C** — Fe vs Mn discrimination diagram for apatites from different granite suites in WC (Broska & Petřík 2008). **D** — Cheralite–Huttonite–Monazite plot for samples NTM7 and NTM12.

biotite and abundance of monazite-(Ce) as main REE carrier along with general absence of minerals typical for hybrid rocks, like magnetite or primary titanite. In Liptovská Lužná area, biotite is Mg richer and allanite is main REE-bearing phase, when monazite-(Ce) occurs as tiny relicts within some allanite grains showing more metaluminous character of melt.

In samples from Liptovská Lužná, the presence of resorbed monazite relicts in some allanite crystals suggest its formation at the expense of the phosphate from presented REEs. The replacement relationship between monazite and allanite could be described by fluid-aided alternation processes (see e.g. Regan et al. 2019).

Mn and Fe (apfu) contents in apatites from all localities are in coincidence with I-type characteristics (Broska & Petrik 2008), some subtle differences are connected with concentration of S and, REEs. Higher content of S generally suggests more oxidised character of crystallization (Sha & Chappell 1999). Low REE contents in sample NTM-7 apatite may be explained by coeval precipitation of monazite (Sha & Chappell 1999).

The changes of Ca and Al activity influenced also micas, causing the replacement of biotite by Ca-Al rich phases towards prehnite, hydrogarnets and chlorite (Tulloch 1979) and exsolution of titanite (Frost et al. 2001). However these secondary phases may also have been formed during post magmatic or sub-solidus alternation in Alpine orogeny.

The presence of K-feldspar and albitic rims (similar to antirapakivis structures) and myrmekitic intergrowths manifest interaction of alkalis rich fluids from residual magmas. It cannot be excluded, that in some cases these alkaline fluids overprinted also the REE minerals (Poitrasson et al. 1996; Poitrasson 2002) and triggered monazite exsolutions from apatite (Harlov & Forster 2003).

Summarising all the differences within Prašivá granite facies, from Magurka and Liptovská Lužná, suggests different input and degree of melt mixing within the Prašivá magmatic body. Proposed model of hybridisation for Prašivá granite body indicate differences in evolution of the different amount of melt injection the mafic melt into partially-solidified differentiated magma in propagation from NW to SE. It may suggest that mafic

input, evidenced by isotope data (Poller et al. 2005) did not result in total mixing of melts.

## References

- Biely A. (Ed.) 1992: Geological map of the Nízke Tatry Mts. 1:50,000. *GÚDŠ*, Bratislava.
- Broska I., Petrik I., Be'eri Shlevin Y., Majka J. & Bezák V. 2013: Devonian–Mississippian I-type granitoids in the Western Carpathian: A subduction-related hybrid magmatism. *Lithos* 162–163, 27–36.
- Broska I., Petrik I. & Uher P. 2012: Akcesorické minerály granitických hornín Západných Karpát. *VEDA*, Bratislava.
- Broska I. & Petrik I. 2008: Genesis and stability of accessory phosphates in silicic magmatic rocks: a Western Carpathian case study. *Mineralogia* 39, 1–2, 53–65.
- Broska I. & Petrik I. 2011: Accessory Fe-Ti oxides in the Western Carpathian granitoids: witness of the granite mixing and the oxidation process. *Mineralogy and Petrology* 102, 87–97.
- Chappell B.W. & White A.J.R. 1974: Two contrasting granite types. *Pacific Geology* 8, 173–174.
- Dupej J. & Siegl K. 1984: Geology of the Kralická granite and its environment (Nízke Tatry Mts, Western Carpathians). *Geologica Carpathica* 35, 3, 395–411.
- Frost B.R., Chamberlain K.R. & Schumacher J.C. 2001: Sphephene (titanite): phase relations and role as a geochronometer. *Chemical Geology* 172, 1, 131–148.
- Harlov D.E. & Förster H.J. 2003: Fluid-induced nucleation of (Y+REE)-phosphate minerals within apatite: Nature and experiment. Part II. Fluorapatite. *Amer. Miner.* 88, 1209–1229.
- Hibbard M.J. 1981: The magma mixing origin of mantled feldspar. *Contributions to Mineralogy and Petrology* 76, 158–170.
- Petrik I. & Broska I. 1989: Mafic enclaves in granitoid rocks of the Tribeč Mts. Western Carpathians: geochemistry and petrology. *Geologica Carpathica* 40, 6, 667–696.
- Petrik I., Broska I. & Uher P. 1994: Evolution of Western Carpathian granite magmatism: age, source rocks, geotectonic setting and relation to the variscan structure. *Geologica Carpathica* 45, 5, 283–291.
- Petrik I., Broska I., Lipka J. & Šiman P. 1995: Granitoid allanite-(Ce): substitution relations redox conditions and REE distributions (on example of I-type granitoids, Western Carpathians, Slovakia). *Geologica Carpathica* 46, 2, 79–94.
- Poitrasson F. 2002: In situ investigations of allanite hydrothermal alteration: examples from calc-alkaline and anorogenic granites of Corsica (southeast France). *Contrib. Mineral. Petrol.* 142, 4, 485–500.
- Poitrasson F., Chenery S. & Bland D.J. 1996: Contrasted monazite hydrothermal alteration mechanisms and their geochemical implications. *Earth and Planetary Science Letters* 145, 1–4.
- Sha L.-K. & Chappell B.W. 1999: Apatite chemical composition, determined by electron microprobe and laser-ablation inductively coupled plasma mass spectrometry, as a probe into granite petrogenesis. *Geochim. Cosmochim. Acta* 63, 3861–3881.
- Tulloch A.J. 1979: Secondary Ca-Al silicates as low-grade alteration products of granitoid biotite. *Contrib. Mineral. Petrol.* 69, 105–117.

# Meteorite Smolenice — a new iron of IVA group from Slovakia

DANIEL OZDÍN<sup>1</sup>, MILAN GARGULÁK<sup>2</sup>, PAVEL POVINEC<sup>3</sup>,  
STANISLAV STREKOPYTOV<sup>4</sup>, VLADIMÍR PORUBČAN<sup>5</sup> and ŠTEFAN FARSANG<sup>6</sup>

<sup>1</sup>Comenius University, Faculty of Natural Sciences, Department of Mineralogy and Petrology, Ilkovičova 6, 842 15 Bratislava 4, Slovakia; daniel.ozdin@uniba.sk

<sup>2</sup>Romanova 11, 851 02 Bratislava 5, Slovakia; milan@gargulak.sk

<sup>3</sup>Comenius University, Faculty of Mathematics, Physics and Informatics, Department of Nuclear Physics and Biophysics, Mlynská dolina, 842 48 Bratislava, Slovakia; Pavel.Povinec@fmph.uniba.sk

<sup>4</sup>Natural History Museum, Science Facilities, Imaging and Analysis Centre, Cromwell Road, London, SW7 5BD, United Kingdom; s.strekopytov@nhm.ac.uk

<sup>5</sup>Astronomical Institute of the Slovak Academy of Sciences, Dúbravská cesta 9, 84504 Bratislava, Slovakia; astropor@savba.sk

<sup>6</sup>University of Cambridge, Department of Earth Sciences, Downing Street, Cambridge, CB2 3EQ, United Kingdom; sf571@cam.ac.uk

**Abstract:** On April 3, 2012 a single piece of a meteorite was found in the forest near Smolenice (Trnava County, Slovakia). The latitude and longitude of the find are 48°31.2'N and 17°23.9'E, respectively. The meteorite was slightly weathered (weathering grade W1) and its total mass was 13.95 kg. The bulk chemical composition is dominated by iron (88.7 wt%) and nickel (8.10 wt%). This, along with concentration of Ga (1.80 µg/g), Ge (< 0.7 µg/g), and Ir (1.67 µg/g), suggest the meteorite being a IVA iron. Based on lamellae width of kamacite (average of 0.22 mm), the meteorite can be classified as fine octahedrite (Of). The mineralogy is very simple, the main minerals are iron (kamacite) (5.16–7.36 wt. % Ni) and taenite (16.73–33.93 wt. % Ni), with rare troilite nodules and daubréelite inclusions and thin veinlets. The meteorite shows Widmanstätten patterns and plesite structure is locally present. Analyses of cosmogenic radionuclides (<sup>26</sup>Al, <sup>14</sup>C, and <sup>40</sup>K) indicate that the radius of the Smolenice meteorite could be in the range of 30–50 cm, its terrestrial age of about 0.1 Ma and its cosmic-ray exposure age of about 0.2 Ma.

## Introduction

A single piece (Fig. 1) of meteorite was found on April 3, 2012 in the cadastral area of Smolenice (latitude 48°31.2'N and longitude 17°23.9'E). The meteorite has an elongated shape with dimensions 25.5×13.5×13 cm. On the oxidized rust-coloured surface of the meteorite, relatively uniform regmaglyptes are observed. The original mass of the meteorite upon recovery was 13.95 kg.

The type specimen of the meteorite Smolenice is deposited in the Mineralogical Museum of Comenius University in Bratislava (24.52 g), other samples are in the Slovak National Museum — Natural History Museum in Bratislava (28.6 g and 37.9 g) and other museums and private collections. The main mass of the meteorite is in the private collection of the finder. On February 9, 2019 the meteorite name Smolenice was approved by the Nomenclature Committee on Meteorites of the Meteoritical Society.

## Methods

Wavelength-dispersion electron-microprobe analysis (EMPA-WDS) was carried out with a CAMECA SX100 microprobe at the State Geological Institute of Dionýz

Štúr in Bratislava. Operating conditions were as follows: acceleration voltage of 20 kV, beam current of 20 nA, beam diameter 3–5 µm. The following standards and lines were used: CuFeS<sub>2</sub> (Cu K $\alpha$ , Fe K $\alpha$ , S K $\alpha$ ), Ni (Ni K $\alpha$ ), Co (Co K $\alpha$ ), ZnS (Zn K $\alpha$ ), Mn (Mn K $\alpha$ ), Ge (Ge K $\alpha$ ), GaAs (As L $\alpha$ ), Cr (Cr K $\alpha$ ), V (V K $\alpha$ ), SiO<sub>2</sub> (Si K $\alpha$ ), TiO<sub>2</sub> (Ti K $\alpha$ ), Al<sub>2</sub>O<sub>3</sub> (Al K $\alpha$ ), GaP (P K $\alpha$ ), and NaCl (Cl K $\alpha$ ).

Bulk chemical composition of the meteorite was determined at the Science Facilities, Imaging and Analysis Centre of the Natural History Museum in London. Major and minor elements (Fe, Ni, Co and P) were determined by inductively coupled optical emission spectroscopy (ICP-OES) using a Thermo iCap 6500 Duo. Trace elements, platinum group elements and Au were determined by inductively coupled plasma mass spectrometry (ICP-MS) using an Agilent 7700x with the collision–reaction cell (CRC) connected to He (99.9995 % purity) and H<sub>2</sub> (99.99999+ % nominal purity produced by H2PD-150 generator) lines.

Accuracy of the Co and Ni determination was verified by the simultaneous digestion and analysis of the certified reference material (CRM) BCS-251 “Low Alloy Steel”. The accuracy of the ICP-MS analysis was checked by analyzing synthetic solutions containing similar amounts of Fe and Ni as studied of meteorite



Fig. 1. Smolenice IVA iron. Width of sample is 25.5 cm. Photo: G. Kučerová.

iron. Due to the extremely high Fe/Ge and Ni/Ge ratio in the Smolenice meteorite and the polyatomic interferences on  $^{74}\text{Ge}$ , only the potential extent of the Ge content in the meteorite could be determined.

Radionuclide (for gamma-ray emitters  $^{26}\text{Al}$  and  $^{40}\text{K}$ ) was measured for 15 days in the Low-Level Gamma-Ray Spectrometry Laboratory of the Department of Nuclear Physics and Biophysics of the Faculty of Mathematics, Physics and Informatics of the Comenius University in Bratislava (Slovakia). A coaxial low-background High-purity Germanium (HPGe) detector (PGT, USA) with relative detection efficiency of 70 % (for 1332.5 keV gamma-rays of  $^{60}\text{Co}$ ) was used. The HPGe detector operated in coincidence–anticoincidence regime (with NaI(Tl) and plastic scintillator detectors) in a large low-level background lead/copper shield with outer dimensions of  $2 \times 1.5 \times 1.5$  m (Povinec et al. 2009, 2015). Because the terrestrial age of the Smolenice meteorite is not known, no decay corrections for investigated radionuclides were applied.

Accelerator Mass Spectrometry (AMS) we used for the  $^{14}\text{C}$  analyses of 200 g sample of meteorite. The cosmogenic  $^{14}\text{C}$  was extracted in a RF induction furnace in a flow of oxygen, and passing the gases to form  $\text{CO}_2$ . The  $\text{CO}_2$  was then converted to graphite and analyzed on a 3 MV AMS machine at the University of Arizona (USA). Methodology of  $^{14}\text{C}$  determination is given in Jull et al. (1993, 2010).

## Results

### Mineralogy

Smolenice meteorite shows very simple composition dominated by iron (kamacite; more than 95 vol. %) with minor taenite, troilite and daubréelite. As shown in the work of Gargulák et al. (in print), the meteorite contains five different types of kamacite. The width of the iron lamellae of the main type of kamacite in the polished section is 0.22 mm (according to Frost 1965 and after correction). Neumann's lines were not observed. The measured lamellae widths correspond to the iron of the fine octahedrite type (Of). Based on 38 analyses, the average chemical composition of kamacite is (in wt. %): Fe 92.66, Ni 6.76, Co 0.52, Ge 0.02, and Cu, P, and Si 0.01.

Taenite occurs in two forms (Fig. 2). The first type of taenite is very abundant and forms individual lamellae in kamacite. The less abundant is the second type forming plessitic texture. Widmanstätten pattern is typical for this meteorite (Fig. 3). The average of chemical composition of kamacite is (in wt. %): Fe 75.13, Ni 24.53, Co 0.28, Cu 0.08, Ge 0.07, Si 0.03, and P 0.01. The range of Ni content in taenite is 16.73–33.93 wt. %. The complex and polyphase structures of the kamacite and taenite point to a complex decomposition of the original kamacite at temperatures below 400 °C (Yang et al. 1996,

1997a; Reuter et al. 1988). The absence of the Neumann's lines in the Smolenice meteorite proves that during the flight in the space no stronger impact, or collision with another object of the cosmos had occurred.

Troilite is rare in Smolenice iron and forms round grains up to 3 mm in the kamacite. Average chemical analysis of the troilite (in wt. %): Fe 62.38, S 36.13, Ni 0.01, Cu 0.02, Ge 0.06, Ga, Si, Ti, and Cl 0.01. Troilite has an increased content of chromium, probably due to nano exsolution of daubréelite.

Daubréelite was observed only in troilite (Fig. 4) where it forms very thin exsolution lamellae with max. width up to 80  $\mu\text{m}$ . The crystallo-chemical formula of daubréelite is  $(\text{Fe}_{1.009-1.085}\text{Ni}_{0.000-0.002}\text{Co}_{0.000-0.001}\text{Cu}_{0.001-0.003}\text{Mn}_{0.019-0.023})_{\Sigma=1.028-1.114}\text{Cr}_{1.978-2.048}(\text{S}_4\text{Cl}_{0.000-0.003})$ . The daubréelite found in the troilite typically has an increased content of manganese (up to 0.42 wt. %=0.023 *apfu*). On the other hand, increased concentrations of Cr are characteristic for the troilite.

According to Wlotzka's (1993) classification, the weathering grade of Smolenice meteorite is W0 and only the marginal part of the iron indicates weathering grade W1.

### Bulk chemistry

The bulk analysis of the Smolenice meteorite suggests two dominant elements, iron and nickel (97.30–99.97 wt. %), cobalt is less abundant (0.38 wt. %). The bulk analysis of the Smolenice meteorite is consistent with the meteoritic iron of the IVA group. This meteorite was classified mainly on the basis of the Ni and Ga content, which clearly ranks it into the IVA group. Similarly, this is also true for the Ni/P ratio, where the Smolenice iron analysis falls to the centre of the IVA group analyses. By comparing the contents of Au to other elements (Ga, Cr, W, Ir, As, Pt), we can see a good match with the data for other IVA iron groups.

### Radionuklides

The examination of meteorite Smolenice included the investigation of cosmogenic radionuclides  $^{40}\text{K}$ ,  $^{26}\text{Al}$ , and  $^{14}\text{C}$ . The half-life of  $^{14}\text{C}$  is 5730 yr,  $^{26}\text{Al}$  — 0.717 Ma, and  $^{40}\text{K}$  — 1.251 Ga).

Initial analyses of radionuclide  $^{14}\text{C}$  indicate a terrestrial age >40,000 yr. Further ongoing AMS analyses can refine and characterise the terrestrial age of the Smolenice meteorite.

The measured  $^{26}\text{Al}$  activity in the Smolenice fragment (3.12±0.24 dpm/kg) suggests that the analysed sample

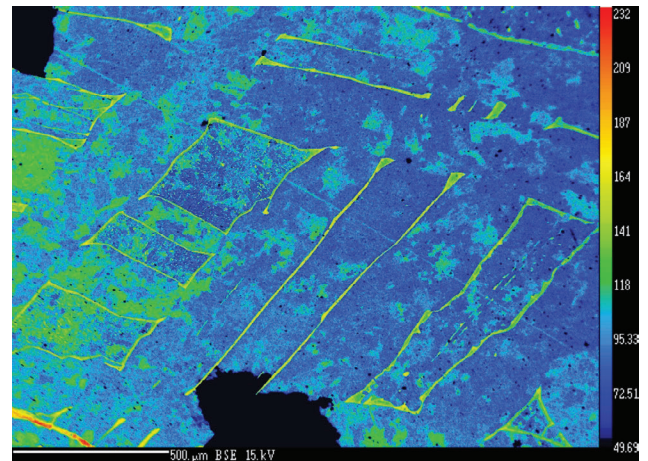


Fig. 2. Two types of taenite – lamellae in kamacite and plessitic texture (in central part).

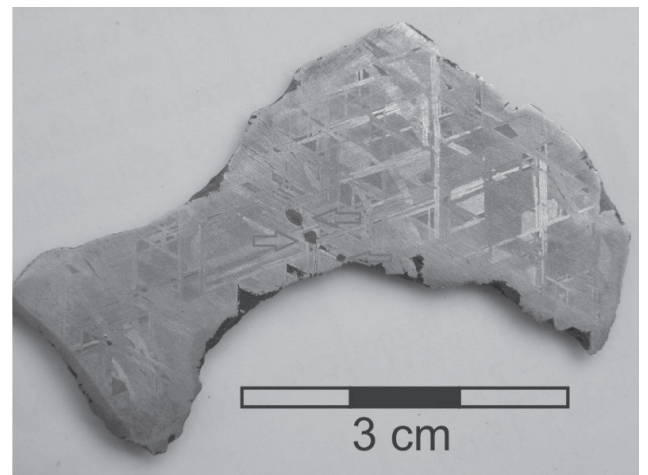


Fig. 3. Characteristic Widmanstätten pattern in the Smolenice iron. The two small dark inclusions are troilite nodules.

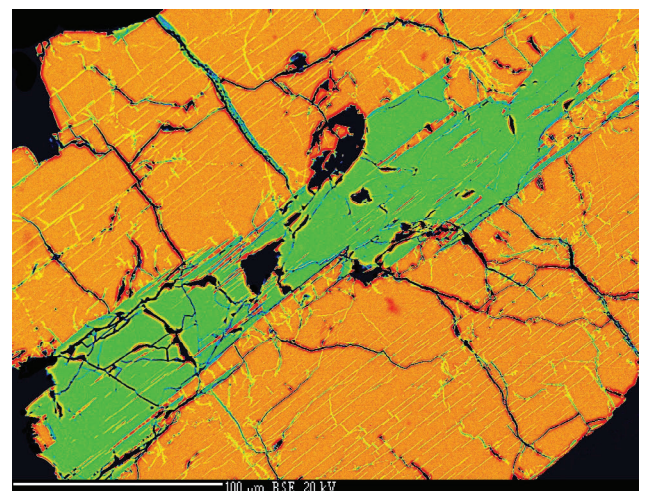


Fig. 4. Daubréelite grain (green) and lamellae (yellow) in troilite (orange). Blue veinlet is form the Fe-oxides. (BSE image)

is extra-terrestrial material. Based on a comparison with other iron meteorites, the measured data fits well with 30–50 cm meteorite radius data, if the terrestrial age of Smolenice would be about 0.1 Ma (Lavrukhina & Ustinova 1990).

The measured cosmogenic  $^{40}\text{K}$  activity (following the gamma-ray peak at 1460.8 keV) in the Smolenice meteorite is  $22.5 \pm 4.9$  dpm/kg, indicating that because of the very long half-life of this radionuclide (1.251 Ga) this value represents an unsaturated  $^{40}\text{K}$  activity. Comparing this experimental value with theoretical calculations of Lavrukhina & Ustinova (1990) we may estimate that the cosmic-ray exposure age of the Smolenice meteorite would be about 0.2 Ma.

**Acknowledgements:** This work was supported by the Slovak Research and Development Agency under the contract Nr. APVV-0516-10 and F.A. Paneth Trust Meteorite Award of the Royal Astronomical Society.

## References

- Frost M.J. 1965: Kamacite plate with estimation in octahedrites. *Mineral. Mag.* 35, 640–642.
- Gargulák M., Ozdín D., Povinec P., Strekopytov S., Porubčan V. & Farsang Š. (in print): Mineralogy, geochemistry and classification a new meteorite Smolenice Slovakia. *Geol. Carpath.*
- Jull A.J.T., Donahue D.J., Cielaszyk E. & Wlotzka F. 1993:  $^{14}\text{C}$  terrestrial ages and weathering of 27 meteorites from the southern high plains and adjacent areas (USA). *Meteoritics* 28, 188–195.
- Jull A.J.T., McHargue L.R., Bland P.A., Greenwood R.C., Bevan A.W.R., Kim K.J., Giscard M.D., LaMotta S.E. & Johnson J.A. 2010: Terrestrial  $^{14}\text{C}$  and  $^{14}\text{C}$ - $^{10}\text{Be}$  ages of meteorites from the Nullarbor, Australia. *Meteorit. Planet. Sci.* 45, 1271–1283.
- Lavrukhina A.K. & Ustinova G.K. 1990: Meteorites probes of cosmic-ray variations. *Nauka*, Moscow, 1–264.
- Povinec P.P., Sýkora I., Porubčan V. & Jeřkovský M. 2009: Analysis of  $^{26}\text{Al}$  in meteorite samples by coincidence gamma-ray spectrometry. *J. Radioanal. Nucl. Chem.* 282, 805–808.
- Povinec P. P., Masarik J., Sýkora I., Kovačik A., Beňo J., Laubenstein M. & Porubčan V. 2015: Cosmogenic radionuclides in the Košice meteorite: Experimental investigations and Monte Carlo simulations. *Meteorit. Planet. Sci.* 50, 880–892.
- Reuter K.B., Williams D.B. & Goldstein J.I. 1988: Low temperature phase transformations in the metallic phases of iron and stony-iron meteorites. *Geochim. Cosmochim. Acta* 52, 617–626.
- Wlotzka F. 1993: A weathering scale for the ordinary chondrites. *Meteoritics* 28, 460.
- Yang C-W., Williams D.B. & Goldstein J.I. 1996: A revision of the Fe-Ni phase diagram at low temperatures (<400 °C). *J. Phase Equilibria* 17, 522–531.
- Yang C-W., Williams D.B. & Goldstein J.I. 1997a: Low-temperature phase decomposition in metal from iron, stony-iron and stony meteorites. *Geochim. Cosmochim. Acta* 61, 2943–2956.
- Yang C-W., Williams D.B. & Goldstein J.I. 1997b: A new empirical cooling rate indicator for meteorites based on the size of the cloudy zone of the metallic phases. *Meteoritics Planet. Sci.* 32, 423–429.

# Two types of titanite in I-type tonalites from Tatric and Veporic units: Magmatic vs. post-magmatic oxidation

IGOR PETRÍK

Earth Science Institute, Slovak Academy of Sciences, Bratislava, Slovakia; igor.petrík@savba.sk

**Abstract:** Titanite, a characteristic mineral of Tatric (Tribeč) and Veporic (Sihla) I-type tonalites crystallizes in two generations: magmatic titanite I originated by slightly different ways, at the expense of Ti-biotite in Tribeč tonalite, and at the expense of Fe–Ti oxides in Sihla tonalite. Both rocks were oxidised in late stages, producing postmagmatic/metamorphic titanite II+magnetite, the Sihla type oxidised more intensely due to oxidising effect of the Alpine overprint.

## Introduction

I-type tonalites and granodiorites represent important rock types building the Variscan basement of the Tatric and Veporic units (Petrík & Broska 1994; Broska et al. 2013; Broska & Petrík 2015). A characteristic accessory mineral assemblage of this granitoid rock, magnetite+titanite+allanite, indicates oxidation conditions during late- to post-magmatic stages (Broska et al. 2007). However, titanite population is not uniform, and at least two types of this mineral can be distinguished in different textural positions. In this contribution I present new interpretation of both titanite types and discuss their petrogenetic significance on the example of Tribeč tonalite (Tatric unit) and Sihla tonalite (Veporic unit).

## Occurrence and petrography of the tonalites

Titanite-bearing tonalites typically occur in Tatric unit (Tribeč. Mts., Nízke Tatry Mts.) and NW part of the Veporic unit (the Sihla type tonalite). By contrast, titanite is not found in more common peraluminous S-type granitoids occurring in both tectonic units.

Medium-grained granitoids are composed of strongly retrogressed plagioclase (saussurite), if preserved with  $An_{28-30}$ , abundant biotite [ $Fe/(Fe+Mg)=0.40-0.42$ ,  $TiO_2$  1.5–2 wt. %], both extensively replaced by epidote/clinozoisite or rare secondary muscovite. The assemblage is completed by a rich accessory assemblage (magnetite, allanite, titanite, apatite, zircon). The presence of accessory amphibole (hornbende) is significant in the Tribeč tonalite, while it is missing in Sihla tonalite. Plagioclase is less altered in Tatric tonalite, and it is replaced by tiny white mica and fine-grained clinozoisite. In contrast, Veporic plagioclase is heavily

replaced by abundant large epidote. Titanite is also different: in the Tatric Tribeč tonalite a euhedral titanite I is associated mostly with plagioclase always containing resorbed grains of Ti magnetite (Fig. 1a). Titanite I in Veporic Sihla tonalite is up to several millimeters in size, sub- to euhedral also associated with plagioclase but without enclosed Ti magnetite (Fig. 1c). Titanite II in both rock types is small anhedral, typically associated with biotite and epidote (Fig. 1d). Titanite II commonly merges with large grains of titanite I (Fig. 1b).

## P-T-X conditions of titanite formation

Magmatic titanite commonly crystallizes from magmas with increased Ca/Al ratio, not necessarily oxidised. High Ca content stabilises titanite at the expense of ilmenite (e.g. Frost et al. 2000). It is stable over wide P–T range including magmatic, postmagmatic and metamorphic conditions.

## Pseudosections

P–T evolution was modelled by pseudosections calculated from whole rock analyses of Tribeč and Sihla tonalites using the Perplex software packet (Connolly 2005). P–T window used were at  $T=500-850$  °C and  $P=1-7$  kbar. Chosen water contents were 1.25 wt.  $H_2O$  for Sihla tonalite and 1.45 for Tribeč tonalite. These contents were estimated from isobaric T- $H_2O$  pseudosections at the  $H_2O$  values, which best correspond to the observed modal mineralogy, especially the presence/absence of amphibole and presence of titanite or ilmenite. Reduced conditions (FeO) were used because an oxidated system in Perplex produces hematite, phlogopite and no Fe–Ti oxide. However, oxidation

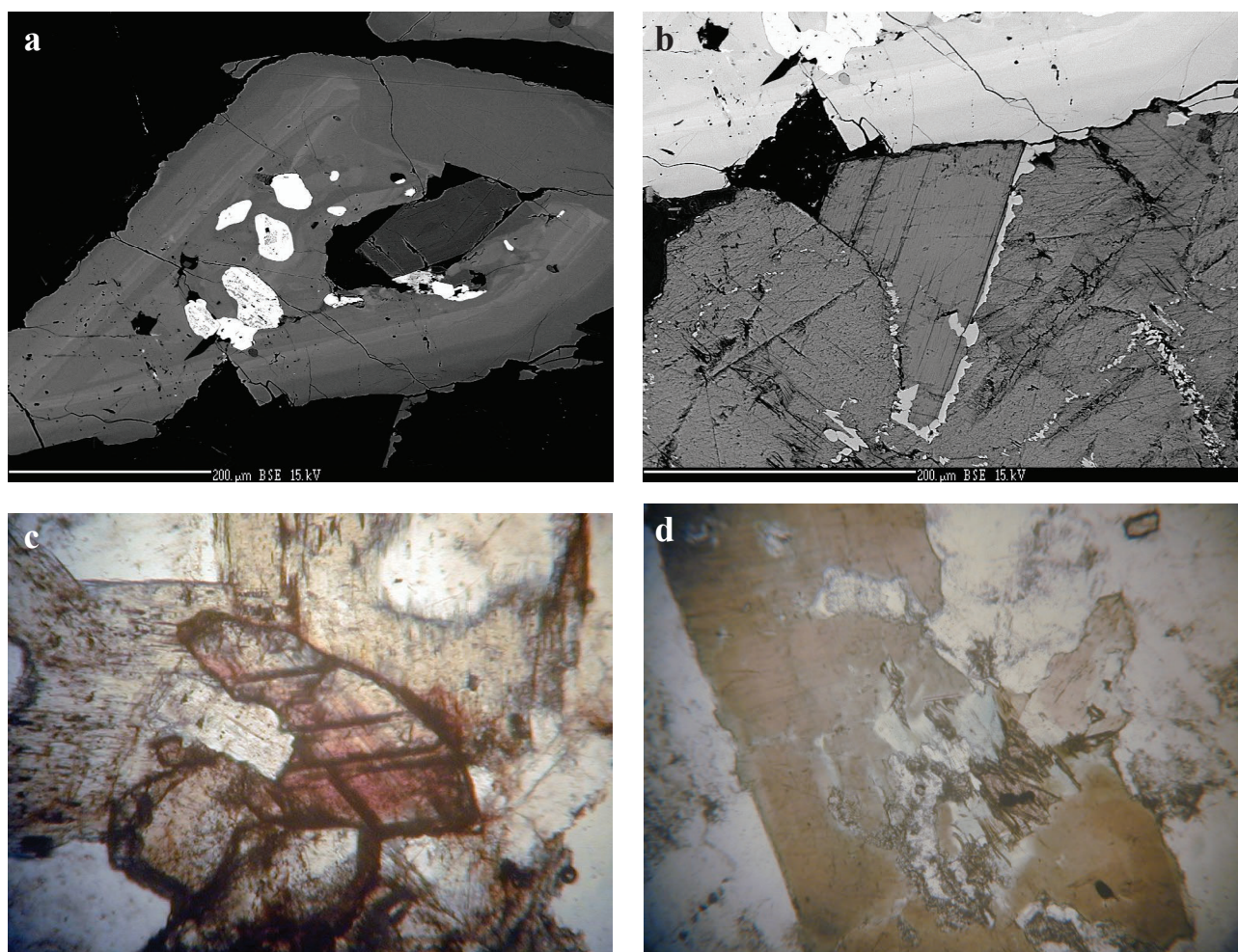


**Fig. 1.** BSE (a–b) and optical microphotos (c–d) images of titanite generations. **a** — Primary titanite with inclusions of early Ti-magnetite and late rims; **b** — secondary titanite “chains” evolved along biotite cleavage coalescing with primary titanite from (a), Tribeč tonalite; **c** — anhedral titanite associated with plagioclase; **d** — secondary titanite associated with biotite, Sihla tonalite.

conditions ( $\text{Fe}_2\text{O}_3$ ) were used for calculation of post-magmatic assemblages involving epidote.

*Sihla tonalite*: At the used value 1.25 %  $\text{H}_2\text{O}$  titanite starts to crystallize  $<760$  °C at 4 kbar, and  $<740$  °C at 3 kbar. Amphibole is not stable and ilmenite is stable over the whole window except  $>6$  kbar, where it is replaced by titanite. The most important feature is that at the beginning of titanite I crystallization the content of ilmenite drops from ca. 0.3 wt. % to 0.05 vol. % indicating that titanite forms at the expense of ilmenite (in real rock ulvöspinel+titanohematite). This can explain the absence of Fe–Ti oxides enclosed in titanite.

*Tribeč tonalite* shows slightly different relations, the system requires higher  $\text{H}_2\text{O}$  (1.45 wt.) to stabilise amphibole, and the beginning of titanite crystallization is accompanied by much lower decrease in ilmenite from 0.2 to 0.15 vol. %. Titanite I, therefore, seems to form at the expense of biotite, enabling ilmenite

(ulvöspinel–titanohematite) to be preserved within titanite crystals.

Crystallization of titanite I does not require oxidation conditions, which is confirmed by compositions of Fe–Ti oxides (Broska & Petřík 2015, fig. 8d).

#### **Late oxidation**

*Tribeč I-type tonalite*: the occurrence of resorbed Ti-magnetite in titanite enabled calculation of late oxidation reactions (Broska & Petřík 2015) involving biotite (annite), ilmenite, actinolite, celadonite and producing magnetite, epidote and titanite II. Intersections of the reactions are at 610, 477 and 471 °C.

*Sihla tonalite*: titanite II originated by reactions involving removal of Ti from biotite, which shows low  $\text{TiO}_2$  contents  $<2$  wt. %. Pseudosections (solution model of Tajčmanová et al. 2009) indicate subsolidus

temperatures for such biotite compositions: Sihla 540 °C (1.83 wt. % TiO<sub>2</sub>), Tribeč 550 °C (1.93 wt. % TiO<sub>2</sub>).

A low temperature alteration was observed in Tribeč tonalite leading to backward replacement of titanite by ilmenite (Broska et al. 2007).

### Discussion and conclusions

I-type tonalites from Tatric and Veporic basement show very similar mineralogy indicating late oxidation conditions (titanite, magnetite, epidote). While the early titanite I associated with plagioclase is magmatic in both rock types, the late secondary titanite II probably originated by differing ways in Tatric Tribeč tonalite as opposed to the Veporic Sihla tonalite. In the first case the Variscan thrusting of altered tonalite (Broska & Petřík 2015) documents that titanite II is product of ulvöspinel oxidation and Ti-rich biotite decomposition during retrogression. On the other hand, titanite II in Sihla tonalite, probably formed during Alpine overprint, both at similar temperature (below 600 °C) but different pressures: much higher in the Sihla tonalite. The Alpine overprint was accompanied by oxidation producing a large amount of new epidote, increasing the Fe<sup>3+</sup>/Fe<sup>2+</sup> ratios in biotite and allanite. Titanite intergrown with epidote in Sihla tonalite indicates formation of titanite below 500 °C.

**Acknowledgements:** This work was financed by grants APVV 14 0278, APVV 18-01107 and Vega 2/0008/19.

### References

- Broska I. & Petřík I. 2015: Variscan thrusting in I- and S-type granitic rocks of the Tribeč Mountains, Western Carpathians (Slovakia): evidence from mineral compositions and monazite dating. *Geol. Carpath.* 69, 365–381.
- Broska I., Harlov D., Tropper P. & Siman P. 2007: Formation of magmatic titanite and titanite-ilmenite phase relations during granite alteration in the Tribeč Mountains, Western Carpathians, Slovakia. *Lithos* 95, 58–71.
- Broska I., Petřík I. & Uher P. 2012: Accessory minerals of the Western Carpathian granitic rocks. *Veda Publishing House*, Bratislava, 1–235.
- Broska I., Petřík I., Beeri-Shlevin Y., Majka J. & Bezák V. 2013: Devonian/Mississippian I-type granitoids in the Western Carpathians: A subduction-related hybrid magmatism. *Lithos* 162–163, 27–36.
- Connolly J.A.D. 2005: Computation of phase-equilibria by linear programming: a tool for geodynamic modeling and its application to subduction zone decarbonation. *Earth Planet. Sci. Lett.* 236, 524–541.
- Frost B.R., Chamberlain K.R. & Schumacher J.C. 2000: Sphephene (titanite): phase relations and the role as a geochronometer. *Chem. Geol.* 172, 131–148.
- Petřík I. & Broska I. 1994: Petrology of two granite types from the Tribeč Mountains, Western Carpathians: an example of allanite (+ magnetite) versus monazite dichotomy. *Geol. J.* 29, 59–78.
- Tajčmanová L., Connolly J.A.D. & Cesare B. 2009: A thermodynamic model for titanium and ferric iron solution in biotite. *J. Metamorph. Geol.* 27, 153–165.

# Geochemical modeling of magmatic–hydrothermal systems: Petrological evaluations and metallogenic application

SERGEY SHNYUKOV, IRINA LAZAREVA, OLEKSANDR ANDRIEIEV,  
OLEKSANDR MYTROKHIN, ANTON ALEKSIEIENKO and LIUBOMYR GAVRYLIV

Institute of Geology, Taras Shevchenko National University of Kyiv, 90 Vasylykivska Str., 03022, Kyiv, Ukraine;  
shnyukov54@gmail.com, lazareva067@gmail.com, andreev@mail.univ.kiev.ua, scr315@gmail.com

**Abstract:** Proposed modeling approach (Shnyukov & Lazareva 2017; Shnyukov et al 2018; Lazareva et al. 2018 etc.) is based on a set of equations for trace element behavior during the melt crystallization/partial melting (Rayleigh–Neumann–Ryabchikov–Shaw et al.) and widespread accessory minerals (WSAM — Ap, Zrn, Mnz etc.) solubility equations (Watson–Harrison–Montel), which are mainly used to derive the model evaluation of the temperature ( $T_{\text{model}}$ ) and fluid regime in the magmatic system from the whole-rock geochemical data. Furthermore, such models include principally new components: (1) calibrated  $\ln K_Y^{\text{Ap/Zrn}}$  vs.  $1/T(\text{K})$  dependence with the equation for the inverse problem solution ( $K_Y^{\text{Ap/Zrn}} = C_Y^{\text{Ap}}/C_Y^{\text{Zrn}}$ ;  $C^{\text{F}}$ ,  $C^{\text{L}} = Y$  content in coexistent apatite and zircon respectively) which allows to verify obtained  $T_{\text{model}}$  values (key input parameter for most of calculations), (2) equations for calculation of the fluid/melt distribution coefficient ( $K^{\text{F/L}} = C^{\text{F}}/C^{\text{L}}$ ;  $C^{\text{F}}$ ,  $C^{\text{L}} = \text{element content in the fluid and melt respectively}$ ) and the model element composition of the hydrothermally altered rocks, (3) procedures for evaluation of ore-generating potential of the system.

## Introduction

Geochemical modeling is crucial for the investigation of magmatic–hydrothermal systems, including evaluation of their ore potential. The main objectives (see Shnyukov 2001, 2002, etc.) are following:

1. Determination of the leading magmatic formation mechanism (fractional crystallization, partial melting, etc.).
2. Determination of major and trace element behavior in the magmatic evolution.
3. Evaluation of physico–chemical conditions of formation.
4. Evaluation of its ore-bearing fluids generation ability corresponding to hydrothermal–metasomatic ore formation.

Theoretical basis and methodology for solving of tasks (1) and (2) proposed by Neumann et al. (1954); Ryabchikov (1965, 1975); Allegre & Minster (1978) etc., are widely used in the study of magmatic complexes. The methodology for the tasks (3) and (4) proposed by Shnyukov et al. (1989, 1993); Shnyukov & Lazareva (2002) etc. It is complex modeling of major and trace elemental distribution in the series of igneous rocks, experimental data on water (Ryabchikov 1975; Holtz et al. 2001, etc.) and widespread accessory minerals solubility in silicate melts (WSAM — Ap, Zrn, Mnz, etc.) (Watson & Harrison 1983; Harrison & Watson 1984; Montel 1993), as well as the data on

the distribution of trace elements in WSAM's associations (Shnyukov & Lazareva 2017, etc.). But the solution of the problem (4) should be considered as incomplete without a quantitative evaluation of the elemental supply from the melt in magmatic–hydrothermal system. The solution was suggested by Shnyukov et al. (2016, etc.).

Modeling procedures are given below on an example of the magmatic system of precambrian Korosten Pluton (KP) in the Ukrainian Shield and hydrothermal–metasomatic ore occurrences and deposits connected with KP and Suschano–Perzhanskaya area (SPA).

## Modeling of the magmatic system

Geochemical model of KP granitoids magmatic evolution was prepared using representative geochemical data set which covers their main varieties (rapakivi, granite–porphyry, veined granites etc.) and Rayleigh fractional crystallization model to approximate the trace element data. Following crucial results have been obtained:

1. Typical incompatible behavior with approximately constant bulk distribution coefficient was determined for Rb ( $D_{\text{Rb}}=0.5$ ). Model  $f$  values (weight fraction of liquid phase in magma chamber) were calculated for each granitoid type (residual melt portion) from Rayleigh equation and Rb content in rocks ( $C_{\text{Rb}}$ )

- assuming minimum concentration in granitoids (169 ppm) as Rb content in parent magma ( $C_0^{Rb}$ ).
2.  $C$  vs.  $f$  curves for trace and major elements were approximated by means of  $C=C_0 \cdot f^{D-1}$  equations or polynomial ones respectively (Fig. 1, Table 1). This set of equations is an idealized model of elements behavior. Corresponding bulk distribution coefficient ( $D$ ) and  $C_0$  values for trace elements are shown in Table 1.
  3. Monotonous decrease of both Zr and P contents indicate melt saturation for zircon and apatite. Therefore, the model temperature ( $T_{\text{model}}$ ) of the melt was estimated using equations for their solubility (Watson & Harrison 1983; Harrison & Watson 1984). The temperature evolution in magma chamber is presented as  $T_{\text{model}}$  vs.  $f$  equation ( $T_{\text{model}}$  range: 900–720 °C).
  4. Inversion in LREE content ( $f=0.185$ ) indicates the apatite/monazite replacement in the crystallizing material. Water content in melt for this  $f$  value for corresponding  $T_{\text{model}}$  was calculated from monazite solubility equation (Montel 1993), which yielded  $C_0^{\text{H}_2\text{O}}=2.36$  wt. % (assuming  $D^{\text{H}_2\text{O}}=0.1$ ) for the liquidus of initial granite melt.  $P_{\text{total}} \sim 6.3$  kbar corresponds to this value (Ryabchikov 1975; Holtz et al. 2001, etc.) (Fig. 1).
  5. Water saturation was reached at  $f=0.165$  and  $\text{H}_2\text{O}$ -fluid was extracted from the melt during its further evolution. Synchronous inversion of  $C$  vs.  $f$

behavior proves fluid enrichment with F, Cl, Nb, Zn, Pb, etc. (Fig. 1).

## Modeling of the magmatic–hydrothermal system

### Fluid/melt distribution coefficient

According to the “magmatic” model (Fig. 1), the behavior of each “inversion” element is described by two equations of Rayleigh type, which correspond to the sections of the magmatic evolution until ( $f > f_{\text{inv.}}$ ) and after ( $f < f_{\text{inv.}}$ ) inversion, which coincides with the beginning of the fluid segregation ( $f_{\text{inv.}}^{\text{Nb}}=0.123$  was accepted as the final  $f_{\text{inv.}}$  value). Concentrations of elements in residual melt, which are calculated by the first and second equations, are rationally denoted as  $C^M$  and  $C^L$ , and efficient bulk distribution coefficients used in these cases —  $D$  and  $D'$  respectively. Both values are constant in the developed model (Table 1).

The final equation for calculation of inversion behavior elements fluid/melt distribution coefficient for any value of  $f_n$  was obtained (see Shnyukov et al. 2016 for explanations):

$$K^{F/L} = \frac{\Delta S_n (D' - D) + D' \Delta F_n}{\Delta F_n}, \quad (1)$$

where  $\Delta S_n$  and  $\Delta F_n$  — the proportion of solid and fluid phases in the system, segregated during period  $\Delta f_n$ . For the elements with  $D'=D$  this equation simplifies to the form  $K^{F/L} = D$ .

### The volume of elements involved to magmatogenic–hydrothermal system

Developed model allows to estimate the *total elemental resource of the fluid* (Fig. 2), i.e. the total weight of each element, extracted from the melt by the aqueous fluid, which is segregated from the magmatic system during its evolution ( $R_F$ ). Really, model provides data not only on the concentration of each element in the residual melt ( $C^L$ ), and the value of its fluid/melt distribution coefficient ( $K^{F/L}$ ), but also estimates the mass fraction of fluid segregated from magmatic system at any stage of evolution at  $f < f_{\text{inv.}}$  ( $\Delta F_n$ ). Therefore:

$$\Delta R_{F_n} = \Delta F_n \cdot C_i^{F_n} \cdot M_{\text{sys}} / 10^6, \quad (2)$$

where  $\Delta R_{F_n}$  — the fluid’s resource, segregated from the magmatic system during the period  $\Delta f_n$  (billion tons);

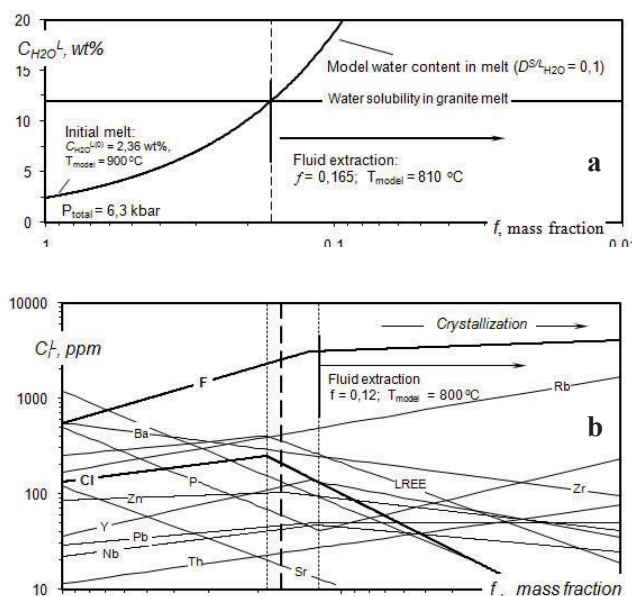


**Fig. 1.** Results of geochemical modeling of the KP granitoid magmatic systems: **a** — segregation of aqueous fluid from the melt during its crystallization; **b** — concentrations of elements in residual melt of the magmatic system.

$C_i^{F_n}$  — the concentration of the element  $i$  in the fluid (ppm) at the moment  $f_n$ ;  $M_{\text{sys}}$  — the mass of the system (billion tons). The total fluid resource of the element  $i$  can be estimated using the expression:

$$R_F = \sum_{n=1}^n \Delta R_{F_n} \quad (3)$$

In these equations the total mass of the parental magmatic system ( $M_{\text{sys}}$ ) is an important input parameter but usually difficult for evaluation. In the case under consideration  $M_{\text{sys}} \geq 200000$  billion tons was accepted. Due to the existing data this estimation is approximate, but realistic.

Additional, but important parameter in the elements behavior analysis during evaluation of ore-generating potential of magmatic–hydrothermal systems is *total elemental resource of the parent magmatic system* ( $R_M$ ), i.e. the total weight of each element in the system. Its calculation is straightforward:

$$R_M = C_{i(0)} \cdot M_{\text{sys}} / 10^6, \quad (4)$$

where  $R_M$  — total resource of the parent magmatic system (billion tons);  $C_{i(0)}$  — concentration of the element  $i$  in the initial melt (ppm) (see Table 1;  $M_{\text{sys}}$  — mass of the system (billion tons).

The model estimations obtained for KP are presented in Figure 2. They indicate that the fluid/melt distribution coefficient ( $K^{F/L}$ ) is the most important factor that controls the total elemental resource of the fluid and ore-generating potential of magmatogenic–hydrothermal systems.

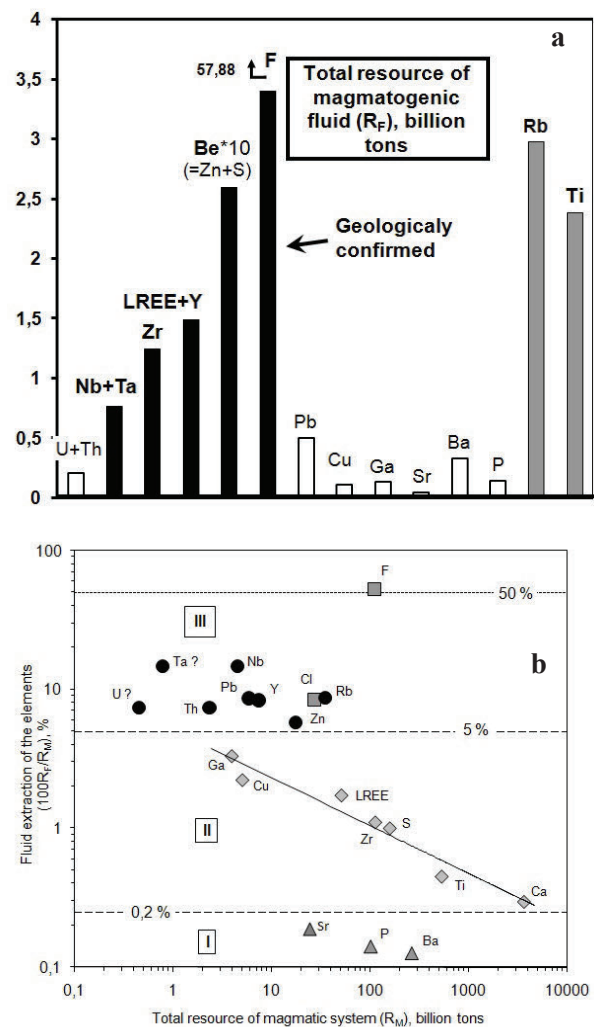


**Fig. 2.** **a** — Total elemental resource of the fluid as a criterion for the evaluation of ore-generating potential of magmatogenic–hydrothermal system. **b** — Extraction of elements with different total elemental resource of the magmatic system to the fluid.

**Table 1:**  $C_0$  and  $D$  values calculated for selected elements on a base of  $C$  vs.  $f$  trends assuming that studied main Korosten granitoids rock types composition is as liquids (melts)

Element	Values calculated for various sections of $C$ vs. $f$ trends			
	Before inversion ( $f > 0.1 \div 0.2$ )		After inversion ( $f < 0.1 \div 0.2$ )	
	$C_0 = a$ (ppm)	$D = b + 1$	$a$	$D' = b + 1$
Zr	555.08	1.381	**	**
Sr	119.99	2.0564	**	**
P	497.04	2.172	9.4801	0.3058
Ti	2622.7	1.7251	**	**
Y	36.104	0.34	412.89	1.5363
LREE	251.6	0.7182	2381.3	2.0511
Rb	169*	0.5*	**	**
Ba	1289.8	2.2094	**	**
Zn	85.55	0.9	191.26	1.3368
Ga	19.314	0.9346	**	**
Th	11.428	0.5872	**	**
Nb	21.991	0.6341	81.164	1.258
Pb	28.841	0.7359	49.842	1.0001
Cu	24.789	1.1069	**	**
F	547.41	0.153	2492.5	0.8963
Cl	132.82	0.6315	2963.4	2.4732
S	780.15	1.418	**	**

Notes: (1)  $a$  and  $b$  are the parameters of the equations of  $y = ax^b$  [ $C(\text{ppm}) = af^b$ ] form obtained for each trace element; (2) \* assumed values; (3) \*\*  $C$  vs.  $f$  trends demonstrate the monotonous behavior of these elements without inversion points; (4) LREE = La+Ce+Nd.

## Conclusions

The method of fluid/melt distribution coefficients and total elemental resource of the magmatic fluids estimation was proposed based on geochemical modeling of parent magmatic systems. The model directly derives from the observed data of elements content in main rock types of magmatic complexes and mostly corresponds to the real conditions of the magmatic evolution. Obtained results allows to use methodology in the regional geological and metallogenic investigations.

**Acknowledgements:** This work was supported by the Scientific Research Department of the Taras Shevchenko National University of Kiev throughout grants 0195U004122, 0195U004123, 0197U003159 and 0116U004784. Authors really appreciate consultations of V.G. Molyavko and O.V. Zinchenko, as well as assistance of V.V. Zagorodny, E.A. Khlon and O.D. Omelchuk in analytical and mineralogical research.

## References

- Allegre C.J. & Minster J.F. 1978: Quantitative models of trace element behaviour in magmatic processes. *Earth Planet. Sci. Lett.* 38, 1–25.
- Greenland L.P. 1970: An equation for trace element distribution during magmatic crystallization. *Am. Miner.* 55, 455–465.
- Harrison T.M. & Watson E.B. 1984: The behavior of apatite during crustal anatexis: equilibrium and kinetic considerations. *Geochim. et Cosmochim. Acta* 48, 1467–1477.
- Lazareva I., Shnyukov S., Aleksieienko A. & Gavryliv L. 2018: Ore-bearing metasomatites of Perga area and Korosten pluton granitoids (Ukrainian shield): genetic relations on the basis of geochemical modelling. *Visnyk Taras Shevchenko National University of Kyiv, Geology* 3, 82, 66–79.
- Montel J.M. 1993: A model for monazite/melt equilibrium and application to the generation of granitic magmas. *Chemical Geology* 110, 127–145.
- Neumann H., Mead J. & Vitaliano C.J. 1954: Trace element variation during fractional crystallization as calculated from the distribution law. *GCA* 6, 90–99.
- Ryabchikov I.D. 1965: Thermodynamic analysis of trace elements behavior during silicate melts crystallization processes. *Nauka*, Moscow, 1–120 (in Russian).
- Ryabchikov I.D. 1975: Thermodynamics of the fluid phase in granitoid magmas. *Nauka*, Moscow, 1–232 (in Russian).
- Shnyukov S.E. 2001: Widespread accessory minerals in geochemical modeling of magmatic processes. *Zbirnik naukovih prats UkrDGRI* 1–2, 41–53 (in Ukrainian).
- Shnyukov S.E. 2002: Geochemical models of magmatic systems and earth crust evolution: potential source of petrophysical and ore-genetic information. *Geophysical Journal* 24, 6, 201–219 (in Russian).
- Shnyukov S.E. & Lazareva I.I. 2002: Geochemical modeling in research of genetic connection of magmatic complexes and spatially associated hydrothermal-metasomatic ore deposits. *Zbirnik naukovih prats UkrDGRI* 1–2, 128–143 (in Ukrainian).
- Shnyukov S. & Lazareva I. 2017: Distribution of yttrium and some other trace elements in wide-spread accessory mineral assemblages: temperature dependence and its application in geochemical modelling. *Visnyk Taras Shevchenko National University of Kyiv, Geology* 2, 77, 13–27 (in Russian).
- Shnyukov S.E., Cheburkin A.K. & Andreev A.V. 1989: Geochemistry of widespread coexisting accessory minerals and their role in investigation of endogenetic and exogenetic processes. *Geological Journal* 2, 107–114 (in Russian).
- Shnyukov S.E., Határ J., Andreev A.V., Gregush J., Cheburkin A.K. & Savenok S.P. 1993: Petrological analysis of accessory zircon and apatite geochemistry in granitoids of Rochovce intrusion (Slovakia). *Geological Journal* 1, 30–41 (in Russian).
- Shnyukov S.E., Lazareva I.I., Portnov V.S., Aleksieienko A.G., Gavryliv L.I., Makat D.K. & Maratova A.G. 2016: Geochemical modeling in the evaluation of ore-forming potential of magmatic–hydrothermal systems. *Bulletin of the Karaganda University, Physics Series* 4, 84, 51–58.
- Shnyukov S., Lazareva I., Zinchenko O., Khlon E., Gavryliv L. & Aleksieienko A. 2018: Geochemical model of precambrian granitoid magmatic evolution in the Korosten Pluton (Ukrainian Shield): petrogenetic aspects and genesis of complex ore mineralization in metasomatic zones. *Visnyk Taras Shevchenko National University of Kyiv, Geology* 2, 81, 12–22.
- Watson E.B. & Harrison T.M. 1983: Zircon saturation revisited: temperature and composition effects in a variety of crustal magma types. *Earth Planet. Sci. Lett.* 64, 295–304.

# Beryllium silicate minerals in granite–pegmatite suites: Tracers of magmatic to hydrothermal and tectonic evolution (examples from Western Carpathians)

PAVEL UHER, PETER BAČÍK and JANA FRIDRICHOVÁ

Department of Mineralogy and Petrology, Faculty of Natural Science, Comenius University, Ilkovičova 6, 842 15 Bratislava, Slovakia; pavel.uher@uniba.sk

**Abstract:** Beryllium silicate accessory minerals (beryl, gadolinite–hingganite, phenakite and bertrandite) represent useful mineral indicators of magmatic to hydrothermal processes and tectonic environment. It is well documented on examples from contrasting Carboniferous to Permian granite–pegmatite suites of the Western Carpathians (Slovakia). Primary magmatic beryl is characteristic accessory mineral in more evolved granitic pegmatites (Tatric Unit); Na–Fe–Mg enriched compositions occur in I-type granodiorite-affiliated pegmatites, whereas Al–(Cs–Li) enriched beryl is typical for S-type granite-related pegmatites. On the contrary, late-magmatic gadolinite-(Y) partly replaced by hingganite-(Y) occurs in rift-related A-type granite (Turčok, Gemeric Unit). Consequently, beryl and gadolinite as the most widespread magmatic accessory minerals of Be show antagonistic relationship in aluminous versus alkaline granite–pegmatite suites. Beryl is frequently replaced by post-magmatic assemblage: secondary Be silicate minerals (phenakite and bertrandite), late quartz, muscovite and K-feldspar. The beryl breakdown clearly documents post-magmatic tectonic event related with late- to post-Variscan uplift or Alpine (Mesozoic to Cenozoic) tectono-metamorphic overprint of the West-Carpathian crystalline basement.

## Beryllium abundance

Beryllium belongs to the rare lithophile elements (RLE) concentrating especially in felsic (Si-rich) peraluminous or alkaline magmatic rocks of the Earth continental crust. Average Be content of common granitic rocks usually attains 2 to 7 ppm (London & Evensen 2002). The highest Be concentrations exhibit some highly evolved F- and alkali-rich magmatic lithologies, such as A-type (topaz-bearing) rhyolites:  $\leq 270$  ppm, rare-element S-type leucogranites: 500 ppm, as well as beryl and complex Li–Cs–Ta granitic pegmatites:  $\sim 50$  to 600 ppm (London & Evensen 2002). An unique combination of low valency and very small effective cation radius of  $\text{Be}^{2+}$  in tetrahedral coordination ( $0.27 \cdot 10^{-10}$  m; Shannon 1976) determine highly incompatible behaviour and very limited incorporation of Be into crystal structure of common granitic rock-forming minerals (quartz, feldspars, biotite, muscovite), probably by  $\text{Be}^{2+} + \text{Si}^{4+} = 2\text{Al}^{3+}$  and  $\text{Ca}^{2+} + \text{Be}^{2+} = (\text{Na}, \text{K})^{+} + \text{Al}^{3+}$  substitutions. However, some silicate minerals could concentrate Be in notable concentrations:  $10^2$  to  $10^4$  ppm, such as cordierite with  $\text{Na}^{+} + \text{Be}^{2+} = \text{Al}^{3+} + \square$  or Ca-micas of bityite–margarite series showing  $\text{Li}^{+} + \text{Be}^{2+} = \square + \text{Al}^{3+}$  substitution (e.g., Černý 2002).

Carboniferous orogenic I-, S-type and Permian rift-related A-type granite to pegmatite suites of the pre-Alpine Paleozoic basement of the Western Carpathians

represent a good example for Be behaviour study in contrasting geochemical and tectonic magmatic series.

## Beryl versus gadolinite antagonism

Beryl [ $(\square, \text{Na}, \text{Cs}, \text{H}_2\text{O})(\text{Al}, \text{Sc}, \text{Fe}, \text{Mg})_2(\text{Be}, \text{Li})_3(\text{Si}_6\text{O}_{18})$ ] and gadolinite–hingganite-(Y) series [ $(\text{Y}, \text{REE})_2(\text{Fe}, \square)\text{Be}_2\text{Si}_2(\text{O}, \text{OH})_2$ ] are generally the most widespread accessory Be minerals in magmatic rocks. However, both minerals precipitate only in highly fractionated, RLE-rich leucogranites and especially in granitic pegmatites due to strongly incompatible nature of Be. Beryl occurs in some evolved peraluminous pegmatites of parental Variscan granitic suites with I- and especially S-type affinity in the Tatric Unit of the Western Carpathians (Uher & Broska 1995; Uher et al. 2010). Beryl commonly associates with primary Nb–Ta oxide minerals (columbite, rarely tapiolite and wodginite groups, Nb–Ta rutile) almandine–spessartine, Hf-rich zircon and locally also gahnite; the pegmatites belong to the beryl–columbite subtype of LCT family. Beryl shows a sequence from Na–Fe–Mg enriched compositions in relatively less evolved pegmatites in I-type biotite granodiorites (Vysoké and Nízke Tatry Mountains) to Na–Fe–Mg poor and Al–(Cs–Li) enriched beryl in more evolved, S-type two-mica granites to granodiorites of the Bratislava and Bojná Massifs (Malé Karpaty and

Považský Inovec Mts.). The Na–Fe–Mg beryl (Prašivá, N. Tatry Mts.) exhibits 1.9–2.5 wt. % Na<sub>2</sub>O (0.35–0.48 Na *apfu*), 2.7–5.0 wt. % FeO (0.21–0.40 Fe *apfu*), 2.0–2.7 wt. % MgO (0.29–0.38 Mg *apfu*), whereas cesium content attains up to 2.0 wt. % Cs<sub>2</sub>O (0.08 Cs *apfu*) in the Jezuitské Lesy pegmatite near Bratislava (M. Karpaty Mts.).

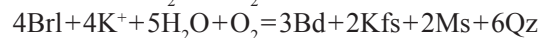
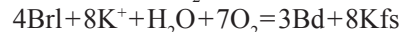
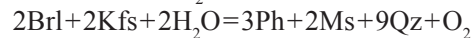
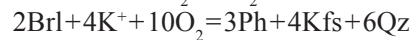
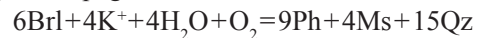
On the other hand, gadolinite-(Y) to hingganite-(Y) are characteristic accessory minerals of the Turčok A-type granites and related aplitic rocks (Gemic Unit, Western Carpathians). The gadolinite associates with zircon, allanite-(Ce), xenotime-(Y) and (Y,REE)–Nb–Ta–Ti oxide minerals [fergusonite-(Y) and aeschynite/polycrase-(Y)] (Uher et al. 2009). Gadolinite-(Y) precipitated at late-magmatic stage consolidation whereas hydroxyl-bearing hingganite-(Y) partly replaced it probably during subsolidus alteration of the Turčok granite.

Consequently, both beryl and gadolinite show antagonistic behaviour in late-magmatic conditions. Beryl is characteristic accessory mineral for evolved mainly peraluminous REE-poor suites (S-, I-, rarely mildly A-type tendency) in contrast to gadolinite-(Y) as typical Be accessory mineral in fractionated metaluminous, REE-Fe-rich A-type granites.

### Phenakite and bertrandite: products of beryl alteration

Investigated beryl is frequently replaced by post-magmatic mineral assemblage including secondary Be silicate phases (phenakite and bertrandite), late quartz, muscovite and K-feldspar. This replacement assemblage forms fine-crystalline (<1 mm) irregular veinlets and cluster aggregates along rims and fractures of primary magmatic beryl crystals. Phenakite and bertrandite were identified by XRD, Raman spectroscopy and EBSD, phenakite shows distinctive cathodoluminescence signal. Based on the mineral assemblage and textural relationships, the following reactions of beryl breakdown

could be assumed in investigated West-Carpathian granitic pegmatites:



(Brl: beryl; Ph: phenakite; Ms: muscovite; Qz: quartz; Kfs: K-feldspar; Bd: bertrandite).

Partial breakdown of beryl to phenakite, bertrandite and associated minerals is connected with post-magmatic (hydrothermal) fluids at T ~250–400 °C; the process has been related with late- to post-Variscan uplift or Alpine (Mesozoic to Cenozoic) tectono-metamorphic overprint of the West-Carpathian crystalline basement.

**Acknowledgements:** The work was supported by the Slovak Research and Development Agency under the projects APVV-18-0065 and APVV-15-0050.

### References

- Černý P. 2002: Mineralogy of beryllium in granitic pegmatites. In: Grew E.S. (Ed.): Beryllium: mineralogy, petrology and geochemistry. *Rev. Mineral. Geochem.* 50, 405–444.
- London D. & Evensen J.M. 2002: Beryllium in silicic magmas and the origin of beryl-bearing pegmatites. In: Grew E.S. (Ed.): Beryllium: mineralogy, petrology and geochemistry. *Rev. Mineral. Geochem.* 50, 445–486.
- Shannon R.D. 1976: Revised effective ionic radii and systematic studies of interatomic distances in halides and chalcogenides. *Acta Cryst.* A32, 751–767.
- Uher P. & Broska I. 1995: Pegmatites in two suites of Variscan orogenic rocks (Western Carpathians, Slovakia). *Mineral. Petrol.* 55, 27–36.
- Uher P., Ondrejka M. & Konečný P. 2009: Magmatic and post-magmatic Y–REE–Th phosphate, silicate and Nb–Ta–Y–REE oxide minerals in A-type metagranite: an example from the Turčok massif, the Western Carpathians, Slovakia. *Mineral. Mag.* 73, 1009–1025.
- Uher P., Chudík P., Bačík P., Vaculovič T. & Galiová M. 2010: Beryl composition and evolution trends: an example from granitic pegmatites of the beryl-columbite subtype, Western Carpathians, Slovakia. *J. Geosci.* 55, 69–80.



**Theme 3:**

Permian evolution: Joining the Variscan and Alpine orogenic events

# From Variscan to Cimmerian Europe as revealed from case studies in the Bohemian Massif and the eastern Mediterranean

GERNOLD ZULAUF

Department of Earth Science, Goethe University, Frankfurt a.M., Germany; g.zulauf@em.uni-frankfurt.de

The crust of Europe shows evidence for Cadomian, Variscan and Cimmerian orogenic imprints. As these orogens developed in entirely different geodynamic settings, their crustal architecture, the amount of horizontal shortening and the crustal thickness differ significantly. The present paper will focus on the Variscan and Cimmerian imprints as exposed in the Bohemian Massif and in the Eastern Mediterranean.

The Variscan orogenic belt developed during the Devonian to Carboniferous collision of peri-Gondwanan terranes with Laurasia. The provenance of these peri-Gondwanan terranes has been revealed using the age of magmatic and detrital zircons (e.g. Dörr et al. 2015). Minoan terranes, which are widespread in the Alpine and Mediterranean realm, are characterized by Tonian zircons derived from NE Gondwana. Armorican terranes of central and western Europe rifted off from N and NW Africa and are free from Tonian and Mesoproterozoic zircons. Avalonian terranes are situated between the Iapetus and the Rheic sutures. They have Amazonian affinity and are characterized by Mesoproterozoic igneous activity. Before these peri-Gondwanan terranes were split off from Gondwana in early Paleozoic times, they underwent Cadomian (Andean-type) orogenic imprints at the northern margin of Gondwana, which did not result in large-scale continent collision and related exhumation of lower crust.

The Variscides, on the other hand, include large areas with exhumed deeply buried high-grade metamorphic rocks, which are characterized by partial melting, complex polyphase deformation and significant amount of finite strain. In contrast to the very-low grade metamorphic rocks of the External Variscides (e.g. Rhenohercynian or Moravo–Silesian Zone), primary structures like bedding are largely destroyed in the high grade rocks of the Internal Variscides and the kinematics of deformation structures like folds and boudins is difficult to constrain. Nevertheless, unraveling the evolution and kinematics of the Variscan Internides is possible in the Bohemian Massif, which is one of the largest outcrops of Variscan basement in Europe where both upper and lower crustal

rocks are resting side by side. It was Franz Eduard Suess, who first recognized that the Tepla–Barrandian rocks were situated at a high structural level during the entire Variscan cycle and escaped Variscan metamorphism, while being surrounded by high-grade Moldanubian s.str. and Saxothuringian rocks. The lack of Variscan metamorphism makes the Tepla–Barrandian Unit an ideal candidate to obtain reliable kinematic data of deformations, which affected the internal part of the Variscides. These data suggest significant changes in the principal shortening directions, which are related to changes in the configuration and arrangement of the lithospheric plates and to major changes in the thermal state of the lithosphere (e.g. Dörr & Zulauf 2010; Žák et al. 2014):

(1) NW–SE shortening due to subduction/collision from ca. 390–345 Ma led to the closure of the Rheic ocean and to a doubly-vergent orogenic wedge with a crustal thickness >50–60 km.

(2) Radial extension from ca. 345–335 Ma was associated with a significant thermal turnover, exhumation of lower crust, and elevator-style slip along the Bohemian shear zone (BSZ), which governed the foci of mantle derived plutonism for >20 m.y. A minimum throw of 10 km was accommodated between 343 and 330 Ma causing the juxtaposition of the supracrustal Tepla–Barrandian unit (the “elevator”) against the hot extruding orogenic Saxothuringian/ Moldanubian root.

(3) N–S shortening at ca. 330 Ma led to a conjugate set of mylonitic strike-slip shear zones related to the closure of the Rhenohercynian ocean and to progressive docking of the collapsing wedge with Baltica. Dextral strike-slip occurred along NW–SE trending shear zones, such as the Bavarian Lode and the Elbe shear zone. Sinistral strike-slip was active along NE–SW trending shear zones as is well documented in the Mid-German crystalline rise (Odenwald).

(4) Subsequent extension at 325–315 Ma is indicated by the opening of E–W trending granitic dikes, which are widespread in the Moldanubian domain, and by the development of steep mylonitic normal faults.

(5) NE–SW shortening at 315–300 Ma is interpreted in terms of collision of Gondwana with the Variscan belt and Laurasia.

At 300 Ma Pangea had already been formed and — apart from the Paleotethys — all oceans of the Variscan realm in Europe had been closed (Stampfli et al. 2013). Orogenic activity continued along the northern active margin of the Paleotethys, which formed an eastward-opening wedge-shaped oceanic tract inside Pangea pinching out in the Iberian realm close to a Euler pole. Accretion of the south and north Minoan terranes to the southern margin of Eurasia occurred at ca. 320 Ma and at 300 Ma, respectively (Zulauf et al. 2015). Ridge subduction might have supported the formation of the late Carboniferous/early Permian Meliata rift. A significant thermal and magmatic event occurred close to 300 Ma as is documented at several places not only in the eastern Mediterranean but also in central and western Europe.

Magmatic activity in the eastern Mediterranean ceased significantly during the Middle Permian (ca. 270 Ma) when the Cimmerian ribbon continent rifted from the northern margin of Gondwana (Stampfli et al. 2013). This rifting event produced a new lithospheric plate, which included the remaining part of the Paleotethys, the Cimmerian ribbon continent and the northern part of the Neotethys. In contrast to the southern margin of Laurasia, the rocks of the Cimmerian ribbon continent are entirely free from Variscan-aged zircons.

Opening of the Neotethys and convergent movements along the southern active margin of Laurasia led to diachronic closure of the Paleotethys, which is regarded to have taken place after the Viséan in Morocco and during Radian time in Sicily, Croatia and the Slovenian Southern Alps (Stampfli et al. 2013). Further to the east, Paleotethys was closed in Triassic times.

In the External Hellenides, revived early Triassic convergent movements along the southern active margin of Laurasia were related to magmatic activity and the formation of back-arc basins (e.g. Tyros basin). Back arc extension ceased in the Ladinian/early Carnian, when the Cimmerian ribbon terrane collided with the southern margin of Laurasia (Zulauf et al. 2018). This collision, referred to as the Eo-Cimmerian phase, was a ‘soft’ collision without major crustal thickening, as is documented from southern Europe to Thailand (Şengör

1979). In the eastern Mediterranean the closure of the Paleotethys led to a complete reorganization of the stress field. Crustal extension in the north led to subsidence of the accreted Cimmerian block resulting in the opening of small oceanic basins (e.g. Pindos ocean). Moreover, there was a striking facies change from siliciclastic rocks towards the Pantokrator-type dolomite, which is a characteristic rock of late Triassic Tethyan carbonate platforms.

It should be emphasized that the Apulian microplate was not part of the Cimmerian block since Permian times. The separation of the Apulian microplate from Gondwana is attributed to the Jurassic break-up of Pangea resulting in the opening of the Mesogean ocean, relics of which are undergoing subduction beneath the Aegean microplate still today.

## References

- Dörr W. & Zulauf G. 2010: Elevator tectonics and orogenic collapse of a Tibetan-style plateau in the European Variscides: the role of the Bohemian shear zone *Int. J. Earth Sci.* 99, 299–325; <https://doi.org/10.1007/s00531-008-0389-x>
- Dörr W. et al. 2015: A hidden Tonian basement in the eastern Mediterranean: Age constraints from U–Pb data of magmatic and detrital zircons of the External Hellenides (Crete and Peloponnesus). *Precambrian Res.* 258, 83–108; <https://doi.org/10.1016/j.precamres.2014.12.015>
- Şengör A.M.C. 1979: Mid-Mesozoic closure of Permo–Triassic Tethys and its implications. *Nature* 279, 590–593.
- Stampfli G.M., Hochard C., Verard C., Wilhem C. & von Raumer J. 2013: The formation of Pangea. *Tectonophysics* 593, 1–19
- Stampfli G.M. & Kozur H. 2006: Europe from the Variscan to the Alpine cycles. In: Gee D.G. & Stephenson R. (Eds.): European lithosphere dynamics. *Geological Society of London, Memoir* 32, 57–82.
- Žák J., Verner K., Janoušek V., Holub F.V., Kachlík V., Finger F., Hajná J., Tomek F., Vondrovic L. & Trubač J. 2014: A plate-kinematic model for the assembly of the Bohemian Massif constrained by structural relationships around granitoid plutons. In: Schulmann K. et al. (Eds.): The Variscan Orogeny: Extent, Timescale and the Formation of the European Crust. *Geol. Soc. London, Spec. Publ.* 405, 169–196.
- Zulauf G., Dörr W., Fisher-Spurlock S.C., Gerdes A., Chatzaras V. & Xypolias P. 2015: Closure of the Paleotethys in the External Hellenides: Constraints from U–Pb ages of magmatic and detrital zircons (Crete). *Gondwana Res.* 28, 642–667; <https://doi.org/10.1016/j.gr.2014.06.011>
- Zulauf G., Dörr W., Marko L. & Krahl J. 2018: The late Eo-Cimmerian evolution of the external Hellenides: constraints from microfabrics and U–Pb detrital zircon ages of Upper Triassic (meta)sediments (Crete, Greece). *Int. J. Earth. Sci.* 107, 2859–2894; <https://doi.org/10.1007/s00531-018-1632-8>

# Whole rock chemistry of the Permian Gemic specialised S-type granites (Western Carpathians) and remark to their correlation

IGOR BROSKA<sup>1</sup> and MICHAL KUBIŠ<sup>2</sup>

<sup>1</sup>Earth Science Institute, Slovak Academy of Sciences, Dúbravská cesta 9, 840 05 Bratislava, Slovakia; igor.broska@savba.sk  
<sup>2</sup>DPP Žilina s.r.o., Legionárska 8203, 010 01 Žilina, Slovakia

**Abstract:** The Permian specialised S-type granite of the Gemic Unit form small bodies of and high potassium calc-alkaline character porphyritic and equigranular granites intruding low grade Paleozoic metamorphic rocks. Magmatic fractionation in situ led to formation of rare-metal (Li, Sn, W, Nb, Ta, B, F) enriched granitic cupolas resulted in vertical chemical step differences in the granite massif. They show also north-south spatial chemical differences. Their age and main chemistry features indicate genetic connection of Gemic granites above Paleotethys subduction zone in extension regime.

## Introduction

The specialised S-type granites known in the Gemic Unit (Western Carpathians, Slovakia) are mostly (1) peraluminous porphyritic syenogranites to monzogranites and (2) fine-grained equigranular monzogranites in granite cupolas. They crop out on six areas of the Spiš–Gemer Ore Mountains (Fig. 1) and in their apexes they contain special rare-metal Li–Sn–W–Nb–Ta–B–F granite mineralization. The chemistry of these granites are distinctly different from the widespread sodic-rich Upper Devonian–Lower Carboniferous Variscan granites known in the Tatric and Veporic units of the Western Carpathians. This contribution introduces the chemistry of Gemic granites and outlines some ideas of their possible correlation and genesis based on the bulk rock composition and age.

## Bulk rock chemistry of granites

Gemic specialised S-type granites show general high contents of Si, Al, K, Na, Rb, P, B, Sn, Nb, Ta, W, F but low Ca, Mg, Sr, Ba, REE (negative Eu-anomaly), Zr and correspond to peraluminous high potassium ( $K_2O/Na_2O > 1$ ) calc-alkaline granites with ASI index  $\sim 1.2$  to 1.4. The bulk rock chemistry and the presence of accessory monazite-(Ce), annite and almandine indicate their S-type character. High primary volatile flux in these granites show high content of boron saturated on tourmaline (schorl to foitite). Boron in cupolas is in hundreds of ppm or even more than 1000 ppm. The concentration of the major and trace elements show quite wide

variability and in general, there are some vertical and spatial compositional differences between the northern and southern granite bodies.

## Vertical compositional differences

The Gemic granites show distinct vertical compositional zoning from deeper situated porphyritic biotite–(muscovite) granite to protolithionite Li–F granite and albitite in granitic cupolas. Contents of Si are relatively high in both upper and bottom parts of the granite intrusions but in contents of P, Li, Rb, Cs, Ga, Nb, Ta, Sn, W increase significantly from the bottom to the cupolas. On the contrary, Ca, Mg, Sr, Ba, Ti, Zr and REE contents decrease in this direction. Some representative rock analyses from DD-3 borehole in Dlhá Valley (Dianiška et al. 2010) are shown in Table 1.

## Horizontal compositional differences

Granite occurrences named Súľová, Delava a Peklisko in northern Hnilec area (see Fig. 1) show many compositional differences with comparison to granite bodies located more to the south demonstrating evident spatial horizontal evolutionary zoning of the granites occurrences. Granites located on south from the Hnilec area show generally higher content of  $K_2O$ ,  $TiO_2$ , and they contain more than double amount of Ba ( $\sim 140$  vs.  $\sim 60$  ppm). Moreover, the southern granite occurrences show distinctly higher Zr concentration ( $\sim 200$  ppm; the Poproč granite) which is analogous to the A-type granite suites. On the other hand, southern granites exhibit generally lower contents of P, Nb, Ta, W and Sn

(e.g., ~50 ppm vs. ~100 ppm Sn in average in the northern and southern occurrences). The chondrite normalised REE pattern from granites in Hnilec area show higher content of LREE and more flat trend on HREEs in comparison towards those southern granite occurrences (Fig. 2).

### Age interval

The Permian ages of Gemic granites (~280 to 250 Ma) were firstly reported by whole-rock Rb–Sr isochrone method (Kováč et al. 1979, 1986; Cambel et al. 1989) and by monazite U–Th–Pb microprobe dating (Finger & Broska 1999). Later their Permian age was confirmed by using zircon U–Pb MS TIMS (Poller et al. 2002),

SHRIMP (Radvanec et al. 2009) and LA-ICP-MS methods (Kubiš & Broska 2010). Kohút & Stein (2005) dated molybdenite from the vein in the Hnilec area by Re–Os isotopes and result ~260 Ma documents the same age and genetic relationship between granite formation and associated Sn–W ore mineralization. The zircon U–Pb dating results (Poller et al. 2002; Radvanec et al. 2009; Putiš et al. this volume) show two principal age intervals for magmatic crystallization of the Gemic granites: (1) ~270–280 Ma for the southern granite bodies (Zlatá Idka, Rudník and Betliar), and (2) ~250–260 Ma for the northern Hnilec area. In this sense, the solidification of Permian Gemic granites show large time interval ( $\leq 30$  Ma) from Cisuralian to Lopingian epochs and their age decreases from south to north.

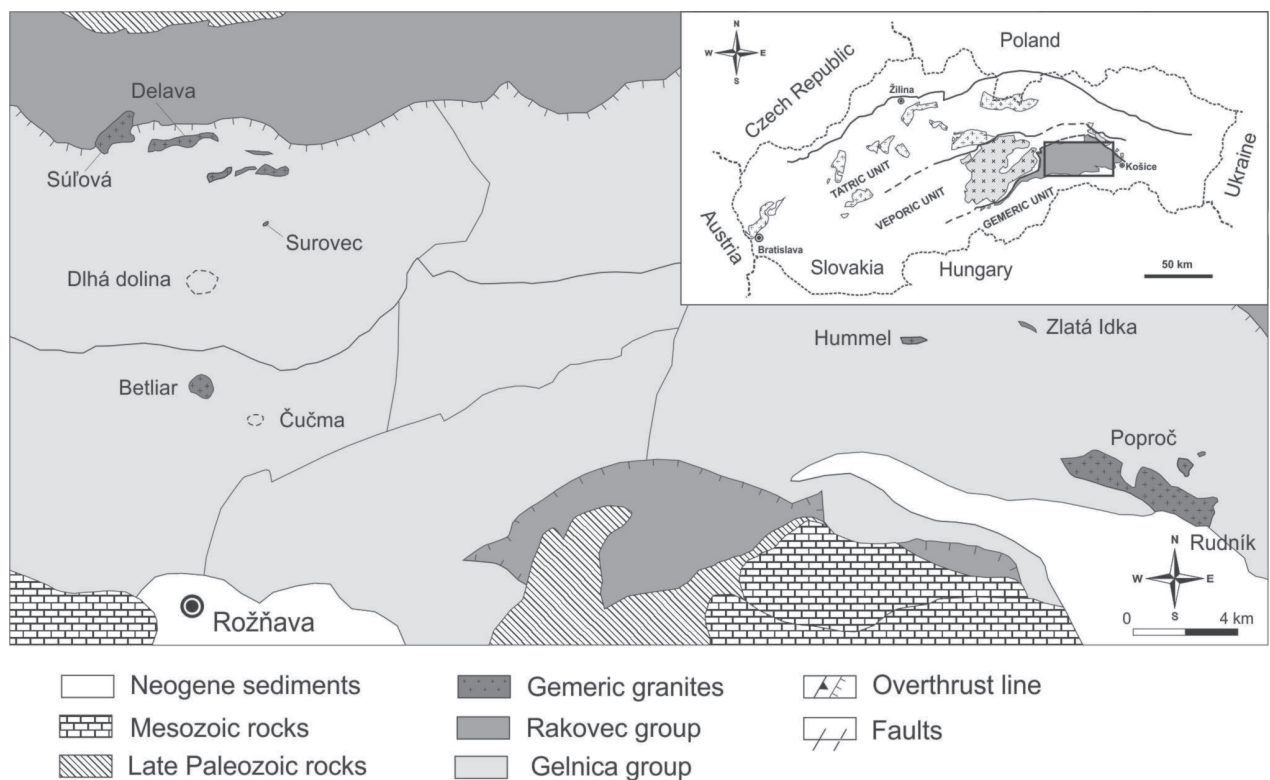


Fig. 1. Position of Gemic granites in the Gemic Unit.

Table 1: Contents of representative elements (oxides in wt. %, trace elements in ppm) from the Dlhá Valley granite. Note the differences in composition between albitite and Li–F granite in cupola and deeper porphyritic granite.

Borehole DD3	Granite type	SiO <sub>2</sub>	P <sub>2</sub> O <sub>5</sub>	Rb	Ga	Sn	Nb	Zr	Ce
DD-504	albitite	74.49	0.31	88	56	347	57	19	1
DD-577	Li–F granite	73.24	0.52	1866	43	79	66	25	3
03GA72	Li–F granite	73.91	0.40	1919	42	n.d.	48	29	2
03GA74	Porphyritic granite	76.70	0.27	650	23	n.d.	15	59	10
DD-783	Bt granite porphyr	76.42	0.16	430	22	31	12	88	32
DD-908	Ms–Bt porphyritic granite	76.72	0.12	440	21	21	9	63	21

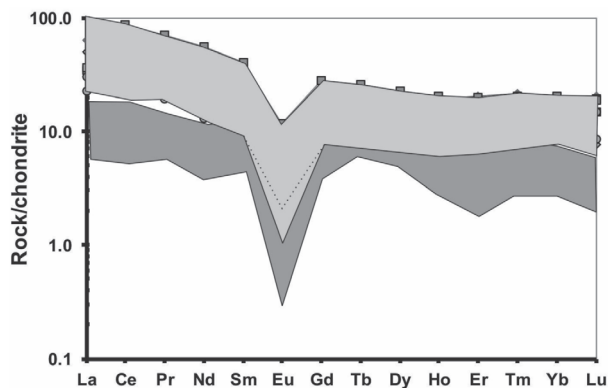


Fig. 2. Comparison of REE patterns normalised acc Evens et al. 1978) from northern (in dark) and southern (in grey) granite bodies.

### Correlation of the specialized S-type Gemicic granites

Understanding the genesis of the specialised S-type granites from Gemicic Unit is possible only by spatial correlation their analogs mainly by comparison of bulk rock chemistry, mineralogical character and reliable age data. The Permian magmatic activity resulted in Europe mainly from continuation of Paleotethys subduction and this process has been probably crucial also for the genesis also Gemicic granites although their eventual rift-related origin cannot be excluded because their age corresponds e.g. to Hronic basaltic magmatic activity connected maybe with plume activity (see Demko in this volume). But the Permian Gemicic granites are K-rich calc-alkaline and in this character resemble the granites from northern Aegean region where K-rich and calc-alkaline originated in continental arc setting recently exposed in Strandzha and Sakar Zone (Bonev et al. 2018) and probably also in the Istanbul Zone. The Permian metamorphic activity is documented in wider central European area and even in the Eastern Alps where the regional Permian prograde metamorphism at moderate pressure conditions in area of Plankogel, Saualpe-Koralpe resulted from extension and heat from ongoing Paleotethys subduction (Thöni & Miller 2009). Magmatic Permian activity connected with Paleotethys subduction is described in external Hellenides (Zulauf et al. 2015), but also in the Asia (Wang et al. 2017). The Paleotethys subduction could triggered the generation of many granite settings including probably also West-Carpathian specialised Gemicic granites. This circumstances should be discussed from different points of view in order to obtain a satisfactory opinion on the reason for such kind of

genesis. Romer & Kroner (2016) proposed genesis of Gemicic granites in similar conditions like Cornubian granites within European extensional province.

**Acknowledgements:** This research was financed by the VEGA Agency (No. 0084/17) and by project APVV-18-0107.

### References

- Bonev N., Filipov P., Raicheva R. & Moritz R. 2019: Timing and tectonic significance of Paleozoic magmatism in the Sakar unit of the Sakar–Strandzha Zone, SE Bulgaria. *International Geology Review* 61, <https://www.tandfonline.com/loi/tigr20>.
- Cambel B., Bagdasarjan G.P., Gukasjan R.C. & Veselský J. 1989: Rb–Sr geochronology of leucocratic granitoid rocks from the Spišsko–gemerské rudohorie Mts. A Veporicum. *Geologica Carpathica* 40, 323–332.
- Dianiška I., Breiter K., Broska I., Kubiš M. & Malachovský P. 2000: First phosphorus-rich Nb, Ta, Sn specialised granite from the Carpathians — Dlhá dolina valley granite pluton, Gemicic superunit, Slovakia. *Geologica Carpathica, Special Issue*, Proceeding of XVII Congress of Carpathian–Balkan Geological Association, CD-ROM.
- Finger F. & Broska I. 1999: The gemicic S-type granites in south-eastern Slovakia: Late Palaeozoic or Alpine intrusion? Evidence from electron-microprobe dating of monazite. *Schweizerische Mineralogische und Petrografische Mitteilungen* 79, 439–443.
- Kováč A., Svingor E. & Grecl P. 1979: New data about age of Gemicic granites. *Mineralia Slovaca* 11, 71–76 (in Slovak).
- Kováč A., Svingor E. & Grecl P. 1986: Rb–Sr isotopic ages of granitoids from the Spišsko–Gemerské rudohorie Mts., Western Carpathians, Eastern Slovakia. *Mineralia Slovaca* 18, 1–14.
- Kubiš M. & Broska I. 2010: The granite system near Betliar village (Gemicic Superunit, Western Carpathians): evolution of a composite silicic reservoir. *J. Geosci.* 55, 131–148.
- Poller U., Uher P., Broska I., Plašienka D. & Janák M. 2002: First Permian–Early Triassic zircon ages for tin-bearing granites from the Gemicic unit (Western Carpathians, Slovakia): connection to the post-collisional extension of the Variscan orogen and S-type granite magmatism. *Terra Nova* 14, 41–48.
- Radvanec M., Konečný P., Ondrejka M., Putiš M., Uher P. & Németh Z. 2009: The Gemicic granites as an indicator of the crustal extension above the Late-Variscan subduction zone and during the Early Alpine riftogenesis (Western Carpathians): an interpretation from the monazite and zircon ages dated by CHIME and SHRIMP methods. *Mineralia Slovaca* 41, 381–394 (in Slovak with English summary).
- Romer R.I. & Kroner U. 2016: Phanerozoic tin and tungsten mineralization — Tectonic controls on the distribution of enriched protoliths and heat sources for crustal melting. *Gondwana Res.* 31, 60–95.
- Thöni M. & Miller C. 2009: The “Permian event” in the Eastern European Alps: Sm–Nd and P–T data recorded by multistage garnet from the Plankogel unit. *Chemical Geology* 290, 20–36.
- Wang Y., Qian X., Gawood P.A., Liu H., Feng Q., Zhao G., Zhang Y., He H. & Zhang P. 2017: Closure of the East Paleotethyan Ocean and amalgamation of the Eastern Cimmerian and Southeast Asia continental fragments. *Earth-Science Reviews* <https://doi.org/10.1016/j.earscirev.2017.09.013>.
- Zulauf G., Dörr W., Fisger-Spurlock S.C., Gerdes A., Chatzaras V. & Xypolias P. 2015: Closure of the Paleotethys in the external Hellenides: Constraints from U–Pb ages of magmatic and detrital zircons (Crete). *Gondwana Research* 28, 642–667.

# The Permian basalts in Hronic Unit (the Western Carpathians): Their physical and regional variations

RASTISLAV DEMKO

State Geological Institute of Dionýz Štúr, Mlynská dolina 1, 817 04 Bratislava, Slovakia; rastislav.demko@geology.sk

**Abstract:** Presented study focused on petrogenesis of the Permian basalts in Hronic unit and their potential relationship with geodynamic analogies from continental flood basaltic provinces connected with mantle plume activity (Paraná, Columbia River, Siberian). Geochemistry of the Hronic basalts shows the special geochemical REE character with steep La/Sm enrichment and slight continual Gd–Yb fractionation. REE modeling indicates melting of fertile subcontinental lithospheric mantle Sp- and Grt-peridotite with volumetrical increase of melt production in the Upper Permian. The Permian Hronic basalts do not show a rifting style of chemistry but rather generation on the periphery of growing mantle plume. The chemical evolution of basalts shows no connections to next rifting or spreading activity and suggests a possible volcanic autonomy of the parental Hronic volcanic province.

## The Hronic Unit in the Western Carpathians and stratigraphical occurrence of basaltic rocks

The Western Carpathians crystalline basement is built by granite–metamorphic rock complexes, covered by sedimentary sequences tectonically arranged into Alpine nappe structures. The Hronic Unit is one of the most spatially extended tectonic upper Alpine nappe structure in the Western Carpathians (Fig. 1). The lithology of the Hronic Unit represents a record of volcanic and sedimentary rocks from the Upper Carboniferous to Upper

Triassic and Jurassic period. The volcanism operated in parental Hronic area forming two main volcanic phases in the Lower (LP) and the Upper Permian (UP) with massive production of basalts, basaltic andesites, basaltic trachyandesites and their pyroclastics.

## The general character of volcanics rocks

Chemistry and petrography of volcanic rocks correspond to two main differentiation trends: B–BA and B–BA–BTA, where tholeiitic basalts (B) and basaltic

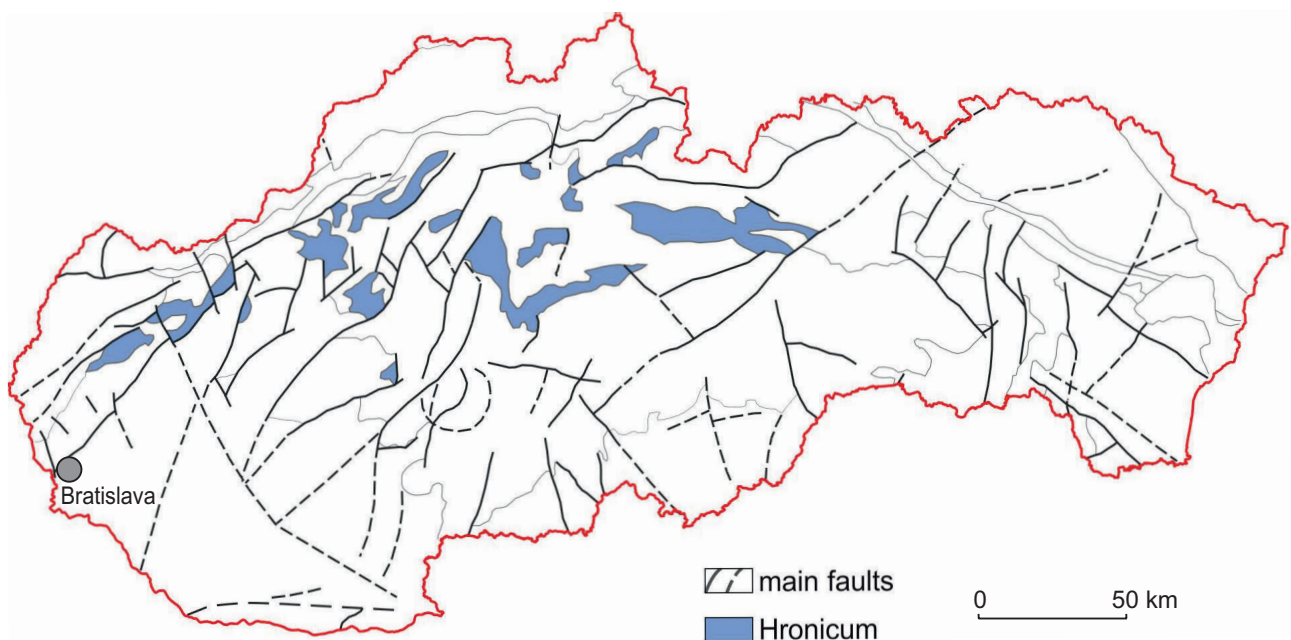


Fig. 1. Simplified tectonic scheme and distribution of the Hronic Unit in the territory of Slovakia (modified after Biely et al. 1996).

andesites (BA) together with basalts–basaltic andesites–basaltic trachyandesites (BTA) of transitional tholeiitic–alkaline series were identified, based on  $\text{SiO}_2-(\text{Na}_2\text{O}+\text{K}_2\text{O})$ .

Tholeiitic basalts and basaltic andesites in to the Upper Carboniferous and the Lower Permian sandstones form many subvolcanic bodies mainly dikes and sills. The Upper Permian basalts dominated as a lava flows and locally generated huge massive bodies as a result of synvolcanic canyon infilling.

The petrographical studies document in magmatic assemblages the presence of augite, diopside, plagioclase, Fe–Ti oxide and spinel. Volcanic glasses are transformed into chlorite, epidote, albite and carbonates. There are some important petrographical differences between the LP and UP basalts as a result of different physical conditions during magma solidification. The LP B and BA rocks have subophitic and interstitial structures formed by evolved 3D plagioclase network infilled by Cpx oikocrysts or altered glass. The UP basaltic lavas show porphyric, glomeroporphyric and vesicular textures marked by abundant plagioclases and occasionally together with amygdalites. Except the association Cpx+Pl+Ilm in magmatic assemblages, pseudomorphoses after olivine and orthopyroxene were identified.

The special feature of erupted lavas is the presence of many small plagioclase crystals as a product of low pressure fractionation in shallow level volcanic chambers, probably in subvolcanic near-surface environment. They are associated with euhedral olivine, clinopyroxenes are rare, or if Cpx is present, it is fixed to plagioclase network to create poikilitic structure. The observed petrographical relation indicates tholeiitic magma differentiation, where Ol+Pl start precipitated before Cpx.

### REE “Hronic” geochemical fingerprint

B–BA–BTA volcanic rocks from the Permian Hronic unit have a very special REE character, which could be qualified as an important petrogenetic fingerprint. The LREEs are very steep fractionated, with La/Sm and next small slight continual enrichment from Gd–Yb or Tb–Yb. Such a REE pattern is found only in several volcanic provinces, namely Siberian traps in Noril’sk area, tholeiites from Paraná volcanic province, Columbia River basalt province (the Saddle Mountains and the Grande Ronde). The identification of geochemical analogues with the same REE pattern suggests within plate

volcanic province as a similar geodynamic type of volcanism for the Hronic unit. The comparisons of basalts from similar provinces are illustrated in Fig. 2.

### The REE modeling of parental magma generation

For a better understanding of the Hronic B–BA rocks generation, numerical simulations of mantle melting has been done at dry conditions using non-modal accumulated fractional melting on fertile lherzolite with initial primordial mantle REE composition, and especially for spinel and garnet peridotites using experimentally determined peritectic melting reactions. The results of modeling are presented in Fig. 3. A characteristic REE pattern, or geochemical fingerprint, of the Hronic LP–UP basaltic rocks could be generated by mixture of melts from different peridotite Grt–Sp facies.

The parental Lower Permian magmas were formed as a mixture of 1/1.7 melts melted in 1.1 % fraction from Grt–lherzolite and 14 % melt fraction from Sp–lherzolite (in wt. %).

The parental Upper Permian magmas were formed as a mixture of 1/2.8 melts melted in 1.9 % fraction from Grt–lherzolite and 13 % melt fraction from Sp–lherzolite.

Another, but similar, petrogenetic explanation is possible by single melting in spinel peridotite facies, previously infiltrated by melts from deeper melted Grt–peridotites or melting of metasomatized mantle.

The results of modeling suggest a progressive increase of melting shifted to the Upper Permian.

### The geodynamic position of tholeiitic Hronic B–BA volcanism

The study of geodynamic position of the Hronic volcanic province during the Permian suggests within plate tholeiitic basalt volcanic province. Hronic WPTB is similar to provinces in Paraná, Columbia River and Noril’sk in Siberian area. All mentioned analogues are petrogenetically connected to mantle plume activity as a engine for volcanism. It should be noted, that the identified analogues are not homogenous with respect to REE “Hronic fingerprint”, because many rocks with different REE patterns are present there as well. In other words, Hronic basaltic rocks show not all geochemical signatures typical for WPB provinces, especially for tholeiitic basalts with  $\text{La}/\text{Ybn}=1$  or alkaline basalts with high La/Yb.

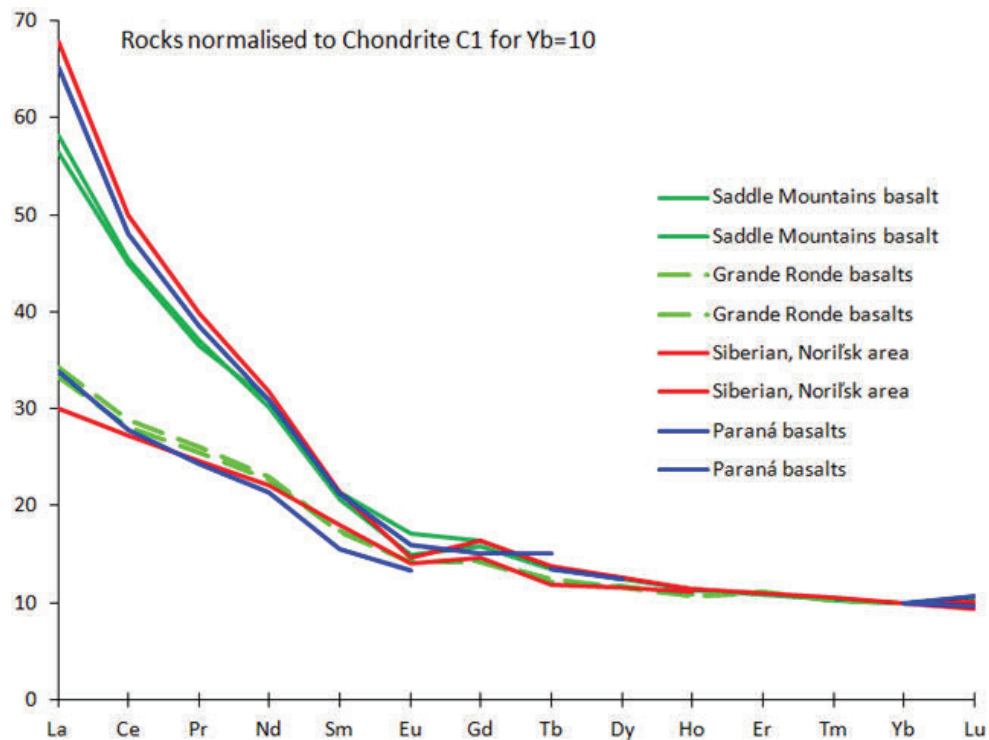


**Fig. 2.** REE of basic volcanic rocks from Siberian traps, Noril'sk area; tholeiites from Paraná volcanic province and Columbia River basalt province, especially from Grande Ronde and Saddle Mountains. REE are chondrite normalized acc. Sun & McDonough (1989) and corrected for Yb=10.

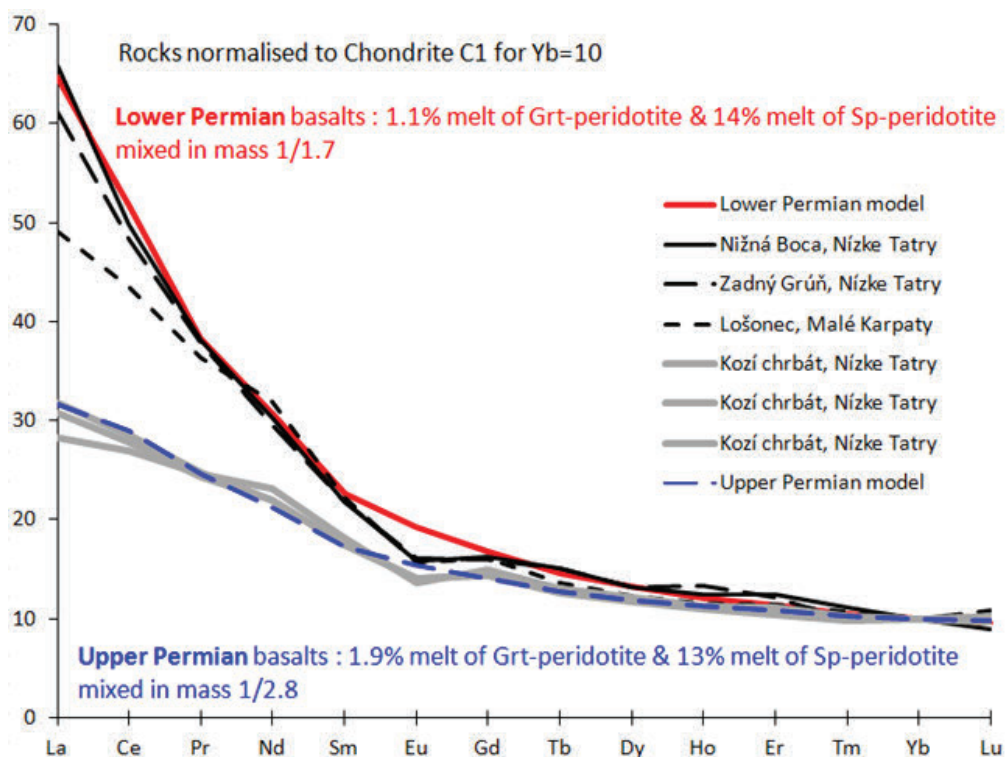


**Fig. 3.** REE in basalts intruded the Upper Carboniferous and lower Permian sandstones (localities Nižná Boca and Zadný Grúň) together with lower Permian basalt from Lošonec, Malé Karpaty mountains, and the Upper Permian basalts from Kvetnica, Lower Tatras Mountains. REE are normalized for C1 (Sun & McDonough, 1989) and Yb=10 to keep equal fractionation level. The REEs model of mantle melting is simulated special for LP and UP basalts with appropriate physical quantification which are presented in a colour. Contrasting REE patterns between LP and UP basalts.

The paleovolcanic reconstruction by Vozár (1997) suggests the rift-related basalt volcanism during the Permian period, but my efforts to find chemically analogues of volcanic rocks from continental rift systems such as the East African and the West and the Central African rifts was not successful. The idea published by Dostal et al. (2003) suggests the Basin and Range type rifting as a motor of parental volcanism also in the Hronic area. The presented results do not require such special rifting type extensional activity influenced by external tectonism. The studied Hronic rock types are simpler compared to the Basin and Range province.

The comparison of B–BA volcanic rocks from the Hronic unit with other Permian volcanic rocks from typical Permian provinces in Europe was also not successful, (for a data source see Wilson et al. 2004) and the Hronic basalts genesis seems to be more complicated.

The Permian CFB volcanic transition to active spreading seems to be a problem, because geochemistry of Hronic CFB does not support any extension increase towards spreading,  $La/Yb_{n} \leq 1$ . It indicates that Hronic area has never reached a rifting event.

Therefore it cannot be excluded that the tholeiitic CFB volcanism in the Hronic unit corresponds to peripheral

plume zone activity, where small extensional tectonics combined with ascent of thermal boundary layer in sub-continental lithospheric mantle caused melting across the Sp–Grt peridotite facies.

## References

- Biely A. (Ed.), Bezák V., Elečko M., Kaličiak M., Konečný V., Lexa J., Mello J., Nemčok J., Potfaj M., Rakús M., Vass D., Vozár J. & Vozárová, A. 1996: Geological map of Slovak republic. M=1:500 000. *Ministry of Environment, Geological Survey of the Slovak Republic, Bratislava*.
- Dostal J., Vozár J., Keppie J.D.D. & Hovorka D. 2003: Permian volcanism in the Central Western Carpathians (Slovakia): Basin-and-Range type rifting in the southern Laurussian margin. *Int. J. Earth Sci.* 92, 27–35.
- Sun S.-s. & McDonough W.F. 1989: Chemical and isotopic systematics of oceanic basalts: implications for mantle composition and processes, *Geol. Soc. London Spec. Publ.* 42, 313–345.
- Vozár J. 1997: Rift-related volcanics in the Permian of the Western Carpathians. In: Grečula P., Hovorka D. & Putiš M. (eds): Geological evolution of the Western Carpathians. *Mineralia Slovaca, Monograph Geocomplex, Bratislava, Slovakia*, 225–234.
- Wilson M., Neumann E.-R., Davies G.R., Timmerman M.J., Heeremans M. & Larsen B.T. 2004: Permo-Carboniferous magmatism and rifting in Europe. *Geol. Soc. London. Spec. Publ.* 223, 1–490.

# Geochronology of Permian–Triassic tectono–magmatic events from the Inner Western Carpathian and Austroalpine units

MARIÁN PUTIŠ<sup>1</sup>, FRIEDRICH KOLLER<sup>2</sup>, XIAN-HUA LI<sup>3</sup>, QIU-LI LI<sup>3</sup>,  
ALEXANDER LARIONOV<sup>4</sup>, PAVOL SIMAN<sup>5</sup>, MARTIN ONDREJKA<sup>1</sup>, PAVEL UHER<sup>1</sup>,  
ZOLTÁN NÉMETH<sup>6</sup>, PETER RUŽIČKA<sup>1</sup> and ONDREJ NEMEC<sup>1</sup>

<sup>1</sup>Comenius University in Bratislava, Bratislava, Slovakia; marian.putis@uniba.sk

<sup>2</sup>University of Vienna, Vienna, Austria; friedrich.koller@univie.ac.at

<sup>3</sup>Institute of Geology and Geophysics, Chinese Academy of Sciences, Beijing, China; lixh@gig.ac.cn

<sup>4</sup>A.P. Karpinsky Russian Geological Research Institute, Saint Petersburg, Russia; alexander.larionov@vsegei.ru

<sup>5</sup>Earth Science Institute, Slovak Academy of Sciences, 840 05 Bratislava, Slovakia; siman@up.upsav.sk

<sup>6</sup>State Geological Institute of Dionýz Štúr, Bratislava, Slovakia; zoltan.nemeth@geology.sk

**Abstract:** This contribution reviews published and our new geochronological data on the Permian–Triassic tectono–magmatic events determined from the researched areas of the Slovak Inner Western Carpathians (IWC) and the Austrian Austroalpine (AA) units by zircon U–Pb SIMS. Most of the dated rocks bear the signatures of the superimposed Late Jurassic and/or Cretaceous tectono–metamorphic overprinting in the greenschist (from the IWC Infratatic, Veporic and Gemic basement complexes), greenschist and blueschist (from the IWC Meliata Unit) or greenschist to eclogite facies (from the Upper AA units) conditions. The reported Permian to Middle Triassic ages constrain a global extension event focused into an equatorial zone thus roughly tracing the accretion zone of the Gondwana-derived Late Variscan basement complexes (~Early Paleozoic basement of the IWC Gemicum, Transdanubicum, Southern Alps of the Pelsó or Noric terranes) to the Early Variscan (~Early Paleozoic to Proterozoic) basement complexes of the Armorican or Galatian affinity following the Devonian Paleotethys closure and the Carboniferous to Early Permian Pangea supercontinent assembly. The Pangea break-up was accompanied by the crust–mantle lithosphere thinning, overheating, melting and formation of the Permian to Middle Triassic magmatic complexes within the rifted shelf areas developed on the thinning Variscan basement. The westward propagation of the Neotethys oceanic rift spreading and the Meliata(–Hallstatt) oceanic basin opening indicate a continuous transition of Late Permian to Early Triassic continental rifting into Middle to Late Triassic Neotethyan oceanic rifting.

## Study area and methodology

Zircon U–Pb SIMS geochronological method was used to determine the Permian and Triassic tectono–magmatic events from the Inner Western Carpathian and some Austroalpine units. We investigated these events in the northern Austroalpine–Inner Western Carpathian (AA–IWC) Block of the Cenozoic ALCAPA microplate (Neubauer et al. 1992) which is separated from the southern Pelsó Block by the Periadriatic–Rába–Hurbanovo–Diósjenő Fault (e.g. Janik et al. 2011). The IWC Orogen can be traced from the Neotethys closure-related Late Jurassic–Early Cretaceous Meliatic–Gemic–South Veporic (ME–GE–SVE) accretionary wedge in the S to the Atlantic (Alpine) Tethys closure-related Late Cretaceous–Eocene North Veporic–Tatric–Infratatic (NVE–TA–IFTA) accretionary wedge in the N (Putiš et al. 2019 and references therein).

Here we dated a gabbro–dolerite dyke crosscutting the Devonian meta–volcanics at the Harmónia village in the Tatric basement, rhyolitic (Bacúch, Závadka n.H.–Burda pass) and A-type granitic (Hrončok) rocks from

the Veporic basement and its Permian volcano–sedimentary cover successions, and A-type (Turčok) granite and specialized S-type granites from the Rudník and Zlatá Idka localities in the Gemic basement.

The GE and SVE units of the IWC can be correlated with the Upper Austroalpine (UAA) structural complexes of the Eastern Alps (sensu Schuster et al. 2004 or Schmid et al. 2004), both representing the inferred Meliata(–Hallstatt) Basin northern passive continental margin (cf. Putiš 1991). The investigated Austroalpine eclogitic complexes represent mostly the Variscan basement that underwent the Permian extension/overheating and the Cretaceous eclogite–facies metamorphism (e.g. Thöni & Jagoutz 1993; Schuster et al. 2004). Granitic orthogneisses from the UAA hanging wall Siegggraben eclogitic complex and the Grobgnais and Wiesmath type meta–granites from the LAA complex were dated in the eastern Austroalpine margin.

The SIMS dating was performed in Beijing and St. Petersburg. Measurements of U, Th, and Pb isotopes were made by Cameca IMS–1280HR SIMS at the Institute of Geology and Geophysics, Chinese Academy of Sciences

in Beijing; the complete instrument description and analytical procedure were published by Li et al. (2009). In situ U–Pb analyses of zircon from Gemic granites were performed on a SHRIMP-II in the Centre of Isotopic Research (CIR) at VSEGEI, St.-Petersburg, applying a secondary electron multiplier in peak-jumping mode following the procedure described by Williams (1998) and Larionov et al. (2004).

### Review of published geochronological data

Both the IWC wedges are quite rich in the Permian mainly calc–alkaline and less A-type acidic to basic volcanic, subvolcanic, lamprophyric or plutonic (mainly granitic) magmatic products (Kotov et al. 1996; Uher and Broska 1996; Poller et al. 2000; Putiš et al. 2000, 2016; Vozárová et al. 2009, 2012, 2015, 2016; Radvanec et al. 2009; Demko & Hraško 2013; Pelech et al. 2017; Spišiak et al. 2018; Ondrejka et al. 2018). All these rock zircon U–Pb SIMS (SHRIMP) ages fall into interval of ca. 280 to 255 Ma. Typical rift-related continental tholeiites occur only in the IWC Hronic Unit Permian succession (Vozárová & Vozár 1988) overlying the Patric and Tatric units as a rootless nappe. The Permian overheating was determined also by the EPMA monazite ages from the IWC North-Veporic Unit (Jeřábek et al. 2008).

The Neotethyan Meliata Unit mid-Triassic (Ladinian) silicites, interlayered with N-MORB, contain the youngest detrital zircon population of  $247\pm 4$  Ma from an inferred (Anisian) acidic magmatic source (Putiš et al. 2011). The Triassic overheating of the Permian Gemic granites up to the Carnian/Norian boundary (ca. 250–225 Ma) was determined by the EPMA ages of the magmatic monazite outer zones and newly-formed monazites (Radvanec et al. 2009).

A clinopyroxenite dyke crosscutting harzburgite was dated at  $252\pm 2$  Ma from the UAA Siegraben structural complex near Steinbach in Burgenland (Putiš et al. 2018). Permian U–Pb age of  $286\pm 14$  Ma as an upper intercept age was dated on zircon by conventional method from a granitic orthogneiss of the UAA Siegraben complex between the Siegraben and Schwarzenbach villages (Putiš et al. 1994, 2000, 2002a). Similar ages of ca. 275 Ma (meta-gabbro) and 260 Ma (meta-pegmatite of Platengneis type) were determined by Grt–wr isochrons plot of whole rock and mineral Sm–Nd data (Thöni and Jagoutz 1993; Thöni & Miller 2000, 2003, respectively) from the UAA eclogitic complexes of Koralm and Saualm areas in Austria. Available

Sm–Nd age data of garnet from metasediments (Wölz, Saualpe, Koralm units) are restricted to a time interval, roughly between 280 and 260 Ma (Thöni & Miller 2009).

### Results from the IWC units

Gabbro-dolerite dyke crosscutting the Devonian meta-volcanics at Harmónia village in the Malé Karpaty Mts. Tatric basement yielded an age of  $269\pm 4$  Ma (HAR-1 sample).

Rhyodacite body from the North-Veporic Permian volcano-sedimentary succession at the Bacúch village was dated at  $267\pm 2$  Ma (BAC-1 sample).

Trachy-rhyolite dyke in the Permian South-Veporic siliciclastic cover from a quarry at the Burda pass, S of the Závadka n.H. village was dated at  $267\pm 2$  Ma (BUR-1 sample) and  $266\pm 2$  Ma (BUR-1 sample retested). The Hrončok A-type granite in the Veporic Variscan basement was dated at  $267\pm 2$  Ma (HK-1 sample).

The Turčok A-type granite in the North-Gemic basement was dated at  $262\pm 4$  Ma (TU-3 sample). Specialized S-type granites from the southern part of the Gemic basement were dated in interval from ca. 280 to 270 Ma at the locality of Rudník ( $276\pm 5$  Ma sample RUD-1;  $277\pm 2$  Ma sample RUD-2;  $271\pm 4$  Ma sample RUD-3;  $269\pm 3$  Ma sample RUD-4;  $281\pm 3$  Ma sample RUD-5). Granite at the Zlatá Idka village was dated to  $265\pm 2$  Ma (sample ZLI-1).

The detrital zircon U–Pb SIMS Concordia ages of  $247\pm 4$  Ma and  $243\pm 4$  Ma from the Ladinian cherty shales of the Meliata Unit near the Jaklovce village in eastern Slovakia, and xenocryst zircon concordia age of  $266\pm 3$  Ma from a 0.5m thick N-MOR basalt layer in these cherty shales, reveal a connection of the evolving oceanic basin to adjacent rifted continental margin Permian to Early/Middle Triassic zircon magmatic sources.

Remarkable are zircon rejuvenation Permian ages found from the North-Veporic Variscan (Ordovician originally) granitic orthogneisses.

### Results from the Austroalpine units

The eclogitized continental crust fragments of the UAA Siegraben structural complex contain Permian ( $256\pm 3$  Ma, sample GS-8) gneissous granite veins between Gschorrhholz and Steinbach in Burgenland, Austria. The underlying calc-alkaline Grobgnais meta-granite was dated at  $265\pm 2$  Ma (sample GRG-1).

In contrast, characteristic Wiesmath A-type meta-granite from the LAA Wechsel complex is Ordovician (484±3 Ma, sample WTH-1 from a small quarry at the Wiesmath village). Surprising are also Triassic (246 and 240 Ma) <sup>40</sup>Ar–<sup>39</sup>Ar white mica plateau ages from a granitic-pegmatitic orthogneiss of the Hochkreuz complex (Putiš et al. 2002b) in the Kreuzeck Massif S of the High Taurus (our unpublished data) which may suggest a Permian age of these pegmatite veins.

### Discussion and conclusion

All these ages indicate a major Permian crust–mantle lithosphere extension, melting and overheating during the Pangea break-up and the Neotethys opening, thus tracing a period from the Permian–Early Triassic continental to the Middle Triassic Neotethys oceanic rifting stages.

The Gemic basement in the southern part of the IWC underwent the most intensive Permian to Early Triassic extension and overheating, connected with the formation of anorogenic specialized S- and A-type granites and volcanites above the inferred Late Paleotethys subduction-related mantle plume zone (“hot lines” in Radvanec et al. 2009 and references therein). The low-grade metamorphics of the Variscan GE basement resemble the basement complexes of the Noric terrane (Frisch & Neubauer 1989; Neubauer & von Raumer 1993) exposed in the Transdanubian Range (Pelsó), Dinarides and Southern Alps, which are however dismembered between the Adria, Alcapia (ALCAPA), Tisia and Dacia Cenozoic microplates together with the Neotethys oceanic crust remnants, including the Meliata Unit. The input of 247–243 Ma old detrital zrn into the oceanic sediments of the Meliata Unit was accompanied by the Ladinian to Carnian ocean-floor N-MORB extrusions. A contemporaneous intra-shelf magmatic activity at 242–227 Ma was reported from the Southern Alps (e.g. Mundil et al. 1996) and the Transdanubian Range (Kövéř et al. 2018; Dunkl et al. 2019) which still may belong to this major Permian–Triassic tectono-thermal-magmatic event.

**Acknowledgements:** This investigation was supported by the Slovak Research and Development Agency (contract APVV-15-0050), VEGA Agency (No. 1/0151/19), and the China Ministry of Science and Technology (2016YFE0203000) scientific grants.

### References

- Demko R. & Hraško L. 2013: Rhyolite body Gregová near the Telgárt village (Western Carpathians). *Miner. Slov.* 45, 161–174 (in Slovak with English summary).
- Dunkl I., Farics E., Józsa S., Lukács R., Haas J. & Budai T. 2019: Traces of Carnian volcanic activity in the Transdanubian Range, Hungary. *Int. J. Earth Sci.*, <https://doi.org/10.1007/s00531-019-01714-w>.
- Frisch W. & Neubauer F. 1989: Pre-Alpine terranes and tectonic zoning in the Eastern Alps. In: Dallmayer R.D. (Ed.): Terranes in the Circum-Atlantic Paleozoic orogens. *Special Paper, Geol. Soc. Am.* 230, 91–100.
- Habler G., Thöni M. & Miller C. 2007: Major and trace element chemistry and Sm–Nd age correlation of magmatic pegmatite garnet overprinted by eclogite-facies metamorphism. *Chem. Geol.* 241, 4–22.
- Janik T., Grad M., Guterch A., Vozár J., Bielik M., Vozárová A., Hegedüs E., Kovács C.A., Kovács I. & Keller G.R. 2011: Crustal structure of the Western Carpathians and Pannonian Basin: Seismic models from CELEBRATION 2000 data and geological implications. *J. Geodyn.* 52, 97–113.
- Jeřábek P., Janák M., Faryad W., Finger F. & Konečný P. 2008: Polymetamorphic evolution of pelitic schists and evidence for Permian low-pressure metamorphism in the Vepor Unit, West Carpathians. *J. Metamorph. Geol.* 26, 465–485.
- Kövéř S., Fodor L., Kovács Z., Klötzli U., Haas J., Zajzon N. & Szabó C. 2018: Late Triassic acidic volcanic clasts in different Neotethyan sedimentary mélanges: paleogeographic and geodynamic implications. *Int. J. Earth Sci.* 107, 2975–2998.
- Kotov A.B., Miko O., Putiš M., Korikovsky S.P., Salnikova E.B., Kovach V.P., Yakovleva S., Bereznaya N.G., Král J. & Krist E. 1996: U/Pb dating of zircons of postorogenic acid metavolcanics and metasubvolcanics: a record of Permian-Triassic taphrogeny of the West-Carpathian basement. *Geol. Carpath.* 47, 73–79.
- Larionov A.N., Andreichev V.A. & Gee D.G. 2004: The Vendian alkaline igneous suite of northern Timan: ion microprobe U–Pb zircon ages of gabbros and syenite. *Mem. Geol. Soc. Lond.* 30, 69–74.
- Li X.H., Liu Y., Li Q.L., Guo C.H. & Chamberlain K.R. 2009: Precise determination of Phanerozoic zircon Pb/Pb age by multi-collector SIMS without external standardization. *Geochem. Geophys. Geosyst.* 10, Q04010.
- Mundil R., Brack P., Meier M., Rieber H. & Oberli F. 1996: High resolution U–Pb dating of middle Triassic volcanoclastics: time-scale calibration and verification of tuning parameters for carbonate sedimentation. *Earth Planet. Sci. Lett.* 141, 137–151.
- Neubauer F., Müller W., Peindl P., Mozschevitz E., Wallbrecher E. & Thöni M. 1992: Evolution of lower Austroalpine units along the eastern margins of the Alps: a review. In: Neubauer F. (Ed.): ALCAPA Field Guide. *Univ. Graz*, 97–114.
- Neubauer F. & von Raumer J.F. 1993: The Alpine basement: linkage between west-European Variscides and Alpine–Mediterranean Mountain Belt. In: von Raumer J.F. & Neubauer F. (Eds.): The Pre-Mesozoic Geology in the Alps: *Springer*, Berlin, 640–663.
- Ondrejka M., Li X.-H., Vojtko R., Putiš M., Uher P. & Sobocký T. 2018: Permian A-type rhyolites of the Muráň Nappe, Inner W. Carpathians, Slovakia: in-situ zircon U–Pb SIMS ages and tectonic setting. *Geol. Carpath.* 69, 187–198.
- Pelech O., Vozárová A., Uher P., Petřík I., Plašienka D., Šarinová K. & Rodionov N. 2017: Late Permian volcanic dykes in the crystalline basement of the Považský Inovec Mts. (Western

- Carpathians): U–Th–Pb zircon SHRIMP and monazite chemical dating. *Geol. Carpath.* 68, 530–542.
- Poller U., Uher P., Broska I., Plašienka D. & Janák M. 2002: First Permian-early Triassic ages for tin-bearing granites from the Gemic unit (W. Carpathians, Slovakia): connection to the post-collisional extension of the Variscan orogen and S-type granite magmatism. *Terra Nova* 14, 41–48.
- Putiš M. 1991: Tectonic styles and Late Variscan–Alpine evolution of the Tatric-Veporic crystalline basement in the Western Carpathians. *Zentralbl. Geol. Paleont.* 1, 181–204.
- Putiš M., Korikovsky, S.P., Pushkarev, Y.A. & Zakariadze, G.S. 1994: Geology, tectonics, petrology, geochemistry and isotope dating of the Siegraben (Grobgneis and Wechsel) Unit in the Eastern Alps. Manuscript, *Geological Survey of Austria*, Vienna.
- Putiš M., Korikovsky S.P., & Pushkarev Y.D. 2000: Petrotectonics of an Austroalpine eclogite-bearing complex (Siegraben, Eastern Alps) and U–Pb dating of exhumation. *Jahrb. Geol. Bundesanst.* 142, 73–93.
- Putiš M., Korikovsky S.P., Wallbrecher E., Unzog W., Olesen N.O. & Fritz H. 2002a: Evolution of an eclogitized continental fragment in the Eastern Alps (Siegraben, Austria). *J. Struct. Geol.* 24, 339–357.
- Putiš M., Korikovsky S.P., Unzog W. & Olesen N.O. 2002b: HP rocks associated with mylonitoclases: a result of polystage overprint of the Austro-Alpine basement (Kreuzeck Massif, E. Alps). *Slovak Geol. Mag.* 8, 65–87.
- Putiš M., Radvanec M., Sergeev S., Koller F., Michálek M., Snárská B., Koppa M., Šarinová K. & Németh Z. 2011: Metamorphosed succession of cherty shales with basalt and diastrophic breccia in olistolith of the Meliatic Jurassic accretion wedge near Jaklovce (Slovakia), dated on zircon (U–Pb SIMS SHRIMP). *Miner. Slov.* 43, 1–18.
- Putiš M., Li J., Ružička P., Ling X. & Nemeč O. 2016: U/Pb SIMS zircon dating of a rhyolite intercalation in Permian siliciclastics as well as a rhyodacite dyke in micaschists (Infrataticum, W. Carpathians). *Miner. Slov.* 48, 135–144.
- Putiš M., Li X.-H., Yang Y.-H., Li Q.-L., Nemeč O., Ling X., Koller F. & Balen D. 2018: Permian pyroxenite dykes in harzburgite with signatures of the mantle, subduction channel and accretionary wedge evolution (Austroalpine Unit, Eastern Alps). *Lithos* 314–315, 165–186.
- Putiš M., Danišik M., Siman P., Nemeč O., Tomek Č. & Ružička P. 2019: Cretaceous and Eocene tectono-thermal events determined in the Inner Western Carpathians orogenic front Infrataticum. *Geol. Quarterly* 63, 2, 248–274.
- Radvanec M., Konečný P., Ondrejka M., Putiš M., Uher P. & Németh Z. 2009: The Gemic granites as an indicator of the crustal extension above the Late-Variscan subduction zone and during the Early Alpine riftogenesis (Western Carpathians): An interpretation from the monazite and zircon ages dated by CHIME and SHRIMP methods. *Miner. Slov.* 41, 381–394 (in Slovak with English summary).
- Schmid S.M., Fügenschuh B., Kissling E. & Schuster, R. 2004: Tectonic map and overall architecture of the Alpine orogen. *Eclogae Geol. Helv.* 97, 93–117.
- Schuster R., Koller F., Hoeck V., Hoinkes G. & Bousquet R. 2004: Explanatory Notes to the Map: Metamorphic Structure of the Alps, Metamorphic Evolution of the Eastern Alps. *Mitt. Öster. Miner. Ges.* 149, 175–199.
- Spišiak J., Vetráková L., Chew D., Ferenc Š., Mikuš T., Šimonová V. & Bačík P. 2018: Petrology and dating of the Permian lamprophyres from the Malá Fatra Mts. (Western Carpathians, Slovakia). *Geol. Carpath.* 69, 453–466.
- Thöni M. & Jagoutz E. 1993: Isotopic constraints for eo-Alpine high-P metamorphism in the Austroalpine nappes of the Eastern Alps: Its bearing on Alpine orogenesis. *Schweiz. Mineral. Petrogr. Mitt.* 73, 177–189.
- Thöni M. & Miller C. 2000: Permo–Triassic pegmatites in the eo-Alpine eclogite-facies Koralpe complex, Austria: age and magma source constraints from mineral chemical, Rb–Sr and Sm–Nd isotope data. *Schweiz. Mineral. Petrogr. Mitt.* 80, 169–186.
- Thöni M. & Miller C. 2003: Garnet Sm–Nd data from the Saualpe and the Koralpe (Eastern Alps, Austria): chronological and P–T constraints on the thermal and tectonic history. *J. Metamorph. Geol.* 14, 453–466.
- Thöni M. & Miller C. 2009: The “Permian event” in the Eastern European Alps: Sm–Nd and P–T data recorded by multi-stage garnet from the Plankogel unit. *Chem. Geol.* 260, 20–36.
- Uher P. & Broska I. 1996: Post-orogenic Permian granitic rocks in the Western Carpathian–Pannonian area: Geochemistry, mineralogy and evolution. *Geol. Carpath.* 47, 311–321.
- Vozárová A. & Vozár J. 1988: Late Paleozoic in West Carpathians. *D. Štúr Geol. Inst. Press*, Bratislava, 1–314.
- Vozárová A., Šmelko M. & Paderin I. 2009: Permian single crystal U–Pb zircon age of the Rožňava Formation volcanites (Southern Gemic Unit, Western Carpathians, Slovakia). *Geol. Carpath.* 60, 439–448.
- Vozárová A., Šmelko M., Paderin I. & Larionov A. 2012: Permian volcanics in the Northern Gemicum and Bôrka Nappe system: U–Pb zircon dating and the implications for geodynamic evolution (Western Carpathians, Slovakia). *Geol. Carpath.* 63, 191–200.
- Vozárová A., Presnyakov S., Šarinová K. & Šmelko M. 2015: First evidence for Permian-Triassic boundary volcanism in the Northern Gemicum: geochemistry and U–Pb zircon geochronology. *Geol. Carpath.* 66, 375–391.
- Vozárová A., Rodionov N., Vozár J., Lepekhina E. & Šarinová K. 2016: U–Pb zircon ages from Permian volcanic rocks and tonalite of the Northern Veporicum (Western Carpathians). *J. Geosci.* 61, 221–237.
- Williams I.S. 1998: U–Th–Pb geochronology by ion microprobe. In: McKissen M.A., Shanks W.C. & Ridley W.S. (Eds.): Applications of microanalytical techniques to understanding mineralizing processes. *Rev. Econ. Geol.* 7, 1–35.

# Calc–alkaline lamprophyres from the Nízke Tatry and Malá Fatra Mts.: Petrology and geochronology

JÁN SPIŠIAK<sup>1</sup>, LUCIA VETRÁKOVÁ<sup>1</sup>, DAVID CHEW<sup>2</sup>, ŠTEFAN FERENC<sup>1</sup>,  
TOMÁŠ MIKUŠ<sup>3</sup> and PAVOL SIMAN<sup>3</sup>

<sup>1</sup>Faculty of Science, Matej Bel University, Tajovského 40, 97401 Banská Bystrica; Slovakia; jan.spisiak@umb.sk

<sup>2</sup>Trinity College Dublin, University of Dublin College Green, Dublin 2, Ireland; chewd@tcd.ie

<sup>3</sup>Earth Science Institute Slovak Academy of Science, Dúbravská cesta 9, 840 05 Bratislava, Slovakia

**Abstract:** Calc–alkaline lamprophyres are known from several localities in the Malá Fatra and Nízke Tatry Mts. They form dykes of varying degree of alteration that have intruded the surrounding granitoid and gneisses. Clinopyroxenes (diopside to augite), amphiboles (kaersutitic), biotites (annite) and plagioclases are major primary minerals. The chemical composition of the lamprophyres indicates their calc–alkaline character. The differences in the chemical composition of the rocks (including Sr and Nd isotopes) probably result from the contamination of primary magma by crustal material during magma ascent. The age of the lamprophyres, based on U/Pb dating in apatite, is of  $263.4 \pm 2.6$  Ma (Malá Fatra Mts.) and  $259.0 \pm 2.8$  Ma (Nízke Tatry Mts.).

Lamprophyres are dyke rocks which differ from intrusive and effusive rocks in mineral composition, structure and, to some degree, in chemical composition. We studied lamprophyre rocks from the Nízke Tatry and Malá Fatra Mountains which occur in the Early Palaeozoic complexes. The lamprophyres from the Nízke Tatry are found in different types of gneisses and those from the Malá Fatra in granodiorites. They are porphyritic dark green rocks with fine-grained to aphanitic matrix. The bodies have a dyke like shape and are mostly several meters thick (in the locality of Jarabá, their thickness is about 25 meters). We focused on the youngest types of rocks with preserved primary structure and minerals in this study. As for mineral composition, they are made from primary (mafic and felsic), secondary and opaque minerals. The Malá Fatra lamprophyres often contain also xenoliths of ambient rocks. The most common mafic minerals occurring in the rocks are clinopyroxenes, amphiboles and biotites. From felsic minerals there are quartz and silica. Based on IUGS classification (Le Maitre et al. 2002; Ondrejka et al. 2015), we classify the studied rocks from both mountains as spessartite or kersantite. The clinopyroxenes correspond to diopside, and/or augite. The amphiboles are quite strongly altered and correspond to Ca-amphibole, tremolite (Hawthorne et al. 2012). We also found kaersutite in Malá Fatra lamprophyres. The biotites are characteristic for high  $\text{TiO}_2$  content, which proves their magmatic origin. Based on Abdel-Rahmana classification (1993), they correspond to amphibole from calc-alkaline rocks. The prevailing felsic minerals are plagioclase, and K-feldspar. The basicity of plagioclases ranges from labradorite to albite.

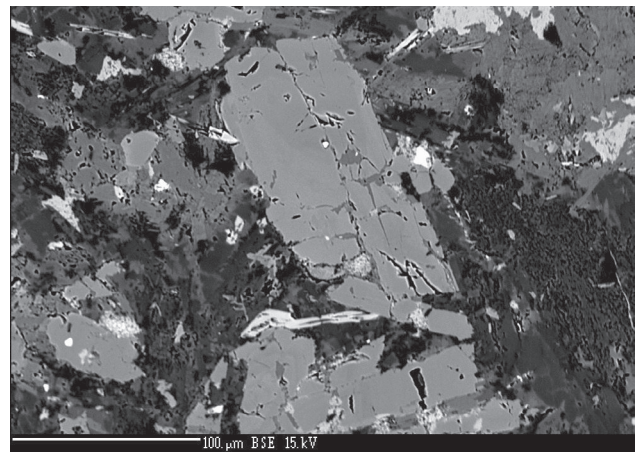


**Fig. 1.** Back scattered electron (BSE) images of lamprophyre texture. Locality: Dubná skala.

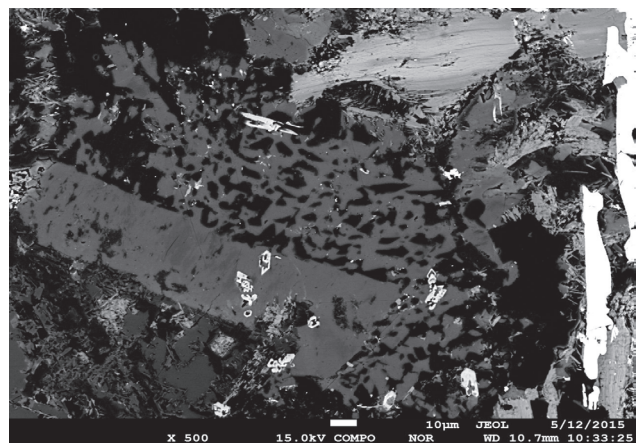


**Fig. 2.** Back scattered electron (BSE) images of lamprophyre texture. Overgrowth of quartz and K-feldspar. Locality: Jarabá.

In addition to different proportions of sodium ( $\text{Na}_2\text{O}$  content up to 3.72 wt. %), alkaline feldspars often have also increased contents of Ba. In some cases ( $\text{BaO}=5.57$  wt. %) we can already speak of barium feldspar. The secondary minerals include chlorite, epidote and carbonates. From opaque minerals, the most common are ilmenite, rutile, pyrite, chalcopyrite, pyrrhotite, while the sulphides are younger than the oxides.

The chemical composition of the lamprophyres from the Nízke Tatry Mts. and Malá Fatra Mts. can be used to reveal their genetic conditions, although it is strongly affected by the alteration of these rocks and amygdalae and xenoliths of the surrounding granitoid rocks (or plagioclases) presence. In the classification diagram of different types of lamprophyre rocks (Rock 1987), the studied lamprophyres correspond to the calc-alkaline type. The contents of compatible elements (Cr, Ni, Co, V, Sc) in the studied lamprophyres are lower (Cr, Ni). We also used discrimination diagrams to classify the studied rocks with different types of magmatic formations — in most diagrams they correspond to calc-alkaline types. The normalized REE curve indicates enrichment in LREE relative to HREE. No Eu-anomaly was observed and therefore, no accumulation or plagioclase fractionation during magma evolution is likely.

The determined age of the rocks using LA-ICP-MS by apatite analysis of  $263.4\pm 2.6$  Ma (Malá Fatra Mts.) and

$259.0\pm 2.8$  Ma (Nízke Tatry Mts.) corresponds to their geological position (Spišiak et al. 2018, 2019).

**Acknowledgements:** This research was supported by grants VEGA 1/0237/18 and APVV 15-0050.

## References

- Abdel-Rahman A.M. 1993: Nature of biotites from alkaline, calc-alkaline, and peraluminous magmas. *J. Petrol.* 35, 525–541.
- Le Maitre R.W., Streckeisen A., Zanettin B., Le Bas M.J., Bonin B., Bateman P., Bellieni G., Dudek A., Efremova S., Keller J., Lameyre J., Sabine P.A., Schmidt R., Sorensen H. & Wolley A.R. 2002: Igneous rocks a classification and Glossary of Terms. Recommendations of the International Union of Geological Sciences. Subcommission on the Systematics of Igneous Rocks. *Cambridge University Press*, 1–236.
- Ondrejka M., Huraiová M., Petrik I., Kohút M., Spišiak J., Šarinová K., Konečný V. & Vančová I. 2015: Klasifikácia a nomenklatura magmatických hornín. *Miner. Slov.* 47, 97–112.
- Rock N.M.S. 1987: The nature and origin of lamprophyres an overview. In: Fitton J.G. & Upton B.G.J. (Eds): Alkaline Igneous Rocks. *Geol.Soc. Spec. Publ.* 30, 191–226.
- Spišiak J., Vetráková L., Chew D., Ferenc Š., Mikuš T., Šimonová V. & Bačík M. 2018: Petrology and dating of the Permian lamprophyres from the Malá Fatra Mts. (Western Carpathians, Slovakia). *Geologica Carpathica* 69, 5, 453–466.
- Spišiak J., Vetráková L., Mikuš T., Chew D., Ferenc Š., Mikuš T., Šimonová V. & Šiman P. 2019: Mineralogy and geochronology of calc-alkaline lamprophyres from the Nízke Tatry Mts. Crystalline complex (Western Carpathians). *Mineralia Slovaca* 51, 1, 61–78.

**Theme 4:**

Stratigraphy, sedimentology, and paleobiology  
of the Tethyan and Paratethyan realms

# An imprint of the middle Miocene paleoceanologic and paleoclimatic events in a satellite sea during the Langhian: A case study from the Central Paratethys

KATARÍNA HOLCOVÁ<sup>1</sup>, FILIP SCHEINER<sup>1,3</sup>, NELA DOLÁKOVÁ<sup>2</sup>,  
SLAVOMÍR NEHYBA<sup>2</sup>, JITKA KOPECKÁ<sup>4</sup>, ROSTISLAV BRZOBOHATÝ<sup>2</sup>,  
ATILLA DEMENY<sup>8</sup>, ŠÁRKA HLADILOVÁ<sup>4</sup>, JURAJ HRABOVSKÝ<sup>6</sup>,  
HENNING KUHNERT<sup>7</sup>, RASTISLAV MILOVSKÝ<sup>5</sup>, JANA RIGOVÁ<sup>5</sup>,  
MICHAL SEKO<sup>5</sup> and TORSTEN UTESCHER<sup>9</sup>

<sup>1</sup>Institute of Geology and Palaeontology, Charles University, Albertov 6, 128 43 Praha 2, Czech Republic; holcova@natur.cuni.cz

<sup>2</sup>Institute of Geological Sciences, Masaryk University, Faculty of Sciences, Kotlářská 2, 611 37 Brno, Czech Republic

<sup>3</sup>Institute of Geology of the Czech Academy of Sciences, Rozvojová 269, 165 00 Praha 6 Lysolaje, Czech Republic

<sup>4</sup>Palacký University, Department of Biology, Faculty of Education, Purkrabská 2, 779 00 Olomouc, Czech Republic

<sup>5</sup>Earth Science Institute of the Slovak Academy of Sciences, Ďumbierska 1, 974 11 Banská Bystrica, Slovakia

<sup>6</sup>Earth Sciences Institute of the Slovak Academy of Sciences, Dúbravská cesta 9, 840 05 Bratislava, Slovakia

<sup>7</sup>MARUM — Zentrum für Marine Umweltwissenschaften, Universität Bremen, Leobener Straße 8, 28359 Bremen, Germany

<sup>8</sup>Institute for Geochemical Research, Hungarian Academy of Sciences, Budaorsi ut 45, H-1112 Budapest, Hungary

<sup>9</sup>Geological Institute, Nußallee 8, D-53115 Bonn, Germany

**Abstract:** The Langhian Central Paratethys sea represents a unique marine environment influenced by many factors as global climatic events, the middle Langhian closure of the Indian-Mediterranean Gateway and the local tectonic events. The multiproxy paleontological and geochemical data confirmed an anti-estuarine circulation regime as the basic circulation pattern during the Langhian. This is supported by a similarity in hydrography of surficial waters (surface mixed layer) between the Paratethys and the Mediterranean Sea which is even more apparent in the upper Langhian. It evokes gradually increased inflow of warm surface water to the Paratethys which might increase terrestrial temperatures. This could explain the delayed onset of cooling after the Middle Miocene Climatic Optimum in the study area. The significant differences between the Burdigalian and Langhian terrestrial climate were recorded only in seasonality of precipitation what might suggest establishment of the monsoon-like climate due to e.g. formation of the Carpathian mountain ridge. Nevertheless, the isotopic data comparison revealed differences regarding the bottom waters, pointing to an existence of the Paratethyan bottom waters especially during the lower Langhian. In the upper Langhian, specificity of this water decreased. We explain this fact by regional shallowing which restricted formation of the Paratethyan bottom water and enabled their substitution by a derivative originating from the intensive inflowing of the Mediterranean surficial waters. This shallowing can be correlated with global Ser-1 sea-level fall. In the study area, the sea-level fall is accompanying by occurrence of euryhaline assemblages what evokes its possible correlation with the Wieliczian Salinity Crisis. The cyclical changes triggered by Milankovitch processes are clearly pronounced in both marine and terrestrial biotops. In marine realm, the cyclical changes reflected variation in intensity of primary productivity which might be connected with cyclical changes of intensity of water masses circulation.

## Introduction

The Langhian epicontinental sea — the Central Paratethys — represents a dynamic environment experiencing many changes influenced by global, regional and local events.

The global changes are represented by the Middle Miocene Climatic Optimum (MMCO) peaking at 15 Ma and followed by cooling with peak at 13.8 Ma (Mi-3b event). This cooling regionally interacted with the middle Langhian closure of the Indian–Mediterranean Gateway which caused a transition from

an estuarine to an anti-estuarine circulation regime in the proto-Mediterranean Sea (Kouwenhoven & van der Zwaan 2006). The opening, depth evolution and closing of marine gateways played a crucial role in the heat, salt and nutrient transport between oceans and marine basins. However, the process is not frequently studied in a chain of epicontinental basins of the Paratethys type which were connected to each other by several different gateways (e.g. Karami et al. 2011).

The interaction of global climatic cooling and sea-level drop at 13.8 Ma with regional paleoceanographic evolution triggered by closure of the Indian–Mediterranean

Gateway formed conditions leading to the Badenian (or Wieliczian) Salinity Crisis (the BSC) in the Central Paratethys (de Leeuw et al. 2010). The BSC is usually considered to be the local Central Paratethys event. However, the evaporites appeared in the comparable time interval e.g. in the SE Mediterranean (Egypt; Ied et al. 2011).

Moreover, the global and regional processes could interact with the local tectonic events during Langhian (the Styrian tectonic phase; Rögl 1998). The tectonic activity might influence the land orography and subsequently atmospheric circulation causing e.g. irregular distribution of rainfalls. (Kováč et al. 2017).

The aim of this work is detailed interpretation of the Langhian paleoenvironment in the Western Carpathian segment of the Central Paratethys and identification of local and global factors which led to establishment of this paleoenvironment.

## Material and methods

We have synthesized previously published multiproxy data from the following cores located in the Moravian segment of the Carpathian Foredeep in the Czech Republic: RY-1 (GPS location: 49°16'27.2" N and 17°04'24.8" E; Kopecká 2012); ZIDL-1 and ZIDL-2 (GPS locations: 49°02'29.9" N and 16°37'19.1" E; 49°02'29.8" N and 16°37'22.8" E, respectively; Doláková et al. 2014); OV-1 (GPS location: 49°06'49.2" N and 16°20'14.2" E; Nehyba et al. 2016); BRUS-1 (GPS location: 49°32'23.8" N 17°01'36.5"; E Kopecká et al. 2018), LOM-1 (GPS location: 49°23'56.7" N and 16°24'32.5" E; Holcová et al. 2015; Scheiner et al. 2018). We also supplemented with newly obtained datasets from the core ŠO-1 (SE part of the Danube Basin; Holcová et al. 2019).

The following datasets were used for paleoceanological interpretations: (i) Paleobiological proxies: composition of calcareous nannoplankton, foraminiferal and mollusc assemblages, palynomorphs, in some sections also otoliths, bryozoa, Ostracoda, dinoflagellates and brachiopods. (ii) Sedimentological proxies: lithofacial analysis, the gamma-ray spectra, in some profiles also analysis of heavy mineral associations. (iii) Geochemical proxies: Carbon and oxygen isotopic values as well as Mg/Ca-ratio using various foraminiferal taxa characterizing different positions within the water column: (1) *Globigerina bulloides*: sub-surficial waters during periods of an enhanced productivity; (2) *Globigerinoides trilobus*: surficial stratified waters during summer

seasons with possible salinity and temperature oscillations; (3) epifaunal *Cibicidoides* spp.: bottom waters; (4) infaunal *Melonis pompiloides*: pore waters. We used the  $\delta^{13}\text{C}_{\text{org}}$ , TOC/TIC and the n-alkane based indices to estimate the production rate and to determine the origin of the organic matter.

## Stratigraphical correlation

The following biostratigraphical events were used for correlation: (1) *Orbulina suturalis* occurs in the whole core sections, i.e. the studied sequences is younger than 14.6 Ma (=the First Occurrence of *Orbulina suturalis* in the Mediterranean; (2) The last common occurrence (LCO) of *Helicosphaera waltrants* is dated at 14.357 Ma in the Mediterranean area; in the Central Paratethys might be slightly older than in the Mediterranean — estimated at 14.38–14.39 Ma. The event was recorded in the majority of studied sections. (3) *Sphenolithus heteromorphus* was recorded in the whole thickness of the cores. Its Last Occurrence in the Mediterranean was dated at ~13.4 Ma which indicates that the top core sediments must be older than 13.4 Ma.

## Paleotemperatures, paleosalinity and precipitation

The Mg/Ca derived temperature ranges of the surface and bottom waters turned out to be comparable with modern subtropical regions what agree with paleontological interpretation (otoliths). However, no cooling trend was recorded in the time interval 14.45–14.35 Ma as was expected at this period following the Middle Miocene Climatic Optimum. However, decreased bottom sea-water temperatures is estimated for the E part of the Danube basin (ŠO-1 core; 14.6–13.4 Ma) from gradually increased  $\delta^{16}\text{O}$ . On the other hand,  $\delta^{16}\text{O}$  is problematic paleotemperature proxy in the epicontinental sea, and increased  $\delta^{16}\text{O}$  values might indicate also salinity changes. Increased salinity in the upper Langhian is expected from occurrence of euryhaline benthic foraminifera as well as from hypersaline dinoflagellates.

The land temperatures (mean annual temperatures, the coldest and the warmest month temperatures) also agree with subtropical climatic belt and they persisted at the same level from the uppermost Burdigalian (Karpatian). The significant differences were recorded in seasonality of precipitation what suggests

monsoon-like climate due to e.g. formation of the Carpathian mountain ridge.

### Paleodepth

Estimation of the maximum paleodepth is very problematic and has not been reliably resolved. While varied biotops of the photic zone (sea-grass meadows, algal bioherms, wave influenced sandy sea-floor...) can be recognized from benthic foraminifera and mollusc assemblages with high certainty, the depocentre paleodepths could be estimated only tentatively. The depocentre paleodepth was interpreted from otoliths, ostracods and Mg/Ca derived temperature of the surface and bottom waters. Depths between 200–300 m is estimated from otoliths, though also deeper conditions cannot be excluded (to 500 m). Ostracods indicate maximal paleodepth around 200–300 m. The Mg/Ca derived temperature showed water thermal gradient  $\sim 7^\circ\text{C}$  between 100 m (*G. bulloides*) and sea-floor (*Cibicidoides* spp.) and  $\sim 8^\circ\text{C}$  between 50 m (*G. trilobus*) and sea-floor. Though thermal gradient strongly depends on circulation patterns, these differences do not contradict the paleontological interpretation of paleodepth.

Though paleobathymetric interpretation of maximum paleodepth is problematic, the sea-level fall correlable with the pronounced global Ser 1 event can be reliably detected in studied sections. The sea-level fall is connected with occurrence of euryhaline markers between planktic as well as shallow-water protists corroborates correlation with the onset of the Wieliczian salinity crisis near the Langhian/Serravallian boundary.

### Cyclical oscillations of paleoenvironmental proxies, nutrients

The cyclostratigraphic analysis based on paleobiological and geochemical proxies in the Langhian of the Vienna Basin was published by Hohenegger et al. 2009. Identified cycles were correlated with cyclical variation in the solar radiation (Milankovitch processes). The cyclical changes of comparable length are very characteristics also for our sections. The cyclicity is the most pronounce in relative abundances of *Globigerinoides* spp., *Globigerina bulloides* and high-nutrient benthic markers what suggests cyclical changes in quantity and/or quality of nutrients. In the central part of basin, the primary

productivity was based on intrabasinal sources (phytoplankton bloom), locally in marginal part of basin also a phytodetritus input may play a role (cyclical bloom of small-sized *Epistominella*). But decisive role of intrabasinal primary production in marine nutrient webs evokes the hypothesis about solar-radiation triggered cyclical changes of intensity of primary productivity which might be connected with cyclical changes of intensity of water masses circulation. It could include the oscillation of intensity of coastal seasonal upwelling suggested e.g. for the eastern coast of the Carpathian Foredeep.

Moreover, the cyclical changes in palynomorph assemblages indicate that solar radiation triggered also cyclical evolution in composition of terrestrial plants.

### Circulation patterns

The comparison of the isotopic and the paleobiological data suggests that an anti-estuarine circulation regime was the prevailing circulation pattern during the studied interval (Fig. 1). The initiation of this circulation regime might be indicated by the Pteropoda event (14.2–14.5 Ma) because the anti-estuarine circulation allowed and simplified migration of planktic organisms to the Central Paratethys. The Paratethyan surficial waters show a high degree of similarity with the Mediterranean during this time interval, which is even more apparent in the upper Langhian.

During the interval with the presence of *Helicosphaera waltrans* ( $\sim 14.6$ – $14.4$  Ma) the Paratethyan bottom waters differed from the Mediterranean ones at the same depth. We assume that the Paratethys probably had its own bottom waters of a regional provenance, which had a different temperature/salinity than the Mediterranean ones at the same depth.

We suggest that the change in the chemistry of the Paratethyan bottom waters in the following time interval ( $\sim 14.4$ – $13.9$  Ma) could be caused by a restriction or isolation of their source area, thus not enabling their formation. It could be due to the shallowing of the basin as indicated by the paleobiological data. The bottom waters were probably not fully evolved or substituted by a derivative originating from the intensive inflowing of the Mediterranean surficial waters during this time interval.

**Acknowledgements:** The study was supported by the projects PROGRES Q45 and by the Center for Geosphere Dynamics (UNCE/SCI/006).

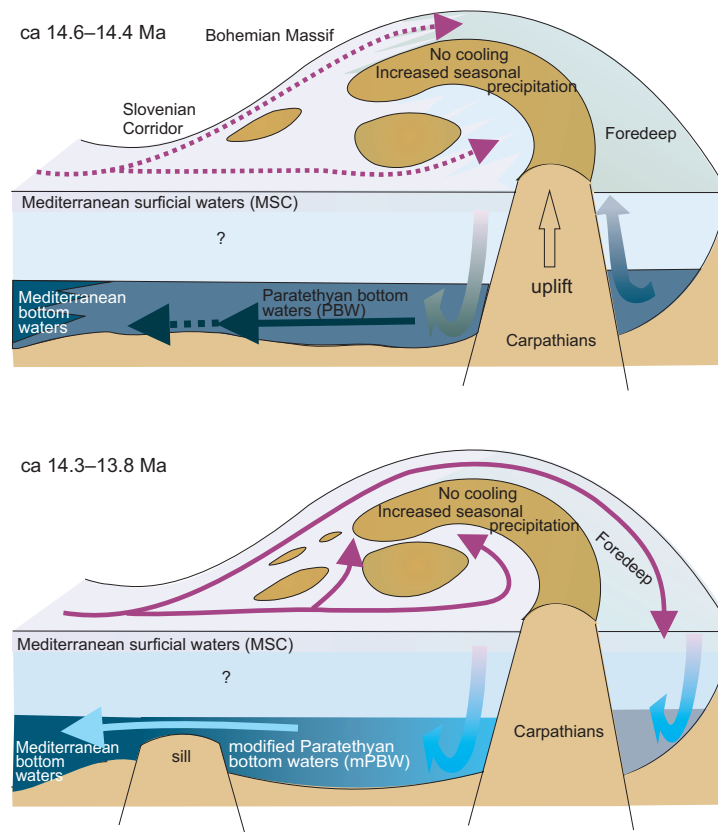


Fig. 1. Simplified model of the Langhian circulation patterns (modified after Holcová et al. 2019).

## References

- de Leeuw A., Bukowski K., Krijgsman W. & Kuiper K.F. 2010: Age of the Badenian salinity crisis; impact of Miocene climate variability on the circum-Mediterranean region. *Geology* 38, 715–718.
- Doláková N., Holcová K., Nehyba S., Hladilová Š., Brzobohatý R., Zágorský K., Hrabovský J., Seko M. & Utescher T. 2014: The Badenian parastratotype at Židlochovice from the perspective of the multiproxy study. *Neues Jb. Geol. Paläontol. Abh.* 271, 169–201.
- Hohenegger J., Čorić S., Khatun M., Pervesler P., Rögl F., Rupp C., Selge A., Uchman A. & Wagreich M. 2009: Cyclostratigraphic dating in the Lower Badenian (Middle Miocene) of the Vienna Basin (Austria) — the Baden-Soos core. *Int. J. Earth Sci.* 98, 915–930.
- Holcová K., Brzobohatý R., Kopecká J. & Nehyba S. 2015: Reconstruction of the unusual Middle Miocene (Badenian) palaeoenvironment of the Carpathian Foredeep (Lomnice/Tisnov denudational relict, Czech Republic). *Geol. Quarterly* 59, 654–678.
- Holcová K., Kopecká J. & Scheiner F. 2019: An imprint of the Mediterranean middle Miocene circulation pattern in a satellite sea during the Langhian: a case study from the 710 Carpathian Foredeep (Central Paratethys). *Palaeogeogr., Palaeoclim., Palaeoecol.* 514, 336–348.
- Ied I.M., Holcová K. & Abd-Elshafy E. 2011: Biostratigraphy and paleoecology of the Burdigalian–Serravallian sediments in Wadi Sudr (Gulf of Suez, Egypt): comparison with the Central Paratethys evolution. *Geol. Carpath.* 62, 3, 233–249.
- Karami M., De Leeuw A., Krijgsman W., Meijer P. T. & Wortel M. 2011: The role of gateways in the evolution of temperature and salinity of semi-enclosed basins: An oceanic box model for the Miocene Mediterranean Sea and Paratethys. *Global Planet. Change* 79, 73–78.
- Kopecká J. 2012: Foraminifera as environmental proxies of the Middle Miocene (Early Badenian) sediments of the Central Depression (Central Paratethys, Moravian part of the Carpathian Foredeep). *Bull. Geosci.* 87, 431–442.
- Kopecká J., Holcová K., Nehyba S., Hladilová Š., Brzobohatý R. & Bitner M.A. 2018: The earliest Badenian *Planostegina* bloom deposit: reflection of an unusual environment in the westernmost Carpathian Foredeep (Czech Republic). *Geol. Quarterly* 62, 1, 18–37.
- Kouwenhoven T.J. & Van der Zwaan G.J. 2006: A reconstruction of late Miocene Mediterranean circulation patterns using benthic foraminifera. *Palaeogeogr. Palaeoclimatol. Palaeoecol.* 238, 1–4, 373–385.
- Kováč M., Hudáčková N., Halásová E., Kováčová M., Holcová K., Oszczytko-Clowes M., Báldi K., Less G., Nagymarosy A., Ruman A., Klučiar T. & Jamrich M. 2017: The Central Paratethys palaeoceanography: a water circulation model based on microfossil proxies, climate, and changes of depositional environment. *Acta Geol. Slovaca* 9, 75–114.
- Nehyba S., Holcová K., Gedl P. & Doláková N. 2016: The Lower Badenian transgressive-regressive cycles — a case study from Oslavany (Carpathian Foredeep, Czech Republic). *Neues Jahrb. Geol. Paläontol.* 279, 209–238.
- Scheiner F., Holcová K., Milovský R. & Kuhner H. 2018: Temperature and isotopic composition of seawater in the epicontinental sea (Central Paratethys) during the Middle Miocene Climate Transition based on Mg/Ca,  $\delta^{18}\text{O}$  and  $\delta^{13}\text{C}$  from foraminiferal tests. *Palaeogeogr. Palaeoclimatol. Palaeoecol.* 495, 60–71.

# Implication of the global and regional tectonics and eustasy on the Central Paratethys paleogeography: Reflection in the regional and standard time scale correlation

MICHAL KOVÁČ & THE NEOGENE TIGERS\*



\*EVA HALÁSOVÁ, JOZEF HÓK, KATARÍNA HOLCOVÁ, NATÁLIA HUDÁČKOVÁ, MATÚŠ HYŽNÝ, MICHAL JAMRICH, PETER JONIAK, MARIANNA KOVÁČOVÁ, ANDREJ RUMAN, SAMUEL RYBÁR, MARTIN SABOL, KATARÍNA ŠARINOVÁ, MICHAL ŠUJAN, RASTISLAV VOJTKO, TAMÁS CSIBRI, PETER KISS, PETRONELA NOVÁKOVÁ, IVICA PAVIČIĆ, LENKA ŠAMAJOVÁ and TOMÁŠ VLČEK

Department of Geology and Paleontology, Faculty of Natural Sciences, Comenius University in Bratislava, Mlynská dolina, Ilkovičova 6, 842 15 Bratislava, Slovakia; kovacm@uniba.sk

**Abstract:** Paleogeography of the Central Paratethys (CP) realm was strongly influenced by the global and regional tectonics and eustasy. Over the past decades these attributes were not sufficiently taken into account what led to misconceptions in CP regional time-scale evaluation. The CP stage boundaries need to be dated by biostratigraphic approaches validated by point-based geochronological data. It would be beneficial to revise the CP time-scale in respect to geodynamics of the orogenic systems. The role of gateways between the Central Paratethys, the Mediterranean, and the Eastern Paratethys should be considered both as a function of local tectonics and the global sea-level changes. To understand original layout of sedimentary basins during distinct time spans an improved paleogeographic–palinspastic model based on an interdisciplinary study is needed in the future.

## The Central Paratethys

The Cenozoic convergence between the African and European plate led to geodynamic processes causing extreme changes in paleogeography, such as uplift of the Alpine type mountain chains and subsidence of the Paratethys basin systems. The Paratethys sea spread from the foreland of the Alps, towards the Carpathians, Dinarides, Balkan, Pannonian domains, and regions of present Black and Caspian Seas on the east. Connections between the Western, Central and Eastern segments of the Paratethys, as well as between its individual depocentres were very unstable. The marine straits/gateways developed and were destroyed depending on tectonics and climate.

## Geochronological data

Depositional sequences originating in semi-enclosed basins, partly or completely isolated from the open ocean, and frequently with endemic biota, do not allow accurate biostratigraphic correlations with the standard geological time-scale (GTS). Exact definition of correlation levels between the Mediterranean, Central

Paratethys, and Eastern Paratethys should be based both on biostratigraphy and geochronological dating. The increase in spatial and temporal coverage of geochronological data is therefore an essential task. In broad-scale paleogeographic analyses requiring correlation of the CP with the Mediterranean, the standard GTS should be used as a reference to avoid problems with the definition of regional stages.

## Eustasy and regional sea-level curve

The Central Paratethys regional time scales often comprise correlation with the global sea-level curve, and the stage boundaries are correlated with boundaries of the 3<sup>rd</sup> order sequence stratigraphy cycles of GTS (Haq et al. 1988; Hardenbol et al. 1998; Piller et al. 2007). However, the research carried out in semi-enclosed basins has shown that the global sea-level change is captured by the sedimentary record only to some degree (Kováč et al. 2018 and references therein). The active tectonics and/or a huge amount of sediment input can intensify, reduce, or completely hide the signal of the global sea-level changes (forced vs. normal regression). In addition, the 3<sup>rd</sup> order sequence stratigraphy cycles

recorded in the CP respond not only to the effects of the Mediterranean, but also to the Eastern Paratethys water masses (Kováč et al. 2017a).

The global trends of the climate changes were found to be obscured by tectonics and by local precipitation patterns, both resulting in the deposition of often coeval coal seams and evaporites in various parts of the CP realm. Nevertheless, dated “disoxic” and “evaporate” events can be used as time correlation levels during the Burdigalian, Langhian/Serravallian boundary, and Early Serravallian time intervals.

The differences between the Mediterranean and Eastern Paratethys sea-level curves indicate that the 3<sup>rd</sup> order sea-level cycles in the CP need to be further validated and the climate evolution should be better resolved.

### Geodynamics and paleogeography

The paleogeographic maps reveal a significant impact of geodynamic processes on the ratio of water covered and continental areas (Kováč et al. 2017b; Sant et al. 2017 and references therein). Similarly, the regional tectonic activity controlled the origin of straits/gateways allowing circulation of water masses between different basin systems. Present-day anti-estuarine and estuarine water exchange regime between the Atlantic, Mediterranean and Black Sea can be used as an example. The sequences deposited during circulation regimes suitably influencing the plankton migration are a prerequisite of a correct correlation between the regional CP and standard Mediterranean biostratigraphic zonations (Fig. 1). Encouraging results were obtained from periods with an anti-estuarine circulation regime, while estuarine circulation led to inaccuracies, or abrupt changes of environment leading to extinction events (Kováč et al. 2017a and references therein).

### Anti-estuarine vs. estuarine water circulation regime

In the early Burdigalian (Eggenburgian–Ottangian, ~20.5–18–17.5 Ma) the final collision of Alps with the platform led to (re)opening of the western gateway in front of the Alps. For this time span an anti-estuarine circulation regime can be assumed due to warming and low precipitation in CP. Isolation of the eastern segment of Carpathian Foredeep led to evaporitic sedimentation. Coeval deposition of coal seams in the southern realm of CP indicates that precipitation was irregularly distributed.

Fluctuations in humidity at the end of this period can be result of the uplift in the Alps and Dinarides.

During the late Burdigalian–early Langhian (Karpatian–earliest Badenian, ~17–15 Ma) the north-eastward movement of crustal segments in the CP realm led to (i) an oblique collision of the Western Carpathians with platform; (ii) the initial rifting in Pannonian domain; (iii) opening of the “pull-apart” Vienna and East Slovakia basins; (iv) thickening of the Outer Carpathian accretionary wedge; and (v) the Carpathian Foredeep subsidence. Marine connection with the Mediterranean through the “Trans-Tethyan-Trench-Corridor” situated between Eastern Alps and Dinarides (re)opened, while gateway towards the Eastern Paratethys was closed. A change from estuarine to anti-estuarine circulation regime was proposed for this time interval based on microfossil proxies. Uplift of the Central Western Carpathian mountain chain can be the reason of fluctuation in humidity and coal seams deposition in their hinterland.

During the Langhian (Early Badenian, ~14.5–13.8 Ma) the area flooded by the Central Paratethys sea reached its maximal extent. In front of the uplifted Western Carpathian mountain chain, the Carpathian Foredeep depocentres showed an eastward shift in subsidence, while a syn-rift subsidence the Pannonian back-arc basin area occurred. Communication of the semi-enclosed sea with the Mediterranean across the “Trans-Tethyan-Trench-Corridor” gained pronounced anti-estuarine pattern, likely due to aridification and salinity increase in surface water level.

At the ~Langhian/Serravallian (Early/Late Badenian) boundary the evaporite deposition, in the Carpathian Foredeep, Transcarpathian, and Transylvanian basins, referred as Badenian Salinity Crisis, took place (de Leeuw et al. 2018). Subsequently, at the beginning of the Serravallian time interval (~Late Badenian), a partial isolation of CP led to low oxic conditions in the whole area despite occasional open circulation regime with the Mediterranean and Eastern Paratethys realm during the Late Badenian (13.8–12.6 Ma).

In the Sarmatian (12.6–11.6 Ma) the water masses from the Eastern Paratethys entered again the semi-enclosed CP basin system resulting in the Badenian–Sarmatian Extinction Event (Harzhauser & Piller 2007). Uplift of the Outer Western Carpathians led to local increase in humidity in this area (coal seams).

In the early Pannonian (~11.6–10 Ma) sedimentation in the Western Carpathian Foredeep ceased. In the hinterland a new phase of subsidence led to the formation of the isolated Pannonian Basin System referred as Lake Pannon.

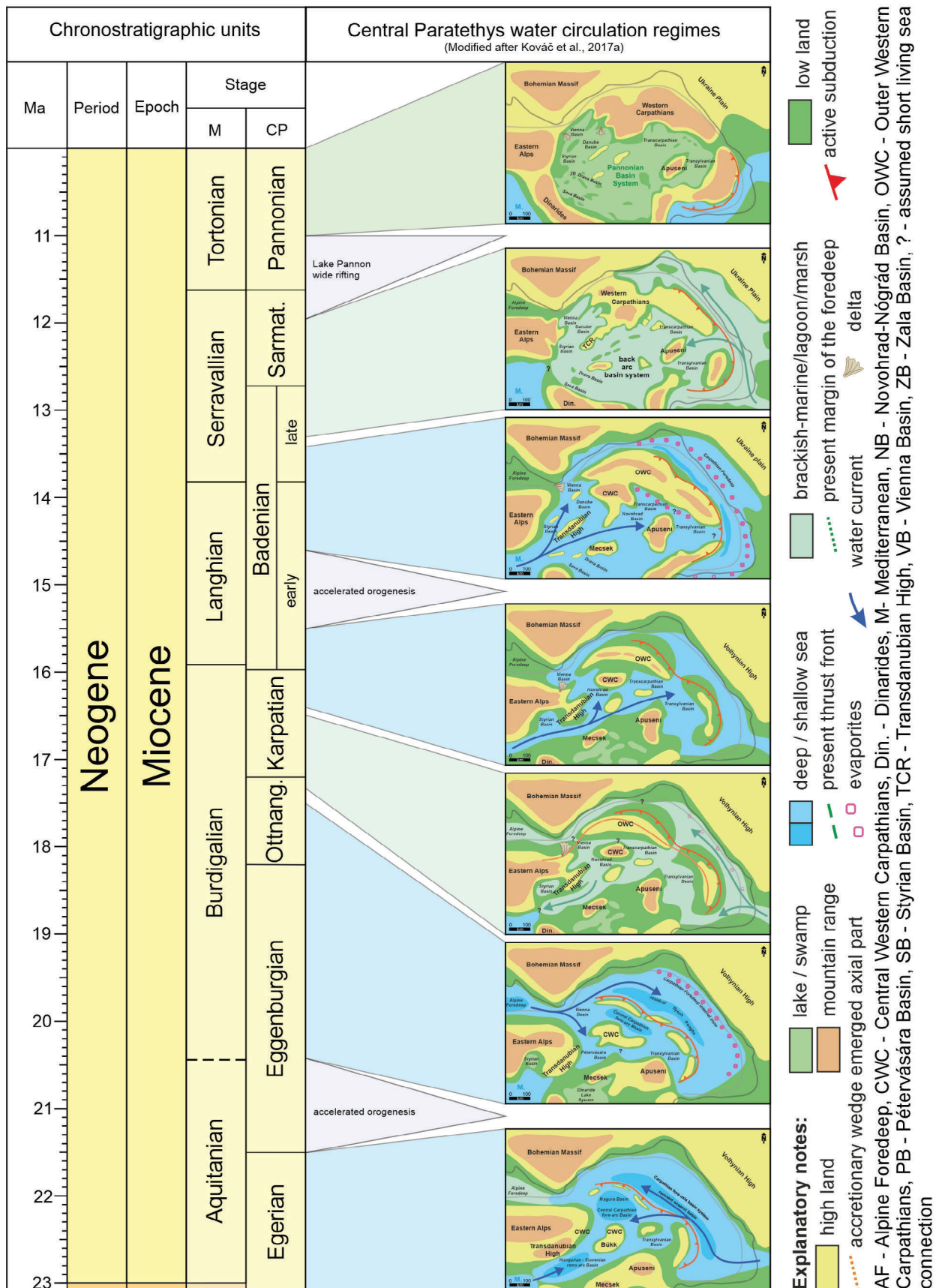


Fig. 1. The Late Cenozoic changes of the Central Paratethys paleogeography — coaction of geodynamic processes and eustasy.

## Conclusions

To conclude, several important factors need to be considered while evaluating regional time-scale in the Central Paratethys realm: (i) the geodynamics of the orogenic system and (ii) the role of gateways between the Central Paratethys, the Mediterranean, and the Eastern Paratethys as a function of both local tectonics and global sea-level changes, (iii) the regional stage boundaries dated by biostratigraphic approaches should be obligatory validated by geochronological methods.

To understand changes in the layout of sedimentary basins during distinct time spans an improved paleogeographic/palinspastic model based on an interdisciplinary approach reflecting the original position and extent of basins which fill was later deformed by folding and thrusting in front of the orogenic system or by the movement of crustal fragments along several hundred km long transform boundaries is needed.

**Acknowledgements:** This research was supported by the Slovak Research and Development Agency under contracts APVV-16-0121, APVV-15-0575, APVV-14-0118, APVV-SK-AT-2017-0010 and VEGA-1-0155-18 project.

## References

- de Leeuw A., Tulbure M., Kuiper K.F., Melinte-Dobrinescu M., Stoica M. & Krijgsman W. 2018: New  $^{40}\text{Ar}/^{39}\text{Ar}$ , magnetostratigraphic and biostratigraphic constraints on the termination of the Badenian Salinity Crisis: Indications for tectonic improvement of basin interconnectivity in Southern Europe. *Global and Planetary Change* 169, 1–15.
- Haq B.U., Hardenbol J. & Vail P.R. 1988: Mesozoic and Cenozoic chronostratigraphy and cycles of sea level changes. In: Wilgus C.K. (Ed.), *Sea-Level Changes — an Integrated Approach*. Society of Economic Paleontologists and Mineralogists, Special Publications 42, 71–108.
- Hardenbol J., Thierry J., Farley M.B., Jacquin T., de Graciansky P. & Vail P.R. 1998: Mesozoic and Cenozoic sequence chronostratigraphic framework of European basins. In: Graciansky C.-P., Hardenbol J., Jacquin T. & Vail P.R. (Eds.): *Mesozoic and Cenozoic sequence stratigraphy of European basins*, SEPM Special Publication 60, 3–13.
- Harzhauser M. & Piller W.E. 2007: Benchmark data of a changing sea — Palaeogeography, Palaeobiogeography and events in the Central Paratethys during the Miocene. *Palaeogeogr. Palaeoclimatol. Palaeoecol.* 253, 8–31.
- Kováč M., Halásová E., Hudáčková N., Holcová K., Hyžný M., Jamrich M. & Ruman A. 2018: Towards better correlation of the Central Paratethys regional time scale with the standard geological time scale of the Miocene Epoch. *Geologica Carpathica* 69, 3, 283–300.
- Kováč M., Hudáčková N., Halásová E., Kováčová M., Holcová K., Oszczytko-Clowes M., Báldi K., Less Gy., Nagymarosy A., Ruman A., Klučiar T. & Jamrich M. 2017a: The Central Paratethys palaeoceanography: a water circulation model based on microfossil proxies, climate, and changes of depositional environment. *Acta Geologica Slovaca* 9, 2, 75–114.
- Kováč M., Márton E., Oszczytko N., Vojtko R., Hók J., Králiková S., Plašienka D., Klučiar T., Hudáčková N. & Oszczytko-Clowes M. 2017b: Neogene palaeogeography and basin evolution of the Western Carpathians, Northern Pannonian domain and adjoining areas. *Global and Planetary Change* 155, 133–154.
- Piller W., Harzhauser M. & Mandic O. 2007: Miocene Central Paratethys stratigraphy-current status and further directions. *Stratigraphy* 4, 71–88.
- Sant K., Palcu D.V., Mandic O. & Krijgsman W. 2017: Changing seas in the Early–Middle Miocene of Central Europe: a Mediterranean approach to Paratethyan stratigraphy. *Terra Nova* 29, 273–281.

# Mesozoic sedimentary basins, current systems and life domains in northern part of the Mediterranean Tethys Ocean

JOZEF MICHALÍK

Earth Science Institute, Slovak Academy of Sciences, Bratislava, Slovakia; geolmich@savba.sk

**Abstract:** Contact of the Mediterranean Tethys with Paleoeurope has been affected by tension, rifting, and by left lateral shift since the Early Triassic. The Late Triassic/Early Jurassic evolution was controlled by convergence along border of the Meliata Ocean and by contemporaneous divergence along the Middle Atlantic/Penninic rift. During Mid Cretaceous, the convergence between Africa and Paleoeurope started, which finally resulted in collision of the Alpine–West Carpathian microcontinent with the Paleoeuropean margin and in the formation of the Alpine nappe pile.

**Keywords:** lithofacies, paleogeography, Mediterranean Tethys, Western Carpathians, Mesozoic.

## Triassic development

Since the Early Permian, the Mediterranean Tethys area becomes a playground of subcrustal movements with variegated microcontinental blocks (Stampfli et al. 2001; Cavazza & Wezel 2003). During the Triassic, Alpine–Carpathian sequences were deposited on fragmented Variscan crust remnants. They formed the Palaeoeuropean shelf between the Armorican and Bohemian massifs and the Ukrainian Shield (Feist-Burkhardt et al. 2008). The Central West Carpathian block, together with the Eastern Alpine fundament, were rimmed by the Meliata Ocean on the south. Triassic sequence of this area is composed of several megacycles deposited under changing climatic, eustatic, and paleoceanographic regime.

The Scythian clastics accumulated in a huge (>100 000 km<sup>3</sup>) deltaic fan system. The source of considerable laterally dispersed terrigenous clastic sediments is assumed to be located in the northern “Vindelician Land” (Michalík 1992, 1993, 2011; Michalík in Feist-Burkhardt et al. 2008). Quartz sandstones, lithic sandstones, and greywackes with conglomeratic layers fining in a southward direction accumulated in a complex delta system (Mišík & Jablonský 2000) with proximal, more terrigenous sediments in the north, and more distal marine facies on the southern margin (Csontos & Vörös 2004). The material was transported by periodical river systems from the area between the Bohemian and the Armorican massifs.

Arid Triassic climate caused accumulation of thick carbonate ramp- and platform complexes, with only several inserted terrigenous clastic formations, indicating more humid intervals during the Scythian, the Early

Carnian, and the Rhaetian. The subsidence (20–30 mm/ka) of wide (300×1000 km) Anisian carbonate ramp of the Gutenstein limestones and dolomites on a submerged alluvial plain was controlled by gradual sea level rise and by compaction of underlying pelitic complexes (60–70 mm/ka). An increasing in late Anisian tectonic activity is documented by tsunamite layers and slump breccias (Michalík et al. 1992). Ladinian carbonate platforms were affected by tensional stress (Michalík 1993, 1994). Sedimentation in intrashelf pull-apart basins was rather slow (4–15 mm/ka) as compared with the rapidly growing reefal margins keeping up with the subsidence rate (up to 400 mm/ka). Differential sedimentation rates accentuated the basinal morphology: the basins attained depths of 1200–1500 m at end of the Ladinian, when sea level began to fall. The Julian humid event was the time of mass transport of clastics (about 10 000 km<sup>3</sup>) that completely filled former tensional basins in the Slovak-Carpathian–Austro-Alpine shelf. Rapidly (500–700 mm/ka) accommodated material has been carried under occasional monsoonal climate from the adjacent Paleoeuropean continent.

Late Triassic regression and tectonic rise in an arid climate led to a re-establishment of carbonate platform system with a continuous reef margin. Extensive back-reef flats (Dachstein Lst and Hauptdolomit formations) separated the sea from Dead Sea-type dry basins with Carpathian Keuper sedimentation. However, the sedimentation rate of the Carpathian Keuper was seven times slower than the sedimentation rate of the Germanic Keuper.

At the end of the Triassic, the Penninic Rift (a continuation of the Mid-Atlantic Oceanic Rift) expanded and detached Mediterranean microcontinents from its

Paleoeuropean foreland. Disintegration of Tethyan shelf resulted in the “mega-shear” model of numerous megablocks separated by strike-slip faults (Michalík 1993, 1994). Lakes and swamps with terrestrial flora and fauna formed in river valleys and depressions, flooded by transgression (Lintnerová et al. 2013). Koessen-type shallow basins have been filled by marine sediments with abundant neritic fauna (Michalík et al. 2013). The Triassic–Jurassic boundary is marked by: termination of carbonate sedimentation; occurrence of spherulite containing beds; C and O isotope excursions; and by the onset of clastic input due to changing climate at beginning of the Hettangian transgression (Michalík et al. 2010). On the other hand, subduction of the Meliata Ocean led to convergence of both Alpine–Carpathian and Adriatic microcontinents.

### Jurassic evolution

The onset of Jurassic sedimentation was affected by emersion and non-sedimentation (Michalík in Pieńkowski et al. 2008). During the Meliata Oceanic crust subduction, the southern margin of the Austroalpine–Central Carpathian microcontinent collided with small blocks in its foreland. Carbonate platforms have been emerged and karstified. The Tatric and Veporic domains much more distant of it have been uplifted. On the other hand, the subsidence continued in the Fatric Domain that was located between these two domains. At the beginning of the Jurassic, marine claystones with occasional sandstone and sandy organodetrital limestones have been deposited in this basin. During the Sinemurian and Lotharingian, quartz-rich sandstone passing distally into sandy limestones documents the last phases of riverine influx in the Central West Carpathians. Crinoidal limestones have been deposited on the slope, while deeper hemipelagic setting was characterized by the deposition of bioturbated marlstones. Red nodular limestones and marls of the Adnet Fm indicated slower sedimentation rate at the end of Early Jurassic. The Lower Jurassic sedimentary cycle in the Hronic Basin started with crinoidal limestones and was terminated with red nodular limestones.

New middle Jurassic sedimentary cycle started with the deposition of organodetrital limestones with calciturbidites, passing basinward into siliceous limestones, radiolarites and dark marls. During the Oxfordian, the bottom of the Fatric Zliechov Basin was covered by dark marlstones, but the adjacent elevated bottom was the location where the Ammonitico Rosso limestones

were deposited. The Mid-Jurassic sedimentary cycle of the Hronic Unit consists of crinoidal limestones. During Late Jurassic, the Ammonitico Rosso facies formed on the shallows. The southernmost part of the West Carpathian inner block is characterized by the deposition of pelagic facies. On the other hand, several elevations with neritic limestone sedimentation have been recorded. The sedimentary record here was terminated by Late Cimmerian deformation of the area.

### Lower Cretaceous evolution

Scarcely preserved source platform limestone complex consists of microsparitic pelletal wackestones with rare oncolites and bioclasts. Shallow marine limestone sequence on more distal elevated blocks starts with Kimmeridgian and Tithonian condensed “Ammonitico Rosso” complex of red nodular limestone. On the other hand, the majority of Lower Cretaceous sequences in the Western Carpathians represents mostly hemipelagic (“Neocomian”) limestones (Vašíček & Michalík 1999) containing calciturbidite debris. The pull-apart Fatric Basin was filled by Upper Jurassic dysoxic marls (Michalík 2007), covered by pelagic Berriasian “biancone” limestones. Hemipelagic limestones are of Late Valanginian age in the Manín Unit, but they comprise Valanginian to Aptian in basinal infill of the Zliechov Basin. The Late Cimmerian compression on south is indicated by input of quartz debris with abundant chromium spinel grains (Michalík in Voigt et al. 2008).

Upper Hauterivian–Lower Albian sequence starts with the deposition of slope- and submarine delta fans derived from carbonate platforms prograding basinwards (Michalík & Soták 1990). The carbonate platforms were mostly destroyed by erosion. Warming during Aptian caused decreasing oxygenation and increasing of carbon content in the basinal sediments.

### Mid-Cretaceous synorogenic formations

During Middle Albian, carbonate platforms submerged being covered by dark marls. The basins in central Carpathians were mostly filled by thick (300–600 m) brownish, often bioturbated gray marls with siltstone intercalations, or even olistoliths, passing into Cenomanian rhythmic sandstone-claystone sequence. At this time, convergence between Gondwana- and Laurasian margins resulted by subduction of the Penninic oceanic bottom, by destruction of former basinal

systems and folding. A complex stacked pile of superposed units comprising the pre-Alpine basement, its Mesozoic cover, and superficial nappes originated during Turonian in Central Carpathians.

## The Upper Cretaceous “Gosau” developments

After the major compression have released, fold structures collapsed. New basins evolved in the middle of orogenic system (Plašienka et al. 1997). Variegated breccias of local material, cemented by yellowish and red argillaceous matrix and Turonian/Lower Coniacian fresh-water algal limestones filled cavities and depressions on surface of carbonate complexes. Marine sequence started by braided river- and subaerial delta clastics composed of alternating graded calcareous sandstones, variegated marls and flysch complexes. In Outer Carpathians, tension and basin opening continued until Oligocene when Alpine and Carpathian orogenic arcs began to form.

## References

- Cavazza W. & Wezel F.C. 2003: The Mediterranean region — a geological primer. *Episodes* 26, 3, 160–168.
- Csontos L. & Vörös A. 2004: Mesozoic plate tectonic reconstruction of the Carpathian region. *Palaeogeogr. Palaeoclimatol. Palaeoecol.* 210, 1–56.
- Feist-Burkhardt S., Götz A.S., Szulc J., Borkhataria R., Geluk M., Haas J., Hornung J., Jordan P., Kempf O., Michalík J., Nawrocki J., Lutz R., Ricken W., Röhling H.G., Ruffer W., Török Á. & Zühlke R. 2008: 13. Triassic. In: Mc Cann T. (Ed.): *The Geology of Central Europe*, vol. 2: Mesozoic and Cenozoic. *Geological Society Book*, London, 749–821.
- Lintnerová O., Michalík J., Uhlík P., Soták J. & Weissová Z. 2013: Triassic–Jurassic climate humidification and Rhaetian kaolinite formation (Western Carpathians, Tatric Unit, the Červený Úplaz section). *Geological Quarterly* 57, 4, 701–728.
- Masaryk P., Lintnerová O. & Michalík J. 1993: Sedimentology, lithofacies and diagenesis of the sediments of the Reifling intra-platform basins in the Central Western Carpathians. *Geologica Carpathica* 44, 4, 233–249.
- Michalík J. 1993: Mesozoic tensional basins in the Alpine–Carpathian shelf. *Acta Geol. Hungarica* 36, 4, 395–303.
- Michalík J. 1994: Notes on the paleogeography and paleotectonics of the Western Carpathian area during the Mesozoic. *Mitteilungen Österreichisches Geologisches Gesellschaft* 86 (1993), 101–110.
- Michalík J. 2007: Rock record and microfacies indicators of the latest Triassic to mid-Cretaceous tensional development of the Zliechov Basin (central Western Carpathians). *Geologica Carpathica* 58, 5, 443–453.
- Michalík J. 2011: Mesozoic paleogeography and facies distribution in the N Mediterranean Tethys from Western Carpathians view. *Iranian Journ. Earth Sci.* 3, 185–193.
- Michalík J. & Soták J. 1990: Lower Cretaceous shallow-marine build-ups in Western Carpathians and their relation to the pelagic facies. *Cretaceous Research* 11, 211–227.
- Michalík J., Masaryk P., Lintnerová O., Papšová J., Jendrejčková O. & Reháková D. 1992: Sedimentology and facies of a storm-dominated Triassic carbonate ramp (Vysoká Fm, Malé Karpaty Mts, Western Carpathians). *Geologica Carpathica* 43, 4, 213–230.
- Michalík J., Biroň A., Lintnerová O., Götz A.E. & Ruckwied K. 2010: Climate change at the T/J boundary in the NW Tethyan Realm (Tatra Mts., Slovakia). *Acta Geologica Polonica* 60, 4, 535–548.
- Michalík J., Lintnerová O., Reháková D., Boorová D. & Šimo V. 2012: Early Cretaceous sedimentary evolution of a pelagic basin margin (the Manín Unit, central Western Carpathians, Slovakia). *Cretaceous Research* 38, 68–79.
- Michalík J., Lintnerová O., Wójcik-Talerzak P., Gaździcki A., Grabowski J., Golej M., Šimo V. & Zahradníková B. 2013: Paleoenvironments during the Rhaetian transgression and the colonization history of marine biota in the Fatric Unit, Western Carpathians. *Geologica Carpathica* 64, 2, 39–62.
- Mišík M. & Jablonský J. 2000: Lower Triassic quartzites of the Western Carpathians: Transport directions, source of clastics. *Geologica Carpathica* 51, 4, 251–264.
- Pieńkowski G., Schudack M.E., Bosák P., Enay R., Feldman-Olszewska A., Golonka J., Gutowski J., Herngreen G.F.W., Jordan P., Krobicki M., Lathuiliere B., Leinfelder R.R., Michalík J., Mönnig E., Noe-Nygaard N., Pálffy J., Pint A., Rasser M.W., Reisdorf A., Schmid D.U., Schweigert G., Surlyk F., Wetzel A. & Wong T.E. 2008: 14. Jurassic. In: Mc Cann T. (Ed.): *The Geology of Central Europe*, vol. 2: Mesozoic and Cenozoic. *Geological Society Book*, London, 823–922.
- Plašienka D., Grecula P., Putiš M., Kováč M. & Hovorka D. 1997: Evolution and structure of the Western Carpathians: an overview. *Mineralia Slovaca — Monographs*, 1–24.
- Stampfli G.M., Borel G.D., Cavazza W., Mosar J. & Ziegler P.A. 2001: Palaeotectonic and palaeogeographic evolution of the W Tethys and PeriTethyan Domain (IGCP Project 369). *Episodes* 24, 4, 222–228.
- Vašíček Z. & Michalík J. 1999: Early Cretaceous ammonoid paleobiogeography of the West Carpathian part of Paleoeuropean shelf margin. *Neues Jahrbuch für Geologie und Paläontologie, Abhandlungen* 212, 1–3, 241–262.
- Voigt S., Wägrich M., Surlyk F., Wałaszczuk I., Uličný D., Čech S., Voigt T., Wiese F., Wilmsen M., Michalík J., Jagt J.W.M., Felder P.J. & Schulp A.S. 2008: 15. Cretaceous. In: McCann Tom (Ed.): *The Geology of Central Europe*, 2: Mesozoic and Cenozoic. *Geological Society Book*, London

# Plankton evolution and biostratigraphy during Late Jurassic and Early Cretaceous

DANIELA REHÁKOVÁ

Comenius University, Faculty of Natural Sciences, Department of Geology and Palaeontology, Mlynská dolina G, Ilkovičova 6, SK-842 15 Bratislava, Slovakia; daniela.rehakova@uniba.sk

**Abstract:** Characteristic morphology, quick turnovers in evolution and assemblages composition of ancient planktonic organisms like phototrophic algae producing cysts or calcite plates, radiolarians, planktonic crinoids, as well as associations of loricated protozoans made them a favourable tools for interregional correlation. Thus nannofossils, calcareous dinoflagellates, radiolarians, sacoccomids, and calpionellids are playing a key role in the biostratigraphy of Upper Jurassic/Lower Cretaceous sequences. In the combination with microfossils like were ammonites or belemnites, also magnetic, chemical, cyclicity and eustatic records are suitable for their high resolution stratigraphy and interpretations of their life conditions. This paper summarize up to date results concerning the evolution of Late Jurassic and Early Cretaceous calcareous dinoflagellates and calpionellids and their interrelationship with another stratigraphically important planktonic groups.

## Introduction

The arrangement of Late Jurassic and Early Cretaceous facies was controlled by interrelated factors, such as by the gradual break-up of Pangea that created individual often interconnected basins and that controlled their subsidence, subsequent thermal subsidence which together with eustasy and climate variation affected the chemistry and the trophic state of ocean water (Baumgartner 2013). At that time rich planktonic assemblages developed in these basins, slopes, intrashelf elevations and partially also in the distal parts of carbonate ramps being characterized by a permanent current regime positively influencing the nutrient input.

Calpionellids and dinoflagellates were sensitive to environmental perturbations such a change of the water temperature, chemistry and the nutrient supply. It is worth to mention, that the abundance and size of calpionellid loricas were influenced by water temperature and fluctuation of the sea-level. These parameters decreased also towards the open sea — they were less frequent in deep basins in which radiolarians prevailed, being very rare or seldom in reefal and lagoonal settings or in proximal settings with permanent river-influenced elevated nutrient level and with changes in surface water chemistry (Reháková 2000a; Kowal-Kasprzyk & Reháková 2019). On the other hand, calcareous dinoflagellates preferring rather more nutritional environments are generally rare elements of assemblages. However, few blooming events probably influenced by such ecological factors as sea-level fluctuations, sea-water

temperature changes were distinguished (Reháková 2000b; Jach & Reháková 2019). Several stages could be selected in the evolution of these two microplanktonic groups.

## Oxfordian stage

The Lower Oxfordian basal ribbon radiolarites with occasional thin shale interbeds were replaced by limy radiolarites and radiolarian limestones (Baumgartner 2013, Jach et al. 2014). The zonation of the silica rich sediments is based on the radiolarian Unitary Association Zones (UAZs) proposed by Baumgartner et al. (1995). UAZs 5-9 were defined for this stage. The concentration of radiolarians in chert beds is regarded as the effect of productivity cycles in response to the Milankovitch climatic oscillations (Baumgartner 2013; De Wewer et al. 2014). The carbonatic basinal deposits contain dinoflagellate cyst associations of the *Parvula* and *Fibrata* acme zones (Reháková 2000b). A rich cyst association of the same age was documented also in shallower coastal parts (Keupp & Ilg 1989). Also fragments of *Bositra* shells formed a persistent part of dysaerobic microfacies. At the end of the Oxfordian *Bositra* filaments slowly decreased in abundance being substituted by planktonic crinoids of *Sacoccoma* sp., and protoglobuligerinid rock-forming foraminifera (Mutterlose & Böckel 1998) the appearance of which may have been related to the sea-level rise and opening of new niches (Reháková 2000a).

### Kimmeridgian stage

The variegated red nodular limestones representing the Ammonitico Rosso type of facies were deposited in the basins and their elevated zones. At the beginning of this stage planktonic foraminifera were still abundant but soon they were replaced by rapid increase of saccocomids and shortly after the blooms of green algae which produced spores of *Globochaete alpina* Lombard. Environmental conditions were favourable for their development up to the Early Berriasian. On the base of morphology of skeletal saccocomid elements and their succession against the ammonite zones seven saccocomid biozones were distinguished by Benzaggagh et al. (2015). Biozones Sc1 and Sc2 were defined for the Late Oxfordian and Kimmeridgian. Abundant calcareous dinoflagellates of the Parvula acme Zone followed by less frequent cysts of Moluccana and Borzai zones were observed in nodular limestones (Reháková 2000b; Jach et al. 2014; Michalík et al. 2016; Grabowski et al. 2019). Nannofossils of this stage were included into the NJT 14 Zone (Casellato 2010). The majority of radiolarians were calcified. Radiolarian UAZ 10 was determined in Kimmeridgian deposits (Baumgartner et al. 1995; Jach et al. 2014).

### Tithonian stage

Thin rhythmic alternation of marls, shales and limestones and their lateral equivalent — variegated pseudonodular limestones passing to the Biancone type of facies dominated in basinal and distal part of carbonate ramps of this stage. Saccocomids and globochaetes dominated in Early Tithonian microfacies in which Saccocoma biozones Sc 3, Sc 4 and Sc 5 were established (Benzaggagh et al. 2015). In microfacies radiolarians are scattered in matrix. Majority of them are calcified, but those replaced by chalcedony or microcrystalline silica allowed to distinguished UAZ 11 in the Lower Tithonian deposits (Baumgartner et al. 1995; Jach et al. 2014). Early Tithonian calcareous dinoflagellate associations are abundant and diversified and offered to events for the establishment of followed cysts zones: Pulla acme, Tithonica, Malmica, Semiradiata, Tenuis, Fortis and Proxima (Lakova et al. 2009; Reháková 2000b). According to Jach & Reháková (2019) the blooms of cysts in some of above mentioned cyst zones could indicate warmer surface seawater corresponding with the arid phase of the “Hudlestoni event” (Hesselbo et al. 2009). In the uppermost part of Early Tithonian the first

calpionellids (chitinoideids of the Dobeni Subzone, Chitinoideida Zone) appeared being followed by their Late Tithonian more advanced descendants of the Boneti Subzone which were the ancestors of the evolutionary lineages of transitional and hyaline calpionellids of the Praetintinnopsella and Crassicollaria zones (Reháková & Michalík 1997). During the first Remanei Subzone of the Crassicollaria Zone saccocomids were still abundant (Sc 6 and Sc 7 biozones of Benzaggagh et al. 2015); during the second, more diversified Intermedia Subzone they declined in abundance and prior to J/K boundary in the third Colomi Subzone they were very seldom among the planktonic assemblages which were dominated by small calpionellid forms of Crassicollaria and Calpionella and by globochaetes. At the end of Late Tithonian dinoflagellate cysts were rapidly reduced; few long living forms persisted up to Late Berriasian. Saccocomids disappeared, those which sporadically were found in Berriasian deposits may be regarded as redeposited fragments due they are often accompanied by reworked Tithonian calpionellids and dinoflagellate cysts (Michalík et al. 2016; Svobodová et al. 2019; Grabowski et al. 2019). Early Tithonian nannofossils of the upper part of NJT14, then NJT 15 zones were rather poor preserved, they increased in abundance and diversity along the Late Tithonian Crassicollaria Zone and provided the marker of the NJT 16 and NJT 17 zones (Casellato 2010). Well-preserved radiolarians allowed to establish the Late Tithonian UAZs 12, 13 /or Loopus primitivus and Pseudodictyomitra carpatica zones (Baumgartner et al. 1995; Matsuoka 1995).

### Berriasian stage

The Biancone type limestones with cherts and locally with rhythmic stratiformed chert layers together with deeper marly limestones intercalated by marls are typical slope, basinal and most distal part of carbonate ramps of this stage. Nannofossils, calpionellids and globochaetes dominated in plankton assemblages. The succession of calpionellids allowed to distinguished Early Berriasian Calpionella Zone with the Alpina, Ferasini and Elliptica subzones and the Late Berriasian Calpionellopsis Zone with the Simplex, Oblonga and Murgeanui Subzones (Remane et al. 1986; Pop 1994; Reháková & Michalík 1997 and further calpionellid zonations summarized in Lakova & Petrova 2013). The Proxima cyst Zone represent the interval of very rare, long living cysts. Shortly before the onset of Late Berriasian Calpionellopsis Zone the widespread cysts event called as

the Fusca Acme appeared which may be also interpreted as the result of the increased temperature in surface seawater layers comparable with those mentioned in Tithonian Semiradiata Zone (Jach & Reháková 2019). Small stomiosphaerid cysts followed by bigger colomisphaerids have been included to the latest Berriasian Wanneri and Conferta cysts zone (Reháková 2000b; Lakova et al. 1999). Nannofossils associations were divided into NKT and NK-1, NK-2a zones (Bralower et al. 1989; Casellato 2010). Radiolarians were splitted into UAZs 13, 14, 15 /or Pseudodictyomitra carpathica Zone (Baumgartner et al. 1995; Matsuoka 1995).

### Valanginian stage

Compared to Berriasian stage, the lithological character of Valanginian deep water deposits did not changed. From the top of the Berriasian the marly limestones and marly intercalations are more frequent and thicker. Locally the cherts and stratiform chert layers are common in Biancone limestones of this stage. Previously highly diversified calpionellid associations rapidly decreased in diversity and abundance. Calpionellites Zone with the Darderi and Major subzones and the Tintinnopsella Zone were distinguished (Reháková & Michalík 1997). The last calpionellid species are supposed from the Late Valanginian, when they extinct. These which were described from Hauterivian or younger deposits are rather reworked. Short flourishing of small cadosinid cysts was described as Acme Minuta Zone. It was followed by the further Vogleri and Valanginiana cyst Zone (Reháková 2000a). Nannofossils associations of this stage were divided into NK-2b and NK-3 zones (Bralower et al. 1989). Planktonic favusellid foraminifera appeared in assemblages once again after a longer break lasting from the Early Kimmeridgian (Reháková 2000a). In sediments of this stage rich in radiolarians the UAZs 16, 17, 18 were distinguished (Baumgartner et al. 1995). In some cases, the laminae rich in radiolaria and sponge spicules could have been linked with the periodically active countour currents which locally persisted until the Hauterivian.

**Acknowledgements:** The paper was supported by the project of the Slovak Grant Agency APVV-14-0118 and by VEGA 2/0034/16 and 2/0057/16 Projects. This work is a contribution of the Berriasian Working Group (BWG) of the International Subcommission on Cretaceous Stratigraphy (ICS).

### References

- Baumgartner P.O., Bartolini A., Carter E.S., Conti M., Cortese G., Danelian T., De Wever P., Dumitrica P., Dumitrica-Jud R., Goričan Š., Guex J., Hull D. M., Kito N., Marcucci M., Matsuoka A., Murchey B., O'Dogherty L., Savary J., Vishnevskaya V., Widz D. & Yao A. 1995: Middle Jurassic to Early Cretaceous radiolarian biochronology of Tethys based on Unitary Associations. In: Baumgartner P.O., O'Dogherty L., Goričan Š., Urquhart E., Pilleveit A., De Wever P. (Eds.): Middle Jurassic to Lower Cretaceous Radiolaria of Tethys: Occurrences, Systematics, Biochronology. *Mémoires de Géologie* (Lausanne) 23, 1013–1048.
- Baumgartner P. 2013: Mesozoic radiolarites — accumulation as a function of sea surface fertility on Tethyan margins and in ocean basins. *Sedimentology* 60, 292–318.
- Benzaggagh M., Homberg C., Schnyder J. & Ben Abdesselam-Mahdaoui S. 2015: Description et biozonation des sections de crinoïdes saccocomidés du Jurassique supérieur (Oxfordien-Tithonien) du domaine téthysien occidental. *Ann. de Paléontol.* 101, 95–117.
- Bralower T.J., Monechi S. & Thierstein H.R. 1989: Calcareous nannofossils zonation of the Jurassic–Cretaceous boundary interval and correlations with the Geomagnetic Polarity Timescale. *Mar. Micropaleont.* 14, 153–235.
- Casellato C. 2010: Calcareous nannofossil biostratigraphy of upper Callovian – lower Berriasian successions from the Southern Alps, North Italy. *Rivista Italiana di Paleontologia e Stratigrafia* 116, 3, 357–404.
- Grabowski J., Bakhmutov V., Kdyr S., Krobicki M., Pruner P., Reháková D., Schnabl P., Stoykova K. & Wierzbowski H. (in press). Integrated stratigraphy and Palaeoenvironmental interpretation of the Upper Kimmeridgian to Lower Berriasian pelagic sequences of the Velykyi Kamianets section (Pieniny Klipen Belt, Ukraine). *Palaeogeography, Palaeoclimatology, Palaeoecology* 532, 109216.
- Hesselbo S.P., Deconinck J-F., Huggett J.M. & Morgans-Bell H.S. 2009: Late Jurassic palaeoclimatic change from clay mineralogy and gamma-ray spectrometry of the Kimmeridge Clay, Dorset, UK. *Journal of the Geological Society* 166, 1123–1133.
- Jach R., Djerić N., Goričan Š. & Reháková D. 2014: Integrated stratigraphy of the Middle Upper Jurassic of the Križna Nappe, Tatra Mountains. *Annales Societatis Geologorum Poloniae* 84, 1–33.
- Jach R. & Reháková D. 2019: Middle to Late Jurassic carbonate-biosiliceous sedimentation and paleoenvironment in the Tethyan Patricum domain, Križna Nappe, Tatra Mts., Western Carpathians. *Annales Societatis Geologorum Poloniae* 89, 1–46.
- Keupp H. & Ilg A. 1989: Die kalkigen Dinoflagellaten im Ober-Callovium und Oxfordium der Normandie/Frankreich. *Berliner-Geowiss. Abh.* A 106, 165–205.
- Kowal-Kasprzyk J. & Reháková D. 2019: A morphometric analysis of loricae of the genus *Calpionella* and its significance for the Jurassic/Cretaceous boundary interpretation. *Newsletters 981 on Stratigraphy* 52 1, 33–54.
- Lakova I., Stoykova K. & Ivanova D. 1999: Calpionellid, nannofossils and calcareous dinocyst bioevents and integrated biochronology of the Tithonian to Valanginian in the West Balkan Mountains, Bulgaria. *Geologica Carpathica* 50, 151–168.
- Lakova I. & Petrova S. 2013: Towards a standard Tithonian to Valanginian calpionellid zonation of the Tethyan Realm. *Acta Geologica Polonica* 63, 220–221.
- Matsuoka A. 1995: Jurassic and Lower Cretaceous radiolarian zonation in Japan and in the western Pacific. *The Island Arc* 4, 140–153.

- Michalík J., Reháková D., Grabowski J., Lintnerová O., Svobodová A., Schlögl J., Sobieñ K. & Schnabl P. 2016: Stratigraphy, plankton communities, and magnetic proxies at the Jurassic/Cretaceous boundary in the Pieniny Klippen Belt (Western Carpathians, Slovakia). *Geologica Carpathica* 67, 4, 303–328.
- Mutterlose J. & Böckel B. 1998: The barremian–Aptian interval in NW Germany: a review. *Cretaceous Research* 19, 539–568.
- Pop G. 1994: Calpionellid evolutive events and their use in biostratigraphy. *Romanian Journal of Stratigraphy* 76, 7–24.
- Reháková D. 2000a: Calcareous dinoflagellate and calpionellid bioevents versus sea-level fluctuations recorded in the West-Carpathian (Late Jurassic/Early Cretaceous) pelagic environments. *Geologica Carpathica* 51, 229–243.
- Reháková D. 2000b: Evolution and distribution of the Late Jurassic and Early Cretaceous calcareous dinoflagellates recorded in the Western Carpathians pelagic carbonate facies. *Mineralia Slovaca* 32, 79–88.
- Reháková D. & Michalík J. 1997: Evolution and distribution of calpionellids — the most characteristic constituents of Lower Cretaceous Tethyan microplankton. *Cretaceous Research* 18, 493–504.
- Remane J., Borza K., Nagy I., Bakalova-Ivanova D., Knauer J., Pop G. & Tardi-Filácz E. 1986: Agreement on the subdivision of the standard calpionellid zones defined at the 2nd Planktonic Conference Roma 1970. *Acta Geologica Hungarica* 29, 5–14.
- Svobodová A., Švábenická L., Reháková D., Svobodová M., Skupien P., Elbra T. & Schnabl P. 2019: The Jurassic/Cretaceous and high resolution biostratigraphy of the pelagic sequences of the Kurovice section (Outer Western Carpathians, the northern Tethyan margin). *Geologica Carpathica* 70, 2, 153–182.

## **Influence of deformation bands on Nubian sandstone reservoir quality, Eastern Desert, Egypt**

AHMED ALI<sup>1</sup>, RAMADAN MOHAMED<sup>1</sup>, KHAIRY ZAKI<sup>1</sup> and MICHAEL WAGREICH<sup>2</sup>

<sup>1</sup>Geology Department, Faculty of Science, Minia University, 61519 Minia, Egypt; ahmad.ali@mu.edu.eg

<sup>2</sup>Department of Geodynamics and Sedimentology, Vienna University, 1090 Vienna, Austria

The importance of the Nubian Sandstone is regarded to the capability of this rock unit to store and produce large volumes of hydrocarbons in the Gulf of Sues, Egypt. The Nubian Sandstone consists of a sequence of sandstones and shales that formed during the Paleozoic to Cretaceous. Samples were examined for the petrographic and petrophysical characteristics. Two sets of deformation bands exist at the study area. There are no differences in the mineralogy between the Nubian Sandstone and the deformation bands, and both consist primarily of quartz. The main petrographic difference is the grain size which is reduced greatly in the bands. Plugs of 1.5” diameter of the Nubian Sandstone with and without bands were examined to

measure gas porosity and permeability. The plugs showed a variation in these two factors along the deformation bands. The porosity in the Nubian Sandstone ranges from 24 to 30 % whereas it is reduced to 9 to 16 % in plugs containing deformation bands. A similar trend is detected for permeability that is strongly reduced from 1200–8400 mD in samples without bands to 0.08–0.3 mD in samples with bands. The orientation of the deformation bands shows a relationship to the regional tectonic settings of the Red Sea rifting. The mineralogical, petrographic and petrophysical investigations document a negative influence of the deformation bands on the capacity of Nubian sandstone reservoir.

# Biostratigraphic and paleoecological evaluation of Lower Jurassic sediments from Myjava Highlands

SILVIA ANTOLÍKOVÁ

Earth Science Institute SAS, Bratislava, Dúbravská cesta 9, 840 05 Bratislava, Slovakia; geolsisa@savba.sk

The study area is located in the Pieniny Klippen Belt, in the Myjava Highlands, and east of the Podbranč locality. The samples for the study calcareous nannofossils were taken from the Lower Jurassic Allgäu Formation. This formation includes dark gray to black, slightly mottled, fine-grained marly limestones and marls. Red and green radiolarities with cherts of the Callovian–Kimmeridgian age overlie this formation. We performed the first biostratigraphic research based on calcareous nanofossils at this locality.

Assemblages of calcareous nanofossils (Fig. 1) are specimen- and species-poor in the studied samples.

Biostratigraphic research of the samples determined calcareous nanofossils assemblage composed almost exclusively of specimens belonging to the genus *Lotharingius* — *Lotharingius hauffii*, *Lotharingius frodoi*, *Lotharingius umbriensis*. Other species include *Biscutum profundum*, *Carinolithus superbus*, *Crepidolithus crassus*, *Schizosphaerella punctulata*, and *Thoracosphaera* sp. (Young et al. 2017)

Based on the identified nano-assemblage, we can determine that layers belong to the Toarcian nannoplankton zone NJ6, according to Bown - Cooper 1998.

The biostratigraphically youngest species is represented by *Carinolithus superbus*, which has its first occurrence in the NJ 6 Zone. Other species are typical of the Toarcian stage.

Species *Lotharingius* began to develop during the Pliensbachian–Toarcian time. During the Toarcian, *Lotharingius* has been diminished in size (Fraguas & Young 2011). The most abundant *Lotharingius* species were *Lotharingius hauffii* and *Lotharingius frodoi*. *Lotharingius frodoi* is, according to Fraguas & Young 2011, a morphotype of *Lotharingius hauffii*, but in our study we distinguish both species individually (Fraguas & Young 2011).

The occurrences of the genera *Lotharingius* are paleoecological significant. *Lotharingius* survived the Early Toarcian anoxic event that was coupled with the biomineralization crisis induced by the high atmospheric pCO<sub>2</sub> and ocean acidification. These conditions led to the crisis and extinguishment of nannofossils. (Fraguas & Young 2011).

**Acknowledgements:** The research has been supported by VEGA 2/0186/17.

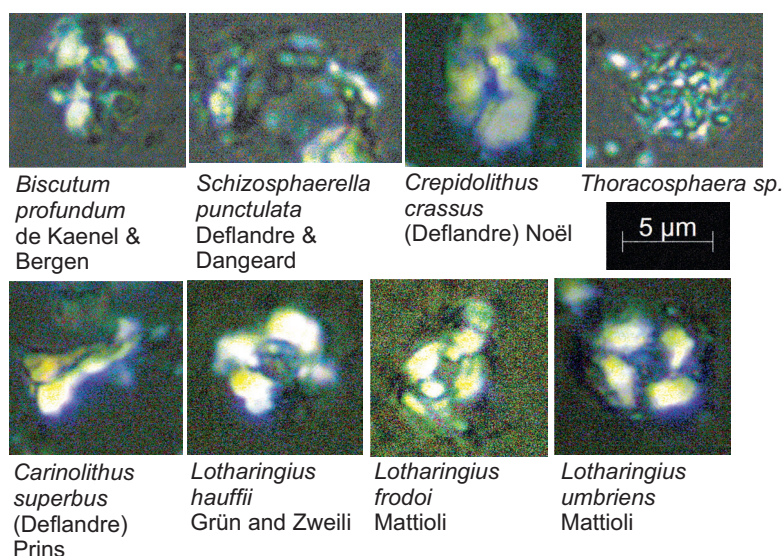


Fig. 1. Phototable of the Lower Jurassic calcareous nannofossil from the study area.

## References

- Bown P.R. & Cooper M.K.E. 1998: Jurassic. In: Bown P.R. (Ed.): *Calcareous Nannofossil Biostratigraphy*. *British Micropalaeontological Society Publication Series*, 34–85.
- Fraguas A. & Young J.R. 2011: Evolution of the coccolith genus *Lotharingius* during the Late Pliensbachian–Early Toarcian interval in Asturias (N Spain). *Consequences of the Early Toarcian environmental perturbations*. *Geobios* 44, 361–375.
- Young J.R., Bown P.R. & Lees J.A. 2017: 'Cylindralithus' Nannotax3 website. Accessed 21 Apr. 2017. <http://www.mikrotax.org/Nannotax3/index.php?taxon=Cylindralithus&module=Mesozoic>

# The paleogeographic distribution of the coralline algae of the genus *Mesophyllum* in Central Paratethys during the Middle Miocene

JURAJ HRABOVSKÝ<sup>1</sup>, DANIELA BASSO<sup>2</sup>, GIOVANNI COLETTI<sup>2</sup>  
and ANDRZEJ PISERA<sup>3</sup>

<sup>1</sup>Earth Science Institute of the Slovak Academy of Sciences, Dúbravská cesta 9, 840 05 Bratislava, Slovakia; geoljuhr@savba.sk

<sup>2</sup>Department of Earth and Environmental Sciences, University of Milano-Bicocca, P.za della Scienza 4, 20126 Milano, Italy; daniela.basso@unimib.it

<sup>3</sup>Polish Academy of Sciences, Institute of Paleobiology, Twarda 51/55, 00-818 Warszawa, Poland; apis@twarda.pan.pl

Despite their common occurrence, the potential of coralline algae is not yet fully exploited in paleoecological reconstructions. The reasons are mainly grounded in the taxonomic inconsistency caused by poor preservation or insufficient knowledge of the type material of many species, and confusion derived from the difficult recognition of the coralline three-phased life cycle in the fossil record. Specimens of fossil coralline algae from newly collected samples, and historical Schaleková's collection of middle Miocene Paratethyan limestone were studied under optical and scanning electron microscopes, revealing the occurrence of the asexual, male gametangial, and carposporangial conceptacles of *Mesophyllum crassiusculum* here documented for the first time. Based on the recent emendation of *Mesophyllum* and consequent circumscription of the genera *Mesophyllum* sensu stricto and *Melyvonnea*, this is the first and oldest finding of a fossil *Mesophyllum* s.s. Moreover, we provide further evidence of the preservation potential of important diagnostic characters, such as the shape of epithallial and subepithallial cells, the shape of the conceptacle roofs, the number and shape of pore canals lining cells in the multiporate roof of the asexual conceptacle chambers. The identification of *M. crassiusculum* led us to revision of the former occurrences of this genus. For purpose of application of emended

generic concept of *Mesophyllum* s.s. we analyzed published material and newly collected Badenian (Langhian–Early Serravallian) samples from Transylvania, Novohrad, Danube, Vienna and Carpathian foredeep basins also. Preliminary results show that (1) roof morphology and pore canal anatomy are available diagnostic characters at species and generic rank for fossil *Mesophyllum*, and (2) closely related tropical genus *Melyvonnea* is probably absent. Although our results suggest that tetra/bisporangial plants far exceed in amount the carposporophyte and gametophyte plants, further research would complete missing data and improve understanding of the paleogeographic distribution of the genus *Mesophyllum* s.s.

**Keywords:** Rhodophyta, Corallinophycidae, *Mesophyllum*, life cycle phases, taxonomy, Miocene, Slovakia.

**Acknowledgment:** Research was supported by Slovak Academy of Sciences grant project VEGA 2/0122/18. This is a scientific contribution of Project MIUR — Dipartimenti di Eccellenza 2018-2022. We thank to Natália Hudáčková (Comenius University, Bratislava, Slovakia) for providing historical collection of Anna Schaleková.

# Badenian/Sarmatian foraminifera shift in the Central Paratethys: Two methods comparison — a morphogroup and species approach

NATÁLIA HUDÁČKOVÁ, ANDREJ RUMAN, IVANA PLAŠIENKOVÁ,  
MICHAL JAMRICH, EVA HALÁSOVÁ, PETER KISS, MARIANNA KOVÁČOVÁ,  
JAROSLAVA BABEJOVÁ-KMECOVÁ and MICHAL KOVÁČ

Department of Geology and Paleontology, Faculty of Natural Sciences, Comenius University in Bratislava, Mlynská dolina, Ilkovičova 6, 842 15 Bratislava, Slovakia; natalia.hudackova@uniba.sk

**Abstract:** Within occasional time intervals during the Late Badenian stage, the connection between the Central Paratethys and Mediterranean was probably closed. Changes in the water circulation regimes were reflected in the development of peculiar conditions on the sea floor. We interpret ecological parameters affecting spatio-temporal prevalence and distribution of foraminiferal assemblages and investigate similarities in functional morphology, which serves as a basis for their morphogroups ordering. The Badenian/Sarmatian boundary, characterized by a major change in the composition of benthic and planktic foraminiferal assemblages in the studied sediments, was proved by both methods.

## Introduction

Due to the great potential of foraminifera and calcareous nannoplankton to preserve in the fossil record and for their relative quick response to changes in ecological factors, they play an important role in paleoenvironmental interpretations of the Middle Miocene northern Paratethyan basins. The main aim of this work is to document the Badenian/Sarmatian boundary based on the correlations of the foraminifera and calcareous nannofossils assemblages and the change in their composition, referred as Badenian–Sarmatian Extinction Event (BSEE) by Harzhauser & Piller (2007), Holcová (2008) and Palcu et al. 2015.

## Material and methods

Rock samples of marine sediments from the key boreholes of the Vienna Basin (MZ-102, IV-19), Danube Basin (ŠVM-1, Poz-4) and East Slovakian Basin (Lo-1, Al-4) were studied and the foraminiferal and calcareous nannoplankton assemblages were quantitatively analyzed. Standard methods were used for microfossils separation and collection (Kováčová & Hudáčková 2009; Jamrich & Halášová 2010). If possible, both foraminiferal and calcareous nannoplankton was studied from the same bulk samples. Published data (Luczkowska 1976; Tóth & Görög 2008; Peryt & Jasionowsky 2012; Gebhart et al. 2009) were used for the correlation and

comparison with our results. Based on statistical analyzes (NMDS and cluster analysis), interpretation of ecological parameters affecting prevalence and distribution of foraminifera assemblages was made. Similarities in the functional morphology of foraminiferal tests enabling effective interpretation of the paleoenvironment were also investigated.

## Results

In total 77 benthic species and 7 planktic species of foraminifera were identified from the 169 samples. Thirty-four taxa stay in open taxonomy due to poor preservation and secondary calcareous coat on the foraminifera test. The Badenian acme zone Tenuitellinata (based on the dominance of *Turborotalia quinqueloba* and *Tenuitella munda*; Filipescu & Silye 2008) and Bulimina-Bolivina, Ammonia, planktic CPN8 zones (Cicha et al. 1975) were identified in the studied samples. Sarmatian sediments were assigned usually based on presence of *Elphidium reginum*, *Ortomorphina dina*, *Elphidium hauerinum*, *Articularia articulinoidea*, and specific calcareous nannofossil assemblages with acme of *Sphenolithus abies* or monoassemblage of *Braarudosphaera bigelowii* a *B. bigelowii parvula*. In the Sarmatian sediments agglutinated foraminifers absent.

From the upper Badenian sediments, based on statistical analyses (cluster analysis, NMDS analysis) of the benthic foraminiferal assemblages and functional

morphology of their tests, three main types of assemblages/paleoenvironments were interpreted: (i) the *Bulimina–Bolivina* assemblage (elongated morphotypes dominates) of the deeper neritic with restricted ventilation on the basin floor, (ii) the *Ammonia–Porosonion* assemblage (motile shallow infauna morphogroup) of the shallow-water with lowered salinity and dysoxia, and (iii) the *Elphidium–Cibicides–Asterigerinata* assemblage (epiphytic facultative motile and non-motile morphogroup) of the shallow-water with substrate covered by algae and sea grass.

From the Sarmatian sediments, beside of (i) the *Elphidium–Cibicides* association (epiphytic, facultatively motile morphogroup) of the shallow-water with the floor covered by algae and sea grass, (ii) the foraminiferal assemblage with strong prevalence of miliolids (epiphytic morphogroup C motile on algae, biconvex, with keel and morphogroup D permanently motile miliolide coiling) documents hyperhaline conditions on the shelf. An another identified special type of very low diversified assemblage dominated by pseudoplanktic *Anomalinodes badenensis* indicates according by Filipescu (2004) restricted benthic life conditions and stimulated associations in the upper, well oxygenated, part of the water column points to stratified water column conditions.

### Conclusion

Across the whole studied area, our results confirm the Badenian/Sarmatian boundary characterized by a major change in the benthic and planktic foraminiferal assemblages. This change was proved by both methods used. Sarmatian sediments differs from the Badenian by the presence of specific assemblage with a strong prevalence of miliolids of the morphogroup D. Agglutinated foraminifers are the most affected group by BSEE which representatives are absent in the Sarmatian deposits. In the studied area the agglutinated foraminifers appear again in the Pannonian stage (Hudáčková et al. 2018).

**Acknowledgements:** This research was supported by the Slovak Research and Development Agency under contracts APVV-17-0555, APVV-16-0121, APVV-15-

0575 and APVV-14-0118. We would like to express our gratitude to Lubomír Sliva for assistance with sedimentology and sample handling and to Nafta a.s. and Pozagas a.s. companies for providing samples.

### References

- Cicha I., Čtyrtek J., Jiříček R. & Zapletalová I. 1975: Principal biozones of the Late Tertiary in the East Alps and West Carpathians. In: Cicha I. (Ed.): Biozonal division of the Upper Tertiary basins of the Eastern Alps and West Carpathians. IUGS Proceedings of the VI Congress Bratislava. *Geological survey*, Prague, 19–34.
- Filipescu S. 2004: Anomalinoidea dividens bioevent at the Badenian/Sarmatian boundary — a response to paleogeographic and paleoenvironmental changes. *Studia Universitatis Babeş-Bolyai, Geologia* 49, 2, 21–26.
- Gebhardt H., Zorn I. & Roetzel R. 2009: The initial phase of the early Sarmatian (Middle Miocene) transgression. Foraminiferal and ostracod assemblages from an incised valley fill in the Molasse Basin of Lower Austria. *Austrian J. Earth Sci.* 102, 2, 100–119.
- Harzhauser M. & Piller W.E. 2007: Benchmark data of a changing sea — Palaeogeography, Palaeobiogeography and events in the Central Paratethys during the Miocene. *Palaeogeogr. Palaeoclimatol. Palaeoecol.* 253, 8–31.
- Holcová K. 2008: Foraminiferal species diversity in the Central Paratethys — a reflection of global or local events? *Geol. Carpath.* 59, 1, 71–85.
- Hudáčková N., Soták J., Ruman A., Rybár S. & Milovský R. 2018: Marsh-type agglutinated foraminifera from Upper Miocene sediments of the Danube Basin. *Micropaleontology* 64, 5-6, 481–492.
- Jamrich M. & Halásová E. 2010: The evolution of the Late Badenian calcareous nannofossil assemblages as a reflexion of the palaeoenvironmental changes of the Vienna Basin (Devínska Nová Ves — clay pit). *Acta Geologica Slovaca* 2, 2, 123–140 (in Slovak with English summary).
- Kováčková P. & Hudáčková N. 2009: Late Badenian foraminifers from the Vienna Basin (Central Paratethys): stable isotope study and paleoecological implications. *Geol. Carpath.* 60, 1, 59–70.
- Łuczowska E. 1974: Miliolidae (Foraminiferida) from the Miocene of Poland Part II. Biostratigraphy, palaeoecology, and systematics. *Acta Palaeontologica Polonica* 19, 1, 3–176.
- Palcu D.V., Tulbure M., Bartol M., Kouwenhoven T.J. & Krijgsman W. 2015: The Badenian–Sarmatian Extinction Event in the Carpathian foredeep basin of Romania: Paleogeographic changes in the Paratethys domain. *Global Planet. Change* 133, 346–358.
- Peryt D. & Jasionowski M. 2012: Sarmatian foraminiferal assemblages of cavern fillings in the Badenian reefs of Medobory (Polupanivka, Western Ukraine). *Biuletyn Państwowego Instytutu Geologicznego* 449, 175–184.
- Tóth E. & Görög Á. 2008: Sarmatian foraminifera fauna from Budapest (Hungary). In: Galász A. (Ed.): 125<sup>th</sup> Anniversary of the Department of Palaeontology at Budapest University. A jubilee volume, *Hantkeniana* 6, 187–217.

# Peperites and other volcano-sedimentary deposits (lowermost Cretaceous, Berriasian) of the Ukrainian Carpathians

MICHAŁ KROBICKI<sup>1</sup>, ANNA FELDMAN-OLSZEWSKA<sup>2</sup>, OLEH HNYLKO<sup>3</sup>  
and JOLANTA IWAŃCZUK<sup>2</sup>

<sup>1</sup>AGH University of Science and Technology, Mickiewicza 30, 30-059 Kraków, Poland; krobicki@geol.agh.edu.pl

<sup>2</sup>Polish Geological Institute – National Research Institute, Rakowiecka 4, 00-975 Warszawa, Poland;  
anna.feldman-olszewska@pgi.gov.pl, jolanta.iwanczuk@pgi.gov.pl

<sup>3</sup>Institute of Geology and Geochemistry of Combustible Minerals of National Academy of Science of Ukraine, Naukova 3a,  
79060 Lviv, Ukraine; ohnilko@yahoo.com

**Abstract:** In two analyzed regions: Kamyanyi Potik Unit of the Fore-Marmarosh Unit (Chyvchyn Mt) and the Pieniny Klippen Belt (Velykyi Kamianets quarry) of the Ukrainian Carpathians classical peperites are developed. It is a very unique consortium of volcanogenic rocks and limestones which occur together as sedimentary episode of submarine eruption of basaltic lavas on the unconsolidated wet carbonate mud. Peperites co-occur with another volcano-sedimentary rocks (basaltic pillow lavas, pyroclastic debris flows and pyroclastic turbidite system) which are perfect proof for age of volcanic activity by dating of limestones both by macro- and micro-fossils and indicate their Berriasian age.

## Introduction

In the frontal part of the Marmarosh Massif in the Ukrainian Carpathians the Outer Dacides–Severinides are represented by the Kamyanyi Potik and Rachiv units (nappes) and are most probably the prolongation of the Black Flysch unit of the Romanian Carpathians (Fig. 1). The Rachiv nappe is represented by folded Lower Cretaceous flysch dipping generally toward the southwest under the Kamyanyi Potik unit and is overthrust on the Porkulets Nappe (Ślącza et al. 2006 with references). The Kamyanyi Potik Unit (Nappe) is the most internal and structurally highest unit of the Fore-Marmarosh units and in many places is directly covered by the Marmarosh nappes of the Central East Carpathians (Marmarosh Massif). But its connection with surrounding units is still matter of discussion by several authors (Boyko 1970; Vialov et al. 1981; Kruglov 1986; Ślącza et al. 2006). By the first author this unit is interpreted as part of the Radomyr zone of the Marmarosh Massif. According to Vialov et al. (1981) it belongs to the Rahiv Nappe, Kruglov (1986) consider this thrust sheet as a part of the Marmarosh Massif, and for Ślącza et al. (2006) this unit is a part of the Marmarosh nappes. The most probably Kamyanyi Potik Unit forms the separate nappe, which extends at the front of the Marmarosh nappes and consists of the uppermost Jurassic Chyvchyn Formation (up to 1000 m thickness) composed mainly by basic effusives, and the earliest Cretaceous (Berriasian–Valanginian(?)) Kamyanyi Potik Formation (thickness 200 m) represented by dark, thin-bedded limestones, black shales, sandstones and conglomerates with

volcanic material, which pass upward into thick-bedded psammities (thickness about 400 m).

## Volcano-sedimentary units of the Ukrainian Carpathians

### *The Kamyanyi Potik Unit*

#### *Chyvchyn Mount (1766.1 m a.s.l.)*

The best places for study of this unit occur both on the Chyvchyn Mount (1766.1 m a.s.l.) — the highest peak of the Chyvchyn Mountains, and in the Rahiv city vicinity (Kamyanyi stream — stratotype of the Kamyanyi Potik Unit) (Fig. 2). First geological structure of this mountains was shown on the geological map published by Zapałowicz (1886) and Pazdro (1934), where volcano-sedimentary deposits were attributed to the Triassic. Recently, geological mapping work showed that this complex forms the tectonic klippe which consists four small tectonic slices (Krobicki et al. 2014; Hnylko et al. 2015) and biostratigraphical investigations (calpionellids — Iwańczuk et al. 2015) indicate Berriasian age at least of lower part of the Kamyanyi Potik Formation. Volcanic–sedimentary complex of the Chyvchyn Mt, does not form a single stratigraphic sequence, as it was considered in previous studies (Hnylko et al. 2007; Matskiv et al. 2009). On the other hand, the basic volcanites of the Chyvchyn Mt have been studied by many geologists (Lomize 1968; Medvedev & Varitchev 2000 with literature cited therein). Recently, geological

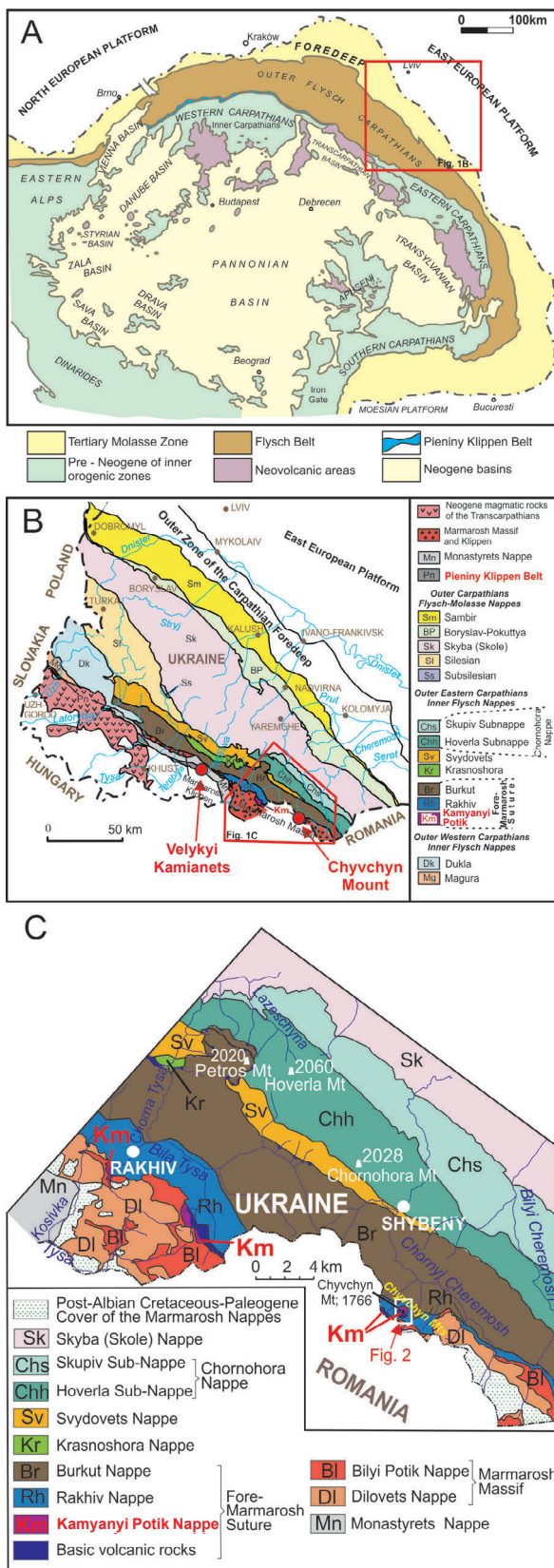


**Fig. 1.** Tectonic sketch map of the Alpine–Carpathian–Pannonian–Dinaride basin system (A — modified after Plašienka et al. 2000) and main tectonic units of the Ukrainian Carpathians (B — Hnylko 2012, modified) with location of study area (C — after Hnylko et al. 2015 with references)

mapping work showed that this complex forms the tectonic klippe which consists four small tectonic slices (Hnylko et al. 2015).

Structurally the lowermost, **first slice** (I) (100–200 m in thickness) (Fig. 2) is developed as thin-bedded light and dark-gray micritic *Maiolica*-type limestones with lenses of dark cherts and is interbedded by coarse/fine-grained calcareous pyroclastic turbidites (flysch) (Kamyanyi Potik Fm.) and is similar to stratotype of this formation in the Kamyanyi Potik stream near Rakhiv (Krobicki 2012; Hnylko et al. 2015). They are thin-bedded layers full of pyroclastic materials with classical features of turbiditic beds manifested by graded fractionation, sharp erosive base of beds, subtle cross-bedding structures, intercalations of shaly–pyroclastic materials between beds — typical Bouma sequence development.

The **second slice** (II) (250–300 m) is filled mostly by calcareous–pyroclastic breccia/conglomerates (“gravelstones”) with volcano-tuffitic matrix and different size of blocks, pebbles and olistoliths of micritic and organo-detritic limestones (often with corals and other benthic fauna; even huge blocks over 5 m), which genetically represent submarine debris flows. From sedimentological point of view this type of sediment represents classical proximal-type of mass movements very close to source area, and records apron-type submarine debris flows with cohesive mechanism of sedimentation.

The **third slice** (III) (up to 30–40 m) is filled by classical peperites — limestones with irregular clasts of basaltic rocks, sometimes as pillow lava fragments (Krobicki 2018). Peperites are special kind of volcano-sedimentary rocks where sharp-boundaries volcanic pieces (usually basaltic) occur within sedimentary deposits (Figs. 2, 3) and were formed on the sea-floor as effect of submarine eruption and disintegration of magma/lavas intruding and mingling with unconsolidated, or at least poorly consolidated, wet sediment and have to be automatically simultaneous with surrounding sediments (e.g., Busby-Spera & White 1987; Skilling et al. 2002; Chen et al. 2016).

The **fourth slice** (IV) (200–250 m) crop out on the Chyvchyn peak and is represented by massive basalts of typical pillow lava structures. The primary volcano-sedimentary sequence was presumably beginning from basaltic pillow lava flows, then peperites, great debris flows with olistoliths and distal pyroclastic turbidities finally, intercalated by micritic, pelagic limestones (*Maiolica*-type). In this case peperites were transitional event between main submarine basaltic flooding and mingling with carbonate mud on the sea-floor (Krobicki 2018).

### The Pieniny Klippen Belt

In the Velykyi Kamianets active quarry (Pieniny Klippen Belt) (Fig. 3) a unique section with continuous Lower Jurassic to lowermost Cretaceous (Berriasian) sedimentary succession occur with precise biostratigraphical data (ammonites, calpionellids and dinoflagellates) (Reháková et al. 2011; Grabowski et al. 2019). In the uppermost part of this section basaltic rocks overlie white *Calpionella*-bearing limestones (Krobicki et al.

2008; Oszczytko et al. 2012), which are dating by this microfossils as Middle Berriasian in age. On the other hand, above basaltic bed occur synsedimentary breccia (so-called Walentowa Breccia Member of the Łysa Limestone Formation — lithostratigraphy after Birkenmajer 1977; see also — Plašienka 2018) with clasts of this, underlying *Calpionella* limestones and with clasts of basaltic rocks. By this reason we have perfect stratigraphical control of the Middle Berriasian age of this basaltic rocks. Additionally, on the contact between *Calpionella*

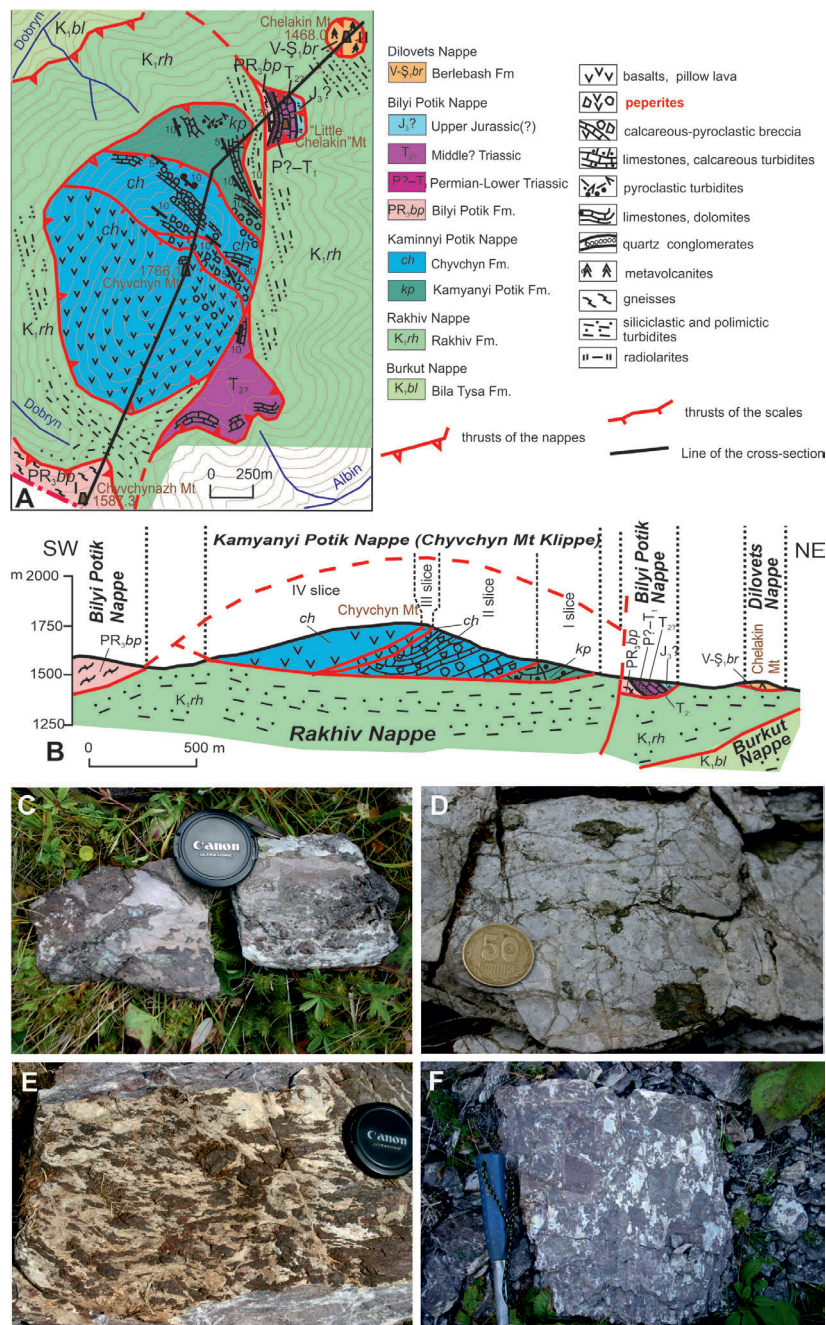


**Fig. 2.** Geological map of the Chyvchyn Mt. area (A) with geological cross-section along the black line (B) (after Hnylko et al. 2015) with examples of peperites: basaltic fragments in limestones (C); small basaltic “bombs” in coral-bearing limestones (D); desintegrated lava flow in limestones (E); pyroclastic flow mixed with limestones (F).

limestones and basalts (sometimes developed as pillow lavas) peperites have been discovered recently.

### Conclusions

In conclusion, in two analyzed cases (Chyvchyn Mt. and Velykyi Kamianets quarry) we have very unique consortium of volcanogenic rocks and limestones which occur together as sedimentary episode of submarine

eruption of basaltic lavas on the unconsolidated wet carbonate mud. Such volcano-sedimentary structure is additional perfect proof for age of volcanic activity by dating of limestones, which are sometimes full both in macro-fossils (e.g., corals of the Štramberg-type limestones — shallow-water carbonates known as olistoliths and exotic pebbles in flysch deposits of the Outer Carpathians; e.g., Eliášová 2008; Kołodziej 2015 with literature cited therein) and micro-fossils (calpionellids) which are Berriasian in age (Iwańczuk et al. 2015).

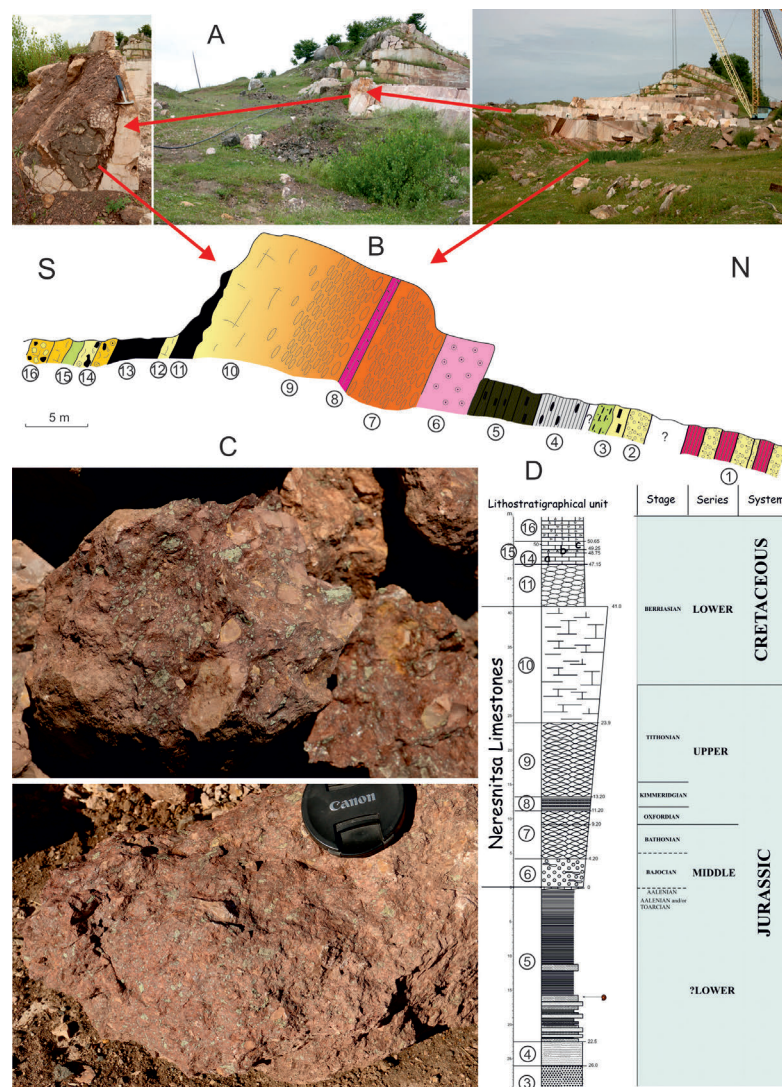


**Fig. 3.** General view of Velykyi Kamianets quarry (A) and studied section (B) with Jurassic and lowermost Cretaceous rocks [after Krobicki 2012; modified; lithostratigraphical names adopted from Birkenmajer 1977]; explanations: 1–5 — Hettangian(?)–lowermost Bajocian: 1 — white-yellowish conglomerates and cherry shales; 2 — yellow sandstones; 3 — fine-grained sandstones and mudstones with coal; 4 — black shales with sphaeroidites; 5 — mudstones with bivalve coquina; Bajocian: 6 — pink crinoidal limestones (Smolegowa and/or Krupianka Limestone Formation); uppermost Bajocian–Oxfordian: 7 — red nodular limestones of the Ammonitico Rosso-type facies (Niedzica Limestone Formation); Kimmeridgian: 8 — red thin-bedded radiolarites (Czajakowa Radiolarite Formation); Upper Kimmeridgian–Upper Tithonian: 9 — red nodular limestones of the Ammonitico Rosso-type facies (Czorsztyn Limestone Formation); 10–16 — Upper Tithonian–Berriasian: 10 — creamy and white Calpionella limestones (Dursztyn Limestone Formation); 11 & 13 — black basalts (including peperites); 12 — creamy biodetritic limestones (Harbatowa Limestone Member of the Łysa Limestone Formation); 14 & 16 — yellowish carbonate breccia (Walentowa Breccia Member of the Łysa Limestone Formation)] with examples of peperites (C — green pieces of volcanogenic material in limestones); 15 — green and purple tuffites; and their stratigraphical position (D — after Reháková et al. 2011).

**Acknowledgements:** This paper was financially supported by AGH UST (MK–16.16.140.315) and PGI-NRI (AF-O, JI).

## References

- Birkenmajer K. 1977: Jurassic and Cretaceous lithostratigraphic units of the Pieniny Klippen Belt, Carpathians, Poland. *Studia Geologica Polonica* 45, 2, 1–159.
- Boyko A.K. 1970: Lower Paleozoic complex of the North-western end of the Marmarosh Massif (Eastern Carpathians). Lviv, 1–247 (in Russian).
- Busby-Spera C.J. & White J.D.L. 1987: Variation in peperites textures associated with differing host-sediment properties. *Bulletin of Volcanology* 49, 765–775.
- Chen S., Guo Z., Qi J., Zhang Y., Pe-Piper G. & Piper D.J.W. 2016: Early Permian volcano-sedimentary successions, Beishan, NW China: Peperites demonstrate an evolving rift basin. *Journal of Volcanology and Geothermal Research* 309, 31–44.
- Eliášová H. 2008: Corals from the Štramberk limestone (Silesian Unit, Outer Western Carpathians, Czech Republic). *Geologia, Kwartalnik AGH* 34, 151–160.
- Grabowski J., Bakhmutov V., Kdýr Š., Krobicki M., Pruner P., Reháková D., Schnabl P., Stoykova K. & Wierzbowski H. 2019: Integrated stratigraphy and palaeoenvironmental interpretation of the Upper Kimmeridgian to Lower Berriasian pelagic sequences of the Velykyi Kamenets section (Pieniny Klippen Belt, Ukraine). *Palaeogeogr. Palaeoclimatol. Palaeoecol.* 532, 109216.
- Hnylko O. 2012: Tectonic zoning of the Carpathians in terms of the terrane tectonics. Article 2. The Flysch Carpathian — ancient accretionary prism. *Geodynamika* 12, 1, 67–78. (in Ukrainian with English summary)
- Hnylko O., Matskiv B. & Ternavskij M. 2007: Pro geologicnje polozenie ta umovi formirovanija trias-jurskich vikladiv Chyvchynskih gir (Ukrainski Karpathi). *Geologija i chemija gorjutschih kopalin* 2, 83–99 (in Ukrainian).
- Hnylko O., Krobicki M., Feldman-Olszewska A. & Iwańczuk J. 2015: Geology of the volcano-sedimentary complex of the Kamyanyi Potik Unit on Chyvchyn Mount (Ukrainian Carpathians): preliminary results. *Geological Quarterly* 59, 1, 145–156.
- Iwańczuk J., Krobicki M., Feldman-Olszewska A. & Hnylko O. 2015: Calpionellid biostratigraphy of the lowermost Cretaceous volcanogenic beds of the Kaminnyi Potik Unit (Ukrainian Carpathians). *Berichte des Institutes für Erdwissenschaften Karl-Franzens-Universität Graz* 21, 179.
- Kołodziej B. 2015: Corals of the Štramberk-type limestones from Poland: Taxonomic and palaeoecological aspects. *Neues Jahrbuch für Geologie und Paläontologie Abhandlungen* 276, 181–199.
- Krobicki M. 2012: Field trip. In: JURASSICA X: Jurassic–Lower Cretaceous deposits of the Pieniny Klippen Belt and surrounding areas (Ukraine – Transcarpathians, Eastern Slovakia), Abstracts and field trip guide-book, Rakhiv-Beňatina 25–30. 06. 2012, 31–56, 100–104, 127–130 (in Polish).
- Krobicki M. 2018: The earliest Cretaceous (Berriasian) peperites in volcano-sedimentary units of the Ukrainian Carpathians. In: Šujan M., Csibri T., Kiss P. & Rybár S. (Eds.): Environmental, Structural and Stratigraphical Evolution of the Western Carpathians, Abstract Book, 11<sup>th</sup> ESSEWECA Conference, 29<sup>th</sup> – 30<sup>th</sup> November 2018, Bratislava, Slovakia, 52–53.
- Krobicki M., Oszczytko N., Salata D. & Golonka J. 2008: Intra-plate alkaline volcanism in the Pieniny Klippen Belt (Eastern Carpathians, Ukraine). In: Németh Z. & Plašienka D. (Eds.): SlovTec 08, 6th CETeG, 23-26 April 2008, Upohlav, Pieniny Klippen Belt, Slovakia. *Proceedings and Excursion Guide*, 73–74.
- Krobicki M., Hnylko O., Feldman-Olszewska A. & Iwańczuk J. 2014: Tectono-stratigraphic position of the Kaminnyi Potik Unit in the Ukrainian Carpathians and volcanogenic rocks of Mt Chyvchyn. In: Roch R. et al. (Eds.): STRATI 2013. *Springer*, 533–537.
- Kruglov S.S. (Ed.) 1986: Tectonics of the Ukrainian Carpathians (explanatory report to the Tectonic Map of the Ukrainian Carpathians, 1:200,000). *Publ. Naukova dumka*, Kyiv (in Russian).
- Lomize M.G. 1968: Late-Jurassic volcanism of the Eastern Carpathians. *Vestnik Moskovskovo Universiteta* 6, 42–58 (in Russian).
- Matskiv B.W., Pukatsch B.D. & Hnylko O.M. 2009: Geological map of Ukraine, 1:200,000, sheet M-35-XXXI (Nadvirna), L-35-I (Viseu-De Sus). Carpathian series. Geological map without Quarternary deposits. *UkrDGRI, Kiev* (in Russian).
- Medvedev A.P. & Varitchev A. 2000: Pra-Carpathians (Construction and de-construction). Lviv (in Ukrainian).
- Oszczytko N., Salata D. & Krobicki M. 2012: Early Cretaceous intra-plate volcanism in the Pieniny Klippen Belt — a case study of the Velykyi Kamenets'/Vilkhivchuk (Ukraine) and the Biała Woda (Poland) sections. *Geological Quarterly* 56, 4, 629–648.
- Pazdro Z.T. 1934: Les Montagnes de Czywczyn. *Rocznik Polskiego Towarzystwa Geologicznego* 10, 3–149 (in Polish with French summary).
- Plašienka D. 2018: Continuity and episodicity in the early Alpine tectonic evolution of the Western Carpathians: how large-scale processes are expressed by the orogenic architecture and rock record data. *Tectonics* 37, 2029–2079.
- Plašienka D., Grecula P., Putiš M., Kováč M. & Hovorka D. 2000: Evolution and structure of the Western Carpathians: an overview. In: Grecula P., Hovorka D. & Putiš M. (Eds.): Geological evolution of the Western Carpathians. *Geocomplex*, Bratislava, 1–24.
- Reháková D., Matyja B.A., Wierzbowski A., Schlögl J., Krobicki M. & Barski M. 2011: Stratigraphy and microfacies of the Jurassic and lowermost Cretaceous of the Veliky Kamenets section (Pieniny Klippen Belt, Carpathians, Western Ukraine). *Volumina Jurassica* 9, 61–104.
- Skilling I.P., White J.D.L. & McPhie J. 2002: Peperites: a review of magma-sediment mingling. *Journal of Volcanology and Geothermal Research* 114, 1–17.
- Ślaczka A., Kruglov S.S., Golonka J., Oszczytko N. & Popadyuk I. 2006: Geology and hydrocarbon resources of the Outer Carpathians, Poland, Slovakia, and Ukraine: general geology. In: Golonka J. & Picha F. (Eds.): The Carpathians and their foreland: geology and hydrocarbon resources. *AAPG Memoir* 84, 221–258.
- Vialov O.S., Gavura S.P., Danysh V.V., Leshchuch R.J., Ponomaryova L.D., Romaniv H.M., Tsarnenko P.N. & Tsizh I.T. 1981: The history of the geologic development of the Ukrainian Carpathians. Kiev (in Russian).
- Zapałowicz H. 1886: Geologische Skizze des östlichen Theiles des Pokutisch-Marmaroscher Grenz-Karpathen. *Jahrbuch der k. k. Geologischen Reichsanstalt* 36, 361–591.

# ***Bathysiphon* microfacies and trace fossils association of the Lower Jurassic Fleckenmergel marly limestone from the Central Western Carpathians, the Pieniny Klippen Belt and the Betic Cordillera**

VLADIMÍR ŠIMO

Earth Science Institute, Slovak Academy of Sciences, Dúbravská cesta 9, 840 05 Bratislava, Slovakia; geolsimo@savba.sk

Agglutinated tests of foraminifera *Bathysiphon* sp. are highly abundant in bioturbated Lower Jurassic (Uppermost Sinemurian to Uppermost Pliensbachian) limestones in the Central Western Carpathians (Šimo & Tomašových 2013) and in the Pieniny Klippen Belt. Similar fragments of agglutinated test have been found in the Betic Cordillera at the Fuente Vidriera section (External Subbetic) and at the Arroyo Mingarrón section (Median Subbetic). Occurrences of isolated pyritic pseudomorphs of siliceous sponge spicules (Mišík 1959) and pyritized radiolarians (Reolid 2014) are typical of the Fleckenmergel facies both in the Betic Cordillera and in the Western Carpathians. Agglutinated *Bathysiphon* tests are mainly formed by pyritized sponge spicules and rarely by other bioclasts (Fig. 1). The tests of *Bathysiphon* sp. are strongly silicified. Many clusters of pyritic sponge spicules in thin sections probably belong to fragments of tests of these agglutinated foraminifers. Sponge spicules arrangement within the walls is random but inner walls of lumen are characteristically smooth. In contrast, the outer side of the wall test is bristly and contains spicules that project out of the wall. *Bathysiphon* tubular tests are oriented either horizontally or vertically/subvertically relative to the bedding planes. Horizontally-oriented tests are probably affected by postmortem displacement owing to bioturbation whereas vertically/subvertically oriented tests are preserved in living position. A diameter of agglutinated tubular test is 1.4 to 6.8 mm. Their length varies from few millimeters to 28 mm in thin sections. The original length thus probably attained several tens millimeters. Diameters of internal lumen vary from 0.4 to 3.6 mm. Width of the test wall is between 0.2 to 2 mm. *Bathysiphon major* (Gooday 1988) has similar morphological parameters with here described *Bathysiphon* sp. *Bathysiphon* microfacies is an important feature on the ichnofacies background of bioturbated Lower Jurassic limestones that contain almost identical trace fossils in the Central

Western Carpathians and the Betic Cordillera. This association of trace fossils is typical for the Lower Jurassic bioturbated Fleckenmergel and Fleckenkalk marls and limestones. Trace fossils association co-occurring with *Bathysiphon* contains *Chondrites intricatus*, *C. targionii*, *Lamellaeichnus imbricatus*, *Nereites* isp., *Paleophycus heberti*, *Pilichnus dichotomus*, *Planolites* isp., *Teichichnus* isp., *Thalassinoides* isp., *Trichichnus simplex*, *Zoophycos* isp. *Nereites* isp. occurs in the Betic only, but *Lamellaeichnus imbricatus* and *Teichichnus* isp. can be considered as characteristic and the most common ichnofacies components of the Lower Jurassic Fleckenmergel type of rock in the Central Western Carpathians, the Pieniny Klippen Belt and the Betic Cordillera. The Central Western Carpathians and the Pieniny Klippen Belt were situated at northern passive margin of the Tethys during Lower Jurassic (Golonka & Wierzbowski 2006). The Betic Cordillera palaeogeographic area was situated in the westernmost part of the Tethys (Bassoulet et al. 1993). Comparison of these distant palaeogeographic areas on the basis of ichnofacies analysis and on the basis of the unique *Bathysiphon* microfacies improves the reconstruction of low-energy palaeoenvironments dominated by the deposition of bioturbated marls and marly limestone during Lower Jurassic.

**Acknowledgements:** This work was supported by the Scientific Grant Agency of the Ministry of Education of the Slovak Republic and the Slovak Academy — VEGA 0186/17.

## References

- Bassoulet J.P., Poisson A., Elmi S., Cecca F., Bellion Y., Guiraud R., Le Nindre Y.M. & Manivit H. 1993: Middle Toarcian (184–182 Ma). In: Dercourt J., Ricou L.E. & Vrielynck B. (Eds.): Atlas Tethys palaeoenvironmental maps. *BEICIP – FRANLAB*, Rueil-Malmaison.

Golonka J. & Wierzbowski A. 2006: Jurassic of Poland and adjacent Slovakian Carpathians In: Wierzbowski A., Aubrech R., Golonka J., Gutowski J., Krobicki M., Matyja B.A., Pieńkowski G. & Uchman A. (Eds.): Field trip guidebook. 7th International Congress on the Jurassic System, 6–18 September 2006, Kraków, Poland, 11–15.

Gooday A.J. 1988: The genus *Bathysiphon* (Protista, Foraminiferida) in the NE Atlantic: revision of some species described by de Folin (1886). *Journal of Natural History* 22, 71–93.

Mišík M. 1959: Litologický profil súvrstviem vyššieho liasu („Fleckenmergel“) Belanských Tatier. *Geologický zborník* 10, 183–187.

Reolid M. 2014: Pyritized radiolarians and siliceous sponges from oxygen-restricted deposits (Lower Toarcian, Jurassic). *Facies* 60, 789–799.

Šimo V. & Tomašových A. 2013: Trace-fossil assemblages with a new ichnogenus in “spotted” (Fleckenmergel–Fleckenkalk) deposits: a signature of oxygen-limited benthic communities. *Geologica Carpathica* 64, 355–374.

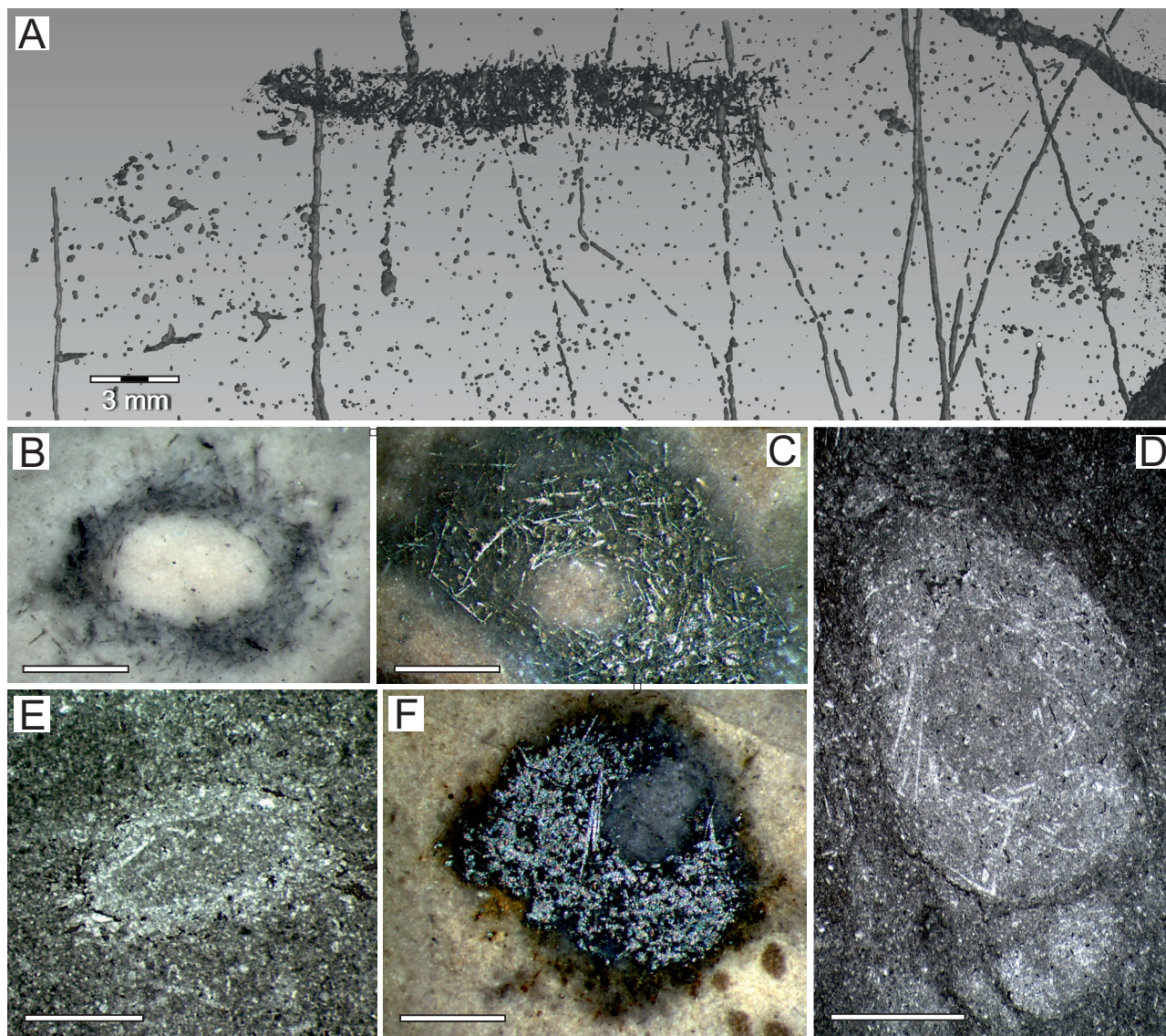


**Fig. 1.** *Bathysiphon* sp. from the Lower Jurassic Fleckenmergel marly limestone of the Central Western Carpathians, the Pieniny Klippen Belt and Betic Cordillera. **A** — Micro computed tomography of sample from the Priborzhavskoe Quarry (Uppermost Sinemurian, Pieniny Klippen Belt, Transcarpathian, Ukraine). *Bathysiphon* sp. is presented as horizontal cylindrical cluster composed from sponge spicules mostly. *Bathysiphon* sp. is situated on the top of the picture. *Trichichnus simplex* is presented by vertically situated wires. **B** — Cross-section of *Bathysiphon* sp. A wall of the lumen is smooth. Internal fill is pale in contrast with background limestone. Pyritic sponge spicules are dark and irregularly arranged. External side of the test has prickly view. (Uppermost Sinemurian, Pieniny Klippen Belt, Transcarpathian, Ukraine). **C** — Cross-section of *Bathysiphon* sp. Pyritic sponge spicules are preserved with central lumen obviously. The Skladaná Skala Quarry, the Veľká Fatra Mts., Central Western Carpathians, Slovakia (Pliensbachian). **D** — Cross-section of *Bathysiphon* sp. not pyritic agglutinated test. The Skladaná Skala Quarry (Pliensbachian). Sponge spicules are light long and thin. **E** — Cross section of not pyritic *Bathysiphon* sp. from the Arroyo Mingarrón locality (Median Subbetic, Uppermost Pliensbachian–Lower Toarcian, Spain). **F** — Sectioned *Bathysiphon* sp. test. With strongly pyritized sponge spicules. Kamenná Poruba (Malá Fatra, Pliensbachian, Central Western Carpathians, Slovakia). *Chondrites intricatus* is presented as a dark spots around the agglutinated test. Scale bars for B–F is 1 mm long.

# Research into mixed turbidite systems: Macro- and microscopic-scale observations — case study from the Szczawa Tectonic Window, the Fore-Magura zone of the Polish Outer Carpathians

PIOTR SIWEK and MAREK WENDORFF

AGH University of Science and Technology, A. Mickiewicza 30 av., 30-059 Kraków, Poland;  
petersiwek18@gmail.com, wendorff@agh.edu.pl

**Abstract:** Lower Oligocene turbiditic succession belonging to the Grybów Unit of the Fore-Magura Zone (the Polish Outer Carpathians) observed in Szczawa Tectonic Window contains mixed siliciclastic–carbonate turbidites, i.e. deposits composed of mixtures of siliciclastic grains, carbonate grains and mixture of silt, clay, carbonate mud and micrite. Co-occurrence of siliciclastic and carbonate components (called bed-scale compositional mixing) is the result of initial entrainment of these two heterogeneous fractions into sediment gravity flows, while bed-scale changes of carbonate content together with microscopic-scale, lamina by lamina segregation of components, indicate the process of hydraulic segregation of particles with different physical properties which were transported and deposited by turbidity currents. In addition to compositional mixing, strata mixing is observed in the studied succession. Strata mixing may have resulted from short-term climatic or relative sea level changes. Mixed turbidite systems, in comparison with shallow-marine mixed deposits, are poorly known and should be the subject of further comprehensive analysis.

## Introduction

Mixed deposits are composed of mixtures of siliciclastic grains (extrabasinal fraction), carbonate grains (intra-basinal fraction, mainly bioclasts and intraclasts) and mixture of silt, clay, carbonate mud and micrite (Mount 1985; Chiarella et al. 2017).

Mixed siliciclastic-carbonate deposits can be recognized and described at different scales of observation, from stratigraphic units, through lithofacies complexes to individual beds (Chiarella et al. 2017). In the first two cases, mixing results from interbedding of siliciclastic and carbonate beds and/or bedsets and it is called strata mixing. In the latter one compositional mixing occurs when siliciclastic and carbonate particles are mixed and deposited contemporaneously in time and space to form millimetre- to meter-scale beds.

Ancient deep water mixed turbidites are poorly recognized, esp. in comparison with e.g. shallow water mixed deposits (e. g. Mount 1984; Longhitano 2011; Chiarella & Longhitano 2012; Flemming 2016). Hardly any papers raise this subject, some authors only describe petrology of mixed deposits and propose their first-order compositional classification (Zuffa 1980; Mount 1985), but there is still striking lack of papers attempting to provide genetic interpretation of composition, textures and structures observed in mixed turbidite systems. Numerous

papers describe mixed shallow marine deposits where mixing of grain composition is due to supply of bioclastic components that constitute the main proportion of carbonate grains. Mount (1984) was the first who proposed conceptual models showing different types of mixing processes in shallow-water marine environments. However, these models are not applicable to deepwater depositional systems. Mixing of different scale in shallow-marine environments can greatly influence compositional mixing in deep-marine turbiditic facies because gravity driven flows transport large volumes of shallow-marine deposits into slope, continental break and basin floor domains. During downslope motion siliciclastic and carbonate components undergo further processes of mixing, sorting and possible segregation within turbulent suspension. Different physical properties (specific density or morphometry) of the grains may result in different behaviour of particles of these two populations during transportation in suspension or near bed traction and, eventually, during sedimentation.

The present authors provide preliminary results of field and microscopic observations of mixed siliciclastic–carbonate turbidites from Szczawa Tectonic Window in order to: (1) present types of vertical changes in terms of compositional and stratal mixing and (2) suggest possible genesis of particular types of mixing.

## Study area

Szczawa Tectonic Window is located in Western Outer Carpathians, 60 km south of Cracow, Poland. Along the course of Kamienica river, good quality outcrops reveal succession of deposits of Grybów Unit of Fore-Magura zone. The studied section is a 60 m thick fragment of a succession comprising lower Oligocene strata described as the Grybów Beds, and Cergowa Beds (Oszczypko-Clowes 2004) or Sub-Cergowa Beds (Uchman & Cieszkowski 2008). The succession is composed of turbiditic Bouma-type sequences (Tbcde, Tcde, Tce, Tde,...), which form very thin to very thick beds intercalated with marls (possibly deposited by turbidity currents), and thick and very thick massive sandstones described as Cergowa-type arenites.

## Materials and methods

The studied succession was chosen for detailed centimetre-by-centimetre logging, photographic documentation and sampling. Microscopic observations including carbonates content estimations were performed on 24 thin sections; moreover, 20 samples obtained from different lithological types were prepared to measure carbonates content using Scheibler's method. Qualitative analysis included description of textures and sedimentary structures, and vertical changes in grains and cements composition between different depositional intervals and within various types of sedimentary structures. Moreover, authors made an attempt to differentiate between carbonate grains, pelitic carbonate matrix and syn- and post-depositional (diagenetic) cements.

## Results

### Lithology

Turbiditic Bouma-type sequences constitute about 75 % of studied succession. They form beds 5–265 cm thick, stacked in complexes of high-frequency (bed thickness 5–55 cm) and low-frequency (bed thickness 25–265 cm) lithofacies variations. Bouma-type sequences are devoid of Ta subdivision. The lowermost parts of beds are developed as parallel-laminated sandstones (Tb), ripple cross-laminated sandstones and coarse siltstones (Tc) and parallel-laminated siltstones (Td). Sandstones and siltstones are grey, dark-grey or

grey-ashen, calcareous. Tbcd, Tcd, Td sequences/intervals can attain 30 cm in thickness. They pass into silt-mud laminations, up to 6 cm thick (Te1 lamination, Piper 1978), or directly into dark-grey, grey or black massive calcareous mudstones, or into grey/light grey massive marls (Te). Thickness of Te subdivisions vary from some centimetres to more than 150 cm (up to 225 cm), but typically does not exceed 100 cm, and commonly constitute more than 60 % of whole thickness of the single turbidite bed.

Within complexes of high-frequency lithofacies changes, there occur depositional rhythms composed of very thin and thin beds of marls alternating with very thin mudstone intercalations, up to 8 beds in one rhythm, which together form packets up to 50 cm thick. Some of marly beds show signs of lamination which may indicate their deposition from very dilute, residual turbidity currents.

The succession contains solitary extremely thick beds: sandstone–calcareous mudstone/marlstone couplets, up to 5.5 m thick. Sandstones which form lower parts of these beds are thick and very thick, medium to fine-grained, massive, with basal several-centimetre thick interval enriched in coarse and very coarse sand-sized grains and mudstone intraclasts dispersed in upper parts, in some cases in form of whole fragments of dark mudstones beds — rafts reaching 100 cm across. Uppermost parts of sandstones exhibit signs of soft-sediment deformation (pore-waters escape) and laminated structures (e.g., dune-like forms or wavy laminations), followed through grain-size break by normally-graded calcareous mudstones enriched in muscovite and grading into massive marlstones.

### Compositional mixing and strata mixing

Almost the entire succession contains carbonates as: (1) skeletal grains (lithoclasts and bioclasts) and matrix/cements or (2) almost only matrix/cements with minor fraction of carbonate grains. The first case corresponds to classical definition of compositional mixing, i.e. mixing of siliciclastic and carbonate skeletal grains with co-occurrence of clay minerals and pelitic carbonate matrix and cements, and it is applicable to sandstones and siltstones. The second case generally refers only to mudstones and marlstones.

Sandstones and siltstones developed as Tb/Tc/Td divisions of Bouma sequence contain relatively high proportion of carbonates, varying from 15 % to more than 50 % of rock total weight. Rarely, carbonates occur only as pore-filling cements with no carbonate grains in

“pure” siliciclastic arenites. Much more common are sandstones and siltstones which contain both pore-filling carbonate matrix or cements, and carbonate grains. The proportion of the latter ones in total grain population changes from less than 1–2 % of bulk volume of framework grains (only single particles are present) to more than 30 % in some laminated siltstones and sandstones. Carbonate grains occur mostly as abraded lithoclasts of micrite/sparry texture, and bioclasts – foraminifera tests and other microplanctonic skeletal remains. Microscopic observations of laminated intervals reveals two regularities: (1) segregation of components in ripple cross-laminations within single cross lamina: lower lamina enriched in heavy minerals (pyrite/hematite, zircon), middle lamina consisting mostly of siliciclastic grains with medium grain coarser than in lower one, and upper lamina enriched in carbonate grains (both bioclasts and intraclasts, occasionally almost only bioclasts); lamina with heavy minerals is sometimes absent; (2) alternating of silt laminae enriched in carbonates and laminae depleted of carbonates; the first are rich in siliciclastic grains, the latter — noticeably enriched in clay minerals and muscovite. What is important, carbonate content correlates with number and size of siliciclastic grains.

Massive sandstones which constitute the lower part of extremely thick beds, are usually lacking significant amount of carbonate grains in total grain number, at least these contain no carbonate grains, matrix and cements. These sandstones are (1) quartz arenites with subordinate feldspar grains and rock fragments of metamorphic rocks, mudstones, sandstones and carbonates, or (2) quartz/sublithic wackes with mudstone and sandstone lithoclasts, and carbonate or carbonate-clayey cements/matrix. In some beds, the first graded vertically into the latter ones.

In the studied succession, there are different patterns of change of carbonates content in vertical profiles of individual beds. In the case of turbidite beds composed of Bouma-type sequence, carbonates content: (1) increases towards bed top — Tbcd, Tcd, Tc, Td intervals usually contain relatively high proportion of carbonates (20–35 % of total weight) and grades into marlstones which contain more than 40 % of carbonates; (2) is highest in laminated intervals (some ripple cross-laminated intervals contain more than 50 % of carbonates in rock total weight) and decreases upward — carbonates are replaced in part by clay minerals. In one extremely thick, bipartite bed, within massive sandstone, carbonate content increases from zero (lower two meters) to about 25 %, then decreases slightly in Te

interval (to 20 % of rock total weight) just above sandstone and eventually increases when grading into marlstone. The highest content of carbonates is recorded from depositional rhythms composed of thin-bedded marlstones, where it ranges from 40 % to 60 % of rock total weight.

In the studied section, only characteristic depositional rhythms composed of thin-bedded marlstones (carbonate beds), which interbed turbidite beds (mixed ones) fit the definition of strata mixing used by Chiarella et al. (2017). Moreover, it is the example of coexistence of compositional and strata mixing.

## Discussion

The structures and textures of laminated intervals, especially segregation of components, were formed due to hydraulic separation of fractions of different physical properties. Hydraulic sorting is most effective in some cross laminae: heavy siliciclastic grains are separated from lighter and coarser bioclasts. Similarly, quartz-carbonate rich and clay-muscovite rich couplets of laminae originated via hydraulic separation of coarse and heavy particles from light and buoyant components. Moreover, a part of pelitic carbonate matrix observed in quartz-carbonates rich laminae may have originated from physical abrasion of carbonate grains, especially those derived from unconsolidated/poorly consolidated carbonate muds.

Changes of carbonate content in vertical profiles of beds may be owing to segregation of carbonate grains and pelitic carbonate matrix within sediment gravity flows and result in deposition of massive, thick sandstones with upper part enriched in carbonates. Decrease of carbonate content in some pelitic intervals just above silt- and sand-sized intervals is associated with increase in content of clay minerals and muscovite deposited from dilute turbidity currents.

Mixing of marlstone rhythms with turbidite beds, classified as strata mixing of bed-scale, can be interpreted, according to Chiarella et al. (2017), as the result of: (1) short-term sea level changes and deposition of marlstone rhythms during relative sea level rise; (2) short-term climate changes from arid (marlstones) to humid (turbidite beds) conditions or (3) tectonic control on the sediment supply from the continent. Moreover, the occurrences of extremely thick sandstone-marlstone beds may indicate catastrophic events, e.g. floods or large-volume submarine slumps triggered by seismic shocks or tsunamis.

## Perspectives

The extensive research into mixed turbidite systems is still missing, both in terms of depositional processes, grain and chemical composition and source areas for different constituents, and their interplay in depositional environment. Similar to mixed turbidites from Szczawa Tectonic Window, compositional and strata mixing is expected from other turbiditic successions with high carbonate content. Therefore, there is a vast field to further analysis.

When mixed turbidite systems are considered, a few specific research problems arise: (1) what is the source area of siliciclastic and carbonate grains and how are they mixed in marine environments; (2) how hydrodynamic processes control the distribution and organization of siliciclastic and carbonate components within turbidity currents and other sediment gravity flows; (3) how analysis of microfossils (mostly foraminifera assemblages) could enable us to interpret depositional environments from which these were redeposited; (4) how porosity and permeability vary throughout mixed turbidite beds and how these properties are affected by depositional and diagenetic processes. In addition, we need to differentiate between carbonate extraclasts and intraclasts in order to get information about the source area (provenance) and to distinguish pelitic carbonate matrix and carbonate cements of different origins.

## Conclusions

On the basis of preliminary research into mixed turbidite succession from the Szczawa Tectonic Window we can conclude that:

- compositional mixing is the major type of mixing observed in the studied succession and manifests itself as the co-occurrence of siliciclastic and carbonate detrital components;
- compositional mixing results from initial entrainment of siliciclastic and carbonate detritus in shallow-marine and slope areas;

- vertical changes of carbonate content at bed-scale and microscopic-scale (lamina by lamina) reflect the process of hydraulic sorting of grains of different physical properties transported and deposited by turbidity currents;
- occurrences of marly packets which interbed the stacked turbidite beds, as well as presence of extremely thick beds (sandstone-marlstone couplets) may point to short-term climatic or relative sea level changes, and result in strata mixing.

## References

- Chiarella D., Longhitano S.G. 2012: Distinguishing depositional environments in shallow-water mixed bio-siliciclastic deposits on the base of the degree of heterolithic segregation (Gelasian, Southern Italy). *J. Sediment. Res.* 82, 962–990.
- Chiarella D., Longhitano S.G. & Tropeano M. 2017: Types of mixing and heterogeneities in siliciclastic-carbonate sediments. *Mar. Petrol. Geol.* 88, 617–627.
- Flemming B.W. 2016: Particle shape-controlled sorting and transport behavior of mixed siliciclastic/bioclastic sediments in a mesotidal lagoon, South Africa. *Geo Mar. Lett.* 37, 397–410.
- Longhitano S.G. 2011: The record of tidal cycles in mixed siliciclastic deposits: examples from small Plio–Pleistocene peripheral basins of the microtidal Central Mediterranean Sea. *Sedimentology* 58, 691–719.
- Mount J.F. 1984: Mixing of siliciclastic and carbonate sediments in shallow shelf environments. *Geology* 12, 432–435.
- Mount J.F. 1985: Mixed siliciclastic and carbonate sediments: a proposed first-order textural and compositional classification. *Sedimentology* 32, 435–442.
- Oszczypko-Clowes M. & Oszczypko N. 2004: The position and age of the youngest deposits in the Mszana Dolna and Szczawa tectonic windows (Magura Nappe, Western Carpathians, Poland). *Acta Geol. Pol.* 54, 339–367.
- Piper D.J.W. 1978: Turbidite muds and silts on deepsea fans and abyssal plains. In: Stanley D.J. & Kelling G. (Eds): *Sedimentation in Submarine Canyons, Fans and Trenches. Dowden, Hutchinson and Ross*, Stroudsburg, Pennsylvania, 163–176.
- Uchman A. & Cieszkowski M. 2008: Stop 4 — Szczawa-Centrum –Grybów Beds (Early Oligocene) and Sub-Cergowa Beds (Early Oligocene): Diplocretarion in deep-sea sediments. In: Pieńkowski G. & Uchman A. (Eds.): *Ichnological sites of Poland. The Holy Cross Mountains and the Carpathian Flysch. The Second International Congress on Ichnology. Cracow, Poland, August 29–September 8, 2008. Polish Geological Institute*, 110–115.
- Zuffa G.G. 1980: Hybrid arenites: their composition and classification. *J. Sediment. Res.* 50, 21–29.

# The Cergowa Sandstone at Stasiana and Iwla: An example of turbidity hyperpycnal flow deposits in the Outer Carpathians (Dukla region)

PIOTR SIWEK<sup>1</sup> and MAREK WENDORFF<sup>1</sup>

<sup>1</sup>AGH University of Science and Technology, A. Mickiewicza 30 av., 30-059 Kraków, Poland;  
petersiwek18@gmail.com, wendorff@agh.edu.pl

**Abstract:** Up to 350 m thick succession of the Cergowa Sandstone (Lower Oligocene) forms lenticular depositional body within the Menilite Formation of the Dukla and Silesian tectonic units. In an axial part of the studied lithosome, in Stasiana and Iwla sections, the Cergowa Sandstone is developed as the succession of deepwater deposits stacked in aggradational pattern. Detailed sedimentological study enabled to document several types of sedimentary structures with their vertical oscillations, and other characteristic sedimentary features. ‘Non-Bouma-type’ sequences, which are typical of studied sections, indicate that studied part of the succession of the Cergowa Sandstone was deposited from sustained long-lived turbidity currents. Many sedimentary features testify that these currents were fed by hyperpycnal flows initiated by river discharges. These are as follow: (1) predominance of sand-prone beds with scarcity of mudstone intercalations; (2) high proportion of tractional structures in thick-bedded sandstones; (3) occurrences of beds called ‘flood hydrographs’; (4) lack of larger erosional features in thick and very thick sandstone beds; (5) presence of partly rounded, aligned mudstone clasts in quasi-massive and massive sandstones; (6) occurrences of lofting rhythmities — a distinctive facies of hyperpycnites. Moreover, the presence of abundant plant debris derived from land and large volume of well-sorted mainly fine-grained sand point to possible supply from shelf-edge deltas fed with considerable amounts of clastic input from the exposed shelf. This was related to relative sea level fall during Oligocene Icehouse and tectonic activity of the Dukla Subbasin.

## Introduction

Hyperpycnal flow is a type of gravity flow which can occur both in lacustrine and marine settings. By its nature, hyperpycnal flows are strictly connected with direct river inflow into standing waters, especially during flood events. To create hyperpycnal discharge, river waters carrying suspended sediments must be denser than waters of the basin in order to sink and continue down the slope as sediment gravity flow. In the case of fresh-water lakes, even small amount of sediment in suspension is enough to cause the plunging of the river waters and consequently, to form hyperpycnal underflow (Mulder et al. 2003). On the contrary, marine environment requires much denser river suspensions to cause plunging of river waters.

Long-lived hyperpycnal flows differ substantially from classical turbidity currents: in terms of initiation, behaviour and related deposits. Surge type flows are related to the collapse of unstable materials in slope areas (Normark & Piper 1991). Initial submarine gravity mass movements, like slides or slumps, transform into bipartite turbulent flows which accelerate during downslope motion and then quickly lose their energy. They deposit individualised or stacked beds composed of Bouma-type sequences. On the contrary, long-lived hyperpycnal flows originate on the land as direct fluvial discharge into ambient marine waters. They are

slow-moving, but can travel for long distances and over long periods of time, as long as the river discharge continues (Zavala et al. 2011). Fluctuating flows produce composite beds: ‘non-Bouma-type’ sequences. Another difference is that hyperpycnal flow contain initially fresh interstitial water.

The Cergowa Sandstone is a lithostratigraphic subdivision of the Cergowa Beds (the Menilite Formation) of the Dukla and Silesian tectonic units, Early Oligocene in age. It comprises elongated, lenticular depositional body dominated by sandstone facies and stretching from NW to SE. An axial complex of sandstone beds, reaching up to 350 m in thickness, is laterally and vertically passing into heterolithic facies and marls. In Stasiana, Iwla or Lipowica the Cergowa Sandstone forms a complex of deposits stacked in aggradational pattern, which reflects syndepositional tectonic activity in the Dukla Subbasin and intensified subsidence coeval with efficient sediment supply to deepwater depositional system (Pszonka 2015).

## Field observations

Detailed sedimentological study enabled to document several types of sedimentary structures and facies in the Stasiana and Iwla sections. The most common sedimentary structures in sandstones are: massive *m*,

quasi-massive (*m*), stratification/spaced lamination including low-angle stratification *s*, and cross-ripple lamination *c*. Plane-parallel or wavy lamination in sandstones and siltstones *l*, occurrences of debrites *D* and massive mudstones/marlstones *M* are rare. Moreover, several intercalation of hard marly limestones *L*, up to 3 m thick, are present. ‘Non-Bouma-type’ sequences, e.g. *m-(m)-m-(m)*, *m-s-m-s* or *s-c-s-c* are commonly observed within single sandstone beds and bedsets. Single intervals of such sequences are separated by non-erosional discontinuity surfaces, amalgamation surfaces or transitional boundaries. Sequences of this type constitute thick- and very thick beds. Some beds composed of several ‘non-Bouma-type’ sequences can reach up to 8 m. Bedsets composed of many such stacked beds and devoid of mudstone intercalations can attain thickness of several tens of meters, as was documented in Iwla. The characteristic feature of the Cergowa Sandstone sections studied is the scarcity of sole structures (if present, they are mostly load casts and grooves) and larger erosional features, i.e. chutes or channels. Two types of vertical oscillations of sedimentary structures were recognized: (1) first-order oscillations of small-scale (alternations of sedimentary structures within single beds), (2) second-order large-scale oscillations distinguished on the basis of changes of *m+(m)/s+c* ratio. In the latter case, they are at the scale of over a dozen to several tens of meters.

The occurrence of mudstone clasts and coalified plant detritus is the another characteristic feature of studied profiles. The first occurs as (1) dispersed lithic grains that occur together with other framework grains (up to very coarse-grained sand), (2) larger (>1 cm across) and partly rounded clasts aligned to diffuse discontinuity surfaces in quasi-massive and massive sandstones (*m*) and *m*), (3) small clay chips and angular, tabular clasts, up to 10 cm in length aligned to stratification/lamination surfaces observed in *s* and *c* intervals; some several-centimeters-thick cross-laminated intervals abound in clay chips. Coalified plant detritus is common in siltstones and sandy siltstones, but was also observed in laminated sandstones. It is present (1) as laminae in laminated siltstones and sandstones or (2) as dispersed material in structureless siltstones. The largest plant fragments are several centimeters in length. Several thin coal intercalations, up to 1 cm thick, were recorded.

### Evidence for hyperpycnal flows

Sedimentary record of the Cergowa Sandstone implies the way this complex originated. ‘Non-Bouma-type’

sequences are here interpreted as deposits of sustained, long lived high- and normal-density turbidity currents. This type of gravity flows can produce thick and very thick composite beds under condition of quasi-steady turbulent flow and incremental aggradation of sand (Kneller & Branney 1995). Fluctuations in velocity and sediment concentration within a flow result in characteristic oscillations of sedimentary structures (Zavala et al. 2011). Therefore, it can be assumed that the discussed flows were driven by long-lived hyperpycnal discharges initiated by river effluents (Zavala et al. 2011).

There are many other indicators that suggest deposition of the Cergowa Sandstone from turbidity hyperpycnal flows. This interpretation is supported by previous work (discussed below) of Plink-Björklund & Steel (2004), Zavala et al. (2011, 2012), Pszonka (2015), Wendorff et al. (2016). Some indicators are related to paleogeography and environmental conditions of the Dukla Subbasin during deposition of the described complex. These are as follows: (1) Deposition of the Cergowa Sandstone coincides in time with relative sea level fall (during Oligocene Icehouse) and forced regression that could have resulted in forming of shelf-edge deltas fed with considerable amounts of clastic input from the exposed shelf platforms. Direct connection of fluvial deltaic system with the basin slope enabled redeposition of large amounts of well-sorted mainly fine-grained sand into deepwater system by hyperpycnal flows sourced from progressive erosion of deltaic deposits; (2) Nannofossil assemblages from the Cergowa Beds, which indicate low salinity of marine waters and even brackish coastal environment. This amplify the density contrast between river effluent and ambient marine waters sufficiently to trigger the hyperpycnal underflow; (3) Predominance of sand-prone beds with scarcity of mudstone intercalations as the effect of separation of coarse and fine populations within the flow due to buoyancy effect on the latter one and deposition of the ‘fines’ in more distal settings; (4) High proportion of tractional structures in thick-bedded sandstones, testifying to recurrences of long-lasting tractional flows; (5) Occurrences of beds called ‘flood hydrographs’. Sedimentary record of these beds is explained by the behavior of river in flood; (6) The lack of larger erosional features in thick and very thick sandstone beds. Hyperpycnal flows are relatively slow and generally not able to erode their substratum in contrary to short-living turbidity currents triggered by slope instability; (7) Presence of partly rounded, aligned mudstone clasts in quasi-massive and massive sandstones. Their position

and roundness reflect bedload transport along depositional boundaries that migrated upward during gradual aggradation of sand from long-lived flow; (8) Occurrence of siltstones with abundant coalified plant detritus and muscovite, which are interpreted as lofting rhythmites — a distinctive facies of hyperpycnites, accumulated from lofting plume, which is a typical feature of hyperpycnal flows. Moreover, the presence of abundant coalified plant material and coal laminae strongly suggest the connection of marine depositional environments with fluvial-deltaic system of sediment supply.

### Conclusions

The studied part of the succession of the Cergowa Sandstone was deposited from sustained long-lived turbidity currents. Many sedimentary features indicate that these currents were fed by hyperpycnal flows initiated by river effluents. Moreover, the presence of abundant plant debris derived from land and large volume of well-sorted mainly fine-grained sand point to possible supply from shelf-edge deltas fed with considerable amounts of clastic input from the exposed shelf. This was related to relative sea level fall during Oligocene Icehouse and tectonic activity of the Dukla Subbasin.

### References

- Kneller B.J. & Branney M.J. 1995: Sustained high-density turbidity currents and the deposition of thick massive sands. *Sedimentology* 42, 607–616.
- Mulder T., Syvitsky J. P. M., Migeon S., Faugères J.-C. & Savoye B. 2003: Marine hyperpycnal flows: initiation, behavior and related deposits. *Marine and Petroleum Geol.* 20, 861–882.
- Normark W.R. & Piper D.J.W. 1991: Initiation process and flow-evolution of turbidity currents: implications for the depositional record. *SEPM Special Publication* 46, 207–230.
- Plink-Björklund P. & Steel R. J. 2004: Initiation of turbidity currents: outcrop evidence for Eocene hyperpycnal flow turbidites. *Sedimentary Geology* 165, 29–52.
- Pszonka J. 2015: Studium sedymentologiczne warstw cergowskich w jednostce dukielskiej i przeddukielskiej Karpat fliszowych. *Instytut Gospodarki Surowcami Mineralnymi i Energią Polskiej Akademii Nauk. Studia, rozprawy, monografie*, 196 (in Polish).
- Wendorff M., Pszonka J. & Zielińska M. 2016: Cechy turbidytów i uwęglonej materii organicznej jako wskaźniki warunków zasilania basenu warstw cergowskich w Lipowicy, jedn. dukielska Karpat Zewnętrznych. In: Olszewska-Nejbert D., Filipek A., Bąbel M. & Wysocka A. (Eds.): VI Polska Konferencja Sedymentologiczna POKOS 6 „Granice Sedymentologii”, 28.06.2016–01.07.2016, Chęciny-Rzepka. *Uniwersytet Warszawski*, 137–138 (in Polish).
- Zavala C., Arcuri M., Meglio Di M., Gamero Diaz H. & Contreras C. 2011: A Genetic Facies Tract for the Analysis of Sustained Hyperpycnal Flow Deposits. In: Slatt R.M. & Zavala C. (Eds.): Sediment transfer from shelf to deep water — Revisiting the delivery system. *AAPG Studies in Geology* 61, 31–51.
- Zavala C., Arcuri M. & Blanco Valiente L. 2012: the importance of plant remains as diagnostic criteria for the recognition of ancient hyperpycnites. *Revue de Paléobiologie, vol. spéc.* 11, 457–469.

# End-Cretaceous extinction and Paleogene recovery of planktonic microfauna in the Western Carpathians: Stratigraphic constraints and paleoenvironmental proxies

JÁN SOTÁK<sup>1</sup>, SILVIA ANTOLÍKOVÁ<sup>2</sup> and TIJU ELBRA<sup>3</sup>

<sup>1</sup>Earth Science Institute, Slovak Academy of Sciences, Ďumbierska 1, 974 11 Banská Bystrica, Slovakia; sotak@savbb.sk

<sup>2</sup>Earth Science Institute, Slovak Academy of Sciences, Dúbravská cesta 9, 840 05 Bratislava, Slovakia

<sup>3</sup>Institute of Geology of the Czech Academy of Sciences, Rozvojová 269, Czech Republic

K/T boundary has been previously constrained in Western Carpathians, but its existence is still uncertain due to Laramian erosion and absence of lowermost P-series biozones (P0–P1). New evidences of the K/T boundary has been gathered from the study of stratigraphic drillings in Middle Váh Valley area, Horná Nitra Depression and Magura Zone.

K/T boundary is most properly marked in the Kršteňany KRS-3 borehole, and that by LO of *Abathomphalus mayaroensis* and FO of *Parvularugoglobigerina eugubina*. Transitional interval is also well dated by microperforate species *Globoconusa daubjergensis*, *Eoglobigerina simplicissima*, etc. The section grades upward to the Selandian formation with *Praemurica inconstans* and *Morozovella angulata*, and Thanetian formation with acme of acarininids (*A. wilcoxensis*, *A. coalingensis*, *A. pseudotopilensis*, etc.). The PETM interval is approximated by negative carbon isotopic excursion, magnetic reversal Chron C24r and appearance of excursion taxa (*Acarenina sibaiyensis*, *Discoaster araneus*). Ypresian formations are rich in diversified morozovellids (*M. formosa*, *M. subbotinae*, *M. aragonensis*, *M. lensiformis*, etc.), and higher up in Lutetian formations by species *Morozovella gorrondatxensis*, *Turborotalia frontosa*, *Acarinina topilensis*, *Globigerinatheka kugleri*, etc. Considering that, the Kršteňany section provides most complete stratigraphical record from the K/T boundary up to the late Middle Lutetian (Zone E10, pre-MECO).

K/T boundary is well constrained in plankton-rich sequence of the Žilina ZA-1 core section and Jasenica section (Fig. 1). The ZA-1 sequence begins with Maastrichtian marlstones containing of rich

globotruncanid and heterohelicid foraminifers like *Abathomphalus mayaroensis*, *Gansserina gansseri*, *Racemiquembelina fructicosa*, etc. This formation passes into dark bioturbated marls with impoverished microfauna, which higher up abruptly change to *Parasubbotina*- and *Subbotina*-rich associations of the lowermost Paleocene formation. Middle Paleocene sequences are significantly enriched in large-sized morozovellids (e.g. *M. angulata*, *M. acuta*), globanolinids (e.g. *G. pseudomenardi*, *G. compressa*) and muricate acarininids (e.g. *A. strabocela*, *A. soldadoensis*). Marly sequence also contains coralgall limestones of Kambübel Formation. Magnetic susceptibility record of Maastrichtian sequence, as well as most of the Paleocene, indicates paramagnetic behavior. A distinct change, with higher magnetic susceptibilities, is seen however at the K-T interval and lowermost Paleocene, and may indicate magneto-mineralogical variations or illustrate the paleoenvironmental changes.

K/T boundary is also inferred in deep-water sequence of the Magura Zone. It is marked by rich microfauna of guembelitrids, which indicates *Guembelitra* bloom at the K/T boundary. Herein, this stress microfauna is well documented by species *Guembelitra cretacea*, *G. danica* and *Woodbringina hornerstownensis*, which correspond to the P0 biozone of Arenillas et al. (2000). Paleocene sediments above *Guembelitra*-bearing formations differ by appearance of *Parasubbotina* species.

**Acknowledgements:** The research has been supported by VEGA project 2/0034/16, project APVV-14-0118 and GAČR project no. 19-07516S.

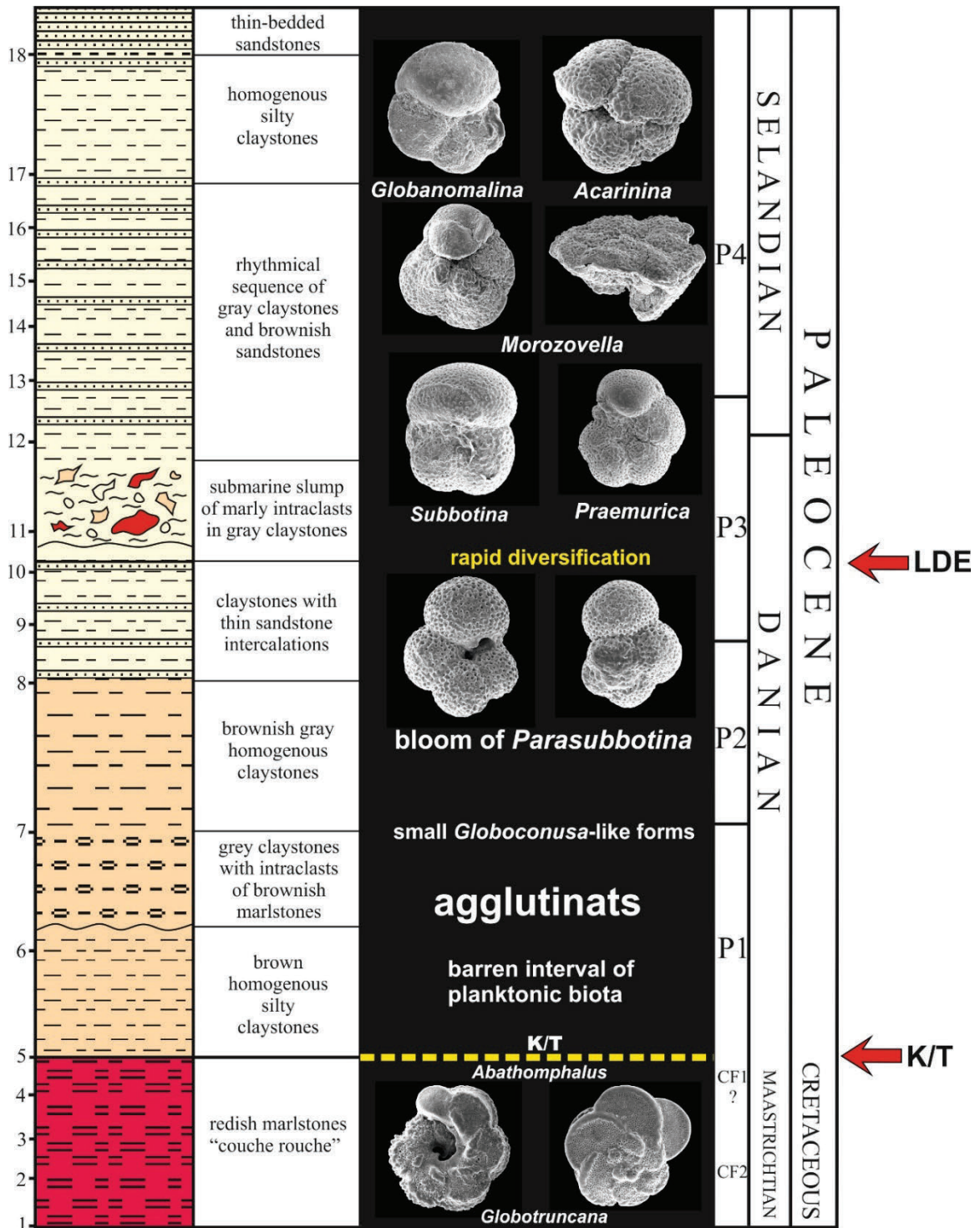


**Fig. 1.** Transitional beds through the K/T boundary showing a distinct lithological changes, disturbances (olistostromes) and turnovers in foraminiferal microfauna (Jasenica section, Mid Váh Valley). Late Danian event (LDE) marked a recovery and new radiation of planktonic foraminifers.

# Provenance of natural chalk used in ground layers of the Bohemian Gothic paintings determined by nanofossils

LILIAN ŠVÁBENICKÁ<sup>1</sup> and RADKA ŠEFCŮ<sup>2</sup>

<sup>1</sup>Czech Geological Survey, Klárov 131/3, 118 21 Prague 1, Czech Republic; lilian.svabenicka@geology.cz

<sup>2</sup>National Gallery in Prague, Staroměstské nám. 12, 110 15 Prague 1, Czech Republic

Nanofossil content found in the chalk ground layers on Bohemian panel paintings created from the 14<sup>th</sup> to the 16<sup>th</sup> century was studied from the collection of National Gallery Prague. The work was focused on markers that offered information about the place of origin of natural chalk. Pieces of painting were disintegrated in a drop of H<sub>2</sub>O<sub>2</sub> and studied by light microscope.

Nanofossils proved that sediments did not come from Bohemia. Most of samples, for example from paintings of the Master of the Vyšší Brod Cycle (ca. 1345) or Master of the Litoměřice Altarpiece (ca. 1515) contained similar assemblages (Švábenická et al. 2017). *Arkhangelskiella maastrichtiana* and *Cribrosphaerella daniae* indicate Maastrichtian, *Prediscosphaera stoveri* gives evidence for cold waters, Boreal province, and genus *Lucianorhabdus* shows on a shallow sea. So, the chalk was deposited during Maastrichtian in the epicontinental sea of North European Platform. In Middle Ages, it had to be imported along the Elbe from N and NW Europe, nowadays N Germany or Denmark. Restores of artworks call it Rügen chalk. Scarce *Micula murus*, low latitude species found in chalk ground layer under silvering (Master of the Puchner Arc) indicates the influence from the Tethyan realm and may demonstrate region located more southwards. This natural

chalk was probably imported from SW France over the Alps and restores call it Champagne chalk.

The source of natural chalk considerably influences the property of the chalk thus playing an important role for the choice of the particular material for its use in the ground layers under gilding or under color layers painting even within one artwork or in one workshop. The practice of using the different sediments of natural chalk may be characteristic for the workshop practice.

**Acknowledgements:** Work was supported by the project of the Ministry of Culture of the Czech Republic: Historical technologies and modern methods of research. The interpretative possibilities of the specialized methods of research of medieval artworks using innovative technologies (DF 13P010V010). Nanofossil analyses were carried out within the internal project of the Czech Geological Survey, No. 310380.

## References

- Švábenická L., Šefců R., Chlumská Š. & Dáňová H. 2017: Původ křídových sedimentů na středověkých deskových obrazech a řezbách na základě studia vápnitých nanofosilií. *Fórum pro konzervátory-restaurátory 2017, podzim*, 48–58.

# Actualistic paleoecology and taphonomy of the Holocene benthic assemblages in the northern Adriatic Sea: Links with the Middle Miocene ecosystems of the Vienna Basin

ADAM TOMAŠOVÝCH<sup>1</sup>, NATÁLIA HUDÁČKOVÁ<sup>2</sup> and TOMÁŠ FUKSI<sup>1</sup>

<sup>1</sup>Earth Science Institute, Slovak Academy of Sciences, Dúbravská cesta 9, 84005, Slovakia; geoltoma@savba.sk

<sup>2</sup>Department of Geology and Paleontology, Comenius University, Mlynská dolina, Ilkovičova 6, 842 15 Bratislava, Slovakia; natalia.hudackova@uniba.sk

Actualistic paleoecological and taphonomic analyses of the present-day northern Adriatic ecosystems and depositional environments can constrain paleoenvironmental and paleoecological inferences when interpreting the dynamic of benthic communities in the Miocene successions of the Central Paratethys and their responses to oceanographic regime changes (e.g., Seneš 1988a–c, 1989; Seneš & Ondrejčková 1991; McKinney & Jaklin 2001; McKinney & Hageman 2006; Zuschin & Stachowitsch 2009; Sawyer & Zuschin 2010). However, the northern Adriatic benthic communities were affected by significant anthropogenic disturbances and stresses over the past centuries and decades (Stachowitsch et al. 2012; Gallmetzer et al. 2019). One of the similarities between the present-day northern Adriatic (affected by anthropogenic impacts) and the Middle Miocene Central Paratethys basins is represented by the so-called *Corbula gibba* community that is characterized by relatively low diversity of molluscan species and by unique size structure of *C. gibba* assemblages, with high abundance of individuals >10 mm. Ecological and paleoecological analyses of the present-day Adriatic communities and Miocene paleocommunities independently indicate that this species is more resistant to seasonal oxygen depletion, pollution and sediment disturbance than most other molluscan species. Here, we show that shell-size distributions of *C. gibba* in the Danube Basin were dominated by small individuals (<5 mm) along the onshore–offshore during the Middle Miocene. In contrast, size distributions in the Vienna Basin show an increase in shell size towards deeper, offshore environments, i.e., with unimodal size-frequency distributions in shoreface sands (with most shells <5 mm), heavy-tailed size-frequency distributions at sandy oyster-reef marginal sites, and bimodal size-frequency distributions with high abundance of individuals >10 mm in deeper muddy embayments. To summarize, size distributions in the Danube Basin do not consist of individuals >10 mm whereas size distributions in the Vienna Basin are domi-

nated by individuals >10 mm. This gradient in shell-size increase correlates with an increase in proportional abundance of *Bulimina* and *Bolivina* in foraminiferal assemblages. Geographic and stratigraphic variation in proportional abundance and size of *C. gibba* can be a useful paleoecological index tracing past changes in the degree of water-column stratification and in bottom-water oxygen concentrations.

## References

- Gallmetzer I., Haselmair A., Tomašových A., Mautner A.K., Schnedl S.M., Cassin D., Zonta R. & Zuschin M. 2019: Tracing Origin and Collapse of Holocene Benthic Baseline Communities in the Northern Adriatic Sea. *Palaios* 34, 121–145.
- McKinney F.K. & Jaklin A. 2001: Sediment accumulation in a shallow-water meadow carpeted by a small erect bryozoan. *Sedimentary Geology* 145, 397–410.
- McKinney F.K. & Hageman S.J. 2006: Paleozoic to modern marine ecological shift displayed in the northern Adriatic Sea. *Geology* 34, 881–884.
- Sawyer J.A. & Zuschin M. 2010: Intensities of drilling predation of molluscan assemblages along a transect through the northern Gulf of Trieste (Adriatic Sea). *Palaeogeography, Palaeoclimatology, Palaeoecology* 285, 152–173.
- Seneš J. 1988a: The Island Banjole — A type region of recent marine ecosystems on North Adriatic shelf. *Geologický Zborník — Geologica Carpathica* 39, 713–738.
- Seneš J. 1988b: Principles of study of Adriatic shelf ecosystems from the viewpoint of applications in geology. *Geologický Zborník — Geologica Carpathica* 39, 285–300.
- Seneš J. 1988c: Quantitative analysis of north and south Adriatic shelf ecosystems. *Geologický Zborník — Geologica Carpathica* 39, 675–712.
- Seneš J. 1989: North Adriatic inter-island shelf ecosystems of the Rovinj area. *Geologický Zborník — Geologica Carpathica* 40, 333–354.
- Seneš J. & Ondrejčková A. 1991: Proposal for the terminology of fossil marine benthic shelf ecosystems. *Geologica Carpathica* 42, 231–240.
- Stachowitsch M., Riedel B. & Zuschin M. 2012: The return of shallow shelf seas as extreme environments: Anoxia and Macrofauna Reactions in the Northern Adriatic Sea. In: *Anoxia*. Springer, Dordrecht, 353–368.
- Zuschin M. & Stachowitsch M. 2009: Epifauna-dominated benthic shelf assemblages: lessons from the modern Adriatic Sea. *Palaios* 24, 211–221.



**Theme 5:**

Applied geophysics: Deep structures in orogenic belts

# Integrated geophysical modelling of the lithosphere in the Carpathian–Pannonian region: A review

MIROSLAV BIELIK<sup>1,7</sup>, HERMANN ZEYEN<sup>2</sup>, ZUZANA ALASONATI TAŠAROVÁ<sup>3</sup>,  
VITALIJ STAROSTENKO<sup>4</sup>, IRINA MAKARENKO<sup>4</sup>, OLGA LEGOSTAEVA<sup>4</sup>,  
HANS-JURGEN GOETZE<sup>5</sup>, †FRANK HORVÁTH<sup>6</sup>, ROMAN PAŠTEKA<sup>1</sup>, JANA DÉREROVÁ<sup>7</sup>,  
JAROSLAVA PÁNISOVÁ<sup>7</sup>, MICHAL GRINČ<sup>8</sup> and BARBORA ŠIMONOVÁ<sup>1</sup>

<sup>1</sup>Department of Applied and Environmental Geophysics, Faculty of Natural Sciences, Comenius University, Bratislava, Slovakia; bielik@fns.uniba.sk

<sup>2</sup>GEOPS, Univ. Paris-Sud, CNRS, Université Paris-Saclay, Orsay, France;

<sup>3</sup>Statoil ASA, Stavanger, Norway

<sup>4</sup>Institute of Geophysics, National Academy of Sciences, Kiev, Ukraine

<sup>5</sup>Institute of Geosciences, Christian-Albrechts-University, Kiel, Germany

<sup>6</sup>Geomega Ltd, Budapest, Hungary

<sup>7</sup>Earth Science Institute, Slovak Academy of Sciences, Bratislava, Slovakia

<sup>8</sup>Inset, s.r.o. Divizia Slovensko, Žilina, Slovakia

**Abstract:** Over the past ten–fifteen years, new, original and extremely valuable results have been obtained about the geophysical–geological structure and dynamics of continental lithosphere in the Carpathian–Pannonian area. These results have been obtained by modern geophysical programs (e.g., CAGES, LitMod, IGMAS+), whose common denominator is that they are able to minimize uncertainties of the estimates derived from forward modelling of various data sets separately. To further constrain our 2D and 3D models we have made use of the vast geophysical and geological data based on experiments performed in Central Europe in the past decades. The paper illustrates resultant geophysical models of the structure and composition of the lithosphere in the Carpathian–Pannonian Basin region obtained by mentioned new integrated geophysical approaches.

## Methodology

### *CAGES 2D approach*

This approach of 2D modelling is based on the joint interpretation of gravity, geoid, topography and surface heat flow data with temperature-dependent density. A finite element algorithm is used to calculate the 2D temperature distribution in the lithosphere in the steady state regime, given its thickness — defined as the 1300 °C isotherm (Zeyen & Fernández 1994).

### *LitMod 3D approach*

LitMod 3D has been developed to perform integrated geophysical–petrological LITHOSPHERIC forward MODEling of the lithosphere and the sublithospheric mantle down to the top of the transition zone at 410 km depth. The forward modelling is performed within a self-consistent thermodynamic framework, where essential physical properties in the mantle are determined as a function of the pressure, temperature, and bulk mineralogical composition. This is done by solving the appropriate heat transfer, thermodynamical, rheological, geopotential, and isostasy equations. The code allows modelling of several geophysical data sets simultaneously (Alasonati Tašarová et al. 2016).

LitMod 3-D uses the finite difference method to solve the thermal conduction equation (Fullea et al. 2010, 2014; Afonso et al. 2013a,b).

### *IGMAS+ 3D approach*

The IGMAS+ 3D (Interactive Geophysical Modelling Assistant) program is based on simultaneous forward modelling of gravity, gravity gradients, and magnetic fields (Schmidt et al. 2011, 2015; Götze 2014). The software platform offers an interdisciplinary modelling approach integrating independent data sets from seismic, boreholes, and geology, and thus reducing the ambiguity of potential field inversion. The superposition of a voxel model and triangulated surfaces gives possibility to produce complex (“hybrid”) models allowing to describe geological structures in a more realistic way (Schmidt et al. 2011; Alvers et al. 2014).

## Results

Joint modeling of surface heat flow, gravimetric, geoid and topographic data (CAGES 2D software), using geological and crustal seismic data as constraints along transects crossing the Carpathians (Dérerová et al. 2006),

allowed us to establish a new model of the lithospheric structure and the lithosphere thickness map of the Carpathian–Pannonian Basin region (Fig. 1), compiled after our results and results published earlier by Babuška et al. (1988), Horváth (1993), Lenkey (1999).

In the paper of Grinč et al. (2013) four new 2D another lithosphere-scale transects (Fig. 2) crossing central Europe from the West European Platform in the North to the Aegean Sea in the South and from the Adriatic Sea in the West to the East European Platform in the East were presented. As a case study the lithospheric model for transect B is shown in the Fig. 3.

The paper Alasonati Tašárová et al. (2016) presents the parameters and the structure of our preferred (best fitting) model obtained by LitMod 3D approach. Our lithospheric model of Central Europe combines

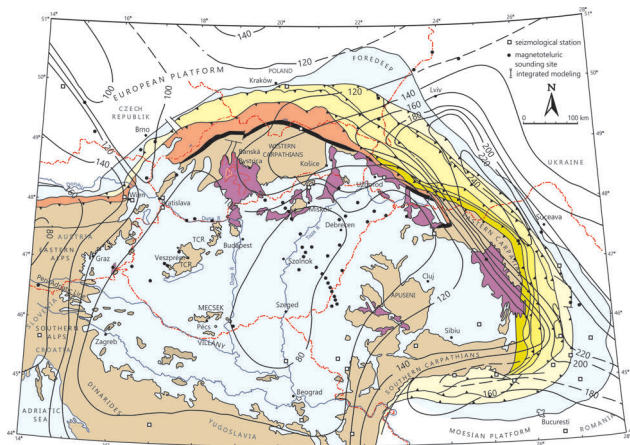


Fig. 1. Lithosphere thickness map of the Carpathian–Pannonian Basin region (modified after Dérerová et al. 2016).

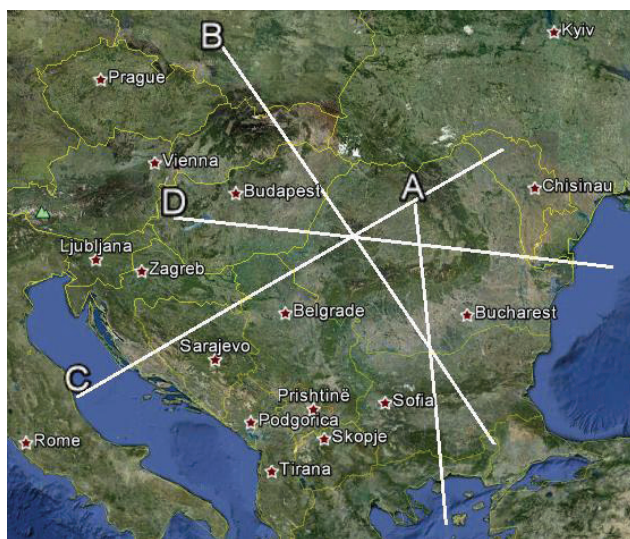


Fig. 2. Location of the interpreted transects A, B, C and D on Google Earth with overlain topography (modified after Grinč et al. 2013).

a large number of geophysical, geological, and petrological data sets at various scales into one robust and self-consistent model.

The model was divided into three main units: ALCAPA; EU, and EEC; and the location of the HVUM (red), slab (grey), and crustal EEC intrusion (blue). Note that the EU mantle has the same composition everywhere except for the shallower part of the HVUM and EEC and the deeper part of the Eastern Alpians slabs (Fig. 4).

Based on the extended modelling (Fig. 5) the following conclusions can be drawn:

1. The lithosphere in Central Europe can be divided into three main tectonic domains, characterized by distinct features:

- Thin, low density, young, hot, and fertile mantle in the Pannonian Basin. Upper/middle crust  $\sim 2750 \text{ kg/m}^3$ ; Lower crust  $< 3000 \text{ kg/m}^3$ , sediment infill up to 7–8 km locally, crust as thin as 22–32 km; and LAB depth varies between 70 and 100 km.
- Thick, cold, dense, and old mantle in the East European craton north of the TESZ; 1–2 km sediments, three-layered and relatively fast and dense crust of up to 45 km thickness. The mantle contains an upper layer composed of depleted (low-density) material.
- Neutral mantle (both in terms of composition and thickness) in the European Platform, Bohemian Massif, and Western Carpathians. No major crustal root is present underneath the Western Carpathians,

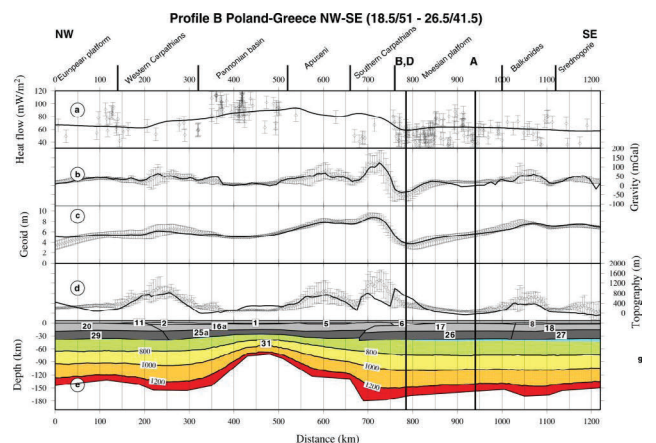
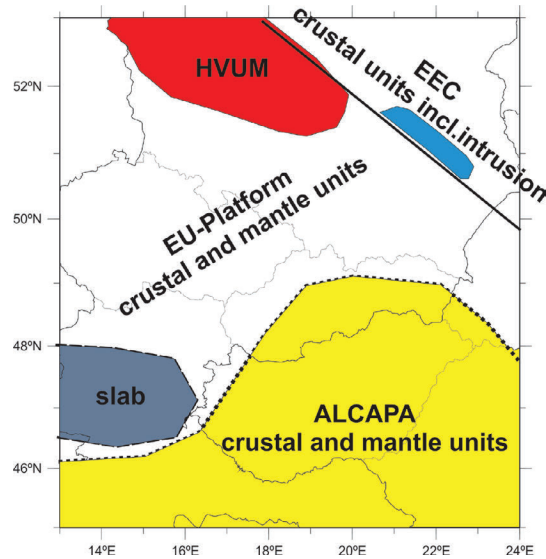
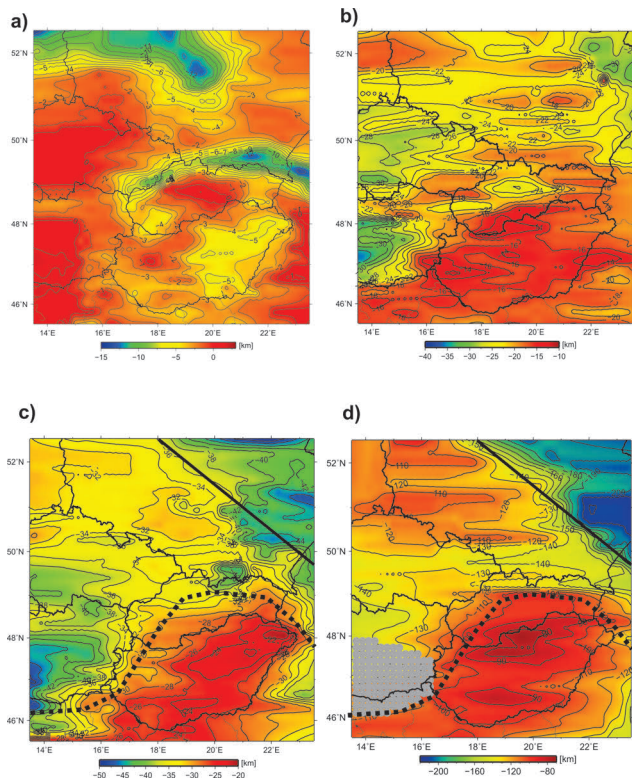


Fig. 3. Lithospheric model for transect B (modified after Grinč et al. 2013). a — Surface heat flow density; b — free-air gravity anomaly; c — geoid; d — topography with dots corresponding to measured data with uncertainty bars and solid lines to calculated values; e — lithospheric structure; numbers in (e) correspond to material number in table 1 of the paper Grinč et al. (2013). In the lithospheric mantle, isotherms are indicated every 200 °C. Numbers on top of the figures indicate the starting and end point coordinates of transects.

with the exception of some local extremes (e.g., ~45 km NE from High Tatras profiles CEL04 and CEL12, Janik et al. 2011).



**Fig. 4.** The model consists of three main units (after Alasonati Tašárová et al. 2016): ALCAPA, European platform (EU) and East European craton (EEC); and the location of the HVUM (high velocity upper mantle — red), slab in the Eastern Alpine region (grey), and crustal EEC intrusion (blue).



**Fig. 5.** Results of the modeling showing the depth to the (a) basement, (b) top of the lower crust, (c) Moho, and (d) LAB. The grey circles denote the area of the 360 km deep Alpinian slab modeled. The black lines denote the three different mantle domains (after Alasonati Tašárová et al. 2016).

2. The Alps are typical collisional orogen, and in contrast to the Western Carpathians, a distinct crustal root is present in our model. The Alpinian “suture” (slab junction) plays an important role. While the orientation of the slabs is still a matter of discussion, the presence of the cold, dense, and thick mantle lithosphere in the triple-junction area is clear from both seismic tomography and the gravity field anomalies.
3. The HVUM south of the TESZ is characterized by high-velocity and high-density material, which is interpreted to be eclogite. The very high values of seismic velocity observed and the high densities required to fit the observed topography and gravity field data rule out interpretation as an underplated magmatic body.
4. The combined geophysical-petrological modeling is a very effective tool and allows estimation of reliable mantle P/T dependent densities, temperatures and velocities (Fig. 6) in the upper mantle. Modeling of

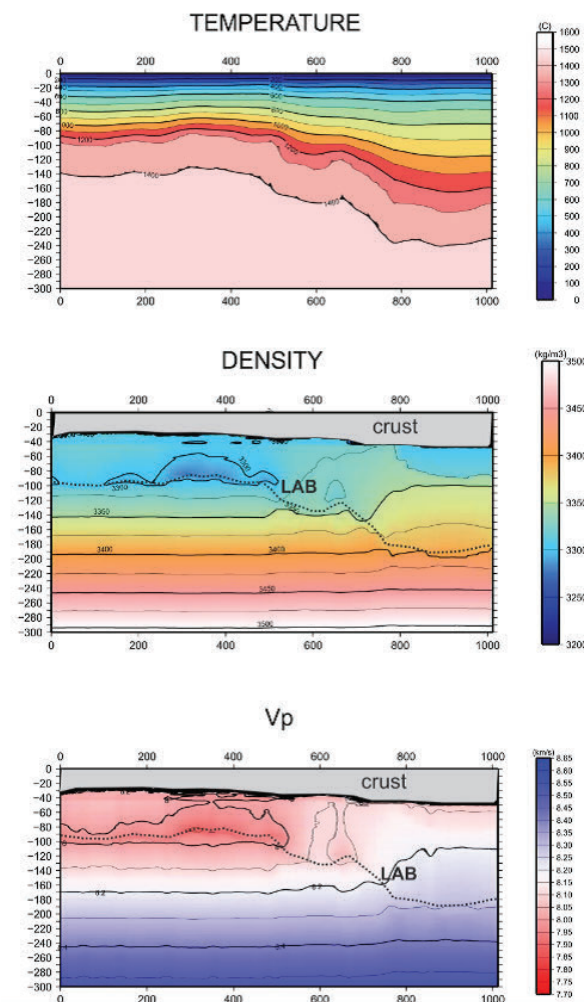


**Fig. 6.** Profile CEL01 showing the temperature, density and seismic distribution (published by Alasonati Tašárová et al. 2016).

several data sets simultaneously further reduces the ambiguity related to modelling/interpreting the different parameters /data sets separately.

The 3D geophysical modelling by IGMS+ 3D approach (Pánisová et al. 2018) was applied for interpretation of the early Late Miocene Pásztori volcano (ca. 11–10 Ma) and adjacent area in the Little Hungarian Plain Volcanic Field of the Danube Basin (Fig. 7). The gridded gravity and magnetic data (Fig. 8), interpreted seismic reflection sections and borehole data combined with re-evaluated geological constraints have been used. Based on petrological analysis of core samples from available six exploration boreholes, the volcanic rocks consist of a series of alkaline trachytic and trachyandesitic volcanoclastic and effusive rocks. The measured magnetic susceptibilities of these samples are generally very low suggesting a deeper magnetic source. The age of the modelled Pásztori volcano, buried beneath a 2 km-thick Late Miocene-to-Quaternary sedimentary sequence, is  $10.4 \pm 0.3$  Ma belonging to the dominantly normal C5 chron. Our model (Figs. 9, 10) includes crustal domains with different effective induced magnetizations and densities: uppermost 0.3–1.8 km thick layer of volcanoclastics underlain by a trachytic-trachyandesitic coherent and volcanoclastic rock units of a maximum 2 km thickness, with a top situated at minimal depth of 2.3 km, and a deeper magmatic pluton in a depth range of 5–15 km. The 3D model of the Danube Basin is consistent with

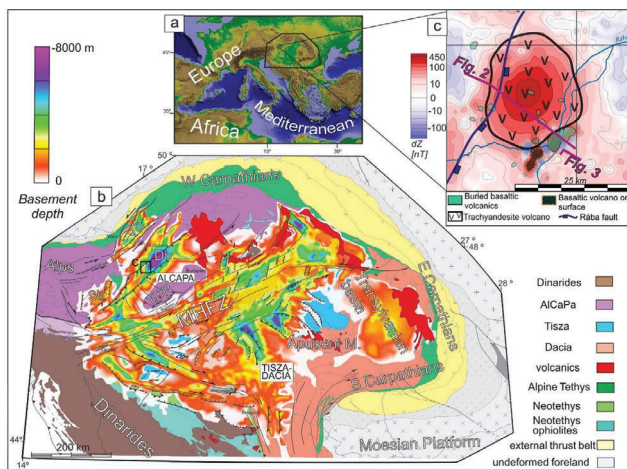


**Fig. 7.** a — Topography and location of the Pannonian Basin system of the Mediterranean region (after Pánisová et al. 2018). b — Simplified tectonic map of the Alps–Carpathians–Dinarides region overlain by the Miocene–Quaternary sedimentary thickness (in meters) of the Vienna (Vb), Pannonian and Transylvanian basins. MHFZ — Mid Hungarian Fault Zone, Db — Danube Basin, TDR — Trans-Danubian Range, Sb — Styrian Basin (modified after Balázs et al. 2017). c — Magnetic  $\Delta Z$  anomaly map of the Danube Basin overlain by the location of surface and subsurface igneous bodies.

observed high  $\Delta Z$  magnetic anomalies above the volcano, while the observed Bouguer gravity anomalies correlate better with the crystalline basement depth. Our analysis contributes to deeper understanding of the crustal architecture and the evolution of the basin accompanied by alkaline intraplate volcanism.

### The refined Moho depth map in the Carpathian–Pannonian region

The paper of Bielik et al. (2018) published a new digital Moho depth map in the the Carpathian–Pannonian region (Fig. 11). The map was produced by compiling

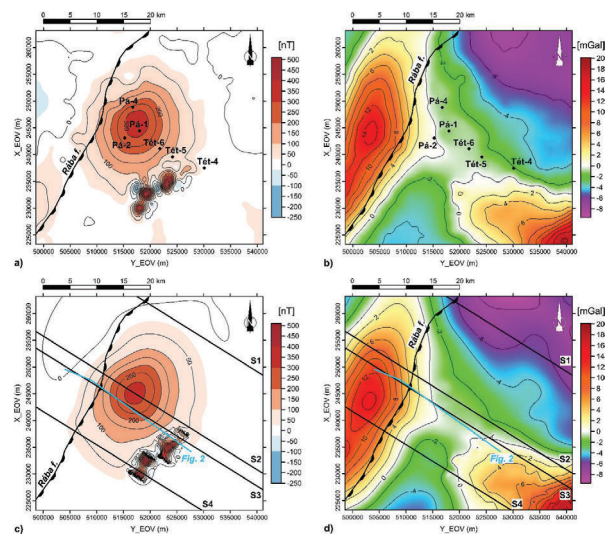


**Fig. 8.** a — Magnetic anomaly above the Pásztori volcano; b — Bouguer gravity anomaly map for a correction density of  $2.0 \text{ g cm}^{-3}$ ; c — modelled magnetic field; d — modelled gravity field. Positions of available wells are depicted by black dots with names (published by Pánisová et al. 2018).

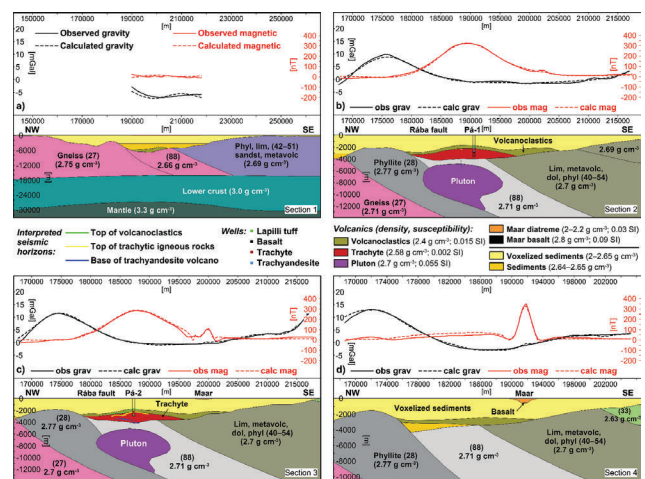


**Fig. 9.** Four selected cross sections of the final model in Section 1 (a), Section 2 (b), Section 3 (c) and Section 4 (d). Locations of particular sections (S1- oriented in NW-SE direction) are drawn by black lines in Fig. 8 (published by Pánisová et al. 2018).

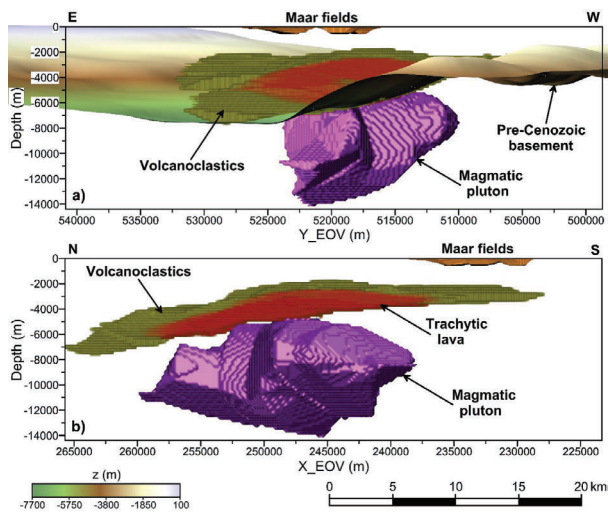


**Fig. 10.** 3D geophysical model of the Pásztori volcano (Pánisová et al. 2018): north view (a), west view (b).

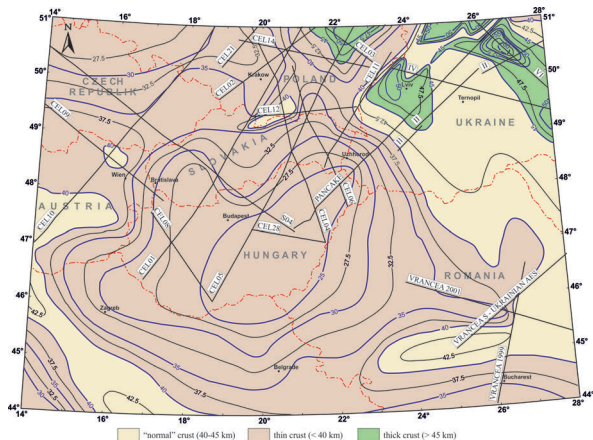


**Fig. 11.** The Moho depth map in the Carpathian–Pannonian region (modified after Bielik et al. 2018).

Moho discontinuity depth data, which were obtained by interpretation of seismic measurements taking into account the results of 2-D and 3-D integrated geophysical modelling. The resultant map is characterized by significant Moho depth variations. The trends and features of the Moho in this region were correlated with the main tectonic units, which built the studied area.

**Acknowledgements:** The work was accomplished with partial support from the grants by the APVV agency by means of projects 16-0146 and 16-0482, and from the Slovak Grant Agency VEGA by means of project 2/006/19.

## References

Afonso J.C., Fullea J., Yang Y., Connolly J.A.D. & Jones A.G. 2013a: 3D multi-observable probabilistic inversion for the compositional and thermal structure of the lithosphere and upper mantle II: General methodology and resolution analysis. *J. Geophys. Res. Solid Earth* 118, 1650–1676.

Afonso J.C., Fullea J., Griffin W.L., Yang Y., Jones A.G., Connolly J.A.D. & O'Reilly S.Y. 2013b: 3D multi-observable probabilistic inversion for the compositional and thermal structure of the lithosphere and upper mantle I: A priori information and geophysical observables. *J. Geophys. Res. Solid Earth* 118, 2586–2617.

Alasonati Tašárová Z., Fullea J., Bielik M. & Šroda P. 2016: Lithospheric structure of Central Europe: puzzle pieces from Pannonian Basin to Trans-European Suture Zone resolved by geophysical-petrological modelling. *Tectonics* 35, 1–32.

Alvers M.R., Götze H.-J., Barrio-Alvers L., Plonka C., Schmidt S., & Lahmeyer B. 2014: A novel warped-space concept for interactive 3D-geometry-inversion to improve seismic imaging. *First Break* 32, 61–67.

Babuška V., Plomerová J. & Pajdušák P. 1988: Lithosphere–asthenosphere in central Europe: Models derived from Presidials. In: Proc. 4<sup>th</sup> EGT Workshop: The Upper Mantle. *Commission of the European Communities, European Science Foundation*, Utrecht, Netherlands, 37–48.

Bielik M., Makarenko I., Csicsay K., Legostaeva O., Starostenko V., Savchenko A., Šimonová B., Dérerová J., Fojtíková L., Pašteka R. & Vozár J. 2018: The refined Moho depth map in the Carpathian–Pannonian region. *Contributions to Geophysics and Geodesy* 48, 2, 179–190.

Dérerová J., Zeyen H., Bielik M. & Salman K. 2006: Application of integrated geophysical modelling for determination of the continental lithospheric thermal structure in the eastern Carpathians. *Tectonics* 25, 3, TC3009.

Fullea J., Fernández M., Afonso J.C., Verges J. & Zeyen H. 2010: The structure and evolution of the lithosphere–asthenosphere boundary beneath the Atlantic–Mediterranean Transition Region. *Lithos* 120, 74–95.

Fullea J., Muller M.R., Jones A.G. & Afonso J.C. 2014: The lithosphere–asthenosphere system beneath Ireland from integrated geophysical–petrological modeling II: 3D thermal and compositional structure. *Lithos* 189, 49–64.

Götze H.-J. 2014: Potential method and Geoinformation Systems. In: Freeden W., Nashed M.Z., Sonar T. (Eds.): *Handbook of geomatics*. Springer, Berlin, 1–21.

Grinč M., Zeyen H., Bielik M. & Plašienka D. 2013: Lithospheric structure in Central Europe: Integrated geophysical modelling. *J. Geodyn.* 66, 13–24.

Horváth F. 1993: Towards a mechanical model for the formation of the Pannonian basin. *Tectonophysics* 226, 333–357.

Lenkey L. 1999: Geothermics of the Pannonian Basin and its bearing on the tectonics of basin evolution. *Ph.D. thesis, Free University*, Amsterdam, 1–215.

Pánisová J., Balázs A., Zalai Z., Bielik M., Horváth F., Harangi S., Schmidt S. & Götze H.-J. 2018: Intraplate volcanism in the Danube Basin of NW Hungary: 3D geophysical modelling of the Late Miocene Pásztori volcano. *International Journal of Earth Sciences* 107, 5, 1713–1730.

Schmidt S., Barrio-Alvers L. & Götze H.-J. 2015: IGMAS+: Interactive Geophysical Modelling ASistant. *Software tutorial*, <http://www.potentialgs.com>, 59.

Schmidt S., Plonka C., Götze H.-J. & Lahmeyer B. 2011: Hybrid modelling of gravity, gravity gradients and magnetic fields. *Geophys. Prospect.* 59, 6, 1046–1051.

Zeyen H. & Fernández M. 1994: Integrated lithospheric modelling combining thermal, gravity and local isostasy analysis: application to the NE Spanish Geo-transsect. *Journal of Geophysical Research* 99, 18089–18102.

Zeyen H., Dérerová J. & Bielik M. 2002: Determination of the continental lithosphere thermal structure in the Western Carpathians: integrated modelling of surface heat flow, gravity anomalies and topography. *Physics of the Earth and Planetary Interiors* 134, 89–104.

# Revision of Bouguer gravity anomalies map of Slovak Republic and interpretation of their enhanced higher derivatives

ROMAN PAŠTEKA<sup>1</sup>, PAVOL ZAHOREC<sup>2</sup>, MIROSLAV BIELIK<sup>1</sup>, VIKTÓRIA SZALAIIOVÁ<sup>3</sup>,  
 JÁN MIKUŠKA<sup>4</sup>, IVAN MARUŠIAK<sup>4</sup>, JURAJ PAPČO<sup>5</sup>,  
 DAVID KUŠNIRÁK<sup>1</sup> and MARTIN KRAJŇÁK<sup>1</sup>

<sup>1</sup>Comenius University, Department of Applied and Environmental Geophysics, Bratislava, Slovakia; pasteka1@uniba.sk

<sup>2</sup>Slovak Academy of Sciences, Earth Science Institute, Geophysical Division, Banská Bystrica, Slovakia

<sup>3</sup>Geocomplex a.s., Bratislava, Slovakia

<sup>4</sup>G-trend s.r.o., Bratislava, Slovakia

<sup>5</sup>Slovak University of Technology, Department of theoretical geodesy, Bratislava, Slovakia

This contribution deals with the revision and enrichment of the present gravimetric database of the Slovak Republic in the frame of the project APVV-0194-10 “Bouguer anomalies of new generation and the gravimetric model of Western Carpathians”. The output of this process is a new version of the complete Bouguer anomaly (CBA) map on our territory. Thanks to the taking into account of more accurate terrain corrections, this field has significantly higher quality and higher resolution capabilities. The excellent features of this map will allow us to re-evaluate and improve the qualitative interpretation of the gravity field in the research of the structural and tectonic geology of the Western Carpathian lithosphere. In the contribution we also

analyse the field of the new CBA based on the properties of various transformed fields - in particular the horizontal gradient, which by its local maximums define important density boundaries in the lateral direction (Fig. 1). Numerical derivatives in both lateral directions have been calculated by means of the concept of regularized derivatives evaluation. All original and new transformed maps make a significant contribution to improving the geological interpretation of the CBA field. Except for the horizontal gradient field, we are also interested in a new special transformation of TDXAS, which in an excellent way separates various detected anomalies of gravity field and improves their lateral delimitation and interpretation.

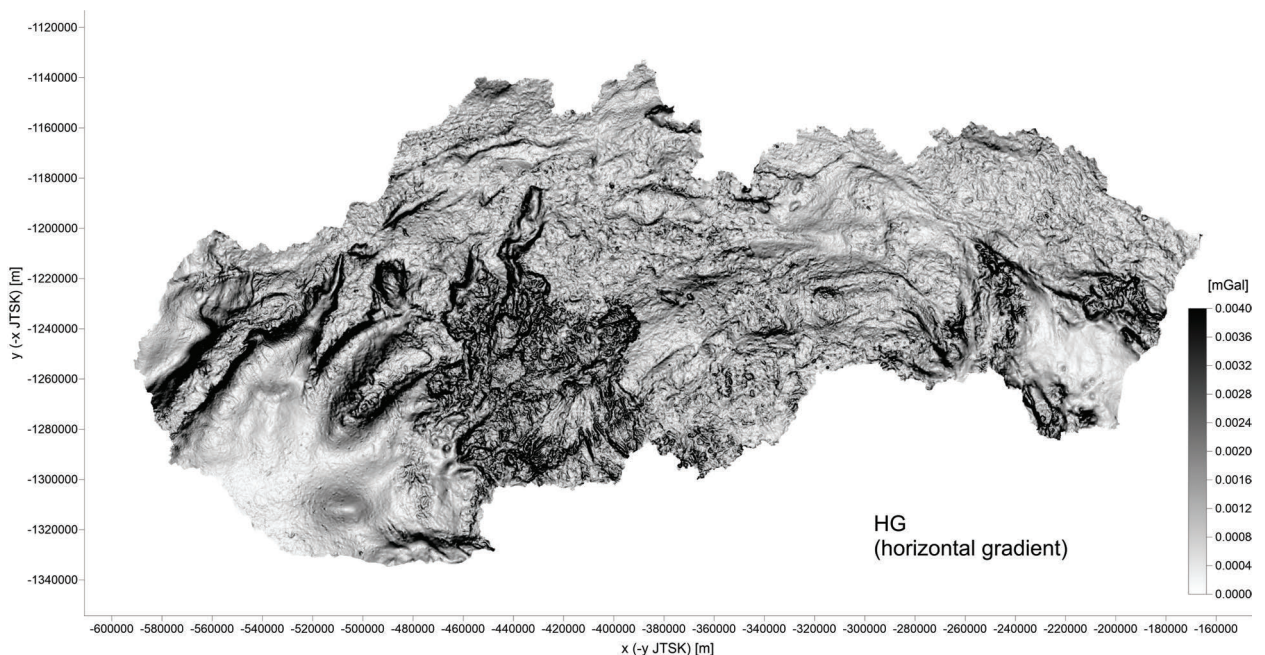


**Fig. 1.** Map of total horizontal gradient amplitudes, calculated from the complete Bouguer anomalies map of Slovak Republic (correction density:  $2670 \text{ kg.m}^{-3}$ ).

# Research of deep crustal structures by electromagnetic sounding and other geophysical methods in the northern part of Slovakia

VLADIMÍR BEZÁK<sup>1</sup>, JÁN VOZÁR<sup>1</sup>, DUŠAN MAJČIN<sup>1</sup>, MIROSLAV BIELIK<sup>1,2</sup>, DUŠAN BILČÍK<sup>1</sup>, JOSEF PEK<sup>3</sup>, RADEK KLANICA<sup>3</sup> and JOSEF TELECKÝ<sup>3</sup>

<sup>1</sup>Earth Science Institute of the Slovak Academy of Sciences, Dúbravská cesta 9, 840 05 Bratislava, Slovakia; geofbezv@savba.sk

<sup>2</sup>Comenius University, Department of applied and environmental geophysics, Ilkovičova 6, 84215 Bratislava, Slovakia

<sup>3</sup>Institute of Geophysics AS Czech Republic, Boční II/1401, 141 31 Praha 4, Czech Republic; jpk@ig.cas.cz

**Abstract:** The new results of integrated geophysical modelling of deep structures in selected areas of northern Slovakia play an important role in the precise description of the geodynamic development of the entire Carpathian–Pannonian region. This knowledge is important from a scientific point of view and has a direct impact on economic activities connected with the shallow structures of the Earth's crust. Over the last years, we are focused on modelling of magnetotelluric (MT), gravimetric, and geothermal data mainly in NW and N part of Slovakia, particularly in the wider zone of the Inner and Outer Carpathian contact.

## Methodology

Integrated modelling consisted of using mathematical algorithms to connect or represent different geophysical images (electrical conductivity, material density, and thermal parameters with depth) into a single geological interpretation model. The magnetotelluric (MT) method provides very important structural characteristics based on electrical conductivity, which is physically distinct from mechanical parameters obtained from the gravimetric and seismic methods. For example, the MT method provides much higher sensitivity to the transport properties of geological units, in particular for water (Blake et al. 2016) and melted rocks (Le Pape et al. 2012). We have used the latest methodologies and programmed tools, like IGMAS+ (Schmidt et al. 2011), JIF3D (Moorkamp et al. 2011) and LitMod (Fullea et al. 2009).

Multiple types of geophysical (electromagnetic, seismic, and gravimetric) methods utilization (Moorkamp et al. 2011) in the multi-dimensional inverse modelling, greatly enhances the correct interpretation of the collected geophysical data (Jegen et al. 2009). This approach based on the coupling between models also provides new information about the physical parameters and their relationships in the examined structures (Moorkamp et al. 2013). The MT data in form of impedance tensor were inverted to 3D geoelectrical MT models by ModEM inversion code (Kelbert et al. 2014).

## Results

For the W and N part of the Inner Western Carpathians the structure of the small mountain ranges (horsts) separated by small basins (grabens) with Tertiary sedimentary filling is typical. It is the result of the youngest stages of tectonic development in Neogene. In this case the old and newly collected geophysical data and methodology have been used concretely to model of the Tatry Mts. horst as the most northern horst in the Inner Western Carpathians and its relation to the so-called Ružbachy island (Bezák et al. 2018). Our magnetotelluric measurements focusing particularly on

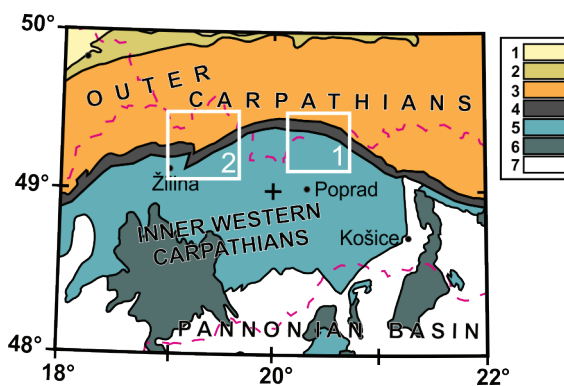


**Fig. 1.** Position of the studied areas (white rectangles). Basic tectonic map was modified after Majcin et al. (2017). Structure description: (1) European platform, (2) Foredeep units, (3) Outer Carpathian Flysch Belt, (4) Klippen Belt, (5) Inner Carpathian units, (6) Neogene volcanites on the surface, (7) Neogene sediments

the nature of the Sub-Tatra fault confirm steep dip of Sub-Tatra fault in the southern border of the Tatry Mts. Measurements show also the connection of Tatry and Ružbachy horsts to the one initially transpressional structure. The structural discordance between the axis of this structure and Klippen Belt direction is a result of younger tectonic processes.

Deep structure of Inner Carpathian Paleogene basin in the Spišská Magura Mts. and the nature of its contact with the Klippen belt units have been also investigated (Majcin et al. 2018). The older measurements from profile MT-04 (from MT continuation of the CELEBRATION 2000 project) were combined with the new perpendicular (the SW–NE oriented) MT profile SL-1 near Stará Ľubovňa, which passes through the Outer Carpathian Flysch Belt, Klippen Belt and ends in the Inner Western Carpathian Paleogene NE from Ružbachy horst structure. The 2-D geoelectrical models were reanalysed by 3-D MT modelling of the studied region, which enabled the evaluation of 3D effects in the original 2D modelling and prepares more robust and complex models (Fig. 2).

The MT data interpretations verified the northern inclination of the Flysch Belt structures and their smaller thickness out of Klippen Belt in direction to the Carpathian electrical conductivity zone (CCZ) axis. We consider this as a consequence of the flower structure—more precisely the southern branch of the suture zone related to the mentioned conductivity zone. Northerly from this zone the thickness of the Outer Carpathian Flysch Belt increases and the structures have an inclination to the south, i.e. to the subduction zone. The contact of Flysch Belt with Klippen Belt has a fault character and it is subvertical, slightly inclined to the North. The southern boundary between Klippen Belt and the Inner Western Carpathians has also fault charac-

ter and is very steep. According to our results, the depth distribution of the pre-Tertiary basement below the Inner Western Carpathian units is non-uniform; the basement is also broken to a number of partial blocks—horsts and grabens.

The interpretation of our new measured MT profile LES-1, crossing the mentioned structures in NNW-SSE direction, allows revealing the overthrusting structure of Klippen belt over Flysch belt complexes. The contact of Flysch belt and Klippen belt is not influenced by a deep fault with shifted structures as in the profile SL-1. The newest MT works confirm, among other results, also the geologic interpretations of contributions (Plašienka & Mikuš 2010; Jurewicz 2018) made in this region of study.

The deep crustal and lithospheric studies with the goal to characterized Carpathian shear corridor and its relation to the Western Carpathian deep-seated structures have been performed along old deep seismic reflection profile 2T (Bezák et al. 2016). The MT, gravimetric and geothermal data were modelled on the section in addition to seismic information and were used for the interpretation. The CCZ was not clearly presented in the older 2D MT model due to offset in linear structure visible also in the Klippen Belt. This complex shape was revealed by recent 3D MT and gravity modelling of the same area (Fig. 3).

Our methods can clearly identified the crustal segments with contrasting physical parameters and thus contrasting geological composition along this profile. Few different tectonic segments can be identified in the north part of Slovakia (North European platform with overlying Flysch Belt nappes, block of the Pienninic crust with relics of the Klippen Belt complexes, block of the Tatricum unit with typical horsts and grabens structure).

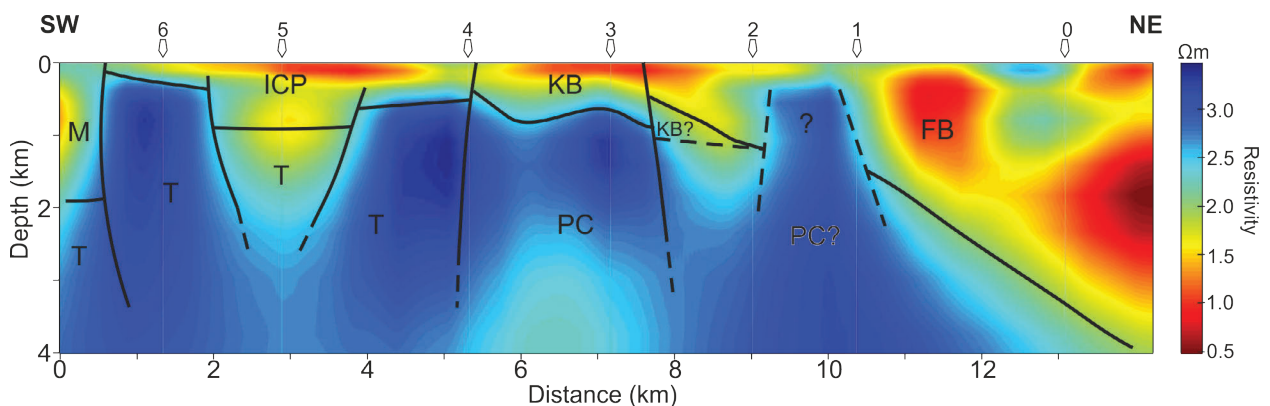


**Fig. 2.** Interpreted geoelectrical section through 3D MT inversion model along SL-01 profile (area 1 in Fig.1). Structure description: M — Mesozoic complexes, T — Tatricum unit, ICP — Inner Carpathian Paleogene, KB — Klippen Belt, PC — Pienninic crust, FB — Flysch Belt.

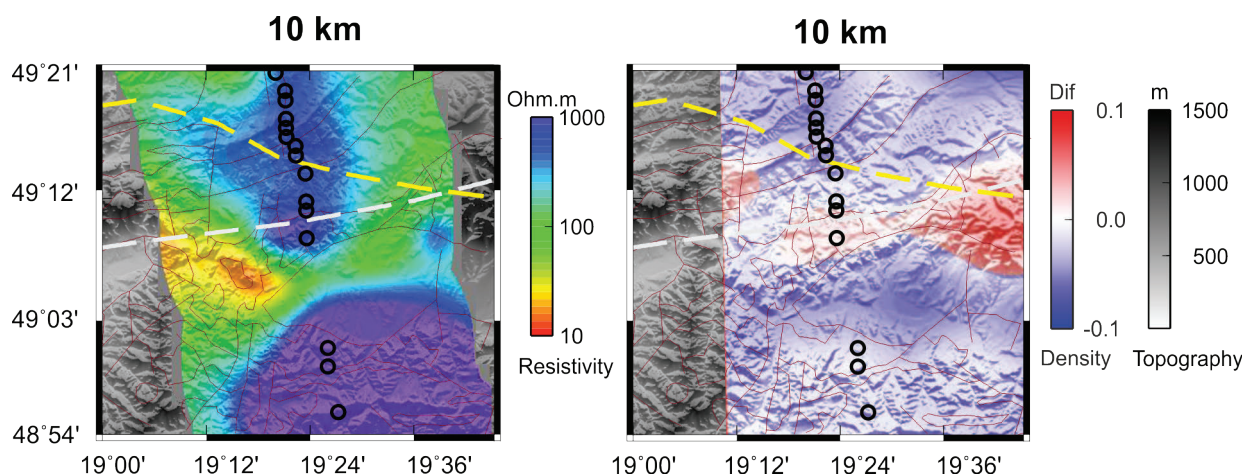


**Fig. 3.** The horizontal slices through 3-D joint inversion geoelectric and differential density models at depth 10 km in the area of northern part of the seismic 2T profile (area 2 in Fig.1). Thick dashed lines indicate expected position of the CCA based on Jankowski et al. (1985) (white) and Červ et al. (2001) (yellow).

Additionally to these regional and deep studies, the new detailed MT measurements north from the Malá Fatra Mts. have been carried out. They are focused on the nature of the offset in Klippen belt zone in this area, which may also be correlated with the shift in the CCZ in the mid-crustal depths.

Knowledge of the thermal state of the lithosphere is based on the results of direct measurements as well as modelling approaches. An important contribution to the direct research methods for whole Slovakia is also currently completed in the project focused on the hot dry rocks energy utilization (Majcin et al. 2017).

## Conclusion

Crustal structures in the northern part of Slovakia were interpreted based on MT data with help of supplementary gravity, seismic and geothermic information. The MT measurements in northern Slovakia along the northern part of seismic profile 2T and MT profile SL-01 were modelled using new processing and inversion methods. Geoelectric model reveals the position and structure of the deep crustal tectonic units and identifies major deep fault zones. The presented northern part of the model exhibits a significant influence of resistive complexes composed of Cadomian crystalline basement of European platform beneath Outer Western Carpathians conductive sediments of Flysch belt. The important contribution of the MT method for the interpretation of the crust structures is the differentiation of high-resistivity and low-resistivity complexes as physically contrasting geological bodies. Young steep shear

zones can be well identified by the MT method due to their high conductive properties.

**Acknowledgements:** The work was accomplished with partial support from the grants by the APVV agency by means of projects 16-0482 and 16-0146 and from the Slovak Grant Agency VEGA by means of project 2/006/19.

## References

- Bezák V., Pek J., Vozár J., Bielík M. & Majcin D. 2016: Magnetotelluric and Gravity Modelling of Crustal Structures in the Northern Slovakia (Western Carpathians). In: *16<sup>th</sup> Int. Multidiscip. Sci. Conf. SGEM2016*, B. 1, 3, 373–380.
- Bezák V., Majcin D., Klanica R., Vozár J. & Bilčík D. 2018: Northernmost horst in the Neoalpine “Horsts and Grabens” structure of the Western Carpathians (Tatra and Ruzbachy horsts in the northern Slovakia) in magnetotelluric data. In: *18<sup>th</sup> Int. Multidiscip. Sci. GeoConference SGEM 2018*, 1–8.
- Blake S., Henry T., Muller M.R., Jones A.G., Moor, J.P., Murray J., Campaña J. et al. 2016: Understanding hydrothermal circulation patterns at a low-enthalpy thermal spring using audio-magnetotelluric data: A case study from Ireland. *J. Appl. Geophys.* 132, 1–16.
- Červ V., Kováčiková S., Pek J., Pecova J. & Praus O. 2001: Geoelectrical structure across the Bohemian Massif and the transition zone to the West Carpathians. *Tectonophysics* 332, 201–210.
- Fullea J., Afonso J.C., Connolly J. a. D., Fernández M., García-Castellanos D. & Zeyen H. 2009: LitMod3D: An interactive 3-D software to model the thermal, compositional, density, seismological, and rheological structure of the lithosphere and sublithospheric upper mantle. *Geochemistry, Geophys. Geosystems* 10, 1–21.
- Jankowski J., Tarlowski Z., Praus O., Pecova J. & Petr V. 1985: The results of deep geomagnetic soundings in the West Carpathians. *Geophys. J. R. astr. Soc.* 80, 561–574.

- Jegen M.D., Hobbs R.W., Tarits P. & Chave A.D. (2009) Joint inversion of marine magnetotelluric and gravity data incorporating seismic constraints. Preliminary results of sub-basalt imaging off the Faroe Shelf. *Earth Planet. Sci. Lett.* 282, 47–55.
- Jurewicz E. 2018: The Šariš transitional zone, revealing interactions between Pieniny Klippen Belt, Outer Carpathians and European platform. *Swiss J. Geosci.* 111, 245–267.
- Kelbert A., Meqbel N., Egbert G.D. & Tandon K. 2014: ModEM: A modular system for inversion of electromagnetic geophysical data. *Comput. Geosci.* 66, 40–53.
- Majcin D., Bezák V., Klanica R., Vozár J., Pek J., Bilčík D. & Telecký J. 2018: Klippen Belt, Flysch Belt and Inner Western Carpathian Paleogene Basin Relations in the Northern Slovakia by Magnetotelluric Imaging. *Pure Appl. Geophys.* 175, 3555–3568.
- Majcin D., Král M., Bilčík D., Šujan M. & Vranovská A. 2017: Deep geothermal sources for electricity production in Slovakia: thermal conditions. *Contrib. Geophys. Geod.* 47, 1–22.
- Moorkamp M., Heincke B., Jegen M.D., Roberts A.W. & Hobbs R.W. 2011: A framework for 3-D joint inversion of MT, gravity and seismic refraction data. *Geophys. J. Int.* 184, 477–493.
- Moorkamp M., Roberts A.W., Jegen M.D., Heincke B. & Hobbs R.W. 2013: Verification of velocity-resistivity relationships derived from structural joint inversion with borehole data. *Geophys. Res. Lett.* 40, 3596–3601.
- Pape F. Le, Jones A.G., Vozar J. & Wenbo W. 2012: Penetration of crustal melt beyond the Kunlun Fault into northern Tibet. *Nat. Geosci.* 5, 1–6.
- Plašienka D. & Mikuš V. 2010: Geological setting of the Pieniny and Šariš sectors of the Klippen Belt between Litmanová and Drienica villages in the eastern Slovakia. *Miner. Slovaca* 42, 155–178.
- Schmidt S., Plonka C., Götze H.-J. & Lahmeyer B. 2011: Hybrid modelling of gravity, gravity gradients and magnetic fields. *Geophys. Prospect.* 59, 1046–1051.

# Contrasting magnetic fabrics in sedimentary rocks of the accretionary prisms of the Flysch Belt of the Western Carpathians and the Rhenohercynian Zone of E Bohemian Massif

FRANTIŠEK HROUDA<sup>1,2</sup><sup>1</sup>Agico Ltd., Ječná 29a, Brno, Czech Republic; hrouda@agico.cz<sup>2</sup>Institute of Petrology and Structural Geology, Faculty of Sciences, Charles University, Prague, Czech Republic

**Abstract:** The magnetic fabric of sedimentary rocks of the Flysch belt of the Western Carpathians is basically sedimentary in origin, in minority of specimens affected by very weak ductile deformation indicating only offscraping during subduction. On the other hand, the rocks of the Rhenohercynian Zone of E Bohemian Massif are often deformed strongly indicating relatively deep burial and return flow.

## Introduction

Sedimentary rocks of the accretionary prisms involved in the process of subduction at convergent margins may undergo variegated deformations ranging from offscraping and frontal accretion to doubling back and flowing up the subduction zone (Moores & Twiss 1995).

The rock deformation can be investigated by various methods of structural analysis among which the anisotropy of magnetic susceptibility (AMS) is of special importance. This is probably because the sediments of accretionary prisms mostly contain no strain markers and the AMS is one of the most sensitive indicators of strain in rocks.

The AMS investigations of accretionary prisms carried out by the present author in the past 50 years revealed large differences in the magnetic fabric of accretionary prisms of the Alpine Flysch Belt of the Western Carpathians and the Variscan Rhenohercynian Zone of the eastern Bohemian Massif (for location of study areas see Fig. 1). The present paper aims to classify the differences in terms of deformation mode during subduction.

## Flysch Belt

The magnetic fabrics in sedimentary rocks of the thrust sheets of the western sector of the Flysch Belt of the Western Carpathians range from essentially sedimentary to weakly deformational in origin (see Hrouda et al. 2009). The former magnetic fabrics are characterized by low degree of magnetic anisotropy, planar magnetic fabric, virtual parallelism of the magnetic foliations

to the bedding and close relationship of magnetic lineations to the current directions, if observable. These magnetic fabrics are typical of the thrust sheets at both margins of the Flysch Belt (Ždánice and Silesian thrust sheets in the west and Bílé Karpaty and Oravská Magura in the east). The sheets were probably detached from the wedge relatively early and underwent deformations as more or less rigid bodies. The latter magnetic fabrics showing in places significant deflections of magnetic foliations from the bedding and of magnetic lineations from the current direction are typical of the central thrust sheets, the Rača and Bystrica ones, indicating the effect of ductile deformation probably associated with creation and motion of the thrust sheets.

## Rhenohercynian Zone

The Variscan thrust sheets of the Rhenohercynian Zone of the E Bohemian Massif show very variable magnetic fabrics and deformation fabric elements (e.g. Hrouda 1979). In the easternmost areas, the Hradec–Kyjovice Formation in the Nížký Jeseník Mts. and the Myslejovice Formation in the Drahany Upland, the degree of AMS is in general weak, the magnetic fabric is oblate, the magnetic foliation is mostly parallel to the bedding, subordinately tending to create a partial girdle in its poles and the magnetic lineation is presumably parallel to current direction. The strata create buckle folds of long wavelength whose magnetic fabric can be unfolded geometrically. In the central areas, represented for instance by the Moravice Formation in the Nížký Jeseník Mts. and the Rozstání Formation in the Drahany Upland, spaced cleavage and relatively

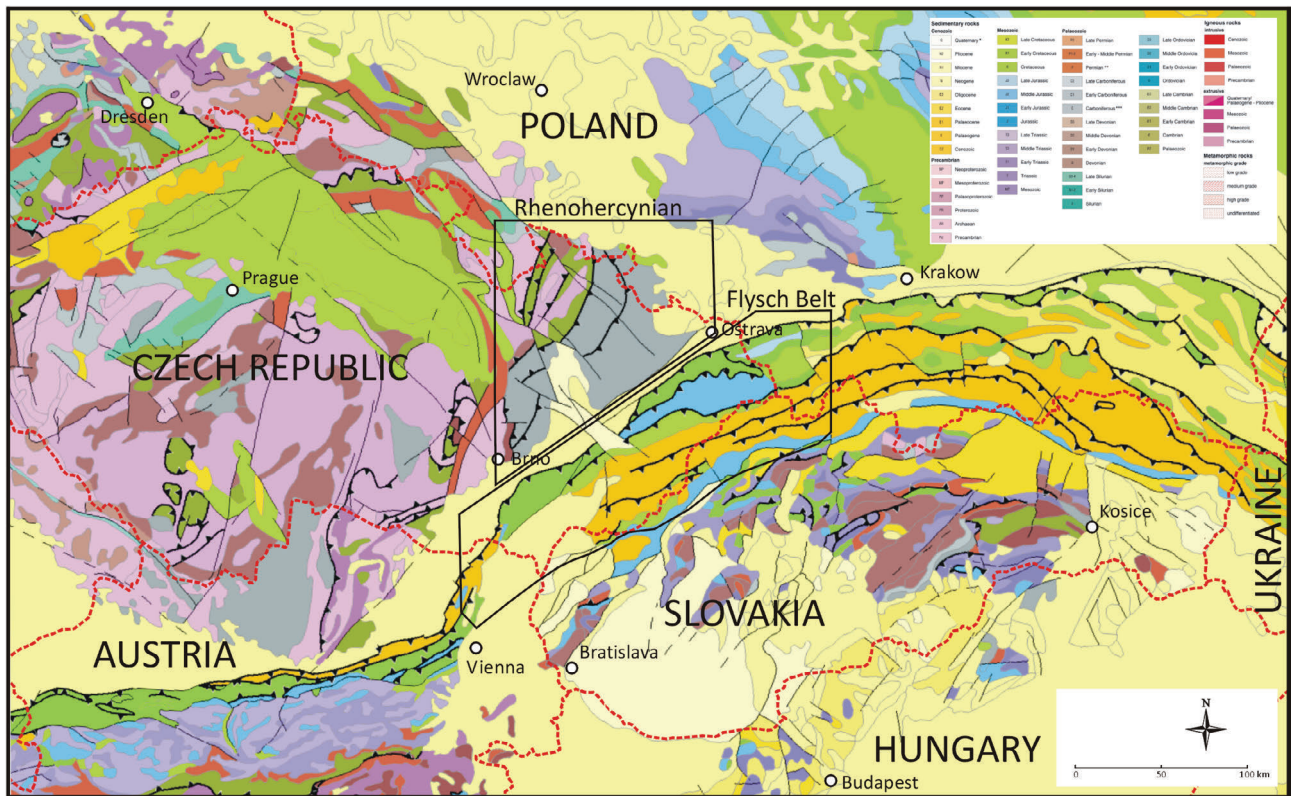


**Fig. 1.** Geological positions of the accretionary prisms of the Flysch Belt of the Western Carpathians and of the Rhenohercynian Zone of the eastern Bohemian Massif.

tight buckle folds can be observed. Magnetic foliation is still mostly parallel to the bedding, but the magnetic lineation is re-oriented into parallelism to the cleavage/bedding intersection lines. The magnetic fabric of the most folds can be unfolded only partially. In the western areas, the Benešov and Andělská Hora Formations in the Nížký Jeseník Mts. and Protivanov Formation in the Drahaný Upland, cleavage folds and very well developed slaty cleavage occur. The degree of anisotropy is high, the magnetic fabric is planar, the magnetic foliation is parallel to the slaty cleavage and the magnetic lineation is parallel to the intersection lines between bedding and cleavage. The magnetic fabric in the folds is homogeneous, the folds cannot be unfolded at all. In the western-most area of the Andělská Hora Formation, the slaty cleavage is transposed into the metamorphic schistosity.

### Tectonic implications

The story of the rocks of accretionary prisms during subduction process can be very concisely described as follows (following Moores & Twiss 1995). If the

supply of the sediment is less than or equal to the capacity of the subduction zone, the sediment entering the subduction zone may be all subducted (Fig. 2a), partly subducted and partly underplated (Fig. 2b) or partly offscraped and frontally accreted, partly subducted, and partly underplated (Fig. 2c). If the sediment supply exceeds the capacity of the subduction zone, part of the sediment doubles back and flows up the subduction zone. If the deformation of the sediment involved in the doubling back and return flow is extreme, it may produce a tectonic mélangé and the incoming sediment is offscraped and subducted, and the mélangé is underplated, offscraped and/or resubducted (Fig. 2d).

The magnetic fabric in rocks of the western sector of the Flysch Belt ranges from almost purely sedimentary in origin to very weakly deformational in origin. It corresponds to the magnetic fabric of the undeformed stage or the earliest deformation stage in terms of the magnetic fabric classification of the accretionary prisms by Parés et al. (1999) (see Fig. 3). In addition, there is no occurrence of the cleavage in the region and no indication of regional meta-morphism (Franců et al. 1999). These observations indicate that during the subduction process there was virtually no doubling back or even

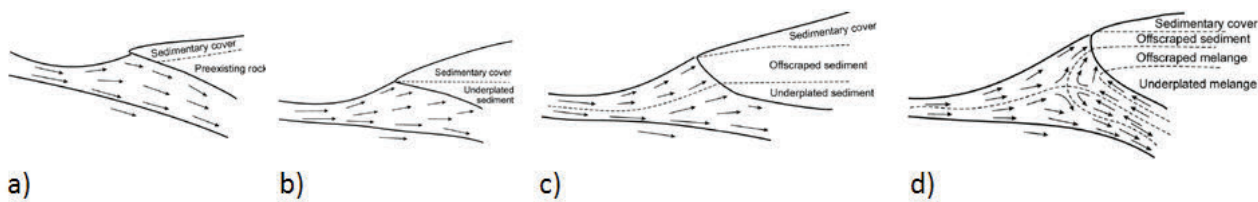


**Fig. 2.** Model of sediment flow at the inlet to the subduction zone. Adapted from Moores & Twiss (1995). Legend: **a** — all sediment is subducted; **b** — sediment is partly subducted and partly underplated; **c** — sediment is offscraped and underplated; **d** — sediment exhibits return flow.

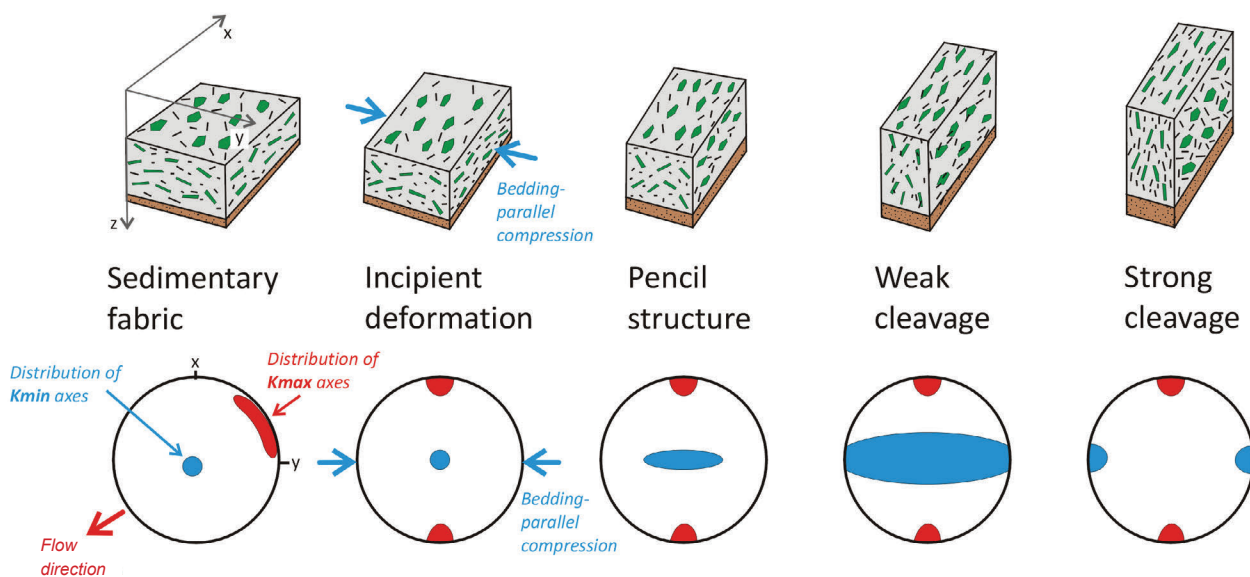


**Fig. 3.** Scheme of magnetic fabric development in progressively deformed sedimentary rocks. Adapted from Hrouda et al. (2009). Legend:  $K_{max}$  — magnetic lineation,  $K_{min}$  — magnetic foliation pole.

return flow. The capacity of the subduction zone was evidently at least equal to or larger than the supply of the sediment that was subducted, partly offscraped and accreted frontally (Hrouda et al. 2009).

The magnetic fabric in rocks of the Rheno-hercynian Zone of the eastern Bohemian Massif ranges from essentially sedimentary to strongly deformational in origin. It corresponds to the *Sedimentary Fabric* stage or the *Incipient Deformation* stage in the Hradec–Kyjovice and Myslejovice Formations, via *Pencil Structure* and *Weak Cleavage* stages in the Moravice and Rozstání Formations, to *Strong Cleavage* stage in the Andělská Hora and Protivanov Formations (see Fig. 3). The regional metamorphism ranges from diagenetic state in the eastern areas, through anchizone in the most areas, to even epizone in the westernmost area of the Andělská Hora Formation.

The strong ductile deformation and anchizone metamorphism suggest that the rocks of the Zone were probably buried relatively deeply. This burial may have taken place during the passage of the sediments to the inlet of the subduction zone. The sediments may have appeared at the surface due to return flow. In addition, the magnetic fabric elements in the crystalline rocks neighbouring this Zone in the west show similar orientations as those of the Zone. This similarity can be interpreted as obtained during the same subduction process resulting in overprinting the older metamorphic fabrics.

**Acknowledgements:** The AMS investigations were financially supported by the Geological Surveys of the Slovak and Czech Republics. The final interpretation was supported by the Czech Science Foundation (Project 18-03160S).

## References

- Franců J. et al. 1999: A model of creation, migration and accumulation of hydrocarbons (in Czech). *Unpublished report of Czech Geological Survey*, Prague, 1–122.
- Hrouda F. 1979: The strain interpretation of the magnetic anisotropy in rocks of the Nížký Jeseník Mountains (Czechoslovakia). *Sbor geol Věd, řada UG* 16, 27–62.
- Hrouda F., Krejčí O., Potfaj M. & Stránil Z. 2009: Magnetic fabric and weak deformation in sandstones of accretionary prisms of the Flysch and Klippen Belts of the Western Carpathians: Mostly offscraping indicated. *Tectonophysics* 479, 254–270.
- Moores E.M. & Twiss R.J. 1995: *Tectonics*. *Freeman and Co.*, New York, 1–415.
- Parés J.M., van der Pluijm B.A. & Dinares-Turell J. 1999: Evolution of magnetic fabrics during incipient deformation of mud-rock (Pyrenees, northern Spain). *Tectonophysics* 307, 1–14.

# The contact of the Bohemian Massif, Western Carpathians and Eastern Alps: Density modelling

LENKA ŠAMAJOVÁ<sup>1</sup>, JOZEF HÓK<sup>1</sup>, MIROSLAV BIELIK<sup>2,3</sup>  
and TAMÁS CSIBRI<sup>1</sup>

<sup>1</sup>Comenius University in Bratislava, Faculty of Natural Sciences, Department of Geology and Palaeontology, Mlynská dolina, Ilkovičova 6, 842 15 Bratislava, Slovakia; samajova7@uniba.sk

<sup>2</sup>Comenius University in Bratislava, Faculty of Natural Sciences, Department of Applied and Environmental Geophysics, Mlynská dolina, Ilkovičova 6, 842 15 Bratislava, Slovakia

<sup>3</sup>Earth Science Institute of the Slovak Academy of Sciences, Dúbravská cesta 9, 840 05 Bratislava, Slovakia

**Abstract:** The Vienna Basin is situated at the contact of the Bohemian Massif, Western Carpathians, and Eastern Alps. Deep boreholes data and existing seismic profile were used in density modelling of the pre-Neogene basement in the Slovak part of the Vienna Basin. Density modelling was carried out along profiles oriented in NW–SE direction, across expected contacts of main geological structures. From bottom to top, the four structural floors have been defined. Bohemian Massif crystalline basement with the autochthonous Mesozoic sedimentary cover sequence. The accretionary sedimentary wedge of the Flysch Belt above the Bohemian Massif rocks sequences. The Mesozoic sediments considered to be part of the Carpathian Klippen Belt together with Mesozoic cover nappes of the Alpine and Carpathians provenance are thrust over the Flysch Belt creating the third structural floor. The Neogene sediments form the highest structural floor overlying tectonic contacts of the Flysch sediments and Klippen Belt as well as the Klippen Belt and the Alpine/Carpathians nappe structures.

## Geological background

Surface geological structure of the investigated area contains the Tatricum, Fatricum and Hronicum tectonic units of the Internal Western Carpathians (IWC). The Pieniny Klippen Belt (PKB) represents the frontal part of the IWC composed mainly of Jurassic and Cretaceous sediments which underwent several phases of folding and faulting during the Late Cretaceous to Miocene (Hók et al. 2016). The Upper Cretaceous to Palaeogene sediments (Gosau Group) are present a top of the Hronicum and PKB tectonic units. The tectonic units of the Northern Calcareous Alps (NCA) are interpreted in pre-Cenozoic basement of the Vienna Basin (Fusán et al. 1987; Wessely 1992a).

The Bohemian Massif (BM) rock complexes below the External Western Carpathians (EWC) sediments are represented mainly by crystalline rocks (Picha et al. 2006). On the other hand, Wessely (1992b) suggested the occurrence of the autochthonous Mesozoic sediments of the BM in the deep substratum of the Vienna Basin. The EWC (Flysch Belt) are in the investigated territory represented by the Magura nappes system characterized by the Palaeogene and Upper Cretaceous flysch sediments on the surface (Biely et al. 1996).

## Density modelling

### *Input data*

The 2D density model was created in GM-SYS software (GM-SYS User's Guide for version 4.9, 2004). It is an interactive software for calculating the gravity field from the geologic models. 2D model is composed of closed polygons with representative density. The calculations of the gravitational effects of the geological bodies are based on the formulae of Talwani et al. (1959), with Won & Bevis's algorithm (GM-SYS User's Guide 4.9, 2004).

The gravity data were obtained from the Bouguer anomaly map with the grid of 200 x 200 m (Pašteka et al. 2017). The topography data were taken from the Topographic Institute (2012). The 2D quantitative interpretation depends on geometry of the modelled polygons that approximate geological bodies and the knowledge of the rock densities.

The surface and subsurface structure of the individual tectonic units was constrained using the geological map, structural data and deep boreholes (lithology, tectonic affiliation and sediment thickness).

The Moho depth (crustal thickness) along the profile is consistent with the Moho depth imaged in the papers of Alasonati Tašárová et al. (2016) and Bielik et al. (2018).

The lithosphere–asthenosphere boundary (lithospheric thickness) has been taken from the papers Dérerová et al. (2006) and Alasonati Tašárová et al. (2016).

The sediment densities were constrained using data summarized in paper of Šamajová & Hók (2018). The natural densities of the tectonic units which built the upper part of the upper crust were taken from the map of the tectonic units of the Western Carpathians (Šamajová & Hók 2018). Input average densities of the lower part of the upper crust, lower crust, mantle lithosphere and asthenosphere were determined by analysis of the results of Bielik (1995); Šimonová & Bielik (2016).

To make the resultant models display a good resolution of the deep and subsurface structures, while the lithosphere–asthenosphere boundary and Moho discontinuity is not shown on final model.

### Profile PF-1

Profile PF-1 passes from the Vienna Basin through the Malé Karpaty Mts. into the Danube Basin (Fig. 1). This profile was constructed parallel to seismic profile 8HR (see Vozár et al. 1999; Bielik et al. 2004). Surface geology is interpreted according to geological maps (Geological map of Slovakia 2013). The calculated gravity of the resultant model consists of the several local anomalies. The density model suggests that the EWC Magura and Krosno nappe systems are overthrust onto the BM. The PKB is interpreted as shallow structure thrust together with Mesozoic cover nappes sediments over the EWC sediments.

The affiliation to the Alpine or Carpathians tectonic provenance of the Mesozoic cover nappes was determined according to the presence or absence of anhydrite-rich strata (Opponitz Fm. the Reichenhall Fm., Haselgebirge Fm.).

The density model indicates of the fault contacts of the Malé Karpaty Mts with the Vienna and Danube Basins Deep contact of the Tatricum tectonic unit

outcropping in the Malé Karpaty Mts is slightly shifted over the Bohemian Massif.

The boundary between the upper and lower crust was modelled in a depths of about 17.5 and 19 km. The deep contact between the EWC nappes and the Bohemian Massif is characterized by a small inclination.

### Profile PF-2

Profile PF-2 (Fig. 1) was constructed across the documented boreholes (Biela 1978; Michalík et al. 1992). The surface geology is interpreted according to geological maps (Geological map of Slovakia 2013) and the structural research. Mainly normal faults with a negligible oblique component of movement disrupt the Brezovské Karpaty elevation structure. The Gosau Group sediments are preserved in the zone continuing from the Vienna Basin area to the Myjavská pahorkatina

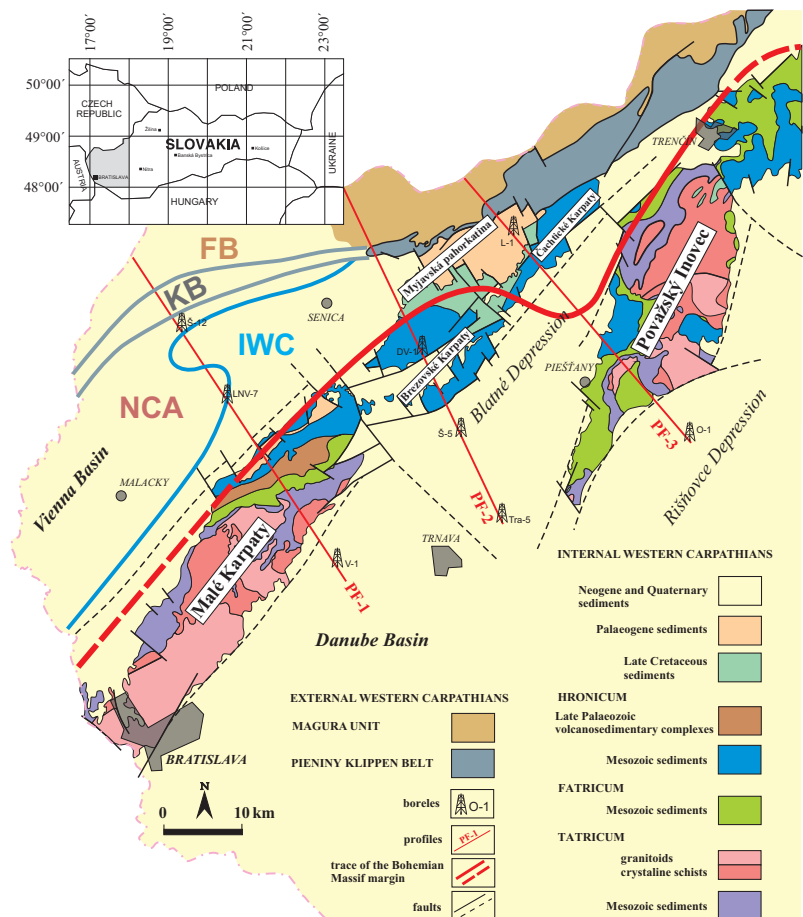


Fig. 1. Simplified geological map with the position of the Alpine and Carpathians nappe systems. FB — Flysch Belt; KB — Klippen Belt; NCA — North Calcareous Alps; IWC — Internal Western Carpathians (map based on Šamajová et al. 2018).

Upland. The calculated gravity includes two gravity lows and one gravity high located between them. A significant gravity high is caused by the structure of the Brezovské Karpaty Mts., which are split by a system of faults with a horizontal gravity gradient of 2.66 mGal/km. The high gravity anomaly of the Brezovské Karpaty Mts. is the result of superposition of gravity effects related to the Mesozoic sediments, the Tatric crystalline basement and the upper/lower crustal boundary, which are in an elevated position. A tectonic contact between the Brezovské Karpaty Mts. and Blatné Depression is confirmed again by the sharp gravity gradient (3.5 mGal/km). Neogene and Quaternary sediments of the Blatné Depression are the cause of a significant gravity low. The shape of the gravity profile in a NW direction from the Brezovské Karpaty Mts. reflects the huge thickness of the Magura nappe system flysch sediments, which are characterized by lower density. The deep contact between the BM and EWC with the IWC along this profile is similar to the situation on profile PF-1. The difference lies in the elevated position of the BM lower crust (0–18 km of the profile). The contact area between the EWC and IWC is very steep (Šamajová et al. 2018).

### Profile PF-3

Profile PF-3 (Fig. 1) is constructed between deep boreholes Lubina-1 (Leško et al. 1982) and Obdokovce-1 (Biela 1978). The geological structures were taken from geological maps (Geological map of Slovakia 2013) and original geological and structural data including geological and structural mapping. The Eocene sediments of the EWC are underthrust below the flat-lying PKB and the Palaeogene sediments (Gosau Group) in borehole Lubina-1 (Leško et al. 1982). From this point of view the PKB is a detached structure thrust above the EWC sediments in the western part of Slovakia during the post-Eocene time. The borehole Obdokovce-1 (O-1) reached the Mesozoic sediments

of the Tatricum cover only (Biela 1978). The resultant density model is characterized by two alternating local gravity highs and gravity lows. The gravity high situated on the NW side of the profile is related to a gravity effect of the Mesozoic sediments belonging to the Hronicum. The elevation of the BM basement contributes to this anomaly, too. Both gravity lows reflect the presence of the Blatné and Rišňovce Depressions. A significant gravity high between them is caused by a horst structure of the Považský Inovec Mts. The top of the BM basement creates an elevation with

a minimum depth of ~8 km beneath the Čachtické Karpaty Mts. Towards to the SE, BM dips sharply under the IWC (Šamajová et al. 2018).

## Conclusion

Geophysical and geological modelling and interpretations along the gravimetric profiles brought new results on the structures of the Western Carpathians, Northern Calcareous Alps and Bohemian Massif (Fig. 1). The gravimetric profile was constructed in the NW–SE direction along deep boreholes and expected tectonic contacts. The data from deep boreholes, especially from Lakšárska Nová Ves-7 (LNV-7) and Šaštín-12 (Š-12), have been reviewed from the point of view of the current lithostratigraphy knowledge of the Mesozoic rock sequences. The obtained results can be summarized as follows:

- The Bohemian Massif (BM) margin is situated internally/southeast from the surface occurrences of the Pieniny Klippen Belt (PKB).
- The accretionary prism of the External Western Carpathians (EWC) is formed by (from the bottom up) the Krosno (Waschberg-Ždánice-Pouzďřany Unit) and Magura units / nappe system thrust over rock sequences of the BM.
- The PKB does not represent topographical manifestation nor geological contact with BM.
- The PKB represents shallow (max. 5 km deep) contact between the EWC and the IWC thin-skinned tectonic units i.e. has not as structural and tectonic importance as has been so far attributed to it.
- The trace of BM margin is apparently bent inward the IWC.
- The deep contact between BM/EWC and IWC propagates as the transtension zone towards the surface.
- The contact between Alpine and Carpathians provenance of Mesozoic sequences is verified by borehole data. The decisive argument for determining the tectonic identity of the cover nappes is the presence or absence of anhydrite-rich strata.

**Acknowledgements:** This work was supported by the Slovak Research and Development Agency under the contracts nos. APVV-0212-12, APVV-16-0146, APVV-16-0121, APVV-16-0482, APVV-17-0170 and APVV SK-AT-2017-0010 by the VEGA Slovak Grant Agency under projects nos. 2/0006/19 and 1/0115/18 and by the grants of Comenius University No. UK/272/2019.

## References

- Alasonati Tašárová Z., Fullea J., Bielik M. & Šroda P. 2016: Lithospheric structure of Central Europe: Puzzle pieces from Pannonian Basin to Trans-European Suture Zone resolved by geophysical-petrological modelling. *Tectonics* 35, 1–32.
- Biela A. 1978: Deep drilling in the covered areas of the Inner Western Carpathians. *Regionálna Geol. Záp. Karpát* 10, *State Geological Institute of Dionýz Štúr*, Bratislava, 1–224 (in Slovak).
- Bielik M. 1995: Continental convergence in the Carpathian region by density modelling. *Geol. Carpath.* 46, 3–12.
- Bielik M., Šefara J., Kováč M., Bezák V. & Plašienka D. 2004: The Western Carpathians — interaction of Hercynian and Alpine processes. *Tectonophysics* 393, 63–86.
- Bielik M., Makarenko I., Csicsay K., Legostaeva O., Starostenko V., Savchenko A., Šimonová B., Dérerová J., Fojtíková L., Pašteka R. & Vozár J. 2018: The refined Moho depth map in the Carpathian-Pannonian region. *Contributions to Geophysics and Geodesy* 48, 2, 179–190.
- Biely A., Bezák V., Elečko M., Gross P., Kaličiak M., Konečný V., Lexa J., Mello J., Nemčok J., Potfaj M., Rakús M., Vass D., Vozár J. & Vozárová A. 1996: Explanations to Geological map of Slovakia 1:500 000. *State Geological Institute of Dionýz Štúr*, Bratislava, 1–76 (in Slovak with English summary).
- Dérerová J., Zeyen H., Bielik M. & Salman K. 2006: Application of integrated geophysical modeling for determination of the continental lithospheric thermal structure in the eastern Carpathians. *Tectonics* 25, 3, 1–12, TC3009.
- Fusán O., Biely A., Ibrmajer J., Plančár J. & Rozložník L. 1987: Podložie terciéru vnútorných Západných Karpát. Pre-Tertiary basement of the Inner Western Carpathians. Monograph. *State Geological Institute of Dionýz Štúr*, Bratislava, 1–103 (in Slovak with English summary).
- Geological map of Slovakia M 1:50 000, 2013. *State Geological Institute of Dionýz Štúr*, Bratislava. Available online: <http://mapservergeology.sk/gm50js>.
- GM-SYS® User's Guide for version 4.9. 2004: *Northwest Geophysical Associates Inc Corvallis*.
- Hók J., Kováč M., Pelech O., Pešková I., Vojtko R. & Králiková S. 2016: The Alpine tectonic evolution of the Danube Basin and its northern periphery (southwestern Slovakia). *Geol. Carpath.* 67, 495–505.
- Leško B. (Ed.), Babák B., Borovcová D., Boučková B., Dubecký K., Ďurkovič T., Faber P., Gašpariková V., Harča V., Köhler E., Kuděra L., Kullmanová A., Okénko J., Planderová E., Potfaj M., Samuel O., Slámková M., Slanina V., Summer J., Sůrová E., Štěrba L. & Uhman J. 1982: Structural borehole Lubina-1 [Oporný vrt Lubina-1]. *Regionálna geológia Západných Karpát*, 17, 7–116 (in Slovak).
- Michalík J. (Ed.), Broska I., Franců J., Jendrejáková O., Kochanová M., Lintnerová O., Masaryk P., Papšová J., Planderová E., Šucha V. & Zatkalíková V. 1992: Structural borehole Dobrá Voda DV-1 (1 140,8 m) (Dobrá Voda-Konča Skaliek) in Brezovské Karpaty Mts. *Regionálna Geológia Západných Karpát*, Bratislava, 3–139 (in Slovak with English summary).
- Pašteka R., Záhorec P., Kušnirák D., Bošanský M., Papčo J., Marušiak I., Mikuška J. & Bielik M. 2017: High resolution Slovak Bouguer gravity anomaly map and its enhanced derivative transformations: new possibilities for interpretation of anomalous gravity fields. *Contributions to Geophysics and Geodesy* 47, 2, 81–94.
- Picha F.J., Stránik Z. & Krejčí O. 2006: Geology and hydrocarbon resources of the Outer Western Carpathians and their foreland, Czech Republic. In: Golonka J. & Picha F.J. (Eds.): *The Carpathians and their foreland: Geology and hydrocarbon resources*. AAPG *Memoir* 84, 49–175.
- Šamajová L. & Hók J. 2018: Density of rock formations of the Western Carpathians on the territory of Slovakia. *Geol. Práce Spr.* 132, 31–52 (in Slovak).
- Šamajová L., Hók J., Bielik M. & Pelech O. 2018: Deep contact of the Bohemian Massif and Western Carpathians as seen from density modeling. *Geol. Carpath.* 69, 6, 545–557.
- Šimonová B. & Bielik M. 2016: Determination of rock densities in the Carpathian–Pannonian Basin lithosphere: based on the CELEBRATION 2000 experiment. *Contributions to Geophysics and Geodesy* 46, 269–87.
- Talwani M., Worzel J.L. & Landisman M. 1959: Rapid gravity computations for two dimensional bodies with application to the Mendocino submarine fracture zone. *Journal of Geophysical Research* 64, 49–59.
- Topographic Institute 2012: Digital terrain model version 3 (online). <http://www.topu.mil.sk/14971/digitalny-model-reliefu-urovne-3-%28dmr-3%29.php>.
- Vozár J. & Šantavý J. (Eds.), Potfaj M., Szalaiová V., Scholtz P., Tomek Č., Šefara J., Magyar J. & Slávik M. 1999: Atlas of Deep Reflection Seismic Profiles of the Western Carpathians and Their Interpretation. *Ministry of environment of the Slovak Republic*.
- Wessely G. 1992a: The Calcareous Alps below the Vienna Basin in Austria and their structural and facial development in the Alpine-Carpathian border zone. *Geol. Carpath.* 43, 347–353.
- Wessely G. 1992b: Outline of Sedimentation, Tectonic Framework and Hydrocarbon Occurrence in Eastern Lower Austria. *Mitt. Österr. Geol. Ges. Guidebook* 85, 5–96.

# Advances in volcano gravimetry: Handling topographic effects

PETER VAJDA<sup>1</sup>, PAVOL ZAHOREC<sup>1</sup>, JURAJ PAPČO<sup>2</sup>, DUŠAN BILČÍK<sup>1</sup>,  
FILIPPO GRECO<sup>3</sup> and MASSIMO CANTARERO<sup>3</sup>

<sup>1</sup>Earth Science Institute, Slovak Academy of Sciences, Bratislava, Slovakia; Peter.Vajda@savba.sk

<sup>2</sup>Dept. of Theoretical Geodesy, Slovak University of Technology, Bratislava, Slovakia

<sup>3</sup>Istituto Nazionale di Geofisica e Vulcanologia (INGV Catania) — Osservatorio Etneo, Catania, Italy

**Abstract:** In volcano gravimetry, spatiotemporal gravity changes are observed, processed and interpreted. This requires the application of proper correction for the sensor height of a gravimeter to reduce the gravity reading from the sensor position to the benchmark on the ground or to a common reference level when executing the repeat surveys using various types of gravimeters or various plates or tripods. Such correction/reduction, called the Free-Air Correction requires the use of true in situ vertical gradient of gravity (VGG). In the absence of in-situ measured VGG values, the constant value of the theoretical (normal) free air gradient (FAG) is commonly used. We propose an alternative to this practice which may significantly reduce systematic errors associated with the use of theoretical FAG. The true VGG appears to be better approximated, in areas with prominent or rugged topographic relief, such as alpine or many volcanic regions, by a value based on the modelled contribution of the topographic masses to the gradient. Such prediction can be carried out with a digital elevation/terrain model (DEM/DTM) of sufficient quality: resolution of 5 m or better and vertical accuracy at the order of 10 cm, depending on the roughness of the relief. We quantify also the need of improving the VGG prediction at gravimetric monitoring networks for benchmarks adjacent to man-made structures (walls, buildings, etc.). We also present the possibility to improve the VGG prediction by locally refining the DEM by drone-flown photogrammetry. The predictability of VGGs in regions of rugged relief was verified by in-situ observations in the Central Volcanic Complex (CVC) of Tenerife (Canary islands) and at Mt. Etna (Italy). We illustrate how strongly and sharply the VGG field deviates spatially from the constant value of FAG. We also analyze the sensitivity of the VGG prediction to the resolution and accuracy of the used DEM. Finally we discuss the role and treatment of the Deformation-Induced Topographic Effect (DITE) in compiling and interpreting residual time-lapse gravity changes in 4D micro-gravimetry.

## Prediction of VGG

The value of VGG at a benchmark consists basically of 3 components: that generated by the normal reference (level) ellipsoid, that generated by the topographic masses (of constant reference density), and that generated by the subsurface density anomalies (geological heterogeneities).

The component due to level ellipsoid (normal reference ellipsoid) can be globally (up to altitude of 9 km) approximated by the constant theoretical free-air gradient ( $FAG = -308.6 \mu\text{Gal/m}$ ) with accuracy better than  $0.5 \mu\text{Gal/m}$  (e.g., Zhao et al. 2015). In regions with prominent and rough topographic relief the contribution of topo-masses to the gradient can be expected to be significantly higher than the contribution of geological heterogeneities. Upon neglecting the geological component we can predict the actual VGG by adding to the constant value of FAG the accurately modelled VGG component due to the topographic masses. It can be modelled with sufficient accuracy suppose a digital elevation (terrain) model (DEM/DTM) of sufficient quality is available. The topo-component is computed by a numerical volumetric Newtonian integration, such as

that facilitated by the Toposk software (Zahorec et al. 2017). Its accurate realization in micro-gravimetric applications in areas of prominent and rough topographic relief requires a DEM with a resolution at the level of several meters and vertical accuracy at the order of 10 cm. In regions with rugged topography the predicted VGG severely deviates from the constant FAG. This deviation is high in amplitude and exhibits sharp spatial variability (Figs. 1 and 2). In absolute sense the high values of VGG are associated with sharp convex terrain features (peaks, ridges), while the small values with the concave ones (canyons, gullies, craters). In alpine regions like the High Tatras of the northern Slovakia the predicted VGGs depart from constant FAG by as much as 88 %. A departure of 77 % was observed in the CVC of Tenerife (Fig. 1). The situation is similar at the Phlegrean fields (Fig. 2).

## In situ verification

The accuracy of predicting the VGGs by adding the computed (modelled) topo-component to the constant FAG was verified in selected volcanic regions by in-situ

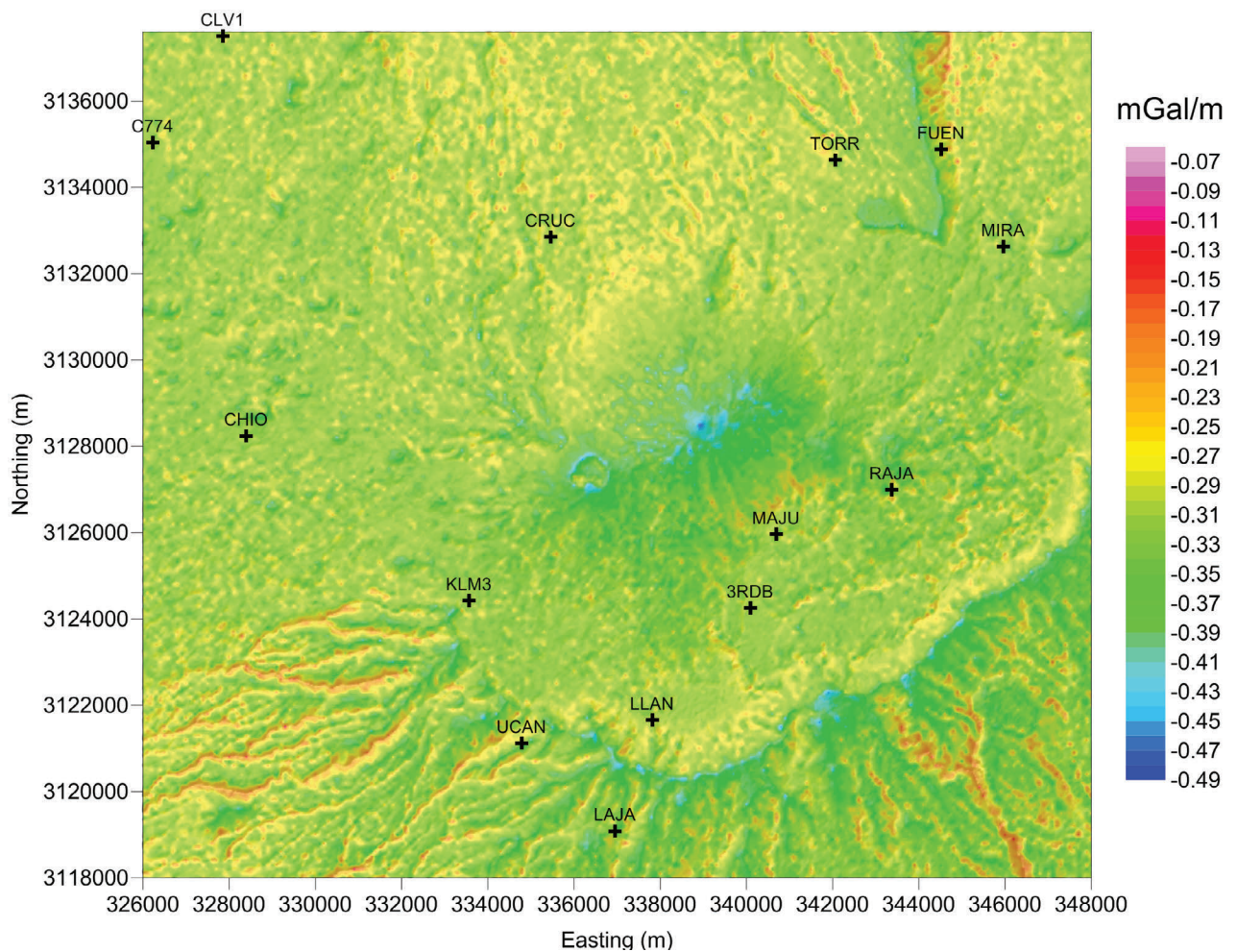


Fig. 1. The predicted VGG field (mGal/m) at the CVC of Tenerife based on a 2 m LiDAR DTM.

observations of VGGs (Fig. 3). Results of the verification campaign in the CVC of Tenerife (Canary islands) and on Mt. Etna (Italy) are presented. When a DEM of adequate quality is used for modelling the topo-contribution to the gradient, the match between predicted and in-situ VGGs is generally very good. Accurate modelling requires LiDAR-derived DEM with resolution at the level of 5 m and accuracy at the order of 10 cm. However, discrepancies may occur at some benchmarks due to geological signal/component (heterogeneities) such as subsurface (near-surface) hydrothermal alteration.

### Refinement of VGG prediction

If benchmarks of a gravimetric network are at or inside (or in close proximity to) man-made structures like walls or buildings, the gravitational effect (on VGG) of these

structures must be accurately modelled in addition to the effect of topographic masses, as it is significant, too. In addition, the nearest-terrain DTM, and its modelled effect on VGG, may be refined by constructing a local drone-borne photogrammetry-derived local DTM within the nearest zone of the modelled topo-contribution (Zahorec et al. 2018).

### Applicability — 3D microgravimetry

Various gravimeters, in combination with various tripods, have various vertical positions of their sensors above the ground. Therefore micro-gravimetric observations require an accurate reduction of the measurement from the meter sensor to the benchmark on the ground or to a common adopted level. This reduction is accomplished based on the true in-situ VGG. If the true VGGs are not available, they can be topo-predicted. The use of

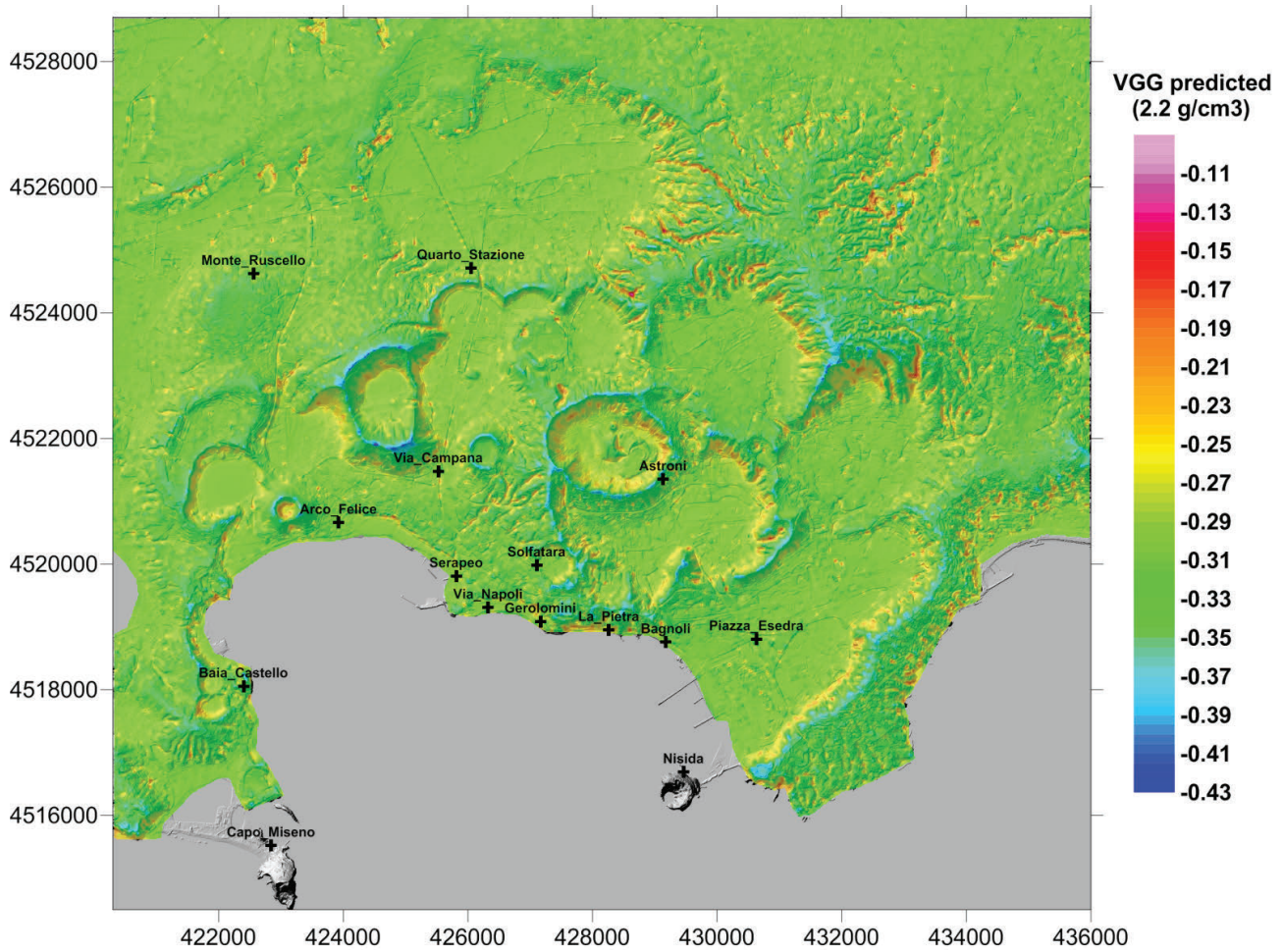


Fig. 2. The predicted VGG field (mGal/m) at Campi Flegrei (Italy) using a 5 m LiDAR DTM.



Fig. 3. In situ VGG observations on Etna (NE crater) using a relative gravimeter in tower mode.

the predicted VGGs in free-air correction is in regions of prominent topography a better choice than the use of the constant FAG.

the VEGA grant agency under projects No. 2/0006/19 and 1/0462/16

### Applicability — 4D microgravimetry

In volcano-gravimetric studies often residual spatio-temporal gravity changes are compiled and interpreted. Some studies apply the free-air effect (FAE) as a correction, which is based on the true in situ VGG, while other studies use the constant FAG instead. The rigorous treatment of deformation-induced topographic effect (DITE) and its numerical realization is outlined here and dealt by in due detail in (Vajda et al. 2019).

**Acknowledgements:** This work was supported by the Slovak Research and Development Agency under the contract (project) No. APVV-16-0482, as well as by

### References

- Vajda P., Zahorec P., Bilčík D. & Papčo J. 2019: Deformation-induced topographic effects in interpretation of spatio-temporal gravity changes: Review of approaches and new insights. *Surveys in Geophysics*, doi: 10.1007/s10712-019-09547-7.
- Zahorec P., Marušiak I., Mikuška K., Pašteka R. & Papčo J. 2017: Numerical Calculation of Terrain Correction Within the Bouguer Anomaly Evaluation (Program Toposk), chapter 5. In: Pašteka R., Mikuška J. & Meurers B. (Eds.): *Understanding the Bouguer Anomaly: A Gravimetry Puzzle*. Elsevier, 79–92. ISBN 978-0-12-812913-5, doi: 10.1016/B978-0-12-812913-5.00006-3
- Zahorec P., Papčo J., Vajda P., Greco F., Cantarero M. & Carbone D. 2018: Refined prediction of vertical gradient of gravity at Etna volcano gravity network (Italy). *Contrib. Geophys. Geod.* 48, 4, 299–317, doi 10.2478/congeo-2018-0014.
- Zhao D., Li S., Bao H. & Wang Q. 2015: Accurate Approximation of Vertical Gravity Gradient Within the Earth's External Gravity Field. In: Jin S. & Barzaghi R. (Eds.): *IGFS 2014*. IAG Symposia, vol 144. Springer, doi 10.1007/1345\_2015\_113.

## Register

- ACKERMAN 79  
 ALASONATI TAŠAROVÁ 166  
 ALEKSIEIENKO 102  
 ALI 141  
 ANCZKIEWICZ 75  
 ANDRIEIEV 102  
 ANTOLÍKOVÁ 142, 160  
 AUBRECHT 33  
 AUDÉTAT 83  
 BABEJOVÁ-KMECOVÁ 144  
 BAČÍK 56, 106  
 BAČO 75  
 BALKANSKA 60  
 BASSO 143  
 BEZÁK 172  
 BIELIK 166, 171, 172, 180  
 BILČÍK 172, 184  
 BIROŇ 75  
 BONDARENKO 87  
 BROSKA 83, 91, 112  
 BRZOBOHATÝ 126  
 BUČOVÁ 33  
 BURET 54  
 CANTARERO 184  
 CAO 16  
 CHEW 123  
 CHOVAN 45  
 COLETTI 143  
 CSIBRI 25, 130, 180  
 DANIŠÍK 75  
 DEMENY 126  
 DEMKO 115  
 DÉREROVÁ 166  
 DOLÁKOVÁ 126  
 ELBRA 160  
 ERBAN 75  
 FARSANG 95  
 FELDMAN-OLSZEWSKA 146  
 FERENC 123  
 FINGER 64  
 FRIDRICHOVÁ 106  
 FRITZ 64  
 FUKSI 163  
 GARGULÁK 95  
 GAVRYLIV 102  
 GENSER 37  
 GEORGIEV 60  
 GEORGIEVA 65  
 GERDES 75  
 GERDJIKOV 60  
 GERŠLOVÁ 71  
 GOETZE 166  
 GRABOWSKI 33  
 GRECO 184  
 GRINČ 166  
 GUAN 37  
 HALÁSOVÁ 130, 144  
 HALTON 75  
 HAUZENBERGER 64  
 HEINRICH 54  
 HEJL 64  
 HLADILOVÁ 126  
 HNYLKO 146  
 HÓK 130, 180  
 HOLCOVÁ 126, 130  
 HORVÁTH 166  
 HRABOVSKÝ 126, 143  
 HROUDA 176  
 HUDÁČKOVÁ 130, 144, 163  
 HYŽNÝ 130  
 IVAN 29  
 IWAŇCZUK 146  
 JAMRICH 130, 144  
 JANÁK 69  
 JANOUŠEK 50  
 JESENÁK 75  
 JIRMAN 71  
 JONIAK 130  
 KIRKLAND 75  
 KISS 130, 144  
 KLANICA 172  
 KODĚRA 45, 83  
 KOHÚT 75, 83  
 KOCHERGINA 75  
 KOLLER 119  
 KOPECKÁ 126  
 KOUNOV 60  
 KOVÁČ 25, 43, 130, 144  
 KOVÁČOVÁ 130, 144  
 KRAJŇÁK 171  
 KRMÍČEK 79  
 KROBICKI 146  
 KRUMOV 65  
 KUBAČ 45  
 KUBIŠ 112  
 KUHNERT 126  
 KURYLO 87, 91  
 KURZ 64  
 KUŠNIRÁK 171  
 LARGE 54  
 LARIONOV 119  
 LAZAREVA 102  
 LAZAROVA 60  
 LEGOSTAEVA 166  
 LEXA 45, 83  
 LI Q.-L. 119  
 LI X.-H. 119  
 LINDNER 64  
 LIU B. 37  
 LIU Y. 16, 37  
 LYZHACHENKO 87  
 MADZIN 33  
 MAGNA 75  
 MAJGIN 172  
 MAKARENKO 166  
 MARASZEWSKA 91  
 MÁRTON 33  
 MARUŠIAK 171  
 MEDVECKÁ 71  
 MÉRES 29, 39  
 MICHALÍK 134  
 MIKUŠ 75, 123  
 MIKUŠKA 171  
 MILOVSKÁ 75  
 MILOVSKÝ 75, 126  
 MOHAMED 141  
 MYTROKHIN 102  
 NEDIALKOV 65  
 NEHYBA 126  
 NEMEC 119  
 NÉMETH 119  
 NEUBAUER 16, 37  
 NOVÁKOVÁ 130  
 ONDREJKA 119  
 OZDÍN 95  
 PÁNISOVÁ 166  
 PAPČO 171, 184  
 PAŠTEKA 166, 171  
 PAVIČIĆ 130  
 PEARCE 75  
 PEK 172  
 PETRÍK 99  
 PEYTCHEVA 54  
 PISERA 143  
 PLAŠIENKA 21, 29, 33, 39, 43  
 PLAŠIENKOVÁ 144  
 PORUBČAN 95  
 POTOČNÝ 39  
 POVINEC 95  
 PRCÚCH 45  
 PUTIŠ 33, 119  
 RECIO 75  
 REHÁKOVÁ 137  
 RIGOVÁ 126  
 ROTTIER 83  
 RUMAN 130, 144  
 RUŽIČKA 119  
 RYBÁR 25, 130  
 SABOL 130  
 ŠAMAJOVÁ 130, 180  
 ŠARINOVÁ 130  
 SCHEINER 126  
 ŠEFCŮ 162  
 SEKO 126  
 SHERLOCK 75

SHNYUKOV 102  
SIMAN 119, 123  
ŠIMO 151  
ŠIMONOVÁ 166  
SIWEK 153, 157  
SOTÁK 43, 160  
SPIŠIAK 123  
STAROSTENKO 166  
STREKOPYTOV 95  
ŠUJAN 130  
ŠURKA 75  
ŠVÁBENICKÁ 162

SYOMKA 87  
SZALAIOVÁ 171  
TELECKÝ 172  
TOMAŠOVÝCH 163  
UHER 106, 119  
UTESCHER 126  
VAJDA 184  
VETRÁKOVÁ 123  
VLČEK 130  
VOJTKO 43, 45, 130  
VON QUADT 54  
VOZÁR 172

WAGREICH 141  
WENDORFF 153, 157  
WESTGATE 75  
YI 83  
YU 37  
YUAN 16, 37  
ZAHOREC 171, 184  
ZAKI 141  
ZEYEN 166  
ŽITŇAN 45  
ZULAUF 110



*Partnership:*



*Sponsors and Supporting Organizations:*



**ISBN 978-80-85754-42-1**